



UNIVERSITY OF  
**LIVERPOOL**

**CHARACTERIZATION OF RENAL CD133<sup>+</sup>  
CELLS AND THEIR THERAPEUTIC EFFICACY IN A  
MODEL OF ACUTE KIDNEY INJURY**

Thesis submitted in accordance with the requirements of the University of  
Liverpool for the degree of Doctor in Philosophy

By

Ilaria Santeramo

September 2016



## **DECLARATION**

I hereby declare that except where specific reference is made to the work of others, the contents of this dissertation are original and have not been submitted in whole or in part for consideration for any other degree or qualification in this, or any other university. This dissertation is my own work and contains nothing which is the outcome of work done in collaboration with others except as specified in the text. This dissertation contains fewer than 65,000 words including bibliography, footnotes, tables and equations and has fewer than 70 figures.

*Ilaria Santeramo*

September 2016



## **ABSTRACT**

Renal 'progenitor' cells expressing CD133 have been proposed as cellular therapeutics for treating patients with kidney disease. In the literature, CD133<sup>+</sup> cells isolated from adult kidneys showed the expression of nephron progenitor markers (Pax2), and broad differentiation plasticity, being able to differentiate towards epithelial cells and podocytes. Most importantly, when injected into preclinical models of kidney injury, CD133<sup>+</sup> cells integrated into damaged renal tissue and improved renal health. Nevertheless, the evidence for CD133 being a bona fide renal progenitor marker is conflicting.

In this study, five renal biopsies belonging to children (from 6 months to 10 years old) were used. The localization of CD133 was consistent with previous studies, as the expression of CD133 was demonstrated on the cells of the Bowman's capsule and in scattered tubular cells. From each sample, a bulk renal population was isolated and was initially characterized for the presence of the CD133 marker. Once placed in culture, most of the renal cells started expressing CD133. A further phenotypical characterization revealed that the vast majority of the cells expressed epithelial (EpCam, E-Cadherin, CD24), and some mesenchymal (CD73, CD44) markers. Also, the CD133<sup>+</sup> population appeared heterogeneous for the expression of other markers. Most notably, CD13, a marker of fully differentiated tubular cells, was found to be significantly expressed in part of the CD133<sup>+</sup> cells, suggesting that either fully differentiated cells started expressing CD13 de novo, or the CD133<sup>+</sup> were committed towards a tubular fate.

The bulk population was sorted by FACS into CD133<sup>+</sup> and CD133<sup>-</sup> sub-populations which were compared in additional experiments to explore the progenitor-like features of the CD133<sup>+</sup> cells.

First, the ability of both CD133<sup>+</sup> and CD133<sup>-</sup> sub-populations to differentiate towards podocytes in vitro was investigated. Both sub-populations were found to express the podocyte markers, nephrin and podocin, to a similar extent following stimulation with retinoic acid. However, the assay did not prove to be consistent and it was not used any further.

Secondly, the potential of both CD133<sup>+</sup> and CD133<sup>-</sup> sub-populations to integrate into ex vivo reaggregated mouse kidney rudiments was determined. Surprisingly, the majority of both cell types died in the chimeric rudiments within two days in culture. Neither the surviving CD133<sup>+</sup> nor the CD133<sup>-</sup> cells showed any propensity to integrate into developing renal structures. Unexpectedly, the CD133<sup>+</sup> cells were found to clump on top of the rudiment and had a negative impact on the developing rudiment, whereas the CD133<sup>-</sup> cells did not. Alongside with the test of the human cells in the chimeric rudiments, the assay itself was modified to suit the imaging of the rudiments in a Light-sheet fluorescent microscope (LSFM). 3D embryonic renal organoids were efficiently produced and the development of their structures could be successfully monitored through the LSFM in proof-of-concept experiments.

The final aim of this work was to assess the therapeutic efficacy of the CD133<sup>+</sup> and CD133<sup>-</sup> sub-populations in a rat model of cisplatin-induced acute kidney injury. The renal function was monitored using a non-invasive transcutaneous device that measures the half-life of an exogenously administered renal marker, FITC-Sinistrin, alongside to the measurement of conventional biomarkers, serum creatinine, and urea. Following intravenous (IV) injection, both CD133<sup>+</sup> and CD133<sup>-</sup> cells ameliorated renal function and preserved renal histology. The data suggest that the human cells passed through the lungs, and probably reached the kidneys. However, no cells were alive at the end of the study (14 days), but traces of PKH26 were retrieved in lungs and, to a lesser extent, in the kidneys, suggesting the possible involvement of paracrine mechanisms, possible through extracellular vesicles in the observed functional amelioration.

Additional biodistribution studies showed that soon after the IV injection the human cells were identified in the lungs of the animals, but not in the kidneys. Phagocytic cells, identified through the marker CD68, were observed around the

human cells in the lungs as early as 1 hour after the injection. By 24 hours, clusters of CD68<sup>+</sup> cells could be found, but not human cells. Therefore, the data suggest that the human cells die in the lungs and that the macrophages might play an active role in the disappearance.

Taken together, this work shows that the expression of CD133 does not confer any advantage to the nephrogenic potential *ex vivo* or to the therapeutic efficacy *in vivo*. Moreover, since the cells were shown to be entrapped in the lungs, the renal repair is probably mediated by cell-derived factors, rather than by CD133<sup>+</sup> cells homing to the kidneys and generating specialised renal cells. The role of macrophages in the resolution or regenerative mechanisms should be considered and further examined in future preclinical studies of cellular therapies for kidney diseases.





# CONTENTS

<b>DECLARATION .....</b>	<b>I</b>
<b>ABSTRACT.....</b>	<b>III</b>
<b>LIST OF FIGURES .....</b>	<b>XI</b>
<b>LIST OF TABLES.....</b>	<b>XV</b>
<b>LIST OF ABBREVIATIONS.....</b>	<b>XVII</b>
<b>1 INTRODUCTION .....</b>	<b>1</b>
1.1 Kidney structure and major components .....	1
1.1.1 Renal development: an overview .....	5
1.1.2 Postnatal development of the kidney .....	8
1.2 Acute kidney injury .....	8
1.3 Chronic Kidney diseases and End Stage Renal Disease .....	10
1.4 The end point: alternatives for ESRD patients .....	11
1.4.1 Transplantation.....	11
1.4.2 Dialysis .....	13
1.5 Biomarkers of acute kidney injury .....	13
1.6 Novel biomarkers of acute kidney injury.....	15
1.7 Human kidney stem/progenitor cells (hKSPCs): CD133 <sup>+</sup> cells.....	19
1.8 CD133 as a marker of stem cells.....	22
1.8.1 Physiological role of CD133.....	24
1.9 Other markers used to isolate hKSPCs.....	26
1.10 Other approaches used to identify hKSPCs.....	28
1.11 The other side of the spectrum: the dedifferentiation theory .....	31
1.12 Methods used to test the potential of hKSPCs.....	33
1.12.1 Differentiation assays.....	33
1.12.2 Kidney Reaggregation Assay.....	34
1.12.3 The light sheet microscope: principles and advantages .....	37
1.13 In vivo models of acute kidney injury.....	38
1.13.1 Pathophysiology of the Cisplatin-induced injury .....	39
1.13.2 Inflammation .....	41
<b>2 MATERIALS AND METHODS.....</b>	<b>45</b>
2.1 Cell Culture Procedures .....	45
2.1.1 Isolation of human renal cells.....	45
2.1.2 Routine cell culture procedures .....	46
2.1.3 Cryopreservation and recovery of the cells .....	47

2.1.4	Maintenance of conditionally immortalized podocytes .....	47
2.1.5	Isolation of primary podocytes.....	47
2.1.6	Population Doublings Time calculations.....	48
2.1.7	Transduction of hK2 cells with GFP lentiviral particle.....	48
2.1.8	clonogenic assay and Giemsa staining.....	48
2.1.9	Podocyte differentiation assay.....	49
2.2	Fixation and immunohistochemistry of samples.....	49
2.3	Immunofluorescence on cells .....	50
2.4	Immunofluorescence on tissues.....	51
2.5	Fluorescence Activated Cell Sorting (FACS) .....	53
2.6	Magnetic Activated Cell Sorting (MACS) .....	55
2.7	Cell Cycle Analysis .....	56
2.8	Kidney Reaggregation Assay .....	57
2.8.1	Immunofluorescence of Kidney reaggregated rudiments .....	58
2.9	Formation of Kidney embryonic spheroids.....	58
2.9.1	Anionic organic transporter functional assay.....	59
2.9.2	Live imaging of the spheroids .....	59
2.10	Cisplatin-Induced acute kidney injury model.....	60
2.10.1	Animal groups, blood and urine collection .....	60
2.10.2	Transcutaneous assessment of renal function.....	61
2.10.3	Two-weeks study using CD133 <sup>+</sup> and CD133 <sup>-</sup> cells.....	63
2.10.4	Short-term study .....	64
2.10.5	Histology: collection and analysis .....	64
2.10.6	Immunohistochemistry procedures on Paraffin-embedded Tissues .....	64
2.10.7	Immunohistochemistry procedures on Frozen Tissues .....	65
2.11	Image processing.....	66
2.12	Statistical analysis .....	67
2.13	Summary of cell culture media.....	67
<b>3</b>	<b>ISOLATION AND CHARACTERIZATION OF RENAL STEM/PROGENITOR CELLS ...</b>	<b>71</b>
3.1	Introduction and aims .....	71
3.2	Results .....	72
3.2.1	Identification of CD133 and CD24 in vivo.....	72
3.2.2	Isolation of renal cells from human kidneys and characterization for CD133 and CD24	76
3.2.3	Characterization of the heterogeneous population at passage 2 .....	79
3.2.4	Sorting of CD133 <sup>+</sup> and CD133 <sup>-</sup> cells .....	87

3.2.5	Characterization of CD133 <sup>+</sup> and CD133 <sup>-</sup> populations by immunofluorescence .....	90
3.2.6	Characterization of the CD133 <sup>+</sup> and CD133 <sup>-</sup> populations in culture.....	92
3.2.7	Clonogenic potential of CD133 <sup>+</sup> and CD133 <sup>-</sup> cells.....	94
3.2.8	Evaluation of the CD133 expression in both sorted populations during expansion	96
3.3	Discussion.....	99
<b>4</b>	<b>INVESTIGATING THE ABILITY OF CD133+ AND CD133- CELLS TO DIFFERENTIATE INTO PODOCYTES AND TO INTEGRATE IN A CHIMERIC RUDIMENT.....</b>	<b>107</b>
4.1	Introduction and aims .....	107
4.2	Results .....	108
4.2.1	Preparation of CD133 <sup>+</sup> and CD133 <sup>-</sup> -GFP-labelled.....	108
4.2.2	Analysing the potential of CD133 <sup>+/-</sup> renal progenitor cells to differentiate into podocytes	110
4.2.3	The kidney reaggregation assay as a tool to evaluate the nephrogenic potential of CD133 <sup>+</sup> human renal progenitor cells cells.....	118
4.2.4	A refined kidney reaggregation assay for light sheet microscopy .....	129
4.2.5	Functionality of the tubuli in the spheroids .....	132
4.2.6	In vivo imaging of kidney spheroids .....	135
4.3	Discussion.....	139
<b>5</b>	<b>AMELIORATION POTENTIAL OF HUMAN CD133+ AND CD133- IN A CISPLATIN-INDUCED RAT MODEL OF ACUTE KIDNEY INJURY.....</b>	<b>149</b>
5.1	Introduction and aims .....	149
5.2	Results .....	151
5.2.1	Preparation of CD133 <sup>+</sup> and CD133 <sup>-</sup> -GFP-labelled.....	151
5.2.2	Two-week Study .....	152
5.2.3	Monitoring serum creatinine and urea to assess functional renal damage.....	155
5.2.4	Biodistribution study.....	167
5.3	Discussion.....	174
<b>6</b>	<b>CONCLUSIONS.....</b>	<b>183</b>
	<b>LIST OF REFERENCES .....</b>	<b>191</b>



## LIST OF FIGURES

FIGURE 1.1 SCHEMATIC REPRESENTATION OF THE STRUCTURE OF THE KIDNEY, NEPHRON AND GLOMERULUS.....	5
FIGURE 1.2 SCHEMATIC REPRESENTATION OF THE RENAL DEVELOPMENT FROM E10.5 TO THE FORMATION OF THE NEPHRON.....	7
FIGURE 1.3 OVERVIEW OF THE NUMBER OF PATIENTS ON THE TRANSPLANT LIST AND THE NUMBER OF AVAILABLE KIDNEYS IN THE UK.....	12
FIGURE 1.4 SCHEMATIC REPRESENTATION OF THE LOCALIZATION OF THE POPULATIONS OF PUTATIVE PROGENITOR CELLS ON THE BOWMAN'S CAPSULE.....	21
FIGURE 1.5 SUMMARY OF STUDIES THAT USED THE KIDNEY REAGGREGATION ASSAY TO VALIDATE THE NEPHROGENIC POTENTIAL OF DIFFERENT POPULATIONS OF HUMAN STEM CELLS, ORDERED BY THEIR POTENCY.....	36
FIGURE 2.1 MINIATURIZED DEVICE USED TO ASSESS THE RENAL FUNCTION IN RATS. ....	62
FIGURE 2.2 REPRESENTATIVE EXCRETION CURVES OF FITC-SINISTRIN IN A HEALTHY (A) AND INJURED (B) RAT. ....	63
FIGURE 2.3 IMAGE PROCESSING PROCEDURE USED TO MEASURE THE TUBULAR DILATATION.....	66
FIGURE 3.1 EXPRESSION <i>IN VIVO</i> OF CD133.....	74
FIGURE 3.2 EXPRESSION <i>IN VIVO</i> OF CD24.....	75
FIGURE 3.3 BRIGHT FIELD IMAGES OF THE FRESHLY ISOLATED CELLS OF ALL SAMPLES.....	76
FIGURE 3.4 EXPRESSION OF CD133 <i>IN VITRO</i> .....	77
FIGURE 3.5 EXPRESSION OF CD24 <i>IN VITRO</i> .....	78
FIGURE 3.6 EXPRESSION OF CD31 AND CD45 <i>IN VITRO</i> .....	79
FIGURE 3.7 EXPRESSION OF MESENCHYMAL MARKERS <i>IN VITRO</i> .....	81
FIGURE 3.8 EXPRESSION OF EPITHELIAL MARKERS <i>IN VITRO</i> .....	83
FIGURE 3.9 EXPRESSION OF RENAL PROGENITOR MARKERS <i>IN VITRO</i> .....	84
FIGURE 3.10 FACS SORTING STRATEGY EMPLOYED IN THE STUDY AND COMPARISON WITH MACS.....	89
FIGURE 3.11 SUMMARY OF THE SORTING FOR ALL SAMPLES (HK1-HK5).....	90
FIGURE 3.12 EXPRESSION OF RENAL PROGENITOR TRANSCRIPTION FACTORS (WT1, PAX2) AND VIMENTIN.....	91
FIGURE 3.13 CHARACTERIZATION OF CD133 <sup>+</sup> POPULATION IN CULTURE.....	93
FIGURE 3.14 BRIGHT FIELD IMAGES OF CD133 <sup>+</sup> AND CD133 <sup>-</sup> CELLS AT PASSAGE 2.....	94

FIGURE 3.15 CLONOGENIC ASSAY .....	95
FIGURE 3.16 CHARACTERIZATION OF CD133 <sup>+</sup> AND CD133 <sup>-</sup> CELLS DURING EXPANSION.....	97
FIGURE 4.1 MICROGRAPHS OF CD133 <sup>+</sup> GFP <sup>+</sup> AND CD133 <sup>-</sup> GFP <sup>-</sup> CELLS AT P3 .....	109
FIGURE 4.2 SORTING STRATEGY USED TO SORT CD133 <sup>+</sup> GFP <sup>+</sup> AND CD133 <sup>-</sup> GFP <sup>+</sup> .....	110
FIGURE 4.3 REPRESENTATIVE BRIGHT FIELD IMAGES OF CD133 <sup>+</sup> AND CD133 <sup>-</sup> CELLS CULTURED IN VRAD CONTROL OR FULL VRAD MEDIUM FOR SEVEN DAYS. ....	111
FIGURE 4.4 REPRESENTATIVE BRIGHT FIELD IMAGES OF DIFFERENTIATED CIPODOCYTES AND PRIMARY HUMAN PODOCYTES IN CULTURE .....	112
FIGURE 4.5 EXPRESSION OF PODOCIN AND NEPHRIN IN HUMAN CD133 <sup>+</sup> AND CD133 <sup>-</sup> CELLS AFTER SEVEN DAYS IN VRAD OR CONTROL MEDIUM.....	114
FIGURE 4.6 REPRESENTATIVE IMMUNOFLUORESCENCE IMAGES SHOWING HK6-DERIVED PRIMARY PODOCYTES AND CIPODOCYTES STAINED FOR PODOCIN AND NEPHRIN.....	115
FIGURE 4.7 CELL CYCLE ANALYSIS OF CD133 <sup>+</sup> AND CD133 <sup>-</sup> CELLS IN CONTROL AND VRAD MEDIUM	117
FIGURE 4.8 REPRESENTATIVE BRIGHT FIELD IMAGES OF HUMAN CELLS TREATED WITH VRAD MEDIUM UNDERGOING CELL DEATH.....	118
FIGURE 4.9 KIDNEY REAGGREGATION ASSAY .....	119
FIGURE 4.10 CONTROL REAGGREGATED RUDIMENTS AT DAY 1, 3 AND 6 .....	121
FIGURE 4.11 CHIMERIC RUDIMENT USING MOUSE MESOTHELIAL CELLS, MONITORED AT 1, 3 AND 6 DAYS .....	123
FIGURE 4.12 CHIMERIC RUDIMENTS USING CD133 <sup>-</sup> CELLS, MONITORED AT DAY 1, 3 AND 6 .....	125
FIGURE 4.13 CONFOCAL IMAGES SERIES OF A Z-STACK SHOWING A DETAIL OF A CHIMERIC RUDIMENT USING CD133 <sup>-</sup> CELLS AT DAY 3.....	126
FIGURE 4.14 CHIMERIC RUDIMENTS USING CD133 <sup>+</sup> CELLS, MONITORED AT DAY 1, 3 AND 6.....	127
FIGURE 4.15 SINGLE FOCAL PLANE CONFOCAL IMAGE OF A CHIMERIC RUDIMENT USING CD133 <sup>+</sup> CELLS ON DAY 6 .....	128
FIGURE 4.16 MODIFIED KRA, DEVISED TO PRODUCE SPHEROIDS TO IMAGE IN THE LSFM.....	130
FIGURE 4.17 COMPACTION OVER TIME OF THE SPHEROIDS .....	131
FIGURE 4.18 REPRESENTATIVE LSFM IMAGES OF THE SPHEROIDS CULTURED FOR SIX DAYS .....	132
FIGURE 4.19 ANIONIC UPTAKE ASSAY ON REAGGREGATED CONTROL SPHEROIDS.....	134
FIGURE 4.20 SERIES OF LSFM IMAGES OBTAINED DURING THE LIVE IMAGING OF A REAGGREGATED SPHEROID FOR TEN HOURS.....	136

FIGURE 4.21 SERIES OF LSFM IMAGES OBTAINED DURING THE LIVE IMAGING OF A CHIMERIC SPHEROID CONTAINING MOUSE MESOTHELIAL CELLS FOR FORTY-FIVE HOURS.....	137
FIGURE 4.22 SERIES OF LSFM IMAGES OF A DETAIL OF THE CHIMERIC RUDIMENT CONTAINING MOUSE MESOTHELIAL CELLS.....	138
FIGURE 5.1 CONFIRMATION OF THE PURITY OF BOTH POPULATION AT P5 BEFORE INJECTION <i>IN VIVO</i> ..	152
FIGURE 5.2 EXPERIMENTAL SET-UP OF THE TWO-WEEK STUDY.....	153
FIGURE 5.3 HALF-LIFE VALUES OF FITC-SINISTRIN OVER THE TWO WEEKS STUDY OBTAINED USING THE GFR DEVICES.....	154
FIGURE 5.4 SERUM CREATININE AND SERUM UREA VALUES OVER THE TWO WEEKS STUDY IN SERUM AND URINE.....	157
FIGURE 5.5 URINARY TIM-1, CYS-C AND ALBUMIN OVER THE LENGTH OF THE STUDY.....	159
FIGURE 5.6 EVALUATION OF THE RENAL INTEGRITY AT DAY 14.....	162
FIGURE 5.7 CORRELATION OF SERUM BIOMARKERS WITH HL-SIN AND LUMINAL AREA VALUES.....	163
FIGURE 5.8 EVALUATION OF FIBROSIS AT DAY 14 AFTER CISPLATIN INJURY.....	165
FIGURE 5.9 LOCALIZATION OF GFP AND PKH26 IN LUNGS AND KIDNEYS AT DAY 14.....	167
FIGURE 5.10 EXPERIMENTAL SET-UP OF THE BIODISTRIBUTION STUDY.....	168
FIGURE 5.11 LOCALIZATION OF HUMAN CD133 <sup>+</sup> CELLS IN THE LUNGS 1, 6 AND 24 HOURS AFTER INJECTION.....	169
FIGURE 5.12 LOCALIZATION OF HUMAN CD133 <sup>+</sup> CELLS IN THE KIDNEY 1 HOUR AFTER INJECTION.....	169
FIGURE 5.13 MACROPHAGE INFILTRATION IN THE LUNGS.....	171
FIGURE 5.14 MACROPHAGES INFILTRATION IN THE KIDNEYS IN THE BIODISTRIBUTION STUDY.....	171
FIGURE 5.15 EFFECTS OF THE HUMAN CELLS ON THE PROLIFERATION OF THE HOST EPITHELIUM AT 14 DAYS.....	173
FIGURE 6.1 SCHEMATIC SUMMARY OF THE KEY POINTS IDENTIFIED IN THIS THESIS.....	184
FIGURE 6.2 BIOLUMINESCENCE IMAGING OF HUMAN CD133 <sup>+</sup> AND CD133 <sup>-</sup> CELLS INJECTED INTO SCID MICE AFFECTED BY ADRIAMYCIN-INDUCED CHRONIC KIDNEY INJURY.....	188





## LIST OF TABLES

TABLE 1.1 LIST OF SOME OF THE BIOMARKERS ALTERNATIVE TO CREATININE AND UREA FOR DETECTION OF AKI (BONVENTRE ET AL., 2010; VAIDYA AND BONVENTRE, 2006; VAIDYA ET AL., 2008)	18
TABLE 1.2 OVERVIEW OF THE IN VIVO MODELS USED TO STUDY ACUTE KIDNEY INJURY. ....	39
TABLE 1.3 CLASSIFICATION OF MACROPHAGES SUBTYPES IN REGENERATIVE MEDICINE BASED ON MARKER EXPRESSION. FROM (CAO ET AL., 2015; MURRAY AND WYNN, 2011) .....	43
TABLE 2.1 DENSITIES USED FOR THE HUMAN CELLS WHEN PLATED .....	46
TABLE 2.2 LIST OF PRIMARY ANTIBODIES USED FOR IMMUNOFLUORESCENCE ON CELLS, TISSUES AND RUDIMENTS .....	52
TABLE 2.3 LIST OF SECONDARY ANTIBODIES USED FOR IMMUNOFLUORESCENCE ON CELLS, TISSUES AND RUDIMENTS *NOW THERMO FISHER.....	53
TABLE 2.4 LIST OF ANTIBODIES USED FOR FACS .....	55
TABLE 2.5 OVERVIEW OF ALL THE BIOLOGICAL REPLICATES PER CONDITION. EACH BIOLOGICAL REPLICATE WAS MADE OF AT LEAST 3 TECHNICAL REPLICATES.....	58
TABLE 3.1 LIST OF SAMPLES USED IN THIS THESIS.....	73
TABLE 3.2 SUMMARY OF THE EXPRESSION OF THE SURFACE MARKERS ANALYSED IN THIS STUDY.....	86
TABLE 4.1 DIRECT COMPARISON BETWEEN THE CONVENTIONAL AND THE NOVEL METHOD TO PERFORM THE KIDNEY REAGGREGATION ASSAY (KRA) .....	144
TABLE 5.1 MEAN VALUES OF HL-SIN, SERUM CREATININE, AND SERUM UREA $\pm$ SEM FOR ALL GROUPS AT ALL TIME-POINTS EVALUATED .....	155
TABLE 5.2 MEAN VALUES $\pm$ SEM FOR TIM-1, CYS-C, AND ACR $\pm$ SEM FOR ALL GROUPS AT ALL TIME POINTS. THE ANOVA ONE-WAY STATISTICAL TEST WITH TUKEY <i>POST HOC</i> ANALYSIS WAS APPLIED FOR GROUP TO COMPARE BASELINE VALUES AND VALUES AT DAY 14. ....	160
TABLE 5.3 SUMMARY OF THE THERAPEUTIC EFFECTS EXERTED BY BOTH CELL TYPES (CD133 <sup>+</sup> AND CD133 <sup>-</sup> ) COMPARED TO THE CONTROL GROUP.....	176
TABLE 5.4 COMPARATIVE TABLE OF ALL STUDIES FOUND IN LITERATURE USING RAT CISPLATIN-INDUCED ACUTE KIDNEY INJURY MODELS. ALL STUDIES REPORTED USE SD RATS.....	182



## LIST OF ABBREVIATIONS

6-CF	5(6)-carboxyfluorescein
ACR	Albumin/creatinine ratio
ALDH	Aldehyde dehydrogenase
ANOVA	Analysis of Variance
AKI	Acute Kidney Injury
APC	Allophycocyanin
ATRA	All-Trans-Retinoic-Acid
BC	Bowman 's capsule
BUN	Blood Urea Nitrogen
BW	Body weight
CD	Cluster of differentiation
CKD	Chronic Kidney Disease
CVD	Cardiovascular Disease
DMEM	Dulbecco's Modified Eagle's Medium
DT	Distal Tubule
E	Embryonic day
EGF	Epithelial Growth Factor
EpCam	Epithelial cell adhesion molecule
ESRD	End Stage Renal Disease
EV	Extracellular Vesicles
FACS	Fluorescence Activated Cell Sorting
FITC	Fluorescein isothiocyanate
FSC	Forward Scatter
FSC-A	Forward Scatter - Area
FSC-W	Forward Side Scatter – Width
GBM	Glomerular Basement Membrane
GDNF	Glial cell-line-derived neurotrophic factor 1
GFB	Glomerular Filtration Barrier
GFP	Green Fluorescent protein
GFR	Glomerular Filtration Rate
HL-Sin	Half Life FITC Sinistrin
hK	human Kidney

HPLC	High-performance Liquid Chromatography
IL	Interleukin
IP	Intraperitoneal
IRI	Ischemia/Reperfusion Injury
IV	Intravenous
Kim-1	Kidney injury molecule-1
KRA	Kidney Rudiment Assay
LSFM	Light-Sheet Fluorescence Microscope
MACS	Magnetic-Activated Cell Sorting
MCP-1	Monocyte chemoattractant protein-1
MIP	Maximum Intensity Projection
MIP-2	Macrophage inflammatory protein-2
MM	Metanephric Mesenchyme
MOI	Multiplicity of infection
MSC	Mesenchymal Stem Cell
NAG	N-acetyl- $\beta$ -glucosaminidase
NCAM1	Neural Cell Adhesion Molecule 1
NGAL	Neutrophil gelatinase-associated lipocalin
p	p-value
Pax2	Paired box gene 2
PBS	Phosphate-buffered saline
PDMS	Polydimethylsiloxane
PD time	Population Doubling time
PE	Phycoerythrin
PDX	Podocalyxin
PNA	Peanut agglutinin lectin
PPAR $\alpha$	Peroxisome proliferator-activated receptor $\alpha$
PT	Proximal tubule
RANTES	Regulated on Activation, Normal T Expressed and Secreted
RCC	Renal Cell Carcinoma
RRT	Renal Replacement Therapies
SCID	Severe Combined Immunodeficiency
SD rats	Sprague Dawley <sup>®</sup> rats
SSC	Side Scatter

SSC-A	Side Scatter-Area
SD	Standard Deviation
SEM	Standard Error of Mean
Six2	Sine Oculis Homeobox Homolog 2
SPIM	Single Plane Illumination Microscope
TIM-1	T-cell immunoglobulin, mucin-1
TNF- $\alpha$	Tumor Necrosis Factor- $\alpha$
UB	Ureteric Bud
VEGF	Vascular endothelial growth factor
VRAD	Vitamin D <sub>3</sub> , All-trans-Retinoic Acid, DMEM/F12
Wt1	Wilms tumor gene 1
WT	Wild type



# 1 INTRODUCTION

## 1.1 KIDNEY STRUCTURE AND MAJOR COMPONENTS

The kidneys are highly complex organs designated for the maintenance of the homeostasis of ions and pH in the body. Moreover, the kidneys have the crucial role of eliminating small molecules, proteins, and toxins from the blood creating urine that will be excreted from the body. Both kidneys account for 0.5% of the total body mass and receive approximately 20% of the cardiac output (Hallgrímsson et al., 2003).

The functional renal units are called **nephrons** (Figure 1.1). It has been estimated that an adult human kidney contains an average of 1 million nephrons (Puelles et al., 2011). Each nephron is a complex tridimensional ensemble constituted by the renal corpuscle and a series of renal tubules. The renal tubule begins at the urinary pole of the Bowman's capsule as the proximal convoluted tubule (PT cells), continues through a hairpin loop, the loop of Henle, and turns into a distal convoluted tubule (DT cells) before reaching the collecting duct (CD). The whole unit counts several types of cells, unique in their properties (Hallgrímsson et al., 2003).

The renal corpuscle consists of the Bowman's capsule, a parietal epithelial layer of cells surrounding the glomerulus that contains the capillary tuft. In the glomerulus, a high-volume, acellular, almost protein-free filtrate of the blood plasma is formed. The blood flows into the glomerulus through the afferent arterioles, is filtered through the glomerular filtration barrier (GFB) and drains through the efferent arteriole. The GFB is a complex structure based on the cross-talk of three crucial components: endothelial cells, podocytes, and the glomerular basement membrane (GBM) (Haraldsson et al., 2008) (Figure 1.1).

The glomerular **endothelial cells** are flattened and extensively fenestrated, without a diaphragm. These features allow a high permeability of water and small

solutes in the glomerulus. The fenestrae represent circa 20% of the endothelial surface and would be big enough (60nm) to let proteins such as albumin (3.6 nm) pass through. However, the endothelial cell is coated on its luminal side with an endothelial cell surface layer (ESL), made of negatively charged glycoproteins and glycosaminoglycans (GAGs), which accumulate within the fenestrae making them less narrow. Therefore, the endothelial cells represent the first layer of the high permselectivity of the glomerular wall, defined as the selective permeation of certain ionic species through the wall (Haraldsson et al., 2008; Jarad and Miner, 2009; Scott and Quaggin, 2015).

The **podocytes** are visceral epithelial cells that face the primary urine in the Bowman's space and embrace the capillary coils. They are characterized by a quite large and arborized cell body from which foot processes protrude, interdigitating cytoplasmic protrusions separated from each other by slit diaphragm (SD) (Brinkkoetter et al., 2013). Nephrin, podocin, and podocalyxin are instrumental in maintaining the structural integrity of the SD and participate in impeding the high-molecular-weight plasma components to end up in the urine (Scott and Quaggin, 2015). Podocytes participate in the secretion of proteins found in the GBM and ensure the survival of endothelial cells, secreting the vascular endothelial growth factor-A (VEGF-A) and angiopoietin-1 (Haraldsson et al., 2008).

Both podocytes and endothelial cells secrete essential components of the **GBM**. The GBM is twice as thick as any other basement membrane in the body (Hallgrímsson et al., 2003). The GBM is a fibrous mix of IV collagen, laminin  $\beta$ 2, entactin, together with glycoproteins and sulphated proteoglycans. Proteoglycans consist of protein cores with attached heparan sulfate and GAGs side chains, contributing to the negative charge of the basement membrane. The network of fibres alone, however, is not sufficient for the permselectivity of the glomerulus (Camici, 2005).

In its entirety, the GFB prevents the passage of exogenous and endogenous macromolecules from the blood into the urine based on their size, shape and charge (Brinkkoetter et al., 2013). Water and small solutes (urea, glucose, amino acids, and mineral ions) can pass undisturbed through the GFB. However, circulating cells (erythrocytes) and high-molecular-weight plasma proteins and anionic



macromolecules, such as albumin are retained in the glomerular capillaries. Generally speaking, the more positive the molecular charge of the solute, the more it will penetrate through the GFB. In fact, in diseases where the GFB is compromised, the primary outcome is represented by the presence of bulk proteins in the urine, a condition called proteinuria or, when albumin is measured, albuminuria (Brinkkoetter et al., 2013).

The glomerular filtration is determined by the equilibrium between the hydrostatic pressure (HP) that drives the fluids out of the capillary lumen, led by the blood pressure and the oncotic pressure (OP), exerted by colloids in the plasma, such as proteins, which pull fluids inside the capillaries. The net filtration pressure (NFP) is equal to the difference between HP and OP and it is optimal to filter 125 ml/min/1.73 m<sup>2</sup> of glomerular fluid from the glomerular capillaries into the Bowman's capsule (glomerular filtration rate, GFR). Autoregulatory pathways are activated when one of the pressures above changes to maintain the GFR constant, mainly because reabsorption of water and solutes depends on how quickly the filtrate flows through the tubules (Hallgrímsson et al., 2003).

The GFR highly depends on age, sex and body size as well as on the physiological status that might affect the nephrons (e.g. pregnancy, protein intake). The GFR is indirectly calculated through the clearance of a filtration marker in the plasma or urine. The ideal filtration marker would be freely filtered across the GBM, would not be bound by plasma proteins and would not be reabsorbed or secreted by the proximal tubule cells. Also, the marker should be physiologically inert (Stevens and Levey, 2005). Inulin, a 5200 Da protein, is an inert uncharged polymer of fructose and represents the best candidate. However, the methods available to measure urinary or plasma clearance of inulin are invasive for the patients, require a bolus administration of the marker and necessitate accurate sampling times. Moreover, inulin is challenging to handle and expensive, so it is not the best option for the clinical practice (Lopez-Giacoman and Madero, 2015). Therefore, the GFR is estimated from prediction equations that exploit endogenous markers, such as creatinine and Cystatin C (Stevens and Levey, 2009). This topic will be further discussed on page 13.

Once in the Bowman's capsule space, the filtrate drains to the urinary pole and enters the tubule. From the proximal tubular cells to the collecting ducts, there is a continuum of specialized cells with a unique range of ion exchangers, cotransporters and channels that will reabsorb all organic nutrients and water. Each cell type has different absorptive capabilities, with the PTC being the most active in reabsorption. The most abundant cation in the filtrate is the  $\text{Na}^+$ . Proximal tubule cells reabsorb the  $\text{Na}^+$  from the luminal filtrate, alongside with water. The first level of transcellular absorption of  $\text{Na}^+$  occurs actively through the  $\text{Na}^+-\text{K}^+$  ATPase. This pump creates a concentration gradient that drives the  $\text{Na}^+$  entry through the apical membrane. Organic nutrients, such as glucose, amino acids, vitamins and most cations are then actively co-transported with the  $\text{Na}^+$ . Water is reabsorbed by osmosis through aquaporins. Finally, negatively charged ions are passively reabsorbed coupled with the active gradient of  $\text{Na}^+$ .

Finally, the kidney is one of the master regulators of the arterial blood pressure, through the activation of the Renin-Angiotensin-Aldosterone System (RAAS). The cascade starts with the release of the enzyme Renin in the intravascular space by juxtaglomerular cells located close to the afferent arterioles. The secretion of renin is positively regulated by the decrease of blood pressure, and by the levels of sodium chloride to the thick ascending limb of the loop of Henle and by the activation of the sympathetic nervous system. Renin is the key enzyme that initiates the cascade formation of Angiotensin II (ANG II). ANG II is responsible for vasoconstriction, through the contraction of the mesangial cells and, therefore, for a reduction in the GFR. It also stimulates the reabsorption of water and  $\text{NaCl}$  in the proximal tubule cells, and the production of the hormone aldosterone in the adrenal glands which stimulate water and  $\text{NaCl}$  reabsorption in the distal tubule cells (Harrison-Bernard, 2009).

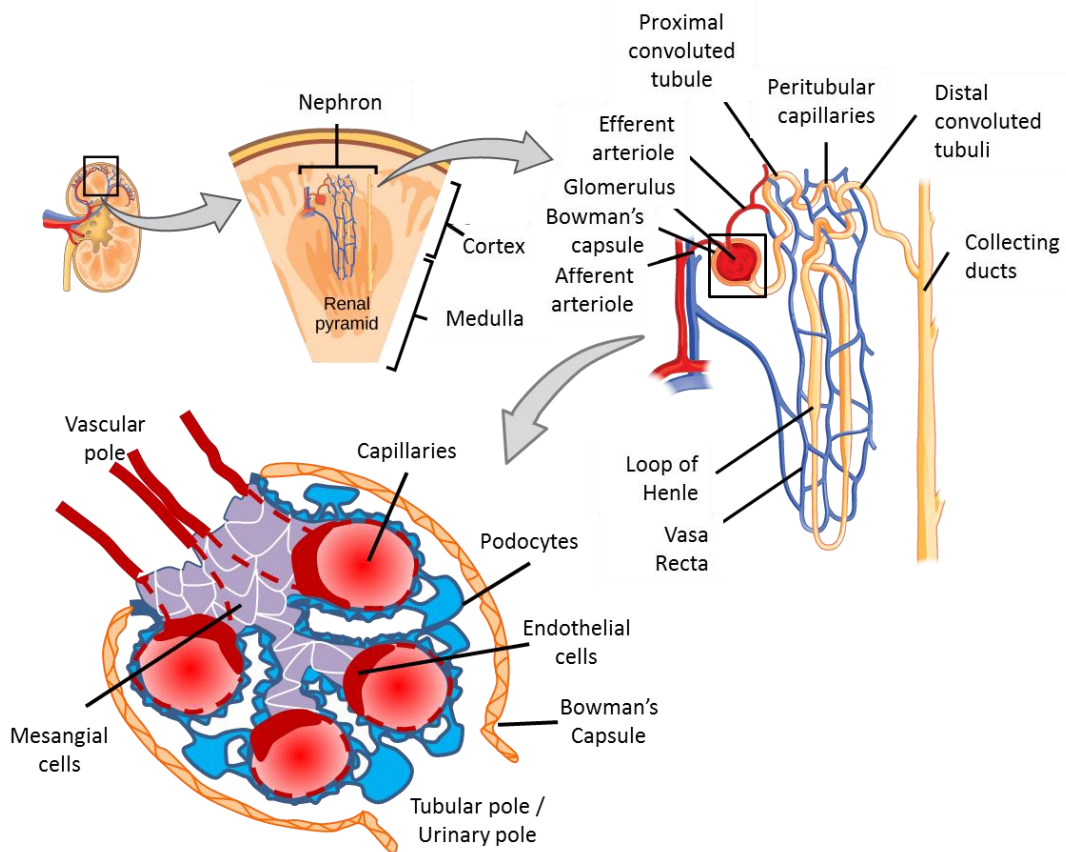


**FIGURE 1.1 SCHEMATIC REPRESENTATION OF THE STRUCTURE OF THE KIDNEY, NEPHRON AND GLOMERULUS**

The kidney is made of thousands of functional units, the nephrons. Each nephron is composed of a series of convoluted tubuli and the glomerulus. Within the glomerulus, the blood gets filtered and the waste, toxins, and ions end up in the urine. Within the tubule, the urine gets concentrated, and relevant nutrients are picked up by tubular cells. Finally, the urine reach the collecting ducts that end up in the ureter. The image was adapted from "The Kidneys and Osmoregulatory Organs" Source: Boundless. "Kidney Structure." Boundless Biology. Boundless, OpenStax College.

### 1.1.1 RENAL DEVELOPMENT: AN OVERVIEW

The mature mammalian kidney, the metanephros, originates from the intermediate mesoderm (IM). From the IM, the Wolffian duct (WD) gives rise to the ureteric bud (UB) and the metanephric mesenchyme (MM). The UB forms the collecting ducts, whereas the MM the nephrons. The two populations secrete reciprocal inductive signals so that the ureteric bud sprouts from the caudal portion of the Wolffian ducts into the metanephric mesenchyme (E10.5 – Figure 1.2 A) (Reidy and Rosenblum, 2009; Vize, 2003). In turn, the cells of the MM send signals to the UB to regulate its invasion and branching in the MM. A subset of the MM cells, the cap

mesenchyme, condensates around the tip of the ureteric bud (Figure 1.2B). Studies in mouse embryos have shown that this population expresses some transcription factors necessary for nephrogenesis (reviewed in (Vainio and Lin, 2002), including *Six2*, *Pax2*, and *Wt1*. *Pax2* (paired box gene 2) is expressed by both the ureteric bud and early MM condensate. *Wt1* (Wilms tumor gene 1) and *Six2* (Sine Oculis Homeobox Homolog 2) are required for nephron formation and prevent apoptosis in MM during growth. Notably, *Six2* defines the cap mesenchyme as multipotent progenitor population. From E11.5, the ureteric bud starts to branch and the cap mesenchyme population undergoes a mesenchymal-to-epithelial transition to give rise to the nephron by forming renal vesicles (Figure 1.2C), comma-shaped bodies (Figure 1.2D) and S-shaped bodies (Figure 1.2E) and, ultimately, glomeruli (Figure 1.2F) (Rak-Raszewska et al., 2015; Vainio and Lin, 2002; Vize, 2003).

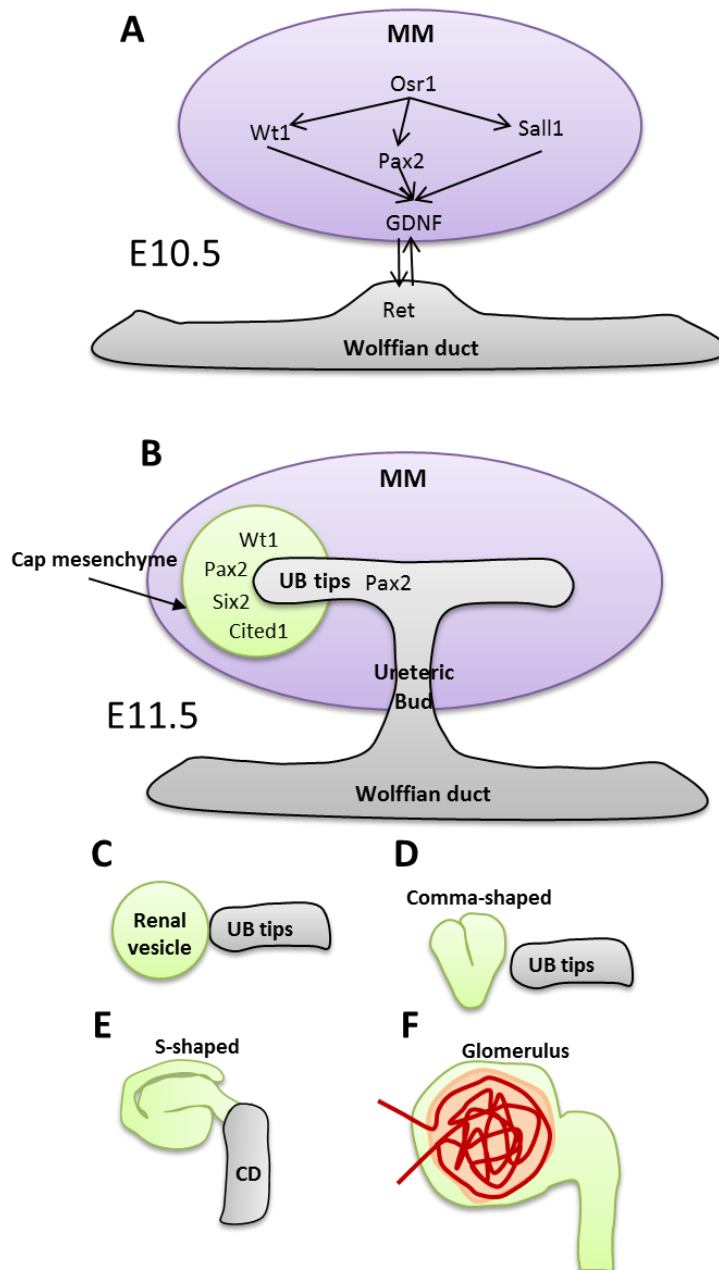


**FIGURE 1.2 SCHEMATIC REPRESENTATION OF THE RENAL DEVELOPMENT FROM E10.5 TO THE FORMATION OF THE NEPHRON**

Adapted from (Rak-Raszewska et al., 2015; Vainio and Lin, 2002). In the mouse, at E10.5, the outgrowth of the UB from the Wolffian duct is orchestrated by essential developmental genes, such as Osr1, Wt1, Pax2, and Sall1. As a result, there is an upregulation of the GDNF production in the MM. GDNF binds the receptor Ret and induces budding of the ureteric bud. (B) After the invasion into the MM, the UB branches following induction from several growth factors, one of which is GDNF. The MM condenses around the ureteric tip. Pax2 is expressed in both components, whereas the expression of Wt1, Six2 and Cited1 is exclusive for the MM. (C) From E11.5, the nephron forms through the sequential shaping of the condensed metanephric mesenchyme: (C) renal vesicles (RV), (D) Comma shaped bodies, (E) S-Shaped bodies, and, finally, (F) the glomerulus.

### **1.1.2 POSTNATAL DEVELOPMENT OF THE KIDNEY**

In an adult kidney, the number of nephrons is stable for the whole lifespan, and it is determined during the gestation period. Therefore, any episode happening during the early steps of development will have tremendous consequences for the individual. For example, preterm infants (born before the 37<sup>th</sup> week of gestation) born with a lower number of nephrons, have a higher risk of developing CKD in their life (Fanos et al., 2015). The functionality of the nephron is achieved by the 32<sup>nd</sup> gestational week with nearly 1 million nephrons, but it reaches the adult levels by two years of age (Sulemanji and Vakili, 2013). As opposed to rodents where nephrogenesis continues until the second week after birth, in humans, nephrogenesis ceases before the 36<sup>th</sup> week of gestation. At birth, the cortex is already mature. However, the glomeruli occupy a higher volume of the cortex in the first two months after birth (18%) compared to adulthood (8.6%). During the first years after birth, the nephron grows, and the tubule elongate. The dimensions of the kidney will grow during childhood and adolescence, reaching a size of about 12 cm in the adult, but the functionality and anatomically maturation is reached during the first year of age (Cukuranovic, 2005; Marchal et al., 1986). However, which cells contribute to the growth of the glomerulus or tubular elongation is not completely understood.

## **1.2 ACUTE KIDNEY INJURY**

Acute kidney injury (AKI) is defined as a rapid decline in the GFR (Edelstein, 2008). It refers to a complex condition that encloses different clinical manifestations ranging from an increase in serum creatinine levels to renal failure. Several risk factors can play a role in the development of AKI, which in turn might lead to increased mortality. As an example, 30% of patients who undergo cardiac surgery are affected by postoperative AKI that increases their mortality risk after the surgery (Ricci et al., 2008; Ricci et al., 2011).

Before 2004, a clear consensus on the definition of AKI was missing, making direct comparisons between studies problematic. As a matter of fact, AKI has been reported to have an incidence between 1% and 25% of intensive care unit (ICU) patients and to have a mortality rate ranging from 15 to 80% (Chawla and Kimmel, 2012; Singbartl and

Kellum, 2012). The RIFLE criteria were therefore introduced to facilitate and uniform a clinical diagnosis of AKI. They provide a list of severity classes, namely Risk, Injury and Failure and, consequently, the possible outcomes, Loss, and ESRD. The assessment of those criteria is based on two parameters: change in blood creatinine levels and GFR from baseline and the urine output per kilogram of body weight in a set period (Ricci et al., 2011). The RIFLE criteria were applied to a cohort of critically ill patients, and the results revealed that the criteria are unambiguous and able to distinguish between functional (vasoconstriction) and structural (acute tubular necrosis) renal dysfunction (Van Biesen et al., 2006). However, several limitations of this model were raised, mostly about the use of serum creatinine or urine output to infer the extent of the tubular injury. Another major drawback of the RIFLE criteria is represented by the necessity to benchmark the creatinine or GFR values against the baseline values, in some cases not available. Even if there are several methods to retrospectively estimate serum creatinine and GFR, none of them appears to be accurate (Ricci et al., 2008; Ricci et al., 2011).

In 2007, the RIFLE criteria were refined by the AKI Network and named AKIN criteria. Besides a change in the name of the risk categories (now divided in stages, from 1 to 3), a subtle, yet important note was added: an absolute change in creatinine of minimum 0.3 mg/dl within 48 hours is sufficient to assign the patient to the first stage. This cut-off was found in previous studies as associated with a higher mortality risk in patients after cardiac surgery (Lassnigg et al., 2004). Also, the two outcome categories have been eliminated; patients in need of a replacement therapy are grouped in stage three, regardless of the creatinine levels or urine output. Those improvements, however, did not change the sensitivity, predictive accuracy, and specificity of the classification of patients with AKI (Ricci et al., 2008; Ricci et al., 2011).

In 2012, the KDIGO (Kidney Disease Improving Global Outcomes) guidelines were published giving precise recommendations to clinicians about the initial classifications of the patients and the management of AKI depending on the stage the patient is in (2012).

In the past, it was believed that patients surviving from AKI would entirely recover the renal function. However, several pieces of evidence point towards the

bidirectional relationships between acute kidney injury and chronic kidney diseases (CKD). AKI was identified as risk factor for the incidence of CKD; patients who experienced AKI once and fully recovered the renal function were more likely to develop CKD than patients who did not experience AKI (Bucaloiu et al., 2012; Leung et al., 2013). Also, the severity of the injury and the frequency of AKI are essential factors that determine the progression to CKD and ESRD and determine higher mortality rates (Chawla et al., 2011). The duration of the AKI episode, instead, was more linked to long-term mortality rate together with the severity of the insult (Chawla and Kimmel, 2012).

Therefore, the paradigm by which patients with AKI do return to the pre-morbid renal function values might be overrated. The KDIGO guidelines advice the physicians to evaluate patients who experienced AKI 3 months after their discharge to better monitor the recovery, onset, and development of CKD or the worsening of pre-existing CKD (Chawla et al., 2014; Chawla and Kimmel, 2012; 2012; Palevsky, 2012).

### **1.3 CHRONIC KIDNEY DISEASES AND END STAGE RENAL DISEASE**

CKD was defined by the National Kidney Foundation in 2002 as an impairment of the renal function and renal damage. Functionally, the loss of kidney function is characterized by a decrease in the GFR levels to a value lower than  $60 \text{ mL/min/1.73 m}^2$  with or without kidney damage. On the other hand, the renal damage is identified through pathologic abnormalities or increase in urinary sediment and proteinuria for more than three months. Importantly, the CKD has been subcategorized in 5 stages, according to the GFR levels. CKD5 represents the level where the GFR is so low ( $<15 \text{ mL/min/1.73 m}^2$ ) that the renal failure is established.

The stratification of the progression of the disease is essential to identify the window of opportunity for therapeutic intervention to slow down the progression of CKD and reduce complications associated with the outcomes, such as ESRD, cardiovascular risk and, most importantly, life quality and survival. CKD takes a long time to develop, and it is asymptomatic until later stages. However, urinary and serum biomarkers available are a fundamental tool to detect the disease (Fink et al., 2012).



## **1.4 THE END POINT: ALTERNATIVES FOR ESRD PATIENTS**

GFR and albuminuria are two strong independent risk factors for ESRD progression. Once the patient reaches the ESRD, the kidney is unable to perform all physiological tasks and requires an external intervention, in the form of dialysis or renal transplantation, referred as Renal Replacement Therapies (RRT). Both alternatives extend the life expectancy of the patients, but they are also associated with higher costs for the society (Vanholder et al., 2015). It has been estimated that transplantation confers an incremental gain in the life expectancy of 3 to 15 years when compared to dialysis, depending on the waiting list time and donor and recipient-specific factors, such as age at transplantation (Wong et al., 2012). Additionally, RRT-related expenses are even greater in the elderly population, who often present co-morbidities and a higher prevalence of CKD than the general population.

### **1.4.1 TRANSPLANTATION**

Between the two options, transplantation is the most cost-effective choice. However, the waiting lists are getting longer and longer as the number of candidates in need of a transplanted kidney greatly exceeds the number of available kidneys. Figure 1.3 depicts a summary of transplant activity for the UK over the last ten years. More than 2000 patients per year are destined to start dialysis while waiting for a kidney.

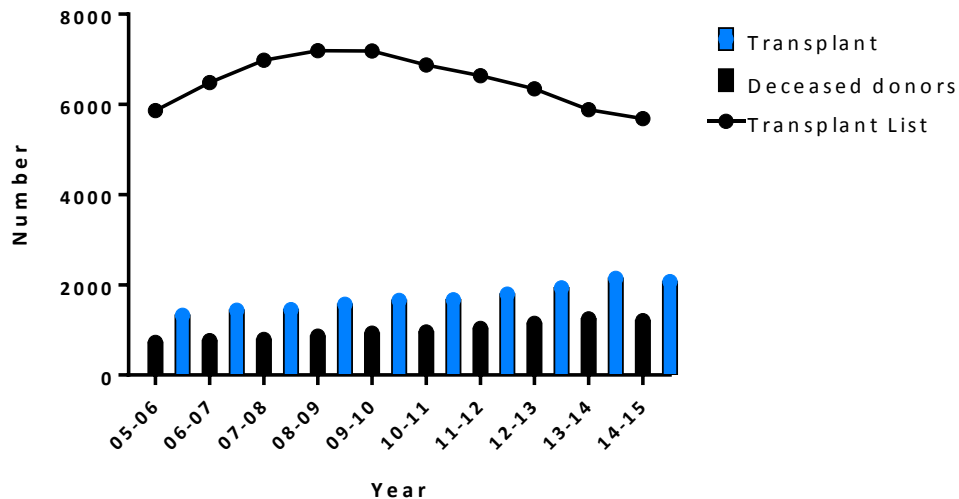


**FIGURE 1.3 OVERVIEW OF THE NUMBER OF PATIENTS ON THE TRANSPLANT LIST AND THE NUMBER OF AVAILABLE KIDNEYS IN THE UK**

The data refer to the last decade from the 1st of April 2005 up to the 31st of March 2015, obtained from the Transplant activity report 2014-2015<sup>1</sup>. The majority of the transplanted organs come from deceased donors. The rest might be supplied by familiars, as live donors.

Another option that is being implemented is to broaden the criteria of the pool of donors, including ‘high risks’ individuals, such as hepatitis C and HIV-positive donors for acceptors with the same disease, or old donors with or without comorbidities (diabetes for example) (Vanholder et al., 2015). Nevertheless, it has still been estimated a gain of life in the acceptors of ‘high risk’ organs over patients on dialysis. A recent study analyzed rejection rates and grafts from subjects transplanted with organs coming from donors with severe AKI compared to subjects who received normal kidneys. They concluded that there were no differences between the two groups in the short-term (1 year) (Heilman et al., 2015). However, the real statistical evidence will be available in few years when the long-term survival and grafts data will be available. In any case, the higher costs associated with the comorbidities of the subjects who received high-risk organs will have to be taken into account (Schold and Segev, 2012).

<sup>1</sup> <https://www.organdonation.nhs.uk/supporting-my-decision/statistics-about-organ-donation/transplant-activity-report/>

### **1.4.2 DIALYSIS**

In case an organ is not available or the patient is not healthy (or well) enough to undergo major surgery, the last option is to start dialysis. In the UK, the NHS provides different options for dialysis, such as hemodialysis (HD) or peritoneal dialysis (PD) in hospitals, satellite units, or in the patients' homes. Home-based options of both HD and PD are more cost-effective than the hospital-based ones (Baboolal et al., 2008). Hemodialysis involves the use of a machine that will clean the blood. It is a process that lasts few hours, and it needs to be done at least three times per week. Peritoneal dialysis uses the peritoneum as a filter: a catheter is inserted into the peritoneal cavity, a cleansing fluid is put in the cavity and after the filtration is over leaves the cavity through the catheter. By the end of the procedure, the fluid will contain all the waste and toxin normally removed by the kidneys. It takes approximately thirty minutes, but it needs to be repeated four times per day. However, it can be done overnight while sleeping. Whichever method the patient is going to prefer, there are serious impairments associated such as impossibility to have a normal working or studying schedule, inability to exercise or go on holiday<sup>2</sup>.

### **1.5 BIOMARKERS OF ACUTE KIDNEY INJURY**

A biomarker is an endogenous biomolecule that infers the disease status of a specific organ. In the kidney, the ideal biomarker would be i) able to solely identify renal damage, and, within the kidney, can pinpoint the site of damage (specificity); ii) it is sensitive, meaning that its levels need to resemble the onset, progression, and recovery from the damage (sensitivity); iii) it can be retrieved through non-invasive sampling or in readily available body fluids; iv) it is conserved in different species, to facilitate the interpretations of therapies in preclinical model. With those features, a good biomarker would help clinicians and researchers to make reasonable decisions on the drug regime to assign or to identify the risk/benefits ratio in preclinical models of renal injury (Bonventre et al., 2010).

Serum creatinine and Blood Urea Nitrogen (BUN) are commonly used to assess the renal function in preclinical models and patients.

---

<sup>2</sup> <http://www.nhs.uk/Conditions/Dialysis/Pages/Introduction.aspx>

Creatinine is a breakdown product of creatine phosphate, released by the muscles into the plasma at a constant rate. Historically, serum creatinine has been used as a renal marker in clinical settings, simply because it is freely filtered by the glomerulus and it is not reabsorbed. However, it can be secreted at very low levels from the tubuli (Uchino, 2010).

There is an increased awareness of the inappropriateness of serum creatinine to measure renal function for several reasons. Firstly, differences in age, sex, dietary intake, muscle mass, exercise levels do influence serum creatinine excretion. Specifically, muscle mass plays a central role in the creatinine measurements (Heymsfield et al., 1983). Secondly, serum creatinine levels do not reflect early changes in GFR. In fact, it has been estimated that between 10% and 40% of creatinine is cleared by tubular secretion into the urine and it is not accumulated in the blood (Ciarimboli et al., 2012). Lastly, several methods are used to measure serum creatinine: Jaffe method, enzymatic, HPLC. The Jaffe method is based on the reaction of creatinine with picric acid in an alkaline environment that produces a solution that can be measured at 420 nm. However, 20% of the colorimetric reaction outcome is due to noncreatinine chromogens, such as proteins and glucose. Therefore, there is often an overestimation of the creatinine concentrations (Delanghe and Speeckaert, 2011). The enzymatic method is based on the conversion of creatinine and derived metabolites by the enzymes creatininase, creatinase and sarcosine oxidase. Hydrogen peroxide, generated by the reaction, is then measured. HPLC (High-performance Liquid Chromatography) is the gold standard to measure serum creatinine. However, is quite time-consuming mainly due to the deproteinization and preparation of the sample. Nevertheless, HPLC and the enzymatic method gave comparable results in mice and rats (Keppler et al., 2007). The three different methods have different costs and difficulties associated, with the Jaffe method being the simplest and less accurate and the HPLC being the most complicated and precise. Inevitably, the use of the various analytical methods to measure creatinine implies a lack of methodological standardization and the difficulties in comparing the results (Delanghe and Speeckaert, 2011).

In the clinic, the serum creatinine is exploited in estimating GFR (eGFR) through equations. Generally speaking, the following equations require stable levels of creatinine, which is not possible to have in subjects with AKI, making them inaccurate for some categories of patients. Over time, three equations have been developed and used in clinical settings, all with their advantages and drawbacks. They are:

- Cockcroft-Gault equation (1976), estimates 24 hours creatinine clearance, not GFR; the variable 'weight' is part of the equation, without adjusting for body surface area;
- MDRD equation (Modification of Diet in Renal Disease) (1999), estimates the actual GFR by measuring the urinary clearance of iothalamate; age, gender and ethnicity are incorporated into the equation, whereas weight is not since it is adjusted for body surface area; the equation was developed in CKD patients. Therefore, GFR in subjects at normal GFR levels is underestimated;
- CKD-EPI (Chronic Kidney Disease – Epidemiology Collaboration) creatinine equation (2009), different coefficients are used depending on age, sex, ethnicity and creatinine condition, it outperforms the MRDR, but it still overestimates GFR for particular categories (Delanaye and Mariat, 2013).

BUN is the other widely used renal biomarker. It is freely filtered by the glomerulus, but the urea is reabsorbed by other parts of the nephrons. A rise in BUN levels can be observed even in the absence of kidney injury, in cases of volume depletion and an increase of endogenous or exogenous protein load, which lead to the production of urea. It is not specific or sensitive (Bonventre et al., 2010).

Despite all those considerations, both serum creatinine and BUN are still the first choices to evaluate renal function in clinical settings and preclinical models.

## **1.6 NOVEL BIOMARKERS OF ACUTE KIDNEY INJURY**

More sensitive and accurate biomarkers of AKI have been identified and validated in preclinical models and the clinic as alternatives to creatinine and BUN. Some of them, such as neutrophil gelatinase-associated lipocalin (NGAL), kidney injury molecule (Kim-1) and IL18, allow an earlier recognition of tubular damage (from 2 hours for NGAL and Kim-1 to 12 hours for IL18) in the urine that would not translate

into a change in GFR. Table 1.1 offers a summary of some of the emerging renal biomarkers for AKI [reviewed in (Vaidya and Bonventre, 2006) and (Vaidya et al., 2008)]. Cystatin C and Kim-1 will be discussed in more detail.

**Cystatin C** (Cys-C) is a low-molecular-weight protein (13 kDa) positively-charged and constantly excreted by most nucleated cells (Abrahamson et al., 1990). Cys-C is freely filtered by the glomerulus, reabsorbed by Megalin-mediated endocytosis in the tubular epithelial cells and catabolized (Tenstad et al., 1996). Serum Cys-C has been indicated as a suitable endogenous marker of GFR, being able to detect AKI 2 days earlier than serum creatinine (Van Biesen et al., 2006). In fact, in contrast to serum creatinine, serum Cystatin-C is unaffected by other non-GFR determinants, such as age, sex, race and muscle mass or change in diet (Baxmann et al., 2008).

There is increasing evidence that urinary Cys-C can be used as a biomarker to detect AKI. In fact, following a tubular injury, the microvillus surface area of the brush border of the proximal tubular cells is compromised, as well as its reabsorptive capacity (Ferguson et al., 2008). Therefore, Cys-C, reabsorbed by the tubular epithelium in a healthy scenario, accumulates in the urine during tubular impairment. In fact, urinary Cystatin C was found elevated in subjects with tubular injuries and was even predictive of subsequent need for RRT (Conti et al., 2006; Herget-Rosenthal et al., 2004; Uchida and Gotoh, 2002).

**Kidney injury molecule (Kim-1)** also known as T-cell immunoglobulin, mucin-1 (TIM-1) is a type I cell membrane glycoprotein containing an immunoglobulin-like domain and a mucin domain in its extracellular region, identified through analysis of the gene expression of ischemic versus healthy kidney tissue (Ichimura et al., 1998). *In situ* hybridization showed high levels of Kim-1 mRNA in the post-ischemic kidney, and immunohistochemistry showed its colocalization with Vimentin on regenerating proximal tubular epithelial cells (Ichimura et al., 1998). High levels of Kim-1 have been reported in renal cell carcinoma (Han et al., 2005), where tubular epithelial cells become dedifferentiated, and in several nephropathies (reviewed in (Vaidya and Bonventre, 2006)).

Specifically, Kim-1 has been validated in a rat model of ischemia/reperfusion and a rat model of cisplatin-induced acute kidney injury. In the latter, urinary Kim-1 was

detected as early as one day after induction of the damage (7.5 mg/kg), whereas BUN and creatinine were significantly elevated from day three onwards (Vaidya et al., 2006). There is evidence that the ectodomain of Kim-1 is shed from injured proximal tubular cells *in vitro*, mediated by a metalloproteinase-dependent cleavage (Bailly et al., 2002). A further evidence of the release of Kim-1 following tubular injury comes from a study where the soluble Kim-1 was found detectable in individuals with ischemic Acute Tubular Necrosis (ATN) as higher than patients with other forms of renal damage and healthy controls (Han et al., 2002).

Also, Kim-1 was compared with several other biomarkers for acute kidney injury. SD (Sprague Dawley<sup>®</sup>) rats were treated with 1mg/kg of Cisplatin for 1, 3, 5, 7 and 14 days. Kim-1 was the only marker to show sensitivity, marking a significant increase from day five and correlating with the extent of the damage. Alongside, immunohistochemical staining for Kim-1 correlated to the urinary Kim-1 changes. From day 1, it was possible to appreciate an increase in the intensity of the staining and spread in the area stained, starting from the outer stripe of the medulla to the cortex. Of note, glomeruli did not show any staining, corroborating the specificity for tubular injuries (Vinken et al., 2012).

The finding that Kim-1 is not detectable in healthy renal tissues and is sensitive to early changes in tubular injury makes it a suitable non-invasive biomarker to detect AKI.

**TABLE 1.1 LIST OF SOME OF THE BIOMARKERS ALTERNATIVE TO CREATININE AND UREA FOR DETECTION OF AKI (BONVENTRE ET AL., 2010; VAIDYA AND BONVENTRE, 2006; VAIDYA ET AL., 2008)**

<b>Biomarker</b>	<b>Type</b>	<b>Produced by</b>	<b>Advantages</b>	<b>Disadvantages</b>	<b>Correlation with diseases</b>
<b>IL-18 (interleukin-18)</b>	Cytokine	Constitutively expressed by distal tubular epithelium. Observe in endothelium and leukocytes.	Early marker of AKI, independent predictor of poor outcome	Involved in several inflammatory diseases	↑ AKI patients ↑ delayed graft function ↑ IRI/Cisplatin in mice
<b>NGAL (neutrophil gelatinase-associated lipocalin)</b>	Protein	Induced in epithelial cells during inflammation or malignancy.	More sensitive than creatinine. Precedes creatinine by 1-3 days.	Not very specific. Found in other organs.	↑IRI (few hours) mice ↑Cisplatin (three hours) mice
<b>NAG (N-acetyl-β-glucosaminidase)</b>	Enzyme	Renal tubular epithelium	Very sensitive, the amount of NAG shredded in the urine is proportional to the damage	Not very specific. Inhibited by endogenous urea Urinary levels of NAG can be detected in non-AKI related pathologies	↑ nephrotoxins damage ↑ delayed graft function ↑ diabetic nephropathy High levels correlate with poor outcome
<b>Clusterin</b>	Glyco-protein	Dedifferentiated tubular cells after injury. The secreted form is anti-apoptotic and prosurvival	Not very sensitive		↑ cisplatin model (5 days after) ↑ IRI
<b>β<sub>2</sub> microglobulin</b>	Protein	Cell surface of all nucleated cells. Filtered by the glomerulus and reabsorbed by the proximal tubule cells	Very sensitive	Unstable in urine, rapidly degraded in pH<6.	↑ nephrotoxins damage ↑renal transplantation



## **1.7 HUMAN KIDNEY STEM/PROGENITOR CELLS (HKSPCs): CD133<sup>+</sup> CELLS**

Unlike the liver, the kidney does not repair itself after partial ablation. In humans, nephrogenesis is completed at the end of the 36<sup>th</sup> week of gestation. The number of nephrons is determined by the intrauterine environment during the gestation period, and *de novo* formation of nephrons has never been documented (Fanos et al., 2015; Little, 2006). Upon damage induced by ischemia or chemical compounds, the mammalian kidney can replenish cells lost and restore the tubular epithelium (Bonventre, 2003; Toback, 1992). In contrast, when the insult aggravates the glomerular compartment, a substantial loss of glomerular cells leads to progressive scarring and fibrosis and, ultimately, to a permanent loss of renal function.

Several repair mechanisms have been proposed over time, from the recruitment of bone marrow stem cells to the dedifferentiation of resident proximal tubular cells to the involvement of a resident progenitor cell population capable of regenerating the damaged area. Over the last decade, however, there has been an inconclusive debate about whether a true progenitor population exists. Bussolati and colleagues were the first to describe a progenitor population in 2005, selecting CD133 (Prominin-1) as a surface marker (Bussolati et al., 2005). The authors do not clearly indicate the rationale of their choice, but use CD133 since it is expressed by undifferentiated epithelial cells in the intestine. Using this marker, they identified interstitial cells in normal portions of cortical regions of kidneys surgically removed, which accounted for circa 0.8% of the total amount of the freshly isolated cells. Once in culture, CD133<sup>+</sup> progenitor cells showed a high proliferative capacity and could be expanded up to eight/nine passages, consistent with a limited life-span of progenitor cells. The phenotypical analysis showed the absence of hematopoietic markers (CD34, CD45), the presence of mesenchymal markers (CD29, CD73 and CD44) and, most importantly, the expression of Pax2, marker of the metanephric mesenchyme. Moreover, CD133<sup>+</sup> clones could be successfully isolated, cultured and differentiated towards epithelial and endothelial cells, losing the expression of CD133 upon differentiation but retaining the expression of Pax2 (Bussolati et al., 2005). Most importantly, this study investigated the potential of this novel progenitor population to ameliorate a severe compromised immunodeficient (SCID) mouse model of glycerol-induced acute kidney

injury. HLA staining and PKH2 staining were identified in the kidney on cells expressing markers of fully differentiated renal epithelia. The authors explained this co-localization by speculating the engraftment and subsequent differentiation of the CD133<sup>+</sup> into the tubular epithelium (Bussolati et al., 2005).

This study paved the way to further investigations on the existence and the nature of renal progenitor cells as therapeutics for regenerative medicine. The Romagnani group has given the major contribution to unraveling the properties of renal progenitor cells. They showed that cells expressing both CD133 and CD24, defined as Parietal Epithelial Cells (PEC), were identified in the Bowman's capsule (BC) of human kidneys (healthy portions coming from patients with localized renal tumours). Virtually 100% of the glomerular outgrowth was shown to be positive for CD133, CD24, CD106, CD105 and CD44 and negative for proximal and distal tubular markers. Stem cell markers, such as Oct4 and Bmi1 were also expressed by double positive, but not double negative cells (Sagrinati et al., 2006). CD133<sup>+</sup>CD24<sup>+</sup>, but not CD133<sup>-</sup>CD24<sup>-</sup> cells were clonogenic and showed an exceptional plasticity, being able to give rise to tubular epithelial cells, osteoblasts, adipocytes and neural cells. Furthermore, PKH26-labelled double positive cells engrafted and differentiated into the tubules of a mouse model of glycerol-induced acute kidney injury, ameliorated the BUN levels and improved renal structure (Sagrinati et al., 2006).

The PEC lie on the BC as a continuum: from undifferentiated cells at the urinary pole, expressing only CD133<sup>+</sup> and CD24<sup>+</sup> to pre-committed podocytes progenitors, expressing the two markers and podocalyxin (PDX), to fully differentiated podocytes on the vascular pole, expressing only PDX (Figure 1.4). To corroborate the finding that double positive cells are progenitors, CD133<sup>+</sup>CD24<sup>+</sup>PDX<sup>-</sup> were shown to be able to differentiate toward tubular epithelial cells and podocytes upon appropriate stimuli *in vitro*. The counterpart CD133<sup>+</sup>CD24<sup>+</sup>PDX<sup>+</sup>, in contrast, did not differentiate, indicating a predetermined commitment to the podocytic compartment (Ronconi et al., 2009). CD133<sup>+</sup>CD24<sup>+</sup>PDX<sup>-</sup> cells were then injected in a mouse model of Adriamycin-induced chronic kidney injury. As shown by PKH26 staining and HLA staining, the CD133<sup>+</sup>CD24<sup>+</sup>PDX<sup>-</sup> cells were found in the glomeruli (11% *ca.*) and the tubules (8%) after three days from the second injection (Ronconi et al., 2009). Proliferative

CD133<sup>+</sup>CD24<sup>+</sup> cells, but not CD133<sup>+</sup>CD24<sup>+</sup>PDX<sup>-</sup> cells populate crescents in collapsing glomerulopathy and crescentic glomerulonephritis in human biopsies (Smeets et al., 2009). However, it cannot be excluded that fully differentiated podocytes dedifferentiate giving rise to the crescentic lesions, acquiring CD133 and CD24 as markers.

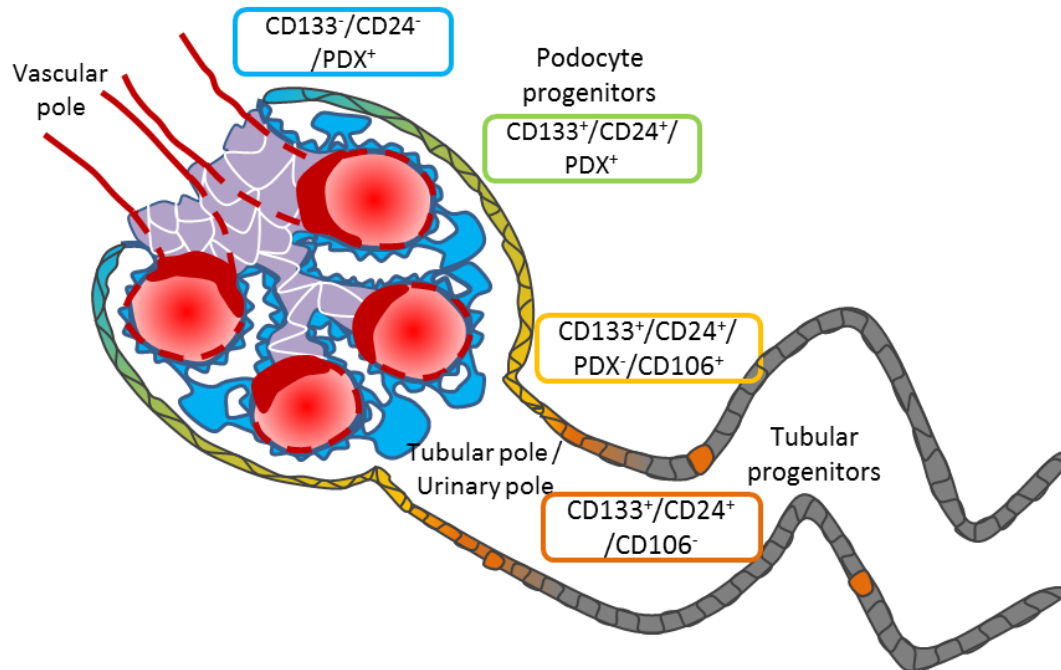


**FIGURE 1.4 SCHEMATIC REPRESENTATION OF THE LOCALIZATION OF THE POPULATIONS OF PUTATIVE PROGENITOR CELLS ON THE BOWMAN'S CAPSULE**

The putative progenitor cells were localized on the BC of the glomerulus: undifferentiated cells, expressing CD133, CD24 and CD106 are confined to the urinary pole of the BC, whereas fully differentiated podocytes expressing PDX, but not CD133 and CD24 are present on the vascular pole. Between these two populations, lies a podocyte-committed cell population with an intermediate phenotype. In the tubuli, a scattered progenitor population was identified, lacking the expression of CD106. The graphic was inspired by (Angelotti et al., 2012)

The researchers went then a step further, comparing the gene expression profile of CD133<sup>+</sup>CD24<sup>+</sup> cells isolated from the glomerulus to CD133<sup>+</sup>CD24<sup>+</sup> cells isolated from the tubuli. VCAM-1 (CD106) was found to be differentially expressed at the urinary pole of the BC. Hence, a new population, expressing CD133<sup>+</sup>CD24<sup>+</sup>CD106<sup>-</sup> was proposed as tubular progenitor population, scattered in the proximal and distal tubule (called 'scattered tubular cells' STCs) (Figure 1.4). Accordingly, CD133<sup>+</sup>CD24<sup>+</sup>CD106<sup>-</sup> cells were able to transdifferentiate *in vivo* into tubular cells (proximal and distal), but not into podocytes. Conversely, CD133<sup>+</sup>CD24<sup>+</sup>CD106<sup>+</sup> cells were able to differentiate

into both, *in vitro* and *in vivo* (Angelotti et al., 2012). This scattered population was observed in the tubuli of patients with ATN and found to express Ki67, Vimentin, and Pax2 (Smeets et al., 2013). The number of proliferative progenitor cells expressing Pax2 was found to correlate positively with the patient outcome (Ye et al., 2011).

Subsequently, the group of Camussi dissected the different parts of the nephron for the presence of CD133<sup>+</sup> cells and focused on the CD133<sup>+</sup> cells found in the inner medulla of the papilla (named pCD133<sup>+</sup> from now on). Marker profile of pCD133<sup>+</sup> cells shows a corresponding pattern to cortical CD133<sup>+</sup> cells (nestin, vimentin, Pax2), but mCD133<sup>+</sup> expressed Six1 and Six2 also. Moreover, Oct4A isoform, involved in stemness, was upregulated in pCD133<sup>+</sup> cells. Progenitor properties were maintained and fostered in hypoxic conditions, so was the expression of Oct4 isoforms (Bussolati et al., 2012). pCD133<sup>+</sup>/CD73<sup>+</sup> cells can produce and release erythropoietin that regulates blood red cells production (Bussolati et al., 2013). mCD133<sup>+</sup> cells were tested for their regenerative potential in a glycerol-induced acute kidney injury model. Biodistribution data at 48 hours post IV injection revealed that CD133<sup>+</sup> cells preferentially homed to the damaged kidneys. Comparatively, small quantities were found in lungs, liver and spleen. Conversely, a larger proportion of the MSCs was found in the same organs. Despite the renal localization, the human CD133<sup>+</sup> cells (identified by HLA staining) were mostly found in the interstitial space in a not proliferative phase, and they did not differentiate in epithelial cells. In the attempt to define the mechanisms of action of the renal CD133 in the AKI model, the cytokine profile from both MSCs and CD133<sup>+</sup> cells was investigated in conditioned medium. Among them, IL15 was found to be exclusively released by the mCD133<sup>+</sup> cells *in vitro*, factor involved in the maintenance of the renal epithelium (Grange et al., 2014a).

## **1.8 CD133 AS A MARKER OF STEM CELLS**

Prominin-1 (CD133) was identified in 1997 on murine neuroepithelial stem cells and named after its location on the protrusion of the apical plasma membrane (Weigmann et al., 1997). In the same year, the human Prominin-1 (CD133) was identified on hematopoietic stem cells from blood and bone marrow and fetal liver cells expressing CD34 (Yin et al., 1997). The gene is located on chromosome 4 in

humans or chromosome 5 in mice, and the protein consists of an extracellular N-domain and five transmembrane domains with two extracellular loops which carry N-linked glycosylation sites and a cytoplasmic C-tail (Shmelkov et al., 2005). It is important to highlight that the human prominin-1 is expressed in many cell types, epithelial and non-epithelial, such as rod photoreceptor cells and bone marrow-derived CD34<sup>+</sup> cells (Corbeil et al., 2010; Fargeas, 2006; Mizrak et al., 2008).

Interestingly, the biological role of CD133/Prominin-1 is still partially elusive. What is known is that CD133 is located on the apical plasma membrane in microdomains, also called lipid rafts, often enriched in cholesterol and sphingolipids. Also, the transmembrane domains are unusually long and might increase the thickness of the membrane to increase interactions with lipids. Therefore, it was suggested that it is implicated in the shaping and organization of the plasma membranes (Bauer et al., 2008; Fargeas, 2006).

Although many cell types express CD133, stem/progenitor cells share a distinct glycosylation pattern on the CD133 protein (Yin et al., 1997). The second extracellular loop, in particular, is subjected to glycosylation. AC133 and 293C2 (Miltenyi Biotech) are the specific monoclonal antibodies able to identify the glycosylated version of CD133 on stem/progenitor cells. CD133 was used to identify endothelial cells, liver stem cells, prostatic epithelial stem cells, pancreatic ductal progenitor cells (Fargeas, 2006).

Karbanova and colleagues derived a different monoclonal antibody (80B258) and showed expression of Prominin-1 in several glandular epithelia in the adult liver, pancreas and uterus (Karbanova et al., 2008). Instead, when using the conventional AC133, the signal is hard to identify or very weak. The authors point out the technical difficulties on using AC133 for immunohistochemistry (IHC). Conventional antigen retrieval procedure and the lipidic environment where CD133 usually resides might not unmask the glycosylated epitopes and make problematic to define its localization. Hence, AC133 might identify a subset of CD133<sup>+</sup> cells, with features commonly ascribed to stem/progenitor cells (Karbanova et al., 2008).

In the adult human pancreas, AC133 was found in the lumen of ductal epithelia together with markers of fully differentiated and specialized cells (CA-II). Similarly to

the kidney, the AC133<sup>+</sup> might identify a facultative progenitor population that undergoes dedifferentiation in the case of injury or regeneration (Lardon et al., 2008). In the normal adult colon, AC133 was expressed on fully differentiated epithelial cells and completely overlapped with EpCam (Epithelial cell adhesion molecule), corroborating its epithelial origin (Shmelkov et al., 2008).

Since Prominin-1 or CD133, but not AC133 is expressed in a wide range of tissues, the activity of its promoter and the relative amount of AC133<sup>+</sup> cells were investigated in colon cancer stem cells during differentiation (Kemper et al., 2010). Upon differentiation, the levels of the transcript and the protein CD133 did not change. Instead, the number of cells that presented the glycosylated epitopes AC133 and 293C decreased, suggesting that the protein might undergo a conformational change in the folding that would mask the glycosylated epitope on the membrane (Kemper et al., 2010).

In the kidney, Prominin-1 was identified in all proximal tubule cells on the apical surface in the study that introduced CD133 for the first time. The antibody used (mAb 13A4), though, was not specifically tested against the glycosylated epitope (Weigmann et al., 1997).

Due to its location, Prominin-1 can be easily released in the extracellular space as membrane vesicles of 50-80 nm, defined prominosomes. In fact, Prominin-1 has been detected in external body fluids in the adult, including saliva, urine, seminal and lacrimal fluid (Bauer et al., 2008; Fargeas, 2006; Florek et al., 2007). Also, to complement its role as stem/progenitor marker, CD133 allowed the isolation of several cancer stem cells from solid tumours, such as breast, colon, liver, lung, melanoma, ovarian, pancreatic and prostate cancer and glioma (Medema, 2013).

To conclude, having a marker with such a broad expression with an unknown biological role is not ideal to isolate progenitor cells or cancer stem cells. However, other markers or different approaches have been employed.

### **1.8.1 PHYSIOLOGICAL ROLE OF CD133**

In the previous paragraph, CD133 was introduced as a ubiquitous marker for stem cells, progenitor cells, and cancer stem cells. However, its specific role remains largely

elusive. Nevertheless, this transmembrane protein has been shown to be involved in several processes, including cell self-renewal, tumorigenesis, metastasis, resistance, metabolism, differentiation, autophagy, apoptosis, and regeneration. In this paragraph, some evidences of the role of CD133 in the context of some of these processes will be briefly presented.

*Tumorigenesis and self-renewal:* CD133<sup>+</sup> cells isolated from colon cancer and gliomas were capable of initiating tumors when transplanted in immunocompromised xenotransplantation models. Importantly, this capacity was maintained when the cells were serially transplanted, highlighting the ability of the CD133<sup>+</sup> cell to self-renew. Both processes were shown to be mediated by the activation of the PI3K/Akt and MAPK pathways (Wang et al., 2010). As a proof that the tumorigenicity and self-renewal depend on the expression of CD133, the silencing of the gene led to a decreased both properties in cancer cells (Neuzil et al., 2007), and the expression of CD133 in HEK293 cells led to an acquisition of both properties (Canis et al., 2013). However, it needs to be mentioned that even the CD133<sup>-</sup> cells from colon cancer were able to form tumours *in vivo*, leading to believe that CD133 is not the exclusive factor that confers this capacity to cells (Shmelkov et al., 2008).

*Metabolism:* as mentioned in the previous paragraph, CD133 is a membrane protein that interacts with cholesterol and sphingolipids on the apical plasma membrane in microdomains, also called lipid rafts. The unusually long transmembrane domains might increase the thickness of the membrane to increase interactions with lipids. Therefore, it was suggested that it is implicated in the shaping and organization of the plasma membranes (Bauer et al., 2008; Fargeas, 2006). Also, CD133 has been reported to be involved in the maintenance of the iron homeostasis through downregulation of transferrin (Bourseau-Guilmain et al., 2011), and of the glucose metabolism. Regarding the latter, the expression and activity levels of the enzyme hexokinase II were found to be lower in CD133<sup>+</sup> hepatocarcinoma cells (Gong et al., 2012), although the relationship between the 2 proteins has not been uncovered yet.

*Apoptosis:* CD133<sup>+</sup> liver cancer cells were shown to be resistant to TRAIL (TGFβ and TNF-related apoptosis-inducing ligand)-induced apoptosis through the high expression of FLIP (FLICE-like inhibitory protein) (Zobalova et al., 2008).

*Regeneration:* CD133<sup>+</sup> cells mainly from bone marrow, cord blood and peripheral blood have been tested in pre-clinical models and are currently used in clinical trials as a regenerative tool. As an example, bone marrow-derived CD133<sup>+</sup> cells proved to be efficacious in a mouse spinal cord injury model, improving angiogenesis, axon growth and functional recovery (Kamei et al., 2013); in a muscle injury rat model, they differentiated into endothelial and myogenic lineages (Shi et al., 2009); in a myocardial infarction model, they improved cardiac function (Ahmadi et al., 2007).

The properties of CD133 have been studied in a wide range of cell types, including primary tumours, opening to the possibility that the involvement of CD133 in a specific mechanism might be cell type-dependant. However, the different pieces of this puzzle certainly point towards a pivotal role of CD133 in a large variety of processes, that are under intense investigation.

## **1.9 OTHER MARKERS USED TO ISOLATE HKSPCs**

The fetal kidney contains pools of stem cells that can be isolated and studied. Since the cells from the MM give rise to the whole nephron during renal development, they have been proposed for regenerative medicine purposes (Pleniceanu et al., 2010; Reidy and Rosenblum, 2009).

Wilms' tumors (WT) are classified as a heterogeneous combination of fully differentiated cells, stromal cells and embryonic cells that closely resemble the MM. Taking advantage of this congruence, Dekel and colleagues investigated by gene expression profile the differences among adult human kidneys (HAK), human fetal kidneys (HFK), Wilms' tumor and renal cell carcinoma (RCC) (Dekel et al., 2006). Genes upregulated in the HFK and WT would represent genes preferentially expressed during development from embryonic renal stem cells. Among the genes, several transcription factors well known to be expressed in the MM were identified (Wt1, Pax2, Lim1, Six1, Eya1, Sall1, Cited1). However, for isolation purposes, surface markers are more convenient. NCAM1 (Neural Cell Adhesion molecule - CD56) emerged as a good candidate for a progenitor population due to its location in the nephrogenic zone (in the condensed mesenchyme and renal vesicles, comma and S-shaped bodies), overlapping with Six2. The expression of NCAM, analysed in conjunction with EpCAM,



marker of epithelial cells, and several transcription factors (Six2, Cited1, Sall1, Wt1, Pax2) led to the conclusion that NCAM1<sup>+</sup> cells represent an MM-derived progenitor population. Interestingly, EpCAM<sup>bright</sup> cells, considered to be the tubular epithelial cells, expressed the largest amount of CD133 and CD24-positive cells, whereas only 20% of NCAM1 positive cells expressed CD133 (Metsuyanin et al., 2009).

In the perspective of a controlled expansion in view of a cell therapy transplantable for the clinic, NCAM1<sup>+</sup> cells were expanded in serum free medium (SFM) or serum-containing medium (SCM). In SFM, NCAM1<sup>+</sup> cells presented a more epithelial profile, upregulating Pax2, Sall1 and E-Cadherin. Next, NCAM1<sup>+</sup> cells were compared to NCAM1<sup>-</sup> cells for clonogenic efficiency, scoring 8% and less than 1%, respectively. The cloning efficiency of NCAM1<sup>+</sup> cells was annulled when a specific antibody-drug conjugate (ADC). Also, CAM (chorioallantoic membrane) grafts with NCAM1<sup>+</sup>, but not with NCAM1<sup>-</sup> cells showed tubular epithelial structures expressing markers of all tubular segments. Finally, the NCAM1<sup>+</sup> cells engrafted into tubuli of *in vivo* in a chronic kidney injury model (5/6 Nephrectomy) and improved renal function, by ameliorating the creatinine clearance (Harari-Steinberg et al., 2013).

The expression of NCAM1 was evaluated also in the adult kidney: approximately 15% of the cells in culture expressed NCAM1. NCAM1<sup>+</sup> cells tick all the boxes for a progenitor/stem population: had a higher clonogenic capacity and proliferation capacity than their counterpart, could differentiate into adipocytes and osteocytes and preferentially form spheroids when cultured in the appropriate environment. Microarray analysis suggests that NCAM1<sup>+</sup> cells undergo first epithelial dedifferentiation and then epithelial-to-mesenchymal transition (EMT), such as downregulation of E-Cadherin and upregulation of Vimentin. Interestingly, they expressed a range of transporters and ion channels proper of proximal tubule cells, suggesting that NCAM1<sup>+</sup> cells descend from the tubular compartment. Even more interestingly, though, both NCAM1<sup>+</sup> and NCAM1<sup>-</sup> cells could ameliorate a glycerol-induced mouse model of acute kidney injury. Following intravenous administration, NCAM1<sup>+</sup> cells were mainly found in the kidneys and lungs, but by 72 hours, the number of human cells in the kidneys decreased (Buzhor et al., 2013).

Also, Tra-1-60, a marker of pluripotent stem cells, was proposed as putative progenitor marker in the kidney, since it was observed in Pax-2 expressing cells in the nephrogenic zone in fetal kidneys. In the adult human kidney, it was identified in scattered cells in the epithelial membrane antigen (EMA) positive cells, representing distal tubules. ATN biopsies were studied and an increase of the Tra-1-60 positive cells, also positive for EMA. Also, these cells were proliferating as indicated by the Ki67 staining and expressed Pax2. However, Tra-1-60 positive cells were not the only cells that expressed Pax2 and proliferated in damaged tubuli (Fesenko et al., 2010). What is still missing is a canonical proof-of-concept that the Tra-1-60<sup>+</sup> cells have a high proliferative, differentiation, and clonogenic potential. Even more importantly, they have not been tested *in vivo*. Hence, definite conclusions cannot be drawn.

### **1.10 OTHER APPROACHES USED TO IDENTIFY HKSPCs**

Different functional approaches have been used to isolate a population with progenitor properties, an alternative to the use of defined surface markers.

Adult stem cells have been identified in other organs for their feature of being quiescent or slow cycling. In fact, quiescent cells would retain labelled thymidine analogues for longer. Hence, such cells are defined “label-retaining cells” (LRCs) (Carlone and Breault, 2012; Fuchs, 2009). This strategy allowed the identification of LRCs in the papilla of the adult kidneys of rats that received BrdU few days after birth. Specifically, the vast majority of BrdU-positive cells were observed in the outer papilla. Three weeks after induction of an ischemic injury, the BrdU signal in the papilla was markedly reduced, suggesting that these cells participated in the regeneration process. In a slightly different experimental set-up, BrdU was administered 36 hours after IRI and chased for 1 hour. Proliferating cells were mainly present in the outer papilla. It was postulated that from the papilla, this putative stem cells population would migrate into the medulla to counteract the cell loss due to ischemia (Oliver et al., 2004). These proliferating papillary cells were also identified using CldU pulse by Humphreys and colleagues. However, in contrast to the study of Oliver et al., LRCs cells in the mouse papilla did not proliferate, nor migrated into the cortex following ischemia/reperfusion (Humphreys et al., 2011). Cells expressing higher levels of

Telomerase were identified in the papilla of mTert-GFP mice. These cells, however, did not increase in number following ischemia-reperfusion, nor migrated towards the outer medulla. Instead, they proliferated following osmotic shock, suggesting a pivotal role in the homeostasis of the papilla (Song et al., 2011).

The enzyme Aldehyde dehydrogenase (ALDH), responsible for aldehydes oxidation, has been used to isolate a wide number of normal and cancer stem cells, due to its involvement in stem cells maintenance, regarding protection against cytotoxic drugs, expansion and differentiation (Ma and Allan, 2011). Lindgren and colleagues used the Aldefluor® assay on freshly isolated tubular renal cells (Lindgren et al., 2011). ALDH<sup>high</sup> cells, accounting for 7% of the total population, when compared to ALDH<sup>low</sup> by microarray, were found to be enriched in anti-apoptotic genes and genes involved in migration and adherence. Instead, the upregulation of HNF1A and HNF1B, transcription factors expressed in fully differentiated renal epithelial cells, in ALDH<sup>low</sup> cells confirmed the tubular origin of the cellular suspension. CD133 (Prominin-1) and CD24, but also Vimentin were found to be upregulated in ALDH<sup>high</sup> cells and their expression in scattered cells in the PT was confirmed by immunohistochemistry. Renal biopsies of patients with ATN in remission were stained as well. Regenerating tubuli showed apical staining of CD133 and basal staining of Vimentin, as will be shown by Smeets and colleagues few years later (Lindgren et al., 2011; Smeets et al., 2013).

Bombelli and colleagues used sphere-forming assays to isolate quiescent cells from primary renal cultures that would retain PKH26 (Bombelli et al., 2013). Cells within the spheres appeared quite heterogeneous, with a PKH26<sup>+</sup> core in the centre. Cells expressing Pax2, epithelial markers, distal and proximal tubular markers as well as Synaptopodin were observed in the spheres. Interestingly, cells isolated from the nephrospheres showed a higher ALDH activity and an upregulation of genes involved in pluripotency, ECM formation, and Notch pathway when compared to primary renal cultures in 2D. The PKH26<sup>high</sup>-sorted cells were the only cells able to create clonal nephrospheres and to differentiate into the epithelial, endothelial and podocytic lineage. In regards to the expression of CD133, both PKH26<sup>high</sup> and PKH26<sup>low</sup> cells have a high expression of CD133, accounting for approximately 70% and 55% respectively. Even 40% of the PKH26<sup>neg</sup> cells expressed CD133. In contrast, only 18% of the primary

renal cultures in 2D expressed CD133. Interestingly, CD24 was not highly expressed in nephrospheres or primary cultures (Bombelli et al., 2013). This finding is in contrast with previous studies outlined at the beginning of this paragraph where *in vivo* and *in vitro* renal progenitor/stem cells express both CD133 and CD24. Those differences were attributed to the different culture conditions used in the study (Romagnani and Remuzzi, 2014).

Buzhor and colleagues applied the same approach using adult kidney epithelial cells. The spheres were not monoclonal but presented a good expression profile regarding nephron progenitor genes. Flow cytometry revealed that the majority of the cells in the spheroids are phenotypically EpCAM<sup>+</sup>CD24<sup>+</sup>CD133<sup>+</sup>CD44<sup>+</sup> and express higher levels of genes involved in cell–cell adhesion/ECM/cell recognition, ion transport, and regulation of cellular component biogenesis, whereas downregulated genes were related to cell growth/mitosis/cell cycle and cell locomotion. Using this system, the group showed that consistent results can be obtained even culturing the cells for a long time before inducing nephrosphere formation (Buzhor et al., 2011).

All the studies presented so far indicate that a progenitor population might exist. However, genetic lineage tracing would be the most powerful tool to help to elucidate the origin of putative progenitor populations in the kidney and the dynamics that lead to the response of the tubular epithelia to injury. Rinkevich and colleagues exploited the so-called ‘rainbow’ mouse to analyse the presence of stem or progenitor cells in kidneys in homeostasis and after injury (Rinkevich et al., 2011). A multicolour (yellow, green, red, blue) Cre-dependent construct in the ROSA26 locus was crossed with an inducible Cre-ER protein under the Actin promoter. Tuning the recombination frequency, this model allows the lineage tracing of single cells labelled with different Cre-dependent reporter constructs regardless of putative markers in the kidney (Rinkevich et al., 2014). By doing so, the group observed that even one single cell can generate clones composed of several cells during the first seven months of the mice life, initiating tubulogenesis. The clone-initiating cells were confined to specific segments of the nephron and did not show any plasticity in the differentiation. The population involved in tubulogenesis appears to be tissue-specific with progenitor characteristics. Upon ischemic and glycerol-induced damage, segment-specific clones

were identified in the kidney cortex, medulla, and papilla. Even when labelled single cells were tested for their potential *in vitro* to generate organoids, they showed a consistent staining for single segment-specific markers. The authors reason this finding with a culture condition that might support all fates, so they did not exclude the possibility that a multipotent population was present. However, the system labels single cells randomly, so fully differentiated cells would be labelled as well, maintaining open the possibility that fully differentiated cells might re-enter the cell cycle in case of tissue maintenance and, most importantly, repair (Rinkevich et al., 2014).

### **1.11 THE OTHER SIDE OF THE SPECTRUM: THE DEDIFFERENTIATION THEORY**

Several studies argue against the existence of a predetermined stem/progenitor population in the adult kidney. In acute kidney injury, it is not uncommon to observe a regenerative process. In this context, several groups advanced the hypothesis that the regeneration is driven by injured fully differentiated proximal tubule cells. Following injury, these cells would dedifferentiate and proliferate to replenish the lost epithelium.

The Bonventre group tackled the question using a combination of DNA-analogues pulse to track cell division in the renal epithelium after IRI. CldU (5-Chloro-2'-deoxyuridine) was injected 24 hours after the ischemia/reperfusion injury (IRI), whereas IdU (5-Iodo-2'-deoxyuridine) was injected at 45 hours after injury, 3 hours before sacrificing the animals. Progenitor cells would display both DNA-analogues in case they are the unique population able to counteract the PTC loss. In contrast, randomly expanding differentiated tubular epithelial cells would have a very low amount of cells labelled with both analogues and a high percentage of single-labelled cells. Indeed, the results showed that replication of PTC after the injury occurs stochastically (Humphreys, 2014; Humphreys et al., 2011).

Genetic approaches provided finer and unequivocal evidence for the theory. Using a more elegant genetic approach, Kusaba and colleagues labelled all fully differentiated proximal tubule cells using a Cre mouse SLC34a1-GFPCreER<sup>T2</sup> crossed with an R26Rt<sup>dTomato/+</sup> mouse. Depending on the dose of tamoxifen used, bigenic mice

would have specifically few or all proximal tubule cells dTomato-labelled (Kusaba et al., 2014). Progenitor cells with a simplified morphology that do not express markers of fully differentiated epithelia would not have been labelled. Therefore, this system was meant to prove whether new epithelial cells after injury originate from fully differentiated PTCs or not. Some significant findings were shown in the study: i) fully differentiated PTCs upon mild or severe injury can undergo one or multiple cell divisions, respectively; ii) injured fully differentiated tubular epithelia do express markers attributed to putative progenitor/stem cells, including CD133, CD24, Pax2, Vimentin and markers of injury, such as Kim-1 (Corbeil et al., 2014; Humphreys, 2014; Kusaba and Humphreys, 2014; Kusaba et al., 2014).

Berger and colleagues reached the same conclusion using a different transgenic mouse, the PEC-rtTA mouse. In this model, all Parietal Epithelial cells and scattered tubular cells (STC) are labelled upon administration of doxycycline. PEC-rtTA cells labelled up to 7 days before the IRI did not expand following injury. Instead, when the PEC-rtTA cells were labelled during the injury, a massive increase of labelled cells was observed (Berger et al., 2014).

Of note, the two antibodies that detect the human glycosylated epitopes CD133\1 and CD133\2 do not cross-react with mouse or rat, so it is difficult to establish whether the CD133<sup>+</sup> population has an equivalent in rodents (Angelotti et al., 2010). Smeets and colleagues provided a link between the rodent and the human studies. They investigated the presence of a scattered CD133<sup>+</sup>CD24<sup>+</sup> population in healthy human kidneys and kidneys from patients with acute kidney injury due to ischaemia–reperfusion injury after transplantation (ATN) (Smeets et al., 2013). The kidneys from ATN patients present complete tubular cross-sections positive for CD24 (and, therefore, CD133) or foci of CD24<sup>+</sup> cells to a larger extent than healthy kidneys. These cells were shown to express also Vimentin, marker of dedifferentiated cells, and Kim-1, a marker of tubular injury. In rats, Vimentin was used to identify the equivalent CD24<sup>+</sup> scattered population. Indeed, following unilateral ureteral obstruction (UUO), more Vimentin-positive cells were identifiable in the cortex. Conversely, kidneys from healthy rats do not show Vimentin or this scattered population even in old age. Both CD24<sup>+</sup> cells in the human kidney and Vimentin<sup>+</sup> cells in the rat kidney show virtually no

brush border, which, after injury, can be attributed to shedding and flattening of the epithelium that is undergoing repair. Altogether, these data indicate the presence of a *de novo* population that participates in the repair of the renal epithelium. Interestingly, the differences in the number of scattered CD24<sup>+</sup> cells and Vimentin<sup>+</sup> cells in healthy human and rat samples were attributed to the possibility that older patients might suffer from nephrosclerosis or mild tubular injury associated with the nephrectomy or adaptive responses to the homeostatic repair (Humphreys, 2014; Smeets et al., 2013).

## **1.12 METHODS USED TO TEST THE POTENTIAL OF HKSPCs**

Once a putative progenitor population has been isolated, regardless of the approach used, it has to be tested for its potential. Usually, differentiation is the first characteristic that is investigated. Also, for the kidney, a kidney reaggregation assay can be used to explore the potential of the cell of interest to integrate into developing embryonic renal structures.

### **1.12.1 DIFFERENTIATION ASSAYS**

The differentiation potential of putative human renal progenitor cells expressing CD133 into intra-lineage and extra-lineage cell types has been investigated by several groups.

Bussolati and colleagues demonstrated the multipotent nature of the CD133<sup>+</sup> population (isolated from cortex and papilla) by differentiating the cells into epithelial and endothelial cells. On the one hand, when cultured in the presence of HGF (hepatocyte growth factor) and FGF4 (Fibroblast growth factor-4), the cells became polarized and expressed markers of proximal and distal tubules (Bussolati et al., 2005). On the other hand, when cultured with VEGF, the cells started expressing endothelial markers. Furthermore, both epithelial and endothelial differentiated cells were able to form tubular structures when embedded in Matrigel, suggesting that the differentiation potential can also be achieved *in vivo* (Bussolati et al., 2005; Bussolati et al., 2012; Ward et al., 2011).

Romagnani and colleagues defined the CD133<sup>+</sup>/CD24<sup>+</sup> population isolated from human kidneys as multipotent after showing that individual clones obtained from the

CD133<sup>+</sup>/CD24<sup>+</sup> population could be differentiated into renal lineages, both tubular and podocytic, and into extra-renal lineages, such as neurogenic, osteogenic and adipogenic cells (Sagrinati et al., 2006). To drive the differentiation of the human progenitor cells into podocytes, CD133<sup>+</sup>/CD24<sup>+</sup> cells were cultured in VRAD (Vitamin D<sub>3</sub>, All-trans-Retinoic Acid, DMEM/F12) medium for seven days (Ronconi et al., 2009). This medium was originally described as the optimum medium to maintain the expression of nephrin which is otherwise lost in a primary culture of podocytes (Takano et al., 2007). Specifically, both Retinoic Acid (All-trans-Retinoic Acid, ATRA), a derivative of Vitamin A, and Vitamin D<sub>3</sub> induce the expression of nephrin by binding to the Retinoic Acid Receptor (RAR) and the Vitamin D Receptor (VDR) (Okamura et al., 2009; Suzuki et al., 2003). Specifically, ATRA has also been shown to induce the formation of foot processes *in vitro* (Vaughan et al., 2005).

### **1.12.2 KIDNEY REAGGREGATION ASSAY**

In the last century, the culture of the forming embryonic kidney *ex vivo* has been used as an experimental approach to investigate its development closely. Since then, the experimental set up has been refined to integrate the progress that the biological sciences were making alongside. In the original culture system, the whole kidney or its metanephric mesenchyme was grown on a surface at the air-medium interface, supported by the embryonic spinal cord, placed underneath the kidney but separated by a filter. The embryonic spinal cord allowed growth and development of the rudiment so that it can be studied *in vitro* (Rak-Raszewska et al., 2015). In 2010, Unbekandt and Davies modified the culture conditions of the assay, simplifying it and opening new avenues which not only enabled the analysis the developmental processes in the embryonic kidney in greater detail but also had considerable implications for tissue engineering and regenerative medicine (Unbekandt and Davies, 2010). In this system, embryonic mouse kidneys at E11.5 post-fertilization were enzymatically dissociated. The single cell suspension was subsequently centrifuged to allow the formation of a pellet that is cultured at the air-medium interface. In this process, nephrogenesis is recapitulated, and both forming nephrons and ureteric buds can be observed. In the first 24 hours of the assay, the pellets are cultured in the presence of ROCK (Rho-associated protein kinase) inhibitor, which enhances survival



of the embryonic kidney cells, thus allowing the formation of epithelial structures that show branching and protein expression typical of ureteric bud in the renal organoids. Also, nephrons display the proper sequence of development, giving rise to renal vesicles, comma-shaped bodies, and S-shaped bodies. The developing nephrons express markers for distal (E-Cadherin) and proximal (megalin) tubules and for glomeruli (Wt1) (Ganeva et al., 2011; Unbekandt and Davies, 2010). One of the strengths of the assay is the ability to investigate the role of single proteins in renal development since siRNA approaches can be incorporated into specifically tailored loss-of-function analysis. For example, reaggregated kidney rudiments containing Wt1-knock-down cells displayed ureteric bud formation, but no nephron formation, suggesting that the genes/proteins in the reaggregated kidney behave as they would *in vivo* (Unbekandt and Davies, 2010). The kidney rudiment assay was further modified with the aim of achieving an accurate cortico-medullary specification and loop of Henle formation (Sebinger et al., 2010).

Through the dissociation and re-aggregation steps, the assay provides a window of opportunity to manipulate the primary embryonic kidney cells; however, it also offers the possibility to introduce exogenous cells and test their engraftment potential in the developing structures of chimeric renal organoids. Stem or progenitor cells can, therefore, be tested to evaluate i) their role and contribution to the recapitulation of nephrogenesis, and ii) their potential to differentiate into specialized cells (Wilm and Murray, 2015). Indeed, a broad range of cell types with different potencies have been mixed with embryonic renal cells at E11.5-E13.5 to test their nephrogenic potential, using ESCs and iPSCs (Takasato et al., 2014; Xia et al., 2013), nephron progenitor cells obtained from ESCs and iPSCs (Takasato et al., 2014; Xia et al., 2013), hMSCs (Kuzma-Kuzniarska et al., 2012), Amniotic Fluid Stem cells (Siegel et al., 2010; Xinaris et al., 2015) and iPSCs-derived podocytes (Song et al., 2012). Ratios and outcomes are summarized in Figure 1.5.

Potency	% of Human cells	Output	Ref.
iPSC undifferentiated ESC	7.5%	Disruption of renal structure formation	Xia et al 2013
	4%	Formation of cysts in the chimera	Takasato et al 2014
N P C	4%	Integration into renal vesicles and nephron progenitors (MM)	Takasato et al 2014
	4%	Integration into the ureteric bud trunk and tip, but not into the metanephric mesenchyme (20-50%)	Xia et al 2013
Human Amniotic Fluid Stem cells	10%	Integration into developing nephrons and ureteric buds	Siegel et al., 2010
	10%	Poor integration into developing structures, improved by genetically modifying the cells to express GDNF	Xiniris et al., 2012, 2015
Human Mesenchymal Stem cells	10%	Disruption of the renal structure formation	Kuzma-Kuzniarska et al., 2012
Human progenitor cells	N/A†	Human cells detected in tubuli	Ward et al., 2011
Fully-differentiated cells	N/A‡	iPSC-derived podocytes expressed Wt1 in developing glomeruli	Song et al., 2013

**FIGURE 1.5 SUMMARY OF STUDIES THAT USED THE KIDNEY REAGGREGATION ASSAY TO VALIDATE THE NEPHROGENIC POTENTIAL OF DIFFERENT POPULATIONS OF HUMAN STEM CELLS, ORDERED BY THEIR POTENCY**

The kidney reaggregation assay was used to test the potential of various human cells of interest to integrate into disaggregated mouse rudiments. The human cells are mixed with the mouse embryonic cells to form a chimeric rudiment in precise ratios, presented in the table as a percentage of human cells per rudiment. The only cells to display a true engraftment were the nephron progenitor cells differentiated from ESCs or iPSCs. † In this paper, the authors injected 1500 CD133+ cells into an E12.5 embryo and cultured the whole organ for four days. The results of this study will be discussed in chapter 4. ‡ In this paper, the authors mechanically disaggregated E13.5-E15.5 kidneys and mixed CFDA-labelled cells into the chimeric rudiments.

Importantly, in the reaggregated rudiments, the developed tubuli displayed the expression of some physiologically-relevant organic anionic and cationic transporters, which were able to selectively uptake their substrates (Lawrence et al., 2015).

One of the major drawbacks of the renal organoid system is the absence of a vascular network, thus preventing the full maturation of podocytes. Xinaris and colleagues circumvented this limitation by pre-treating the rudiment with VEGF and, after implantation under the kidney capsule, by regularly injecting VEGF into the animals. Subsequently, the rudiments developed a Bowman's capsule that contained cells expressing the podocyte marker set, including Synaptopodin, CD2AP, and Nephtrin (Xinaris et al., 2015; Xinaris et al., 2012).

So far, the integration and differentiation potential of CD133<sup>+</sup> cells has only been assessed in an alternative rudiment approach by Ward and colleagues. In their study, the authors did not use the aggregation-disaggregation assay. Instead, they injected a suspension of 1500 cortical or papillar CFDA-labeled CD133<sup>+</sup> cells into the embryonic kidneys and evaluated the integration of the cells into tubular structures after four days in culture. Both cortical and papillar CD133<sup>+</sup> cells were shown to have integrated into developing tubules, whereas the unsorted population of kidney cells occupied the interstitium of the kidneys (Ward et al., 2011).

The reaggregated rudiments are routinely imaged using confocal microscopy. The Light-sheet microscope can offer an alternative for a more gentle imaging method.

### **1.12.3 THE LIGHT SHEET MICROSCOPE: PRINCIPLES AND ADVANTAGES**

The Light sheet fluorescent microscopy (LSFM) has been developed over the past 15 years and demanded the efforts of a multi-disciplinary team due to its complexity. The novelty of the light sheet microscope also called selective plane illumination microscope (SPIM), resides in the presence of an illumination lens positioned orthogonally to the detection lens. This configuration allows the generation of sheets of light from the illumination lens to excite thin sections of the samples. The arrangement eliminates the light emitted from the out-of-focus areas of the sample, thus reducing the phototoxicity and photobleaching of the specimen. Furthermore, the sample is presented vertically, is moved through the light sheets and can be rotated freely. Hence, multiview imaging of live samples is possible (Reynaud et al., 2015).

In the SPIM, a single exposure of milliseconds is enough to achieve the optical sectioning of the entire plane, and the image is recorded fast. Conversely, in a conventional laser-scanning confocal microscope, the laser beam needs to travel from one pixel to the other, thus maintaining a longer exposure on the whole sample and increasing the time necessary to acquire the images, which subsequently can lead to phototoxicity and photobleaching of the specimen. It is not surprising, therefore, that the light sheet microscope has been a very appealing tool for biologists aiming to image over days the developmental processes in *Caenorhabditis elegans*, zebrafish or *Drosophila* (Ebeling and Jorgensen, 2013).

This technology enables a long-term gentle imaging of three-dimensional organoids; therefore, it might be a powerful tool to study the behaviour of progenitor/stem cell populations into a three-dimensional environment as it is the reaggregation assay described in the past paragraph.

### **1.13 IN VIVO MODELS OF ACUTE KIDNEY INJURY**

Several models have been developed to study the onset of renal damage and to test pharmacological interventions to treat renal diseases. As far as AKI is concerned, the most used *in vivo* models can be categorized in toxic AKI, where the insult is represented by a nephrotoxin (Cisplatin, Gentamycin, Folic Acid), ischemic AKI, where the blood supply to the kidney is interrupted for a short period of time, and sepsis, where the renal damage is due to a massive inflammatory response, induced by a surgical procedure or injection of lipopolysaccharide (LPS). All these damages are relatively easy to induce. However, their simplicity often makes the models less clinically significant. For instance, Cisplatin is typically administered to cancer patients regularly. Therefore, the renal damage develops slowly. In animal models, a low dose of nephrotoxin (or a lower clamping time) can increase the variability of the outcome enormously. As a result, a single dose of the toxin, or longer times for clamping is preferred. Table 1.2 summarizes the most common *in vivo* models used to study AKI. The pathophysiology of the cisplatin-induced model of acute kidney injury will be discussed in more detail in the following paragraph (Heyman, 2010; Singh et al., 2012).

**TABLE 1.2 OVERVIEW OF THE IN VIVO MODELS USED TO STUDY ACUTE KIDNEY INJURY.**

Abbreviations: C – cortex; T – tubuli; PT – proximal tubular cells; M – medulla; OM – outer medulla; IM – inner medulla; IMu – intramuscular injection; IP – intraperitoneal injection; IV – intravenous injection; IR – ischemia reperfusion; LPS endotoxemia; CLP – Cecal Ligation and Puncture. Details are taken from (Singh et al., 2012, Heyman et al., 2010)

<b>Model type</b>	<b>Agent inducing the damage</b>	<b>Induction of damage (Route of administration)</b>	<b>Localization of injury</b>	<b>Clinical Relevance</b>
<b>Toxic</b>	Gentamicin	80-100 mg/kg (IP)	C	++
	Cisplatin	M: 20-40 mg/kg R: 7 mg/Kg (IP)	C (S3 - PT)	+++
	Folic Acid	M/R: 250 mg/kg (IV)	C (T)	++
	Glycerol	8-10 ml/Kg (IMu)	C (PT)	+++
<b>Hypoxic</b>	Warm IR	20-45 min clamping	OM	+/-
	Cold IR	20-45 min clamping	IM	++++
<b>Sepsis</b>	LPS	2.5-15 mg/kg (IP)	OM	+/-
	CLP	cecal ligation and puncture	C, M	+++

### 1.13.1 PATHOPHYSIOLOGY OF THE CISPLATIN-INDUCED INJURY

Cisplatin (cis-diamminedichloroplatinum [II]) is a widely used platinum-based chemotherapy drug, highly effective against a wide range of solid tissue tumours (Hanigan and Devarajan, 2003). It has been used alone or as an adjuvant to other procedures, like surgery or radiotherapy (dos Santos et al., 2012). Nephrotoxicity, neurotoxicity, ototoxicity and emetogenicity (capacity to induce vomit) have been reported as side effects. Although nephrotoxicity can be managed through hydration and the use of diuretics, it still represents a dose-limiting factor for the success of the therapy (dos Santos et al., 2012; Wang and Lippard, 2005). Cisplatin-induced AKI is the major presentation of nephrotoxicity with a reduction of 20–40% of their GFR, increased serum BUN and creatinine levels as well as reduced concentrations of serum magnesium and potassium (Kintzel, 2001; Miller et al., 2010; Ries and Klastersky,

1986). Approximately, one-third of patients treated with cisplatin develop a renal impairment within days after the initial dose (Sahni et al., 2009).

Cisplatin gets concentrated in the kidney during the excretion process. The primary targets of cisplatin are the renal proximal tubules, principally the epithelial tubular cells of the S-3 segment (Werner et al. 1995). In fact, it has been reported that the concentration of cisplatin in tubular epithelial cells is five-fold higher than in plasma therefore even nontoxic blood levels of cisplatin might reach toxic levels in kidneys (Ozkok and Edelstein, 2014). Subsequently, glomeruli and distal tubules can be affected.

Ctr1 (high-affinity copper transporter) and OCT2 (organic cation transporter) are the transporters responsible for the uptake of cisplatin in mice, rats and human kidneys (Ciarimboli et al., 2010; Ciarimboli et al., 2005; Ishida et al., 2002; Ozkok and Edelstein, 2014). In fact, the knock-down of Ctr1 in yeast and mouse cells *in vitro* and OCT2 *in vivo* provides protection from the tubular damage induced by cisplatin (Ciarimboli et al., 2005; Ishida et al., 2002).

Once inside the cell, the cisplatin is hydrolysed, and the chloride ions dissociate from the molecule due to low intracellular chloride concentrations (Miller et al., 2010). The resulting positively charged cisplatin binds to a great variety of molecules, like RNA, DNA, and proteins. In the nucleus, it causes intra- and inter-strand cross-linking events, causing disruptions in the replication, transcription, and repair of the DNA (Sanchez-Gonzalez et al., 2011).

In addition to nuclear DNA damage, the positively charged platinum molecules accumulate into the negatively charged mitochondria, generating mitochondrial dysfunctions. It has been reported that Cisplatin inhibits the oxidation of fatty acids, impeding the activity of PPAR- $\alpha$ , resulting in a decreased energy production (Portilla et al., 2002). Also, a drop in the electrochemical membrane potential, the considerable decrease in mitochondrial calcium uptake as well as a disruption of mitochondrial respiratory complexes and function have been reported as consequences of accumulation of cisplatin *in vitro* (Miller et al., 2010).

Apoptosis plays a major role in the histological changes in the renal tissue associated with cisplatin damage, together with necrosis (Pabla and Dong, 2008). *In vitro*, the dose used defines the cut-off between the two types of cell death (Lieberthal et al., 1996). Also, their role in the development of cisplatin-induced AKI has been confirmed *in vivo* (Faubel et al., 2004; Ramesh and Reeves, 2003).

Apoptosis can be activated through different pathways, both caspase-dependent and -independent, including:

- extrinsic pathways, initiated by the activation of Caspase-8 by the death-cell receptors, such as Fas, and TNFR2 (TNF $\alpha$  Receptor), triggered by cisplatin (Kaushal et al., 2001; Pabla and Dong, 2008; Ramesh and Reeves, 2003; Razzaque et al., 1999);
- intrinsic pathways, or mitochondrial pathways; the cisplatin activates Bax, which in turn induces the release of Cytochrome C, prompting a caspase-dependent apoptosis (Wei et al., 2007);
- ER-stress pathway, through activation of caspase-12 (Pabla and Dong, 2008).

### **1.13.2 INFLAMMATION**

Inflammation is one of the major components of the pathophysiology of cisplatin-induced AKI. The impairment of the integrity of the endothelial barrier, caused by nephrotoxic agents, facilitates the migration and infiltration of the immune response cells, initiating early inflammatory cascades (Akcaay et al., 2009; Jang and Rabb, 2015).

T cells have a pivotal role in the pathophysiology of cisplatin injury. An increase of infiltrated T cells was observed in mice within 1 hour from the cisplatin injection, peaked at 12 hours and declined by 24 hours. In the absence of T cells in a nu/nu mouse model, the amelioration of the renal function and histological damage was reported. And, when T cells were restored in nu/nu mice, a higher degree of damage was observed, but not comparable to the wild-type animals. Among the T cells, CD4<sup>+</sup> cells were shown to be more detrimental in the cisplatin pathology, due to their secretion of pro-inflammatory cytokines, such as IL-12 and TNF- $\alpha$  (Yokota et al., 2003). Indeed, CD4-deficient mice produce less TNF- $\alpha$  in the kidney than wild-type and are

more protected from renal damage than the CD8- deficient mice (Liu et al., 2006). However, in the context of cisplatin injury, TNF- $\alpha$  is not only produced by immune cells but also by intrinsic renal cells, such as tubular epithelial cells in response to cisplatin *in vivo* and *in vitro* (Ramesh and Reeves, 2005; Zhang et al., 2007).

TNF- $\alpha$  plays a major role in the development of the cisplatin-induced pathology. Cisplatin can specifically activate caspase 8, which in turn activates TNF- $\alpha$ . In fact, TNF- $\alpha$  protein and mRNA were upregulated following cisplatin administration in serum, kidney tissue, and urine. Inhibition of TNF- $\alpha$  resulted in a downregulation of the IL-1 $\beta$ , RANTES, MIP-2, MCP-1, TGF- $\beta$ , IP-10 transcripts and an amelioration of the renal function (Ramesh and Reeves, 2002, 2004). As a further piece of evidence, caspase-1 deficient mice show a marked decreased secretion of IL-1 $\beta$ , IL-18, and IL-6. Notably, mice with singular KO for this three cytokine were not protected by cisplatin (Faubel et al., 2007). Hence, these cytokines/chemokines represent pro-inflammatory mediators that activate and recruit components of the innate and adaptive immune response from the circulation, leading to exacerbation of the ongoing kidney damage.

On the other hand, anti-inflammatory cytokines are produced by the renal tissue to foster the remodelling of the injured tissue, such as IL-4, IL-13, TGF- $\beta$ , and IL-10. IL-10 is produced by Th-2, Treg cells, DC cells and macrophages. IL-10 KO mice treated with cisplatin show a significant rise in markers of renal function (creatinine and urea) when compared to the wild-type. Interestingly, the infiltration of neutrophils was largely increased in IL-10 KO mice treated with cisplatin suggesting a role as an inhibitor of monocytes and neutrophils recruitment in the renal tissue (Tadagavadi and Reeves, 2010). In the same reports, the authors demonstrate a protective role for DC in the cisplatin nephrotoxicity, partially due to the secretion of IL-10 (Tadagavadi and Reeves, 2010).

Neutrophils are the most abundant type of white blood cells that can be found in the bone marrow, spleen, liver, and lung, under physiological conditions. During acute inflammation, neutrophils are the first type of leukocytes to be attracted by chemotaxis in a damaged organ (Kolaczowska and Kubes, 2013). The role of neutrophils has been studied in cisplatin-induced injury. In mice, the number of neutrophils increased by twenty-four hours of the injection of cisplatin in the blood



and by 48 hours in the kidney. Ablation of the neutrophils through specific antibodies did not induce an improvement in the renal function (Faubel et al., 2007; Tadagavadi et al., 2015). The role of neutrophils in AKI is still controversial.

Macrophages are ‘professional’ phagocytic cells usually presents in healthy tissues. *In vivo*, upon injury or infection, resident tissue macrophages can easily switch phenotypes, depending on the stimuli from the local environment. Pan-macrophages markers include CD68 and F4/80. Once activated, mature macrophages can either exert a more phagocytic and pro-inflammatory role (so called, classically activated M1 macrophages) or an anti-inflammatory and regenerative role (alternatively activated M2 macrophages). Major details are provided in Table 1.3. However, this categorization in M1 and M2 macrophages has been recently challenged, since it is believed that, due to the high diversity of the macrophage phenotypes, it is not possible to have a clear distinction in M1 and M2 only. Instead, it was proposed to refer to macrophages depending on the factors that activate them (Lee et al., 2006; Murray et al., 2014; Murray and Wynn, 2011).

**TABLE 1.3 CLASSIFICATION OF MACROPHAGES SUBTYPES IN REGENERATIVE MEDICINE BASED ON MARKER EXPRESSION. FROM (CAO ET AL., 2015; MURRAY AND WYNN, 2011)**

Name	Markers	Role	Subcategories	Markers	Activated by
<b>M1</b>	MHC-II, CD86	Pro-inflammatory, anti-microbial, anti-tumoral activity	N/A	MHC-II, CD86	LPS or IFN $\gamma$
			M2a	CD206, CD163	IL-4 IL-13
<b>M2</b>	Arg1, CD206	Anti-inflammatory, wound healing	M2b	MHC-II, CD86	immune complexes, LPS, IL-1 $\beta$
			M2c	CD206, CD150	IL-10, TGF $\beta$ , glucocorticoids, apoptotic cells

In the cisplatin nephrotoxicity, a positive correlation between the number of interstitial macrophages and the degree of kidney injury was identified, suggesting that kidney macrophages play a pathogenic role in the progression of the damage.

Cisplatin induces an increase of the infiltrating macrophages as early as 24 hours in mice, as shown by the increase of the F4/80 positive cells and up to at least 72 hours. Inhibitors of the TNF- $\alpha$  and NF- $\kappa$ B reduced the extent of the macrophage infiltration and led to an amelioration of the renal function. Once again, TNF- $\alpha$  has been shown to be the responsible for the macrophages infiltration and, therefore, for the exacerbation of the renal function. Depletion of macrophages, achieved using liposome-encapsulated clodronate (LEC), did not restore completely renal function upon cisplatin damage (Lee et al., 2006).

## **2 MATERIALS AND METHODS**

### **2.1 CELL CULTURE PROCEDURES**

Cell culture procedures were performed under sterile conditions in a Laminar Flow Cabinet safety class II. All surfaces, materials, and mediums in direct or indirect contact with the working area were either sterile or disinfected with 70% ethanol. All solutions were pre-warmed to 37°C before use.

#### **2.1.1 ISOLATION OF HUMAN RENAL CELLS**

The samples employed in this study were identified with hK# (human Kidney #number) and listed on page 73. All biopsy tissues were obtained from anonymised donors, previous informed consent from donor families. The samples were obtained from Mr. Simon Kenny, a renal urologist at the Alder Hey Hospital (Liverpool, UK). hK2, the only healthy kidney in the cohort, was collected from the Royal University Hospital (Liverpool, UK). The study received full approval from the NHSBT (National Health Service Blood and Transfusion), and it is registered in the UK Clinical Research Network Study Portfolio (ID 6403).

Upon reception, the tissue fragments were rinsed few times with cold PBS (Dulbecco's Phosphate Buffered Saline, Sigma, D8537) to remove external blood. Where necessary, fatty tissue was removed using a forceps. The tissue was dissected in a 10 cm dish placed in a bucket of ice; pieces of approximately 2 mm<sup>2</sup> were obtained using a surgical blade (size 22, 0108, Swann-Morton, UK) in sterile conditions. The pieces were digested using Collagenase I (1mg/mL, C0130, Sigma) for 1 hour and 30 minutes at 37°C. During this incubation period, the tubes were agitated by inversion every ten minutes to avoid the deposition of the tissue at the bottom of the tube. At the end of the incubation period, the solution was centrifuged at 1500

rpm for 5 minutes and washed with cold PBS once. The pellet still comprising some fragments was then resuspended in DMEM/F12 containing Deoxyribonuclease I (1%) (DNase I, D4263, Sigma) and incubated for 15 minutes at room temperature. The solution was centrifuged at 1500 rpm for 5 minutes, and the pellet was washed with cold PBS twice. The suspension was passed through a 70 µm and a 40 µm sterile sieve (352350, 352340, respectively, Corning) to obtain a single cell suspension. The pellet was plated in the Human renal progenitor cell (HRPC) medium used for fetal progenitor cells (Price et al., 2007). For the media protocols, please consult page 67. The following day the medium was collected, centrifuged and the pellet was replated in HRPC medium. Fresh HRPC medium was added to the original plates. The medium was changed every two days until the cells reached confluence.

### **2.1.2 ROUTINE CELL CULTURE PROCEDURES**

Cells were grown at 37°C in a humidified incubator supplied with 5% CO<sub>2</sub> and passaged when at 80%/90% confluence. For subculturing, the culture medium was discarded, the cells were firstly washed with PBS, and the cells were detached from the dish by incubating the cells at 37°C with Trypsin/EDTA (Sigma, 59427C) for 2-3 minutes. The detachment was monitored under the inverted microscope to avoid excessive exposure to Trypsin. At the end of the incubation period, double the trypsin volume of culture medium containing FBS was used to neutralize the trypsin. The suspension was collected in a falcon tube and centrifuged at 1500 rpm for 3 minutes. The pellet was resuspended in 1 ml of the fresh medium so that the cells could be counted. For the counting, the cell suspension was diluted 1:1 with Trypan Blue (0.4% T8154, SIGMA) and counted using a TC20™ Automated Cell Counter (Bio-rad). The appropriate number of cells was then plated accordingly or cryopreserved. The day after plating, the medium was replaced to eliminate dead cells and debris and subsequently changed every two days. Cell densities used in this thesis are listed in Table 2.1.

**TABLE 2.1 DENSITIES USED FOR THE HUMAN CELLS WHEN PLATED**

<b>Plate</b>	<b>Number of cells</b>
<b>10 cm dish</b>	<b>200.000 cells</b>

---

<b>6 cm dish</b>	70.000 cells
------------------	--------------

---

### **2.1.3 CRYOPRESERVATION AND RECOVERY OF THE CELLS**

When the cells were at 80%-90% confluence, they were trypsinized and counted using a TC20™ Automated Cell Counter (Biorad) to assess viability and resuspended in freezing medium (12648-010, Life-technologies) at a density of  $10^6$  cells per ml of medium. The cell suspension was stored in cryovials (1 or 2 ml each) and frozen using a freezing container filled with 2-propanol (P/7507/17, Fisher Chemical) stored at -80°C for 24 hours before long-term storage in the liquid nitrogen tank.

When needed, the vial was quickly thawed in a water bath at 37°C and thawed drop-wise in 10 ml of pre-warmed medium. The suspension was centrifuged at 1500 rpm for 3 min, and the supernatant was discarded. The cells were resuspended in the appropriate culture medium and maintained according to Section 2.1.2.

### **2.1.4 MAINTENANCE OF CONDITIONALLY IMMORTALIZED PODOCYTES**

The conditionally immortalized Podocytes (ciPodo) were obtained from Professor Moin Saleem (University of Bristol, UK) (Saleem et al., 2002). The cells were maintained at 33°C for expansion purposes in a dedicated incubator or at 37°C for at least nine days for differentiation purposes. When needed to be trypsinized, the cells were passaged at a ratio 1:3.

### **2.1.5 ISOLATION OF PRIMARY PODOCYTES**

hK6 was used to isolate human podocytes. Upon reception of the sample, the nephrectomy was bluntly dissected using surgical blades under sterile conditions, using a modified procedure described in (Koitabashi et al., 2011). Briefly, the pieces were passed through a metallic 200  $\mu$ m sieve inserted in a 50 ml falcon. The resultant suspension was made of both tubules and glomeruli, was centrifuged and resuspended in fresh medium and passed through a 40  $\mu$ m sieve inserted in a 50 ml falcon. In this step, the glomeruli are withheld in the sieve and the rest of the tissue is collected at the bottom of the tube. The 40  $\mu$ m sieve was then turned upside-down, and the glomeruli collected and plated. Several glomeruli were obtained, either with or without Bowman's capsule. The glomeruli were plated in the primary podocyte medium. Outgrowths were observed after 8 days in culture. Five days after the

outgrowth was observed, the cells were trypsinized and sieved through a 40 µm sieve to remove the glomeruli.

### **2.1.6 POPULATION DOUBLINGS TIME CALCULATIONS**

To calculate the Population Doubling Time, the software Doubling Time was used (<http://www.doubling-time.com/>). The following equation was used to compute the doubling time:

$$T = t \times \frac{\ln 2}{\ln N1 - \ln N0}$$

Where

$T$  = Population Doubling Time

$t$  = time of culture

$N1$  = number of cells at the end of the culture period

$N2$  = number of cells at the beginning of the culture period

At each passage, the number of cells obtained was recorded, and the cells were always plated at the same density, according to Table 2.1.

### **2.1.7 TRANSDUCTION OF hK2 CELLS WITH GFP LENTIVIRAL PARTICLE**

The hK2 cells were labelled using the lentiviral expression vector pHIV-eGFP plasmid (3<sup>rd</sup> generation, Addgene, 21373), kindly prepared in HEK293 cells by Dr. Sofia Pereira or Dr. Arthur Taylor (University of Liverpool). An MOI (multiplicity of infection) of 5 was used to transfect the cells to have >90% labelling efficiency. Typically,  $2 \times 10^5$  cells were plated 8 hours before transfection in a 10 cm dish. Once attached, their medium was replaced by the complete medium containing the appropriate amount of lentiviral particles (depending on the batch of the titration) containing 8 µg/ml of Polybrene (Sigma, H9268). The cells were incubated in these conditions for 16 hours. The medium was then appropriately discarded, and the cells were grown in normal medium.

### **2.1.8 CLONOGENIC ASSAY AND GIEMSA STAINING**

For the clonogenic assay, 100 and 200 sorted hK2 CD133<sup>+</sup> or CD133<sup>-</sup> cells were seeded in a 6 cm dish in presence of fresh medium and conditioned medium (1:1). After three weeks in the incubator, the dishes were washed once with PBS and fixed in

Methanol (100%, Sigma), and stained in a solution of Giemsa (Sigma) in PBS (1:10) for 25 minutes. The dishes were then washed three times in PBS and once in dH<sub>2</sub>O before letting them dry overnight. Once dry, the dishes were observed under the inverted microscope and the number of colonies was recorded.

### **2.1.9 PODOCYTE DIFFERENTIATION ASSAY**

To verify the differentiation potential of the primary human renal cells, the hK2 sorted populations, CD133<sup>+</sup> and CD133<sup>-</sup> cells, were induced to differentiate *in vitro* into podocytes. The protocol used for the differentiation was adapted from (Okamura et al., 2009).

Human CD133<sup>+</sup> and CD133<sup>-</sup> at passage 2 or 3 were seeded at a density of 1x10<sup>4</sup> cells per well in a 6-well plate and left to attach overnight in HRPC medium. The following morning, the medium was replaced with podocyte differentiation medium (VRAD) or control medium. The media were changed every 2 days, and the assay lasted for 7 days in total (2 changes of the medium in total). In some dedicated wells, coverslips were used for immunofluorescence purposes. At day 7, the coverslips were fixed in 4% (v/v) PFA solution and the immunofluorescence was performed according to paragraph 2.3. Three wells per condition per experiment were used for cell cycle analysis. The assay was repeated 2 times successfully, and a number a time without success.

## **2.2 FIXATION AND IMMUNOHISTOCHEMISTRY OF SAMPLES**

Upon collection, part of the renal biopsies was collected in a 50 ml falcon and incubated in 4% PFA (28908, Thermo Scientific) for 2 hours at room temperature, washed with PBS three times, and incubated in 30% Sucrose (w/v) in PBS (S7903, Sigma) overnight or until the tissue sunk to the bottom of the falcon. The tissue was then washed 3 times with PBS and embedded in cryo-embedding solution (Cryomatrix™, 6769006, Thermo Scientific) in cryo-embedding moulds (Polysciences Europe GmbH, Germany). The mould was placed in liquid nitrogen-chilled isopentane (154911, Sigma) until frozen, and stored in -80°C freezer.

6 µm thick sections were cut on a Cryostat HM 505 using a microtome blade (MX35 ULTRA, Thermo Scientific). The sections were placed on microscope slides

Superfrost (10149870, Fisher Scientific,) and stored at -80°C if not immediately stained.

### **2.3 IMMUNOFLUORESCENCE ON CELLS**

The immunofluorescence experiments on cells were performed on 8-wells chamber slides (354108, Corning). The primary renal cells were plated at passage 0 without counting the cells and grown until confluent; the cells at any other passage were seeded at 50,000 cells per well and grown overnight. When appropriate, the cells were washed with PBS once and fixed in 4% PFA in PBS for 10 minutes at room temperature. The cells were then washed and blocked with blocking buffer [2% (w/v) BSA (Bovine Serum Albumin, A1470, Sigma) in PBS, 0.1% (v/v) Triton-X 100 (T-8787, Sigma)] for one hour at room temperature. A list of all antibodies used in this thesis is provided in Table 2.2 and Table 2.3. The primary and secondary antibodies were diluted in blocking buffer. The cells were incubated with primary antibody solution overnight at 4°C in a humidified chamber. The day after, the cells were washed 3 times with PBS and incubated for 2 hours in secondary antibody solutions at room temperature in the dark in a humidified chamber. At the end of the incubation period, the cells were washed with PBS three times and incubated in DAPI (4', 6-diamidino-2-phenylindole, dihydrochloride, D1306, Invitrogen) solution (1:100,000 in PBS or blocking solution) for 10 minutes in the dark. Negative controls were included to test the secondary specificity, by omitting the primary antibodies and replacing it with blocking buffer. After the DAPI staining, the cells were washed with PBS three times; the plastic grid was removed, and the slides were mounted with Fluorogel with Tris buffer (17985-10, EMS) and sealed with nail polish. All fluorescence micrographs of cells shown in chapter 3 were obtained using the epifluorescence Leica DM2500 microscope coupled to a Leica DFC420C camera, except the figures 3.1 and 3.2, taken using a spinning disk confocal microscope CSU-X1 coupled to a digital camera (CMOS, Hamamatsu, C11440).

The immunofluorescence experiment to evaluate the colocalization of CD133 and CD24 in chamber slides was performed using the Antibody Labeling Kit Zenon®Alexa



Fluor® Mouse IgG<sub>1</sub> (ThermoFisher Scientific, Z-25002), according to the manufacturer instructions.

The immunofluorescence experiments on cells in VRAD or control medium shown in chapter 4 were performed on coverslips. Coverslips of the diameter of 13-19 mm were placed in 6 well plates, and the cells were seeded on top. The staining procedure is as explained in the previous paragraph, but the coverslips were mounted on microscope slides.

## **2.4 IMMUNOFLUORESCENCE ON TISSUES**

6 µm thick frozen sections were removed from the -80°C freezer and left for 30 minutes at room temperature to defrost. The slides were washed once in PBS for 5 minutes and the area occupied by the tissue was delineated with a hydrophobic pen (S2002, DAKO). The human tissues were blocked for one hour at room temperature with 0.1% (v/v) Triton-X 100 and 10% (v/v) Goat serum (G9023, Sigma) in PBS; the rat tissues were blocked in 2% (w/v) BSA with 0.1% (v/v) Triton-X 100 in PBS. This blocking solution was used to dilute primary, secondary antibodies and DAPI. After one hour, the sections were incubated with the primary antibody solution and incubated overnight at 4°C in a humidified chamber. The next day, the sections were washed 3 times with PBS and incubated with a secondary antibody solution for two hours at room temperature in the dark in a humidified chamber. Finally, the sections were incubated with DAPI solution for 10 minutes at room temperature in the dark, washed with PBS three times, mounted and sealed using nail polish. Negative controls were included to test the secondary specificity, by omitting the primary antibodies and replacing it with blocking buffer. All fluorescence micrographs of human tissues shown in chapter 3 were obtained using the spinning disk confocal microscope CSU-X1 coupled to a digital camera (CMOS, Hamamatsu, C11440).

**TABLE 2.2 LIST OF PRIMARY ANTIBODIES USED FOR IMMUNOFLUORESCENCE ON CELLS, TISSUES AND RUDIMENTS**

Type	Description	Host Isotype	Dilution	Company Cat. Num.
<b>Primary Antibodies</b>	CD133/1	M IgG <sub>1</sub>	1:50	Miltenyi, 130-090-422
	CD24	M IgG <sub>1</sub>	1:75	Santa Cruz, sc-19585
	CD44	M IgG <sub>2a</sub>	1:200	Abcam, ab6124
	Pax2	Rb	1:200	Abcam, ab37129
	Wt1	M IgG <sub>1</sub>	1:200	Millipore, 05-753
	Vimentin	Gt	1:200	ICN, 647401
	Podocin	Rb	1:200	Abcam, ab50339
	Nephrin	Rb	1:200	Abcam, ab72908
	Megalin	M IgG <sub>1</sub>	1:200	Acris, DM3613P
	Laminin	Rb	1:1000	Sigma, L2020
	Synaptopodin	M IgG <sub>1</sub>	1:2	Acris, BM5086
	GFP	Rb	1:5000	Abcam, ab6556
	CD68	M IgG <sub>1</sub>	1:500	Abcam, ab31630
	CD206	Rb	1:500	Abcam, ab64693
Ki67	Rb	1:500	Abcam, ab15580	

**TABLE 2.3 LIST OF SECONDARY ANTIBODIES USED FOR IMMUNOFLUORESCENCE ON CELLS, TISSUES AND RUDIMENTS** \*NOW THERMO FISHER

Type	Description	Host Isotype	Dilution	Company Cat. Num.
<b>Secondary antibodies</b>	AF® 488nm	Gt α Ms IgG1	1:1000	Life Technologies* A-21121
	AF® 633nm	Gt α Ms IgG1	1:1000	Life Technologies* A-21126
	AF® 488nm	Gt α Ms IgG2a	1:1000	Life Technologies* A-21131
	AF® 594nm	Gt α Rb IgG (H+L)	1:1000	Life Technologies* A-11012
	AF® 488nm	Gt α Rb IgG(H+L)	1:1000	Life Technologies* A-11034
	AF® 594nm	Gt α Gt IgG (H+L)	1:1000	Life Technologies* R37117
	AF® 594nm	Ck α Gt IgG (H+L)	1:1000	Life Technologies* A-11058

## 2.5 FLUORESCENCE ACTIVATED CELL SORTING (FACS)

The human renal cells were analysed by FACS for the expression of several surface markers, listed in Table 2.4. The FACS characterization experiments were performed with single or dual labeling, according to the excitation and emission spectra of the antibody used, using a BD FACSCalibur (BD Biosciences). All steps were performed on ice.  $2 \times 10^5$ - $1 \times 10^6$  cells were aliquoted in a 1.5 ml Eppendorf and washed once with PBS. The cells were then washed once with 1 ml of FACS buffer, composed of 0.1% (w/v) NaAzide (S2002, Sigma) and 1% (w/v) BSA in PBS. After 5 minutes of centrifugation at 500xg, the cells were resuspended in 50 µl of FACS buffer and the appropriate antibodies were added. The samples were incubated, according to the manufacturer instructions, for 10 minutes at 4°C in the dark. At the end of the incubation period, 950µl of FACS buffer were added, and the sample was centrifuged for 5 minutes at 300g. The samples were then resuspended in approximately 1 ml of FACS buffer of in 1% (v/v) FBS in PBS and analysed using the FACSCalibur. When possible, isotype-matched control antibodies were used to confirm the specificity of the antibody used. Unlabeled cells were used as baseline control, to set the threshold of SSC, FSC and the

fluorescence channels (FL) in use. The peak of the unlabeled control during acquisition and analysis was set to be in the  $10^0$ - $10^1$  regions of the FL axis. At least 10,000 events per sample were recorded. The .fcs (flow cytometry standard) files were analysed using Flowing software (Cell Imaging Core, Turku Centre for Biotechnology, Finland) and FlowJoV10 (Ashland, USA).

For the sorting of the cells, the BD FACSAria (BD Biosciences) was used. The cells were labeled with the appropriate antibodies according to the procedure explained in the previous paragraph. The FACS sorting buffer was different: for the actual sorting, the cells were resuspended in PBS containing 1% (v/v) FBS at a concentration of  $5$ - $7.5 \times 10^6$  cells/ml.  $5 \times 10^5$  of unlabeled or labeled cells were provided to set the gates correctly. The sorting was performed by specialized personnel after the discussion of the gatings that were to be applied to the sortings. To increase the viability of the sample after sorting and to increase the recovery of the cells, the tubes were coated with 100% FBS for at least 30 minutes before the sorting. 1 ml of FBS was left in the tube of the sort. In the end, the sorted populations were re-analysed to define the purity of the sorting and, once in the lab, resuspended in growth medium, counted and plated accordingly. The FACSAria was used to sort single cells of  $CD133^+$  or  $CD133^-$  into each well of the 96 well plate (2 plates each cell type).

**TABLE 2.4 LIST OF ANTIBODIES USED FOR FACS**

Description	Fluorescence channel	Dilution	Company Cat. Num.
CD133/1-PE	FL2	1:10	Miltenyi, 130-098-826
CD133/2-APC	FL4	1:10	Miltenyi, 130-090-854
CD24-FITC	FL1	1:10	Miltenyi, 130-099-118
CD45-PerCP	FL3	1:10	Miltenyi, 130-098-145
CD31-PE	FL2	1:5	BD Bioscienc 555446
CD326-FITC	FL1	1:10	Miltenyi, 130-098-115
CD324-APC	FL4	1:10	Miltenyi, 130-099-723
CD13 - FITC	FL1	1:10	Abcam, ab46882
CD90 - FITC	FL1	1:10	Miltenyi, 130-097-930
CD73 - PE	FL2	1:10	Miltenyi, 130-097-943
CD56 - PE	FL2	1:10	Miltenyi, 130-098-137
Tra-1-60 - PE	FL2	1:10	Miltenyi, 130-100-350
Control IgG <sub>1</sub> FITC	FL1	1:10	Miltenyi, 130-098-847
Control IgG <sub>1</sub> PE	FL2	1:10	Miltenyi, 130-098-845
Control IgG <sub>1</sub> APC	FL4	1:10	Miltenyi, 130-098-846
Control IgG <sub>2b</sub> APC	FL4	1:10	Miltenyi, 130-098-890

## 2.6 MAGNETIC ACTIVATED CELL SORTING (MACS)

The MAC sorting of hK2 cells for CD133 was performed by labeling the cells with the CD133/1-PE antibody (Table 2.2) according to the procedure described in the previous paragraph. After labeling, the cells were washed with ice-cold MACS buffer, consisting of 0.5% (w/v) BSA, 2 mM EDTA (E4884, Sigma) in PBS (pH 7.2) and centrifuged at 300g for 5 minutes. The supernatant was aspirated completely, and the pellet was resuspended in 60 µl of MACS buffer and 40 µl of Anti-PE Microbeads (130-048-801, Miltenyi) (double the quantity recommended by the manufacturer). The

suspension was then incubated for 15 minutes at 4°C. At the end of the incubation period, the cells were washed with MACS buffer and centrifuged at 300xg for 5 minutes. The supernatant was aspirated completely, and the cells were resuspended in 500 µl of MACS buffer. In the meantime, an LD column (130-042-901, Miltenyi) was placed on a MidiMACS Separator (130-042-302, Miltenyi) and rinsed twice with 1 ml of MACS buffer. Afterwards, the cellular suspension was applied to the column. The flowthrough was meant to contain the unlabeled fraction of the cells. No pressure was applied to the column while the suspension was passing through. The column was then rinsed with 2 ml of MACS buffer, without applying any pressure onto the column. The flow-through was collected and analysed using the FACSCalibur for the number of PE<sup>+</sup> cells, which represent the CD133<sup>+</sup> cells (FL2). After rinsing twice with MACS buffer, the column was detached from the MACS Separator, 1 ml of MACS buffer was applied to the column, and the plunger was used to obtain the purified labeled fraction. This fraction, which should contain the specifically selected CD133<sup>+</sup> cells, was also analysed using the FACSCalibur for the number of PE<sup>+</sup> cells (CD133<sup>+</sup> cells; FL2).

The MACS efficacy was determined by using the following equation, taken from (Fong et al., 2009):

**EQUATION 1 MACS EFFICACY**

$$E \text{ (efficacy)} = 1 - \frac{\% \text{ CD133 + cells in the 'flow - through' }}{\% \text{ CD133 + cells in the unsorted population}}$$

## **2.7 CELL CYCLE ANALYSIS**

Each well was processed separately; the cells were trypsinized according to the procedure explained in the paragraph 2.1.2, and fixed in 70% (v/v) cold ethanol in water: Specifically, the ethanol was added drop-wise to the cell pellet while vortexing to avoid cell clumping. The cells were kept on ice for 30 minutes and centrifuged at 6000rpm for 3 minutes. The ethanol was aspirated, and the cells were washed twice with PBS. Ribonuclease A (RNase A, Sigma, R6513, 100µg/ml in PBS) solution was firstly added to the pellet and 400 µl of PI solution (Propidium Iodide, P-3566, Molecular Probes, 50µg/ml in PBS) was added to the cell solution. The cell solution was then incubated for 10 minutes at room temperature in the dark, before analysis using the FACSCalibur. At least 10,000 events per sample were recorded. The .fcs (flow

cytometry standard) files were analysed using Flowing software (Cell Imaging Core, Turku Centre for Biotechnology, Finland) and ModFitLT (Verity Software House, USA).

## **2.8 KIDNEY REAGGREGATION ASSAY**

Pregnant CD-1 mice (Charles River, UK) were sacrificed at embryonic day 13.5 by CO<sub>2</sub> exposure, followed by cervical dislocation, and the embryos were isolated. The kidneys were dissected in kidney dissection medium under the Leica MZ16F dissection microscope and collected on ice in a 1.5 ml Eppendorf containing PBS. All following steps were performed in a tissue culture cabinet. The kidneys were washed few times in PBS and transferred in a 15 ml falcon. 3 ml of Trypsin/EDTA were added directly to the kidneys, and the kidneys were incubated for 10 minutes at 37 °C, in the incubator. After five minutes, the suspension was resuspended gently with a micropipette. After the 10 minutes incubation, 10 ml of kidney dissection medium were added to the disaggregated kidneys and the falcon was incubated for 5 minutes in a water bath at 37°C. The suspension was centrifuged at 3000rpm for two minutes and washed once in kidney dissection medium. Finally, the cells were resuspended in 1 ml of kidney reaggregation medium and counted. The volume corresponding to 1x10<sup>5</sup> cells (or 9x10<sup>4</sup> cells in the chimeric reaggregation experiments) was aliquoted in a 0.5 ml Eppendorf and centrifuged at 3000rpm for 2 minutes to obtain a compact pellet. The pellet was then collected with a pipette and placed on a 1.2 µm isopore membrane (RTTP02500, Millipore) positioned on a stainless steel metal grid inside a 6-well plate. Each well contained 1.5-2 ml of kidney reaggregation medium that reached the sample by capillarity. The pellets were cultured for 24 hours in kidney reaggregation medium supplemented with 20µM of Rho-kinase inhibitor (ROCK, Y27632, Calbiochem). On day 1, at least 3 pellets per condition and cell type were fixed in 4% (v/v) PFA in PBS for 15 minutes in the dark and washed twice in PBS. For the other samples, the medium was the replaced with kidney reaggregation medium and cultured at 37°C and 5% CO<sub>2</sub>. Additional 3 pellets per condition and cell type were fixed on day 3 and 6, as described above.

For the chimeric reaggregation experiments, GFP-mouse mesothelial cells (kindly provided by Sumaya Dauleh, University of Liverpool), human GFP-CD133<sup>+</sup> and GFP-

CD133<sup>-</sup> cells were thawed two days before the assay. On the day of the assay, the cells were trypsinized, and 10<sup>4</sup> cells were added to 9x10<sup>4</sup> mouse embryonic cells and centrifuged at 3000rpm for 2 minutes to obtain a compact pellet. The pellets were then processed as explained above. Numbers of biological replicates are indicated in Table 2.5.

**TABLE 2.5 OVERVIEW OF ALL THE BIOLOGICAL REPLICATES PER CONDITION. EACH BIOLOGICAL REPLICATE WAS MADE OF AT LEAST 3 TECHNICAL REPLICATES.**

Replicates \ Samples	Reaggregation control	Positive control	GFP-CD133 <sup>+</sup> cells	GFP-CD133 <sup>-</sup> cells
Biological replicates	6	2	4	3

### 2.8.1 IMMUNOFLUORESCENCE OF KIDNEY REAGGREGATED RUDIMENTS

For the immunofluorescence of the rudiments, the whole membrane was placed on a microscope slide and delineated with an hydrophobic pen. The staining procedure of the rudiments followed the one explained in paragraph 2.4 for the immunofluorescence of the tissues. The GFP cells were imaged without the aid of primary antibodies. The primary and secondary antibodies used in the whole study are listed in Table 2.2 and Table 2.3. The Laser Scanning Microscope 510 Meta (Zeiss) was used to image the samples.

## 2.9 FORMATION OF KIDNEY EMBRYONIC SPHEROIDS

The PDMS (Polydimethylsiloxane) multiwell support was obtained using the Sylgard 184 elastomer kit (761036-5EA, Sigma). The prepolymer was mixed with the curing agent in a 10:1 ratio. The mixture was then thoroughly mixed and degassed for 20 minutes. The mixture was finally poured slowly into a 3 cm dish and cured for an hour at 70°C. The final PDMS disc was approximately 5 mm thick, and the wells were obtained by punching the disc with a biopsy punch (4 mm, BP-40F, Kai Medical). The PDMS multiwell support was autoclaved, the polycarbonate membrane with 1.2 µm pores (RTTP02500, Millipore) was applied at the bottom of the multiwell support as shown in Figure 4.16. Four PDMS supports were made to prevent the sinking of the multiwell in the medium. Once arranged, the dish was filled with 2 ml of Phenol-Free



MEM (51200-046, Thermo Fisher) containing 10% of FBS. Each pellet, processed according to paragraph 2.8, was transferred to each well after centrifugation and grown for six days at 37°C and 5% CO<sub>2</sub>. On day six, the pellets were transferred to a 96 well plate with u-bottom using a Wiretrol®II micropipette (5-000-2100, Drummond Scientific) and fixed for 15 minutes in 4% (v/v) PFA and washed in PBS twice before commencing the immunofluorescence staining, according to the procedure explained in paragraph 2.4 using some of the antibodies listed in Table 2.2. On the day of the imaging, the fixed spheroids were embedded in 1.5% Low-melt Agarose (A9045, Sigma) and 3% gelatin from porcine skin (G9136, Sigma) in a glass Wiretrol®II micropipette for imaging. The images were taken by Dr Marie Held on a Z1 Light-sheet Microscope (Zeiss), using the W Plan-Apochromat 20x/1.0 UV-VIS objective lens.

### **2.9.1 ANIONIC ORGANIC TRANSPORTER FUNCTIONAL ASSAY**

The functional assay was carried out on live spheroids. At day 5 or 6, the spheroids were moved from the multiwell PDMS support to a 96 well plate (U-bottom Costar®, 3367, Corning Incorporated), washed with PBS twice in sterile conditions and incubated with a solution of 1 µM 5(6)-Carboxyfluorescein (6-CF, 21877-1G-F, Sigma), 20 µg/ml of PNA (B-1075, Vector Laboratories) in PBS with or without 2.5 mM of Probenecid (P8761, Sigma) for 1 hour at 25C. The samples not receiving Probenecid were designated as control samples, where eventual functional tubuli would be able to uptake the 6-CF. At the end of the incubation period, the samples were washed with ice-cold PBS for 10 minutes. Both samples received a solution of 10mM Probenecid in PBS and were incubated for 15 min at room temperature in the dark. Finally, the spheroids were washed with PBS three times and images at the Z1 Light-sheet Microscope (Zeiss), using an objective lens W Plan-Apochromat 20x/1.0 UV-VIS.

### **2.9.2 LIVE IMAGING OF THE SPHEROIDS**

For the live imaging, the spheroids were cultured as described previously for 1 day before being embedded in 1.5% Low-melt Agarose (A9045, Sigma,) and 3% gelatin from porcine skin (G9136, Sigma) in a glass Wiretrol®II micropipette for imaging. The embedding medium was proved to be bio-compatible with the growth of the spheroid

over time. Major details about the imaging parameters are provided in the respective figure legends.

## **2.10 CISPLATIN-INDUCED ACUTE KIDNEY INJURY MODEL**

### **2.10.1 ANIMAL GROUPS, BLOOD AND URINE COLLECTION**

All *in vivo* experiments were conducted at the University of Heidelberg in accordance with the German Animal Protection Law and approved by the local authority (Regierungspräsidium Nordbaden, Karlsruhe, Germany, in agreement with EU guideline 2010/63/EU). Zeneida Herrera Perez performed the injections of Cisplatin, FITC-Sinistrin, and cells.

In this study, immunodeficient athymic nude rats (Crl:NIH-Foxn1<sup>nu</sup>, Charles River Laboratories), 8-9 weeks old, were used. All animals were housed in pairs in individually ventilated cages to maintain sterile conditions and acclimated for 1 week before the start of the experiment.

Plasma samples were collected via ophthalmic venous plexus (orbital sinus) in lithium-heparinized tubes (Microvette 500 LH, Sarstedt, Nümbrecht, Germany) using capillaries for blood collection (Micropipettes 20µl, Blaubrand, Wertheim, Germany) by specialized research technicians. The samples were then centrifuged for 5 minutes at 2000xg at 4°C and collected in 1.5 ml tubes (Ratiolab GmbH, Dreieich, Germany) and stored at -20°C until analysis. For urine collection, the animals were housed for 16 hours in individual metabolic cages with free access to water and food. At the end of each collection period, the urine volume was recorded, and the samples were centrifuged (78g, 5 minutes) to remove precipitates. Centrifuged urine aliquots were placed in 2 ml tubes (Eppendorf AG, Hamburg, Germany) and immediately frozen at -20°C until analysed.

Routine blood and urine chemistry parameters, including serum creatinine and urea, were determined using the Cobas c311 analyzer (Roche Diagnostics GmbH, Mannheim, Germany) by the research technicians. Albumin in urine was determined by ELISA and osmolarity was analysed using an osmometer (2020 Multi-Sample Osmometer, Advanced Instruments Inc., Norwood, MA). Tim-1 and Cystatin-C were

measured using the Rat TIM-1/KIM-1/HAVCR Quantikine ELISA kit (MKM100, R&D systems) and Mouse/Rat Cystatin C Quantikine ELISA kit (MSCTC0, MKM100, R&D systems) respectively at the University of Liverpool by myself. The urine was diluted 4 and 400 times, respectively and the assay was performed according to the manufacturer instructions. The plates were analysed for their optical density using the FLUOstar Omega microplate reader (BMG Labtech).

### **2.10.2 TRANSCUTANEOUS ASSESSMENT OF RENAL FUNCTION**

For the transcutaneous measurement of renal function, the marker fluorescein isothiocyanate (FITC)-sinistrin (Fresenius Kabi, Linz, Austria) was used. After its IV administration to the animals, the fluorescence emitted by the marker is measured transcutaneously using a miniaturized device (Mannheim Pharma and Diagnostic, Mannheim, Germany) shown in Figure 2.1.

The core components of the device are:

- Two light-emitting diodes (LEDs), with an emission maximum for FITC at 470 nm (KPTD-3216QBC Kingbright Electric);
- One photodiode that detects the fluorescent light with maximum sensitivity at 525 nm (EPD-525-1-0.9-1; EPIGAP Optoelektronik);
- Removable Lithium polymer rechargeable battery (voltage of 3.7V and capacity of 50 mAh) to supply energy during the measurement.

For this work, the device was configured to perform a measurement each 1757 ms (34.149 samples per minute) with an excitation time of 8 ms.

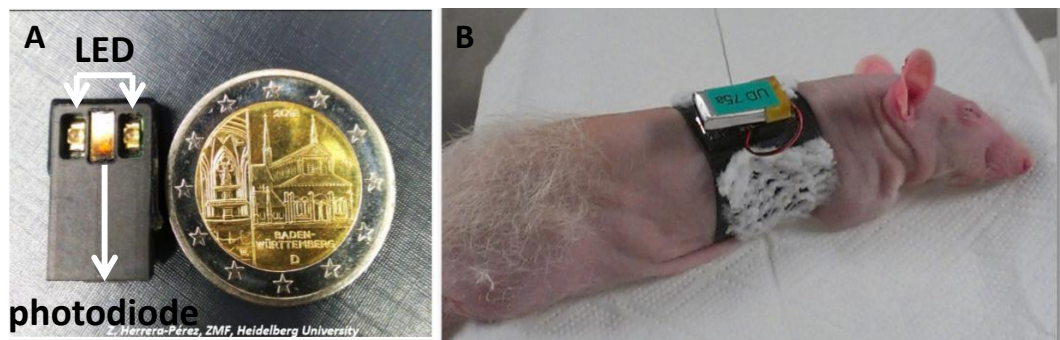


**FIGURE 2.1 MINIATURIZED DEVICE USED TO ASSESS THE RENAL FUNCTION IN RATS.**

(A) A miniaturized device utilized in this study. The LEDs and the photodiode represent the optical component. (B) The device is small enough to fit on the back of the an RNU rat. For the fixation, the animals were under short inhalable anesthesia, to then be awake for the rest of the measurement. Image courtesy of Zeneida Herrera Perez.

The recorded digital data are stored in the internal memory of the device (MSP430f2013 Texas Instruments; maximum storage capacity 256 data points).

On the day of the measurement, the animals were prepared for the measurements by depilating a region of the back of approximately 3 cm<sup>2</sup> if necessary using an electrical shaver for small rodents (Aesculap®). Also, in some cases, a depilation cream (Veet® sensitive skin) was applied to the area for 2 minutes to ensure that all hair was removed. During the fixation of the device, the rats were kept under short inhalable anaesthesia (Isoflurane, Abbott Laboratories, Abbott Park, IL). The device was fixed on the depilated area using a double-sided adhesive patch (Lohmann, Neuwied, Germany). The measurements started when the battery was connected to the device. After the fixation of the device on the back of the animal, a background signal was recorded for about 4 minutes before the injection of FITC-Sinistrin. 5mg/100g body weight (BW) of FITC-Sinistrin was administered into the tail vein. The measurements were carried out for at least 2 hours. In this period, the animals were placed singularly in the cage in the absence of water and free to move. At the end of the measurement, the battery was disconnected, and the device was detached from the animal. Figure 2.2 shows typical curves from a healthy and a cisplatin-injured animal.

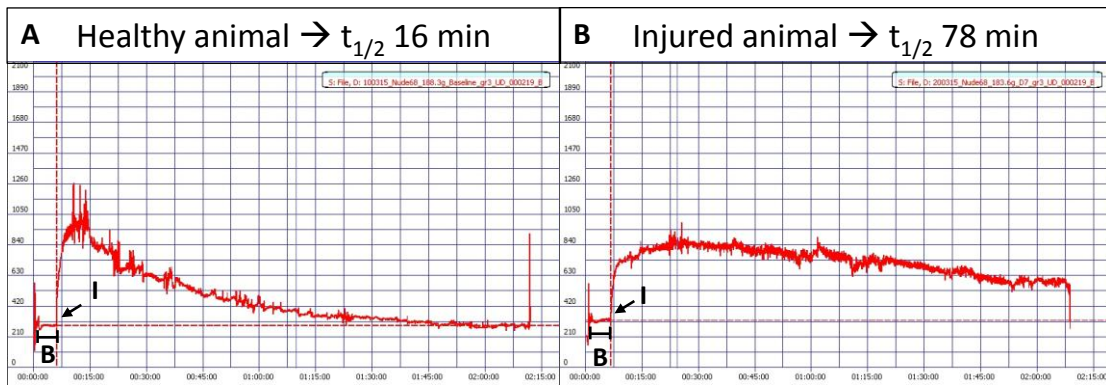


**FIGURE 2.2 REPRESENTATIVE EXCRETION CURVES OF FITC-SINISTRIN IN A HEALTHY (A) AND INJURED (B) RAT.**

The transcutaneous measurements were carried out for two hours. The device was fixed on the back of the animal for 5 minutes, before the injection of the FITC-Sinistrin, to establish the background reading (B, in image A and B). Once the FITC-Sinistrin was injected (I), the fluorescent signal initially increased but then decreased over time, according to the renal function of the animal. The Half-Life of FITC-Sinistrin was calculated from the curves using a specialized software using a three-compartment model.

The data were downloaded to a computer through a USB cable. The half-life ( $t_{1/2}$ ) excretion of the administered FITC-sinistrin was computed using a specifically designed software for the device. By using the software, the data were analysed with a 3-compartment model, which allows calculation of the half-life of the FITC-Sinistrin even from abnormal curves due to renal impairment.

### 2.10.3 TWO-WEEKS STUDY USING CD133<sup>+</sup> AND CD133<sup>-</sup> CELLS

A total of 32 male 8-9 weeks old immunodeficient athymic nude rats (CrI:NIH-Foxn1<sup>fnu</sup>, Charles River Laboratories) were used for the two-weeks study. Renal damage was induced by a bolus injection of Cisplatin (Sigma-Aldrich, Germany) intraperitoneally (IP) with a dose of 7mg/100g of BW under short isoflurane anaesthesia. Cisplatin solution was prepared freshly in sterile 0.9% saline (AlleMan Pharma, Rimbach, Germany) at a concentration of 1 mg/ml. Control animals received the same volume of sterile saline as a vehicle. At the start of the experiment, all animals were randomly divided in 3 groups, to facilitate the handling and sacrifice of the animals, and the measurements and injections. All 32 animals received cisplatin at day 0. At day 2, the cell-treated and control groups were determined by a randomization of the animals. At least 2 petri dishes containing CD133<sup>+</sup>GFP<sup>+</sup> or CD133<sup>-</sup>GFP<sup>+</sup> were available, and, after the FITC sinistrin Half-Life measurements, the animals

that did not show any sign of injury were excluded. The others animals received the required amount of cells: animal 1 received CD133<sup>+</sup> cells, animal 2 received CD133<sup>-</sup> cells, animal 3 received saline, and so on.

The renal function was assessed before the induction of the damage (baseline), at day 2, 7 and 14 post cisplatin administrations. The day of Cisplatin administration was considered as day 0. The day before the measurements, the animals were placed into metabolic cages for 16 hours as previously described. The following morning, the urine and blood were collected, the animals were weighted, and the renal function was assessed by the transcutaneous device, as described at the beginning of the paragraph. On day 2 and day 7, the animals that were randomly assigned to cell-treated groups received  $1 \times 10^6$  GFP-CD133<sup>+</sup> or GFP-CD133<sup>-</sup> cells in 500  $\mu$ l volume of sterile PBS. All cells were labeled with PKH26 (PKH26GL-1KT, Sigma-Aldrich, Germany) before injection, following manufacturer's instructions.

#### **2.10.4 SHORT-TERM STUDY**

For the short-term study, a total of 8 male 8-9 weeks old immunodeficient athymic nude rats were used. The renal function was assessed at baseline and day 2.  $1 \times 10^6$  GFP-CD133<sup>+</sup> cells were injected in 6 animals at day 2 after the transcutaneous measurement. 2 animals were sacrificed 1, 6 and 24 hours after the injection of the cells.

#### **2.10.5 HISTOLOGY: COLLECTION AND ANALYSIS**

On the day of the sacrifice, a complete physical examination was performed, and the BW was recorded for all rats. Animals were euthanatized by CO<sub>2</sub> exposure and the kidneys were weighed. Additionally, 2 portions of lungs, kidney and liver were collected for immunohistological analysis and fixed in 4% PFA for 24 hours at 4°C.

#### **2.10.6 IMMUNOHISTOCHEMISTRY PROCEDURES ON PARAFFIN-EMBEDDED TISSUES**

One portion of the fixed tissue was processed for paraffin embedding, cut (3 $\mu$ m) and stained with hematoxylin and eosin (H&E) by research technicians. The paraffin block was also used to cut 4 $\mu$ m sections to perform the Ki67 staining. Slides were deparaffinized and rehydrated by washing the slides twice in HistoClear II (HS-202,

National Diagnostics) for 5 minutes each, twice in Absolut Ethanol for 5 minutes each, once in 95% Ethanol (5 minutes), once in 70% Ethanol (5 minutes), once in dH<sub>2</sub>O (5 minutes) before performing the antigen retrieval procedure (Sodium Citrate 10 mM in dH<sub>2</sub>O, pH 6, C2404, Sigma). After the antigen retrieval, the slides were washed with PBS once (5 minutes) and treated with 0.3% H<sub>2</sub>O<sub>2</sub> in MetOH for 30 min (Hydrogen Peroxide 30, H1009, Sigma; Methanol, 322415, Sigma). The slides were then washed three times (3 minutes) in TBS 0.1% (v/v) Tween (SRE0031, Sigma). After that, the procedure follows the one used for immunofluorescence staining in tissue reported in paragraph 2.4.

For Masson Trichrome staining, one slide for each animal was deparaffinized and rehydrated as previously described. The slides were then immersed in Weigert's iron hematoxylin working solution (HT1079, Sigma) for 10 minutes, stained with Biebrich scarlet-acid fuchsin solution (HT151, Sigma) for 10-15 minutes, differentiated in Phosphomolybdic-phosphotungstic acid solution (319279, HT152, Sigma) for 10 minutes, and stained with aniline blue solution (B8563, Sigma) for 5-10 minutes and differentiated in 1% acetic acid solution (695092, Sigma) for 3 minutes. In between all steps the slides were rinsed with distilled water before proceeding to the following step. Finally, the slides were dehydrated by immersing them twice in 70% ethanol (30 seconds), three times in 95% ethanol (30 seconds), three times in absolute ethanol and twice in Histoclear (30 seconds). The slides were finally mounted with DPX (12658646, Thermo Scientific) and left to dry under a chemical hood overnight before visualization.

### **2.10.7 IMMUNOHISTOCHEMISTRY PROCEDURES ON FROZEN TISSUES**

The other portion of the fixed tissue was washed with PBS three times, and placed consecutively in 15% (w/v) sucrose solution in PBS and 30% (w/v) sucrose solution in PBS until the sample sank to the bottom of the container due to exchange of water with sucrose (approximately 1 day). After three more washes, the samples were embedded in Tissue-Tek® O.C.T™ medium and stored at -80 until cut. The frozen samples were then cut using the cryostat in 5-6 µm slices and stored at -80 until use. For the immunofluorescence stainings, the slides were processed as described in paragraph 2.4.

## 2.11 IMAGE PROCESSING

**Count of Pax2<sup>+</sup> cells:** a total of 10 images were taken for each subpopulation (CD133<sup>+</sup> and CD133<sup>-</sup>) for each sample in the red channel (Pax2), green channel (Wt1) and blue channel (DAPI). Once at the computer, the images were transformed from 16 to 8 bit, and the Black and White Threshold was applied. The number of cells Pax2<sup>+</sup> and DAPI<sup>+</sup> was then counted.

**Spheroid area:** at least 9 spheroids were imaged every day for 6 days using a Leica MZ16F dissection microscope with a DFC420C camera. A black and white threshold was applied in the Fiji software and the area of the spheroid was computed.

**Tubular dilation:** H&E procedures were performed by research technician at the University of Heidelberg. Microphotographs of all the animals were acquired using Leica M651 microscope. To study the tubular dilation induced by cisplatin in the three groups, 10 random fields of the renal cortex per animal were taken using a 20X objective. The images were transformed into black and white and Fiji software was used to compute the area of the tubular luminal dilatation, by applying a black and white threshold to all images and measuring each black area (Figure 2.3).

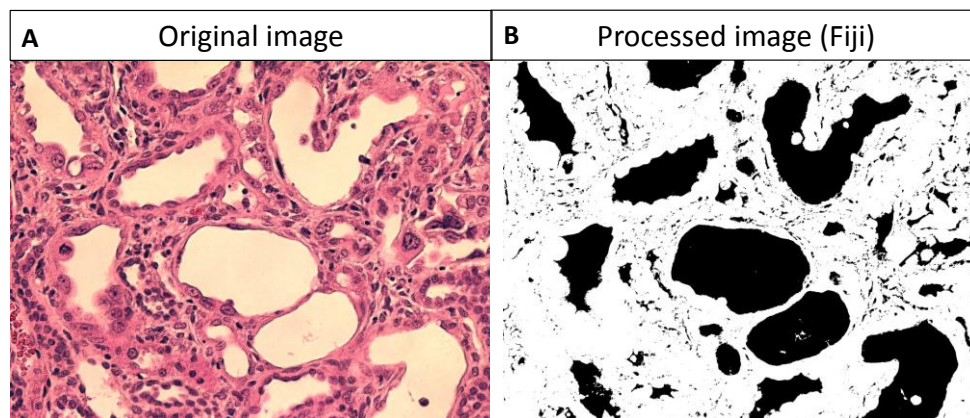


**FIGURE 2.3 IMAGE PROCESSING PROCEDURE USED TO MEASURE THE TUBULAR DILATATION.**

A random numerical code was assigned to each slide. The images were transformed from 16 to 8 bit (Image > Type > 8 bit), a black and white threshold was applied (Image > Adjust > Threshold). A cut-off was measured in order to count only luminal areas of dilated tubule, and the black areas were computed (Analyze > Analyze Partides). The luminal areas on the edge of the image were eliminated. At least 12 images per kidney per animals were included in the analysis of a total of 480 images.



**Masson's Trichrome (MT) staining:** Microphotographs of all the animals were acquired using Leica. To study the amount of collagen staining per slide, Fiji software was used by applying colour threshold (blue) to all images and measuring the blue area. Also, 5 MT images per two animals per group were stitched together using the 'stitching' plug-in of the Fiji software.

**Ki67<sup>+</sup> cells counting:** one paraffin embedded slide per animal was processed according to the protocol described in paragraph 2.10.6. Each slide was randomised so that the group could not be identified. At least 10 images per slide were randomly taken, and the number of positive nuclei for Ki67 was counted by an external observer not aware of the group distribution.

**General image processing:** routine image processing was performed using the Fiji software.

## 2.12 STATISTICAL ANALYSIS

Each figure legend reports which statistical test was applied to that experiment. All data are generally represented as mean  $\pm$  standard error means (SEM), unless stated otherwise. The statistical tests were based on the assumption that the data follow a Gaussian (normal) distribution. In chapter 3 and 4, the t-test was used to determine whether the differences between the means of two independent groups were significant. In chapter 5, the ANOVA one-way test was used to determine whether the differences between the means of more than two groups were significant. All statistical analysis was performed using the GraphPad Prism software. The statistical significance is expressed with the p-value (p), considered *significant* when  $0.05 > p > 0.01$  (\*); *very significant* when  $0.01 > p > 0.001$  (\*\*) and *extremely significant* when  $p < 0.001$  (\*\*\*)).

## 2.13 SUMMARY OF CELL CULTURE MEDIA

<b><u>Human renal progenitor cells (HRPC)</u></b>	<b>C<sub>f</sub></b>	<b>Manufacturer, Cat. num.</b>
FBS	5%	Gibco, 10270-106
hEGF	10 $\mu$ g/L	Sigma, E9644
Hydrocortisone	36 $\mu$ g/L	Sigma, H0135

3,3',5-triiodo-L-thyronine sodium salt	4 ng/L	Sigma, T5516
ITS (Insulin, Transferrin, Selenium)	1x	Gibco, 41400 - 045
MycoZap™	1x	Lonza, VZA-2021
DMEM/F12	to final volume Lonza, BE12-719F/12	

#### **Conditionally Immortalized Podocytes**

FBS	10%	
RPMI-1640	to final volume Sigma, R8758	

#### **Primary Podocytes**

FBS	10%	
MycoZap™	1x	
RPMI-1640	to final volume Sigma, R8758	

#### **Mouse Mesothelial cell**

FBS	10%	
DMEM-High Glucose	to final volume Sigma, D5796	

#### **Kidney Dissection Medium**

FBS	10%	
DMEM	to final volume Sigma, D6546	

#### **Kidney Rudiment Medium**

FBS	10%	
Penicillin/Streptomycin	1%	Sigma, P4333
MEME	to final volume Sigma, M4655	

#### **Kidney Spheroid Medium**

FBS	10%	
MEM-phenol free	to final volume Gibco, 51200-046	

#### **Podocytes Differentiation Medium (VRAD)**

FBS	10%	
ATRA (in EtOH)	100 µM	Sigma, R2625
1α, 25- Dihydroxyvitamin D3	100 nM	Sigma, D1530

DMEM/F12 to final volume

**Podocytes Differentiation Control Medium (Control)**

FBS 10%

EtOH Abs 10% Sigma, E7148



## **3 ISOLATION AND CHARACTERIZATION OF RENAL STEM/PROGENITOR CELLS**

### **3.1 INTRODUCTION AND AIMS**

In the last decade, the field of renal regenerative medicine has blossomed. The search for a renal stem or progenitor cell became paramount, in the view of formulating a cell therapy as an option for patients with acute and chronic kidney diseases to prevent progression to ESRD. In the general introduction, seminal studies were introduced, where CD133 was identified as a possible marker of renal stem/progenitor cells (Bussolati et al., 2005; Ronconi et al., 2009; Sagrinati et al., 2006). Notably, these studies made use of tissue nephrectomies derived either from the healthy region of a kidney of patients affected by renal cell carcinoma (Angelotti et al., 2012; Ronconi et al., 2009; Sagrinati et al., 2006) or elderly deceased donors (Angelotti et al., 2012). As healthy as these regions can be, there is always the risk of cancerous cells in that region. Consequently, cells isolated from kidneys with tumours would not be appropriate for clinical use. On the other side, cells from older kidneys are likely to be suboptimal, being more susceptible to ischaemic damage. Therefore, there is a need to assess the therapeutic potential of CD133<sup>+</sup> cells isolated from young potentially healthy kidneys.

In all previous studies, the CD133<sup>+</sup> cells were isolated exclusively using magnetic-activated cell sorting (MACS) conjugated to CD133 antibodies (Ronconi et al., 2009; Sagrinati et al., 2006). With MACS, the cells are labeled using antibodies conjugated to magnetic beads. The bead-labelled cells are then passed through a column within a magnetic field. In the column, the labelled cells are retained by the magnetic field (positive selection) whereas the cells that are not labelled go through the column (negative selection). The whole cell population is passed simultaneously through the column, reducing the time of sorting. With FACS (Fluorescence-Activated Cell Sorting)

sorting, the cells are labeled using fluorescently-labelled antibodies. FACS is typically the method of choice when high purity or the sorting of a very rare population is desired (Gross et al., 2015; Jahan-Tigh et al., 2012). How FACS and MACS affect stem cell properties is mostly unexplored (Li et al., 2013b).

In this chapter, the general aim is to investigate the presence of a cell population expressing CD133 in tissue biopsies obtained from children and to understand whether this population represents the putative progenitor population reported by the literature in adult kidneys. It was hypothesised that the expression of CD133 (and CD24) in the children's kidneys would be comparable to the one previously described in adult kidneys. In addition, it would be expected that following eventual isolation the CD133<sup>+</sup> cells would display to a certain extent a proliferation capacity consistent with their progenitor status.

In specific, the following objectives will be investigated:

- I) Analyse the expression of CD133 and CD24 in intact children's kidneys
- II) Determine if CD133 and CD24 are expressed in renal cells following isolation and culture *in vitro*
- III) Characterize the primary renal cultures *in vitro* by FACS
- IV) Assess the suitability of MACS or FACS for isolating CD133<sup>+</sup> and CD133<sup>-</sup> cells.

## **3.2 RESULTS**

The biopsy tissues were collected at the Alder Hey Hospital (Liverpool) from Mr Simon Kenny, a consultant paediatric surgeon, and transported in ice boxes to the University of Liverpool. All samples were obtained following informed consent from the parents of the patients.

### **3.2.1 IDENTIFICATION OF CD133 AND CD24 IN VIVO**

A list of all samples is shown in Table 3.1. Renal tissue was obtained from biopsy tissue samples obtained from children, age between 15 months and 15 years. hK2 was the only healthy sample in the cohort, obtained from a deceased donor. All the other samples were obtained from patients hospitalized mainly for recurrent infections. Four of these patients presented a duplex kidney. Duplex kidneys represent the most

common congenital abnormality of renal development, where a duplication of the pelvicalyceal system of the kidney results in the presence of two ureters, called upper and lower moiety ureters. The anomaly is asymptomatic in most cases but carries several complications, such as vesicoureteral urinary reflux (VUR). VUR is defined as the retrograde flow of urine from the bladder to the ureter and kidney and causes acute infections, renal scarring and nephropathy (Doery et al., 2015). No additional information about the renal condition of the patients was obtained after their hospitalization and reception of the samples. Among all samples, hK6 was processed differently (see Material and Methods) and the cells isolated from its glomeruli were used as positive control for the differentiation assay (shown in the following chapter).

**TABLE 3.1 LIST OF SAMPLES USED IN THIS THESIS**

All samples (hK1-hK5) were processed according to the protocol reported in the Material and Method Section. hK6 was processed differently: the glomeruli were separated from the tubuli and plated.

<b>ID</b>	<b>Age (m/y)</b>	<b>Condition</b>	<b>Portion received</b>
<b>hK1</b>	15 m	Duplex kidney	cortex
<b>hK2</b>	24 m	healthy	whole
<b>hK3</b>	10 y	Duplex kidney	cortex
<b>hK4</b>	8 y	Recurrent infections	cortex
<b>hK5</b>	8 y	Duplex kidney + recurrent infections	cortex
<b>hK6</b>	6 m	Duplex kidney	cortex

As mentioned in the general introduction, the glycosylated isoforms of CD133 are reported to be stem cell markers, and two monoclonal antibodies are commercially available to detect the glycosylated epitopes, AC133 (CD133/1) and 293C2 (CD133/2) (Angelotti et al., 2010).

CD133/1 was used to evaluate the expression of CD133 on frozen sections. CD133 was expressed in the glomeruli of all samples, specifically on the parietal epithelial cells of the Bowman's capsule (BC), regardless of the age of the patient or the status

(healthy vs. not healthy) (Figure 3.1 A-D). Interestingly, few CD133-expressing cells were detected inside the glomerulus, as shown in hK4 (Figure 3.1 C). In this sample, the staining was not confined to a thin layer of cells. Instead, the images suggested that either the BC is thicker or there were visceral glomerular cells (podocytes) that expressed CD133. In hK5, instead, a relative big Bowman's space was observed. However, in the sections belonging to that patient only one glomerulus was spotted, so limited conclusion can be drawn.

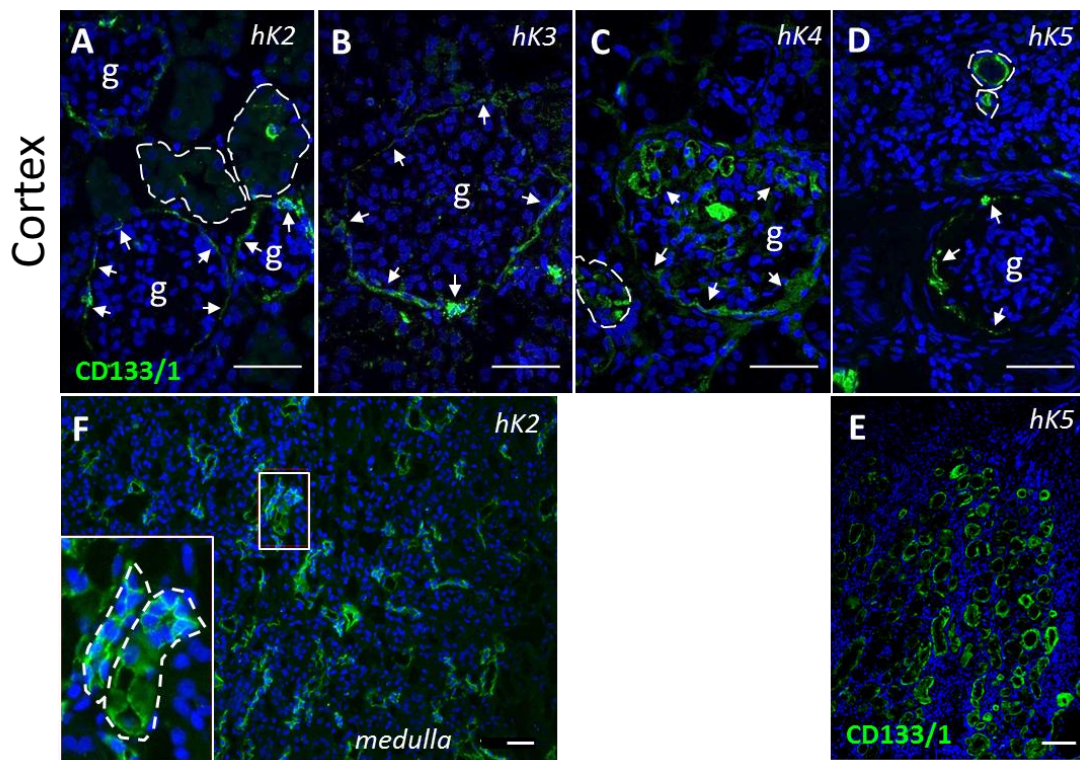


**FIGURE 3.1 EXPRESSION *IN VIVO* OF CD133**

(A-D) Representative immunofluorescence images showing the cortex of four samples (hK2, hK3, hK4, hK5) stained for CD133/1 (green). CD133/1 can be identified on the PEC cells and on scattered tubular cells. The glomeruli (g) are annotated and the arrows indicate the cells on the BC. The tubuli are highlighted by a dotted line. (E) Immunofluorescence images of hK5 section stained with CD133/1 at low magnification that shows tubular injury. (F) Immunofluorescence images of the medulla of hK2 showed positive staining with CD133/1. The inset shows in higher magnification a completely stained tubule. The scale bars represent 50  $\mu$ m.

In addition to the PEC, CD133 staining was found on the luminal surface of scattered tubular cells. In hK5, the entire cross-section of some tubuli is stained for CD133 (Figure 3.1D-E). Of note, hK5 displayed extensive tubular injury, demonstrated by the dilated luminal area of the tubules (Figure 3.1 E).



In the case of hK2, the whole kidney was available. Since CD133<sup>+</sup> cells were previously identified in the inner medulla (Bussolati et al., 2013), the medulla of hK2 was stained for CD133/1. Cross-sections of most of the tubuli present in the medulla (thick segments of the Loops of Henle and Collecting ducts) demonstrated expression of CD133 throughout. CD133 was specifically detected on the luminal surface as well as on the basolateral surface of the tubular cells, as shown in the small inset in Figure 3.1 F.

CD24 was described as marker of putative stem/progenitor cells in adult kidneys, together with CD133 (Sagrinati et al., 2006). Its expression, therefore, was assessed on frozen sections (Figure 3.2). CD24 was spotted not only on the PEC, but also inside the glomerulus, and on some tubular cells (Figure 3.2 A-B). Also, entire tubuli were CD24-positive. In the medulla, most of the tubular cells expressed CD24 on their entire cell surface.

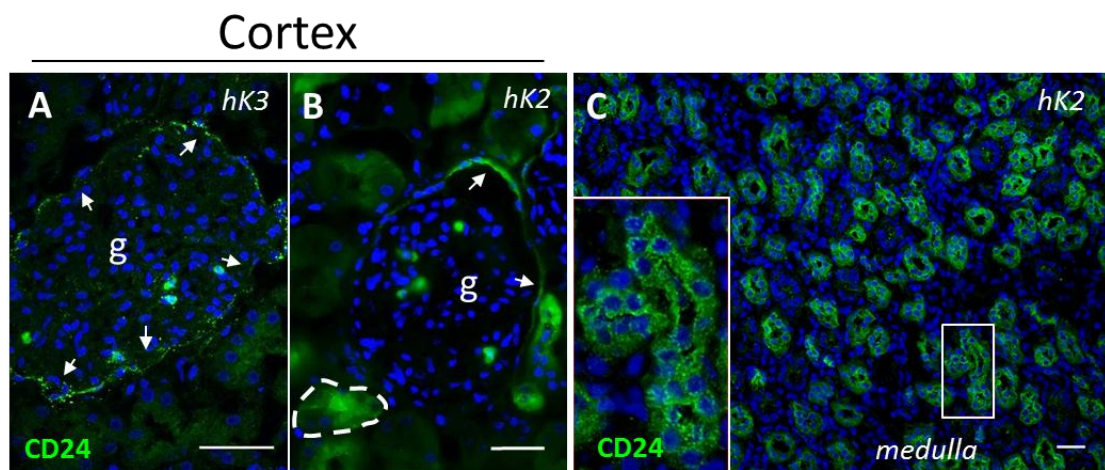


**FIGURE 3.2 EXPRESSION *IN VIVO* OF CD24**

(A-B) Representative immunofluorescence images showing the cortex of two samples (hK2, hK3) stained for CD24 (green). CD24 could be identified on the PEC cells, inside the glomeruli and on tubular cells. Some tubuli are highlighted by a dotted line. (C) Fluorescence image of the medulla of hK2 stained with CD24. The inset shows in higher magnification a completely stained tubule. The scale bars represent 50  $\mu$ m.

Altogether, the *in vivo* localization of CD133 and CD24 suggests that both markers are expressed in the PECs and in scattered tubular cells, as previously shown (Hansson et al., 2014; Sagrinati et al., 2006). However, qualitatively, it appeared as more CD24<sup>+</sup>

cells were present. For the medulla, limited conclusions can be drawn, since the medulla was available for one sample only.

### 3.2.2 ISOLATION OF RENAL CELLS FROM HUMAN KIDNEYS AND CHARACTERIZATION FOR CD133 AND CD24

Each human kidney sample went through the isolation procedure, explained in detail in the material and methods section (page 45). Five cell lines (hK1-hK5) were successfully established in culture. A representative set of bright field images of each sample is shown in Figure 3.3. The isolated cells appeared phenotypically highly heterogeneous: compact colonies of small, cuboidal, epithelial-like cells were spaced-out by elongated, mesenchymal-like cells. The images in Figure 3.3 were taken after six days in culture, and all isolated cells reached confluence in that time frame, except the cells isolated from hK5 that took 12 days. Also, in hK5, less compact colonies were visible.

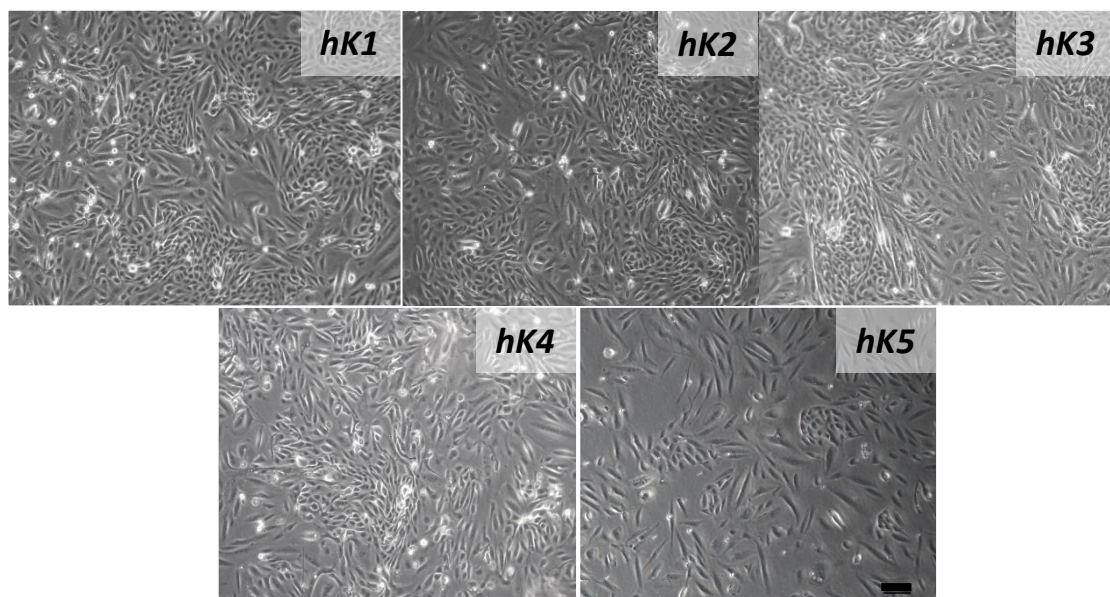


**FIGURE 3.3 BRIGHT FIELD IMAGES OF THE FRESHLY ISOLATED CELLS OF ALL SAMPLES**

Bright field images of freshly isolated cells taken six days after the isolation from the tissue. Phenotypically, the cells appeared highly heterogeneous, with epithelial-like cells alternating with elongated mesenchymal-like cells. Scale bar represents 100  $\mu\text{m}$ .

The first aim was to assess the expression of CD133 on freshly isolated cells. To achieve that, the primary cells were seeded into chamber slide immediately after isolation and when confluent, stained with the CD133/2 antibody. As shown in Figure 3.4 A, a high number of hK2 cells was CD133-positive.

Consequently, the expression levels of both glycosylated epitopes of CD133 were quantitatively evaluated by FACS in all cell lines. All cell lines were cryopreserved at passage 1. Upon thawing, the cells were plated, and the expression of CD133 by FACS was evaluated at passage 2. At passage 2, the percentage of cells expressing CD133 was not insignificant. In average, more than 70% of the renal cells isolated expressed both CD133/1 and CD133/2. However, some differences were detected in the individual samples: hK2 presented significantly more CD133/2-expressing cells ( $p < 0.01$ ), whereas hK4 and hK5 presented more CD133/1-expressing cells (hK4:  $p < 0.01$ ; hK5:  $p < 0.01$ ).

Therefore, the FACS analysis at passage 2 showed a notable increase of the cells expressing CD133 in one or both isoforms on their surface.

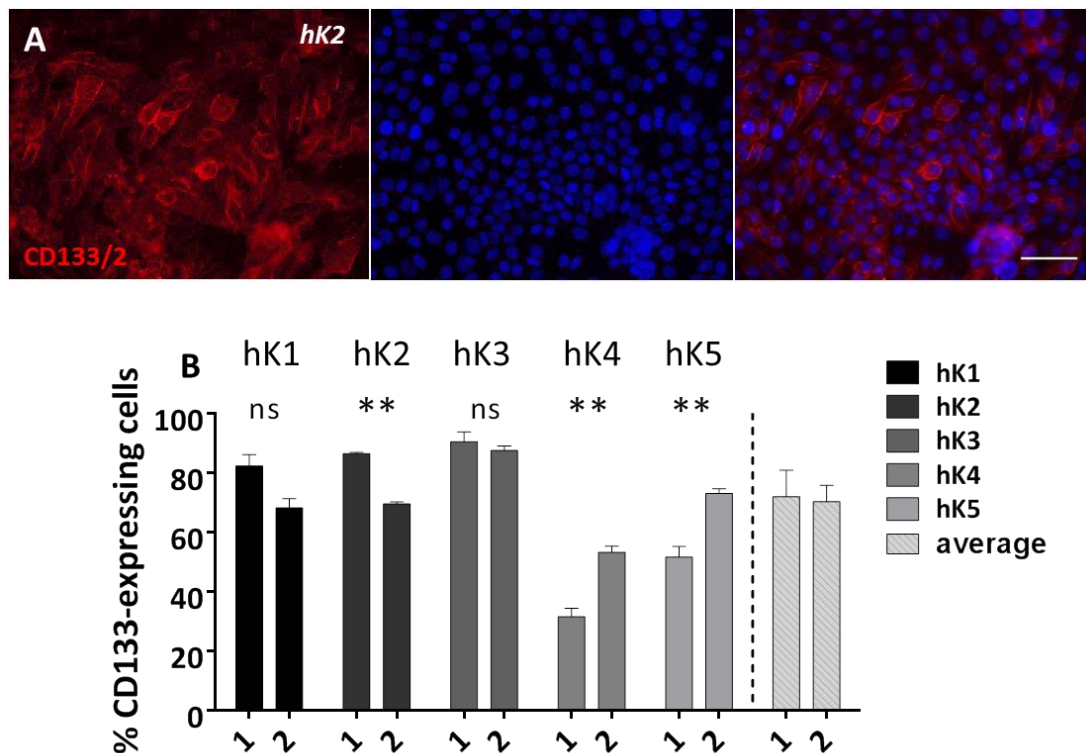


**FIGURE 3.4 EXPRESSION OF CD133 *IN VITRO***

(A) Immunofluorescence image of freshly isolated cells stained for CD133/2 (red). Most cells appeared stained. The scale bar represents 50  $\mu\text{m}$ . (B) FACS analysis showing the amount of the two glycosylated epitopes of CD133, CD133/1 and CD133/2, in all samples. The analysis was conducted in duplicate, starting from frozen aliquots of the cells at passage 1. The error bars represent SEM. A t-test was applied to determine significance, \*\*  $p < 0.001$ .

In the literature, isolation of renal progenitor cells has been reported based on the expression of CD133 in combination with CD24 (Romagnani and Remuzzi, 2014).

Therefore, the expression of CD24 was evaluated by FACS at passage 2 in the five primary cell lines (Figure 3.5). On average,  $88\% \pm 7.8$  of the renal cells expressed CD24 on their surface. Of the CD24<sup>+</sup> cells, almost two thirds also expressed CD133/2 ( $65.16\% \pm 13.57$ ). The co-expression of CD133 and CD24 was confirmed by immunofluorescence, where some colonies displayed both markers (Figure 3.5 C). However, almost a quarter ( $23.5 \pm 8\%$ ) of the CD24<sup>+</sup> renal cells did not express CD133. In comparison, only  $4.6 \pm 1.4\%$  of the renal cells expressed CD133 but not CD24 (Figure 3.5 B).

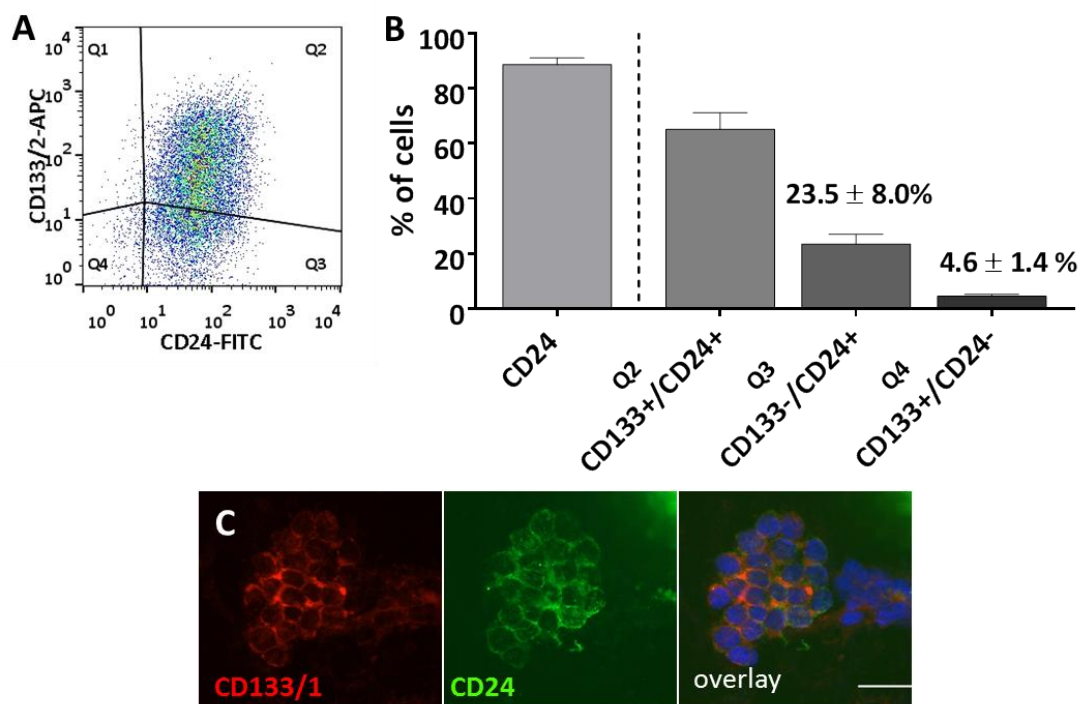


**FIGURE 3.5 EXPRESSION OF CD24 *IN VITRO***

(A) Representative dot plot, obtained staining the heterogeneous population at passage 2 for CD24-FITC and CD133/2-APC. The different quadrants are displayed: Q1, CD133<sup>+</sup>/CD24<sup>-</sup>; Q2, CD133<sup>+</sup>/CD24<sup>+</sup>; Q3, CD133<sup>-</sup>/CD24<sup>+</sup>; Q4, CD133<sup>-</sup>/CD24<sup>-</sup> (B) Histogram bars summarizing the FACS data about the expression of CD24 in the whole population and in conjunction with CD133/2. The FACS analysis was performed in duplicate for each sample, starting from separate aliquots of frozen cells and for each duplicate a technical replicate was performed. The scale bars represent the SEM (C) Representative immunofluorescence image stained for CD24 (green) and CD133 (red). The scale bar represents 50  $\mu$ m.

Thus, virtually all CD133<sup>+</sup> cells expressed CD24, but not all CD24<sup>+</sup> cells expressed CD133. As a result, we decided to base the isolation of the putative renal progenitor cells on the expression of CD133 only (see paragraph 3.2.4).

### 3.2.3 CHARACTERIZATION OF THE HETEROGENEOUS POPULATION AT PASSAGE 2

The heterogeneous population of all samples was characterized by FACS at passage 2. Generally, the data are presented separately for each cell line, where interesting differences among the samples were found, or pooled together, where all samples followed the same trend.

#### 3.2.3.1 CD31 AND CD45

At first, the heterogeneous population was characterized by FACS for the expression of CD45 and CD31, to rule out the possibility that the heterogeneous population obtained is derived from the hematopoietic (CD45) or endothelial (CD31) component (Figure 3.6). A small subset of the overall renal population was characterised by the CD31 expression, being less than 5% across the five cell lines (Figure 3.6 A and C). In regards to CD45, its expression was evaluated in conjunction with CD133. An average of  $6.18 \pm 4.17\%$  cells of CD133-positive cells also expressed CD45 (Figure 3.6 B and C). CD45 expression was not detected in the CD133/2-negative subset of cells (Data not shown).

This FACS analysis shows that the isolation procedure did not lead to the accumulation of endothelial cells in the bulk population. Also, since CD133 was originally identified on hematopoietic stem cells (Yin et al., 1997), it was important to exclude an enrichment for hematopoietic cells expressing CD133.

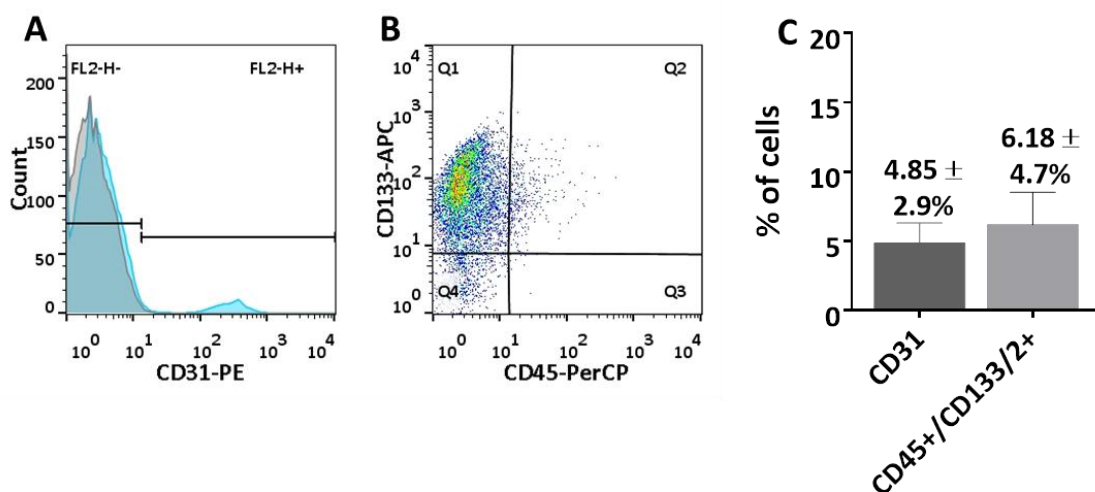


**FIGURE 3.6 EXPRESSION OF CD31 AND CD45 *IN VITRO***

(A) Representative FACS histogram showing the distribution of the whole population of renal



cells stained with an anti-CD31-PE antibody, to identify the endothelial population. The grey histogram represents the control sample (unstained), whereas the blue histogram is a representative stained sample. (B) Representative dot plot depicting the heterogeneous population at passage 2 after staining for CD45-PerCP and CD133/2-APC. (C) Histogram bars showing the mean values of CD31<sup>+</sup> cells and CD45<sup>+</sup>/CD133/2<sup>+</sup> cells in all samples. The FACS analysis was performed in duplicate for each sample, starting from separate aliquots of frozen cells; for each duplicate a technical replicate was performed. The scale bars represent the SEM.

### **3.2.3.2 MESENCHYMAL MARKERS**

The next aim of the present study was to define the phenotype of the isolated cells for mesenchymal markers. CD73 (5'-nucleotidase), CD90 (Thy1.1) and CD44 were chosen as indicated by the international society for cellular therapy position statement (Dominici et al., 2006).

All cells from all samples in culture at passage 2 were found to express CD73. Therefore, all CD133<sup>+</sup> cells were also CD73<sup>+</sup> (Figure 3.7A). By contrast, the amount of CD90<sup>+</sup> cells was below 20% in all samples except hK4, where the number of CD90<sup>+</sup> cells exceeded 40%. In the CD90<sup>+</sup> subpopulations, only in hK1 and hK4 showed significant differences between the amount of CD133<sup>+</sup>/CD90<sup>+</sup> and CD133<sup>-</sup>/CD90<sup>+</sup> cells (hK1:  $p < 0.05$ ; hK4:  $p < 0.05$ ). Finally, immunofluorescence analysis of CD44 revealed that all cell lines expressed this marker (Figure 3.7 C).

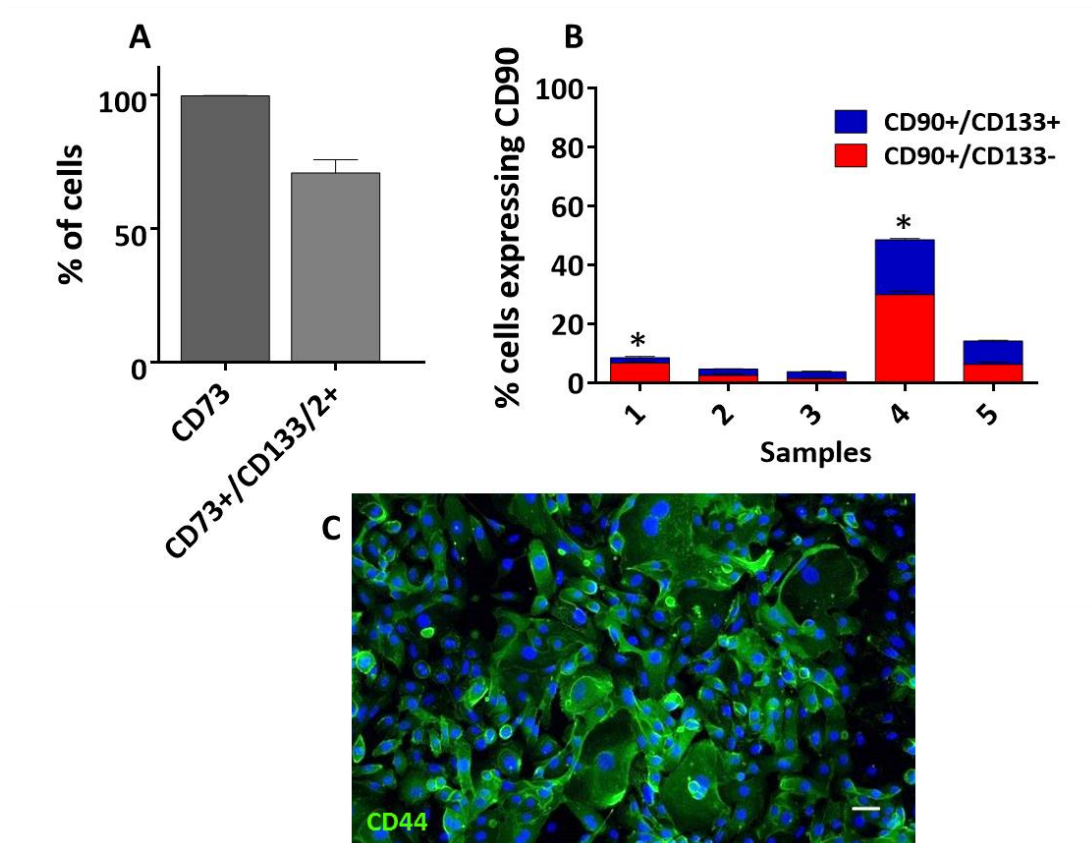


**FIGURE 3.7 EXPRESSION OF MESENCHYMAL MARKERS *IN VITRO***

(A) Histogram showing the mean values of all samples for the amount of CD73<sup>+</sup> cells in the heterogeneous population and in conjunction with CD133. The error bars represent the SEM. (B) Histogram showing the amount of CD90<sup>+</sup> cells in each sample in relation to the expression of CD133. The FACS analysis was performed in duplicate for each sample, starting from separate aliquots of frozen cells and for each duplicate a technical replicate was performed. The scale bars represent the SEM. A t-test was applied to determine significance, \*p<0.05 (C) Representative immunofluorescence image stained for CD44 (green) in the heterogeneous population. The scale bar represents 50 μm.

Thus, all cell lines except hK4 expressed CD73 and CD44, but not CD90. hK4, instead, had the highest amount of CD90<sup>+</sup> cells and most of them were part of the CD133<sup>-</sup> fraction. Although not all recommended mesenchymal markers were tested (e.g. CD105), the data suggest that the renal cells show an incomplete mesenchymal profile, since they lack CD90. However, CD90 has been also used to identify and purify fibroblasts in human primary cell lines (Kisselbach et al., 2009). It is therefore a possibility that following the isolation procedure hK4 was enriched for fibroblasts.

### **3.2.3.3 EPITHELIAL MARKERS**

Next, we aimed at characterizing the renal population for epithelial markers. Specifically, CD324 (E-Cadherin) and CD326 (EpCam) were chosen (Kalluri and Weinberg, 2009; Metsuyanin et al., 2009; Trzpis et al., 2007). Virtually all cells isolated in this study expressed both E-Cadherin and EpCam (Figure 3.8 A-D). Thus, all CD133<sup>+</sup> cells expressed the two epithelial markers.

CD13 (Aminopeptidase N) was evaluated by FACS as an additional epithelial marker on the five cell lines. CD13 is expressed on tubular epithelial cells, specifically proximal tubular cells (Van der Hauwaert et al., 2013). Interestingly, at least 50% of the cells of each sample expressed CD13 (Figure 3.8 C) and, most importantly, in each sample, the number of CD133<sup>+</sup>CD13<sup>+</sup> cells was significantly higher than the counterpart (t-test; hK1, hK2, hK3, hK4:  $p < 0.01$ ; hK5:  $p < 0.001$ ). The data indicate that a fraction of the CD133<sup>+</sup> cells expressed markers of the proximal tubular cells, which are fully differentiated cells.



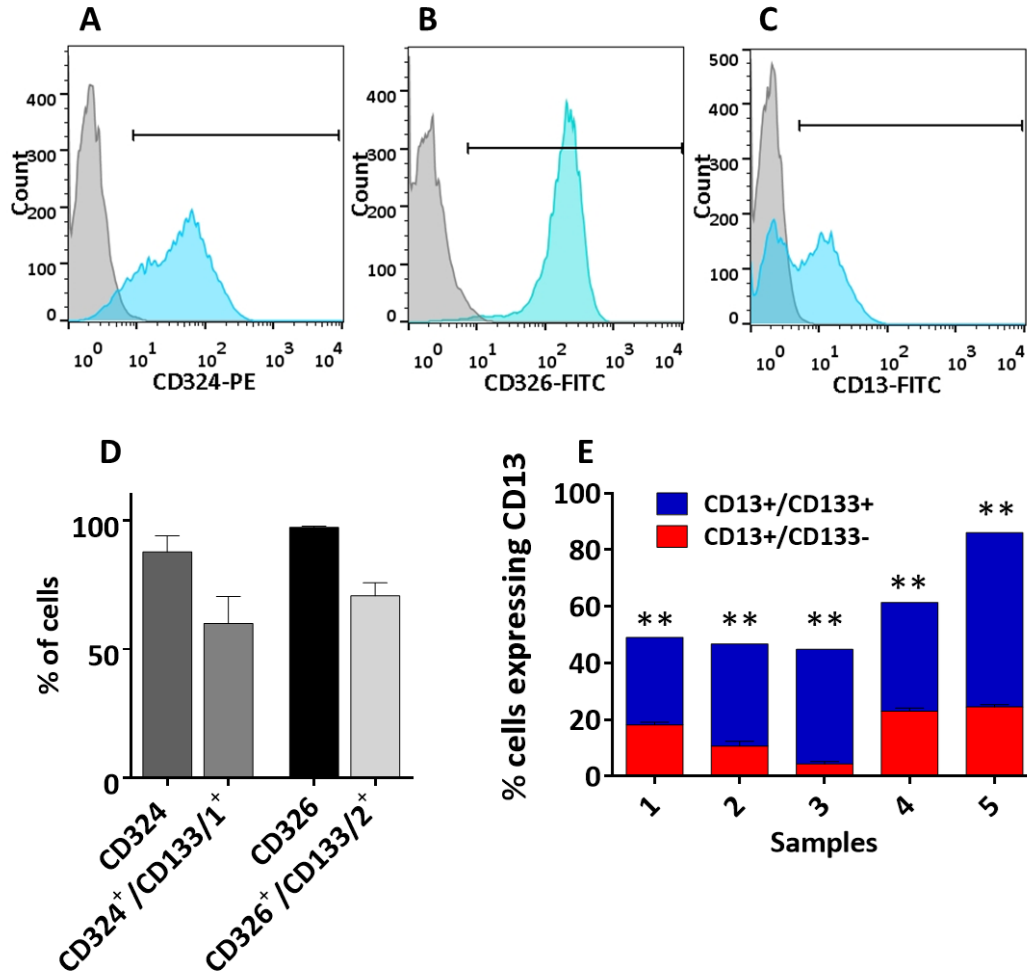


**FIGURE 3.8 EXPRESSION OF EPITHELIAL MARKERS *IN VITRO***

(A-C) Representative FACS histograms showing the distribution of the whole renal cell population stained with an anti-CD324-APC (A), anti-CD326-FITC (B) or anti-CD13-FITC antibody (C). The grey histograms represent the control sample (unstained), whereas the blue histograms are representative stained samples. (D) Histogram showing the mean values of all samples for the percentage of CD324<sup>+</sup> cells and CD326<sup>+</sup> cells in the whole populations or in conjunction with CD133. Note that CD324-APC was used with CD133/1-PE and CD326-FITC and CD13-FITC were used with CD133/2-APC. The error bars represent the SEM. (E) Histogram showing the percentage of CD13<sup>+</sup> cells in each sample in relation to the expression of CD133. The FACS analysis was performed in duplicate for each sample, starting from separate aliquots of frozen cells; for each duplicate a technical replicate was performed. A t-test was applied to determine significance, \*\* p < 0.001.

### 3.2.3.4 RENAL PROGENITOR MARKERS

To make the phenotypical analysis more thorough, other putative markers of renal progenitor cells were evaluated in the heterogeneous population of all cell lines by FACS.

NCAM1 (CD56) had been identified as marker of progenitor/stem cells in the human fetal and adult kidney (Buzhor et al., 2013; Metsuyanin et al., 2009), whereas Tra-1-60 had been proposed as marker of progenitor cells in the adult kidneys (Fesenko et al., 2010). Very few cells expressed CD56. Similar to the results for CD90, all samples presented less than 10% CD56-expressing cells, with the exception of hK4, where as many as 40% of the cells expressed CD56. Among the CD56<sup>+</sup> cells, there were significant differences between the number/percentage of CD56<sup>+</sup>/CD133<sup>+</sup> and CD56<sup>+</sup>/CD133<sup>-</sup> cells depending on the cell line (Figure 3.9A). The CD133<sup>-</sup> population of hK1 and hK4 contained a higher number of CD56<sup>+</sup> cells (hK1, hK4: p<0.01) than the CD133<sup>+</sup> population, whereas it was the opposite situation for hK3 and hK5 (hK3, hK5: p<0.05).

Tra-1-60 expression showed a more homogeneous trend across the samples: approximately 50% of the cells expressed Tra-1-60. Among these, expression of Tra-1-60 was significantly higher in the CD133<sup>+</sup> fraction (Figure 3.9 B).

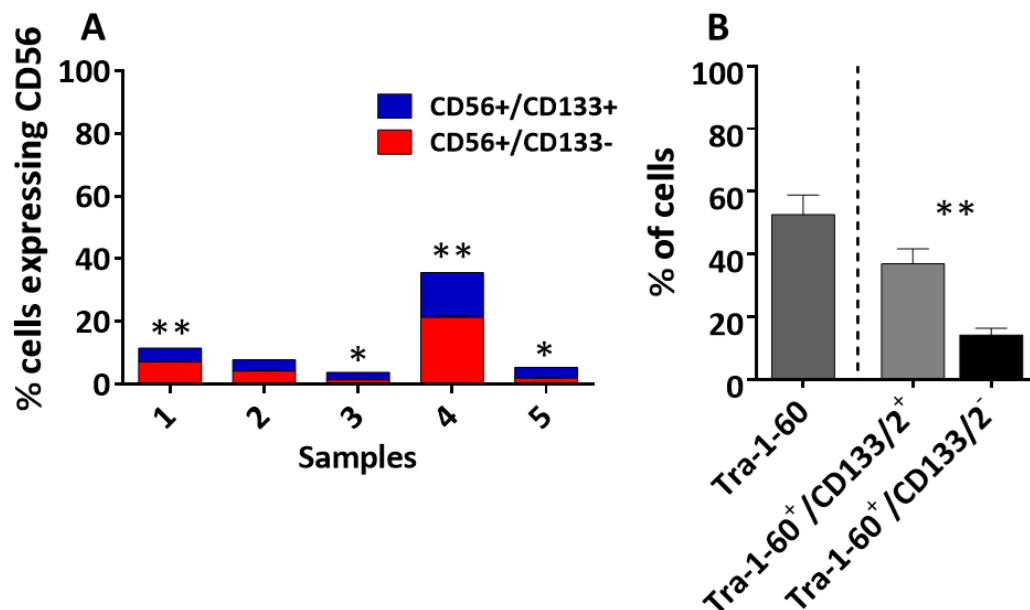


**FIGURE 3.9 EXPRESSION OF RENAL PROGENITOR MARKERS *IN VITRO***

(A) Histogram showing the amount of CD56<sup>+</sup> cells in each sample in relation to the expression of CD133. (B) Histogram showing the mean values of all samples for the amount of Tra-1-60<sup>+</sup> cells in the whole populations and in conjunction with CD133. The error bars represent the SEM. The FACS analysis was performed in duplicate for each sample, starting from separate aliquots of frozen cells and for each duplicate a technical replicate was performed. A t-test was applied to determine significance, \*\* p<0.001.

In summary, the renal primary cell lines appeared quite heterogeneous, expressing mesenchymal markers (CD73 and CD44) and epithelial markers (E-Cad and EpCam). Of note, the amount of fully differentiated tubular epithelial cells, detected through the expression of CD13, accounted for more than 50% of the population. However, a proportion of the CD133<sup>+</sup> cells also expressed Tra-1-60, and CD56, even if at very low levels. In conclusion, it appeared that even if most of the cells expressed CD133, several sub-populations were present.

**TABLE 3.2 SUMMARY OF THE EXPRESSION OF THE SURFACE MARKERS ANALYSED IN THIS STUDY**

All markers were analysed using the heterogeneous populations of all biological samples (hK1-hK5) at passage 2 by FACS in conjunction with the expression of CD133. \* hK4 showed the highest amount of CD90+ cells (50%) and CD56. The role of the markers and where they are found in mammalian cells is reported.

Legend: expression levels in the heterogeneous population: +, 0%<X<25%; ++, 25%<X<50%; +++, 50%<X<75%; +++, 75%<X<100%; >10% expression ✓ ; <10% expression ✗ . For significance levels, consult the respective section in the results.

Markers	Main function	Expressed in	Percentage of +ve cells in the heterogeneous population	Present in	
				CD133 <sup>+</sup>	CD133 <sup>-</sup>
<b>CD24</b>	not fully understood	granulocytes, normal and cancer stem cells	++++	✓	✓
<b>CD45</b>	activation of lymphoid cells	haematolymphoid cells	+	✗	✗
<b>CD31</b>	leukocyte transmigration, angiogenesis, and integrin activation	endothelial cells	+	✗	✗
<b>CD73</b>	atalyzes production of extracellular adenosine from AMP, involved in inflammation and injury	MSCs, leukocytes	++++	✓	✓
<b>CD90</b>	wound repair, cell-cell and cell-matrix interaction	MSCs, endothelial cells, hematopoietic stem cells, fibroblasts, mesangial cells	+	✗	✗
<b>CD44</b>	involved in cell-cell interactions, cell adhesion and migration	MSCs, large number of mammalian cell types	++++	N/A	N/A
<b>E-Cad</b>	calcium-dependent cell-cell adhesion glycoprotein	epithelial cells	++++	✓	✓
<b>EpCam</b>	calcium-dependent cell-cell adhesion glycoprotein, involved in cell signaling, migration, proliferation, and differentiation	epithelial cells	++++	✓	✓
<b>CD13</b>	aminopeptidase activity	small-intestinal cell, proximal tubular cells	+++	✓	✓
<b>CD56</b>	homophilic binding glycoprotein, n cell-cell adhesion, neurite outgrowth, synaptic plasticity	neurons, glia, skeletal muscle and natural killer cells	+	✓	✓
<b>Tra-1-60</b>	cell adhesion protein podocalyxin	pluripotent stem cells, embryonal carcinoma (EC)	+++	✓	✓
<b>Pax2</b>	transcription factor, essential in kidney development	nephron progenitor cells	+++	✓	✓
<b>Wt1</b>	transcription factor, essential in kidney development	nephron progenitor cell, nephron precursors, podocytes, mesothelial cells	++++	✓	✓
<b>Vimentin</b>	type III intermediate filament (IF) protein	mesenchymal cells, non-epithelial cells	++++	✓	✓

### 3.2.4 SORTING OF CD133<sup>+</sup> AND CD133<sup>-</sup> CELLS

In order to analyse the CD133<sup>+</sup> and CD133<sup>-</sup> populations separately in further experiments, the heterogeneous population was sorted based on the expression of CD133. The feasibility and efficacy of MACS and FACS in separating the two populations was compared using the hK2-derived heterogeneous population.

The FACS sorting strategy of the heterogeneous population is shown in Figure 3.10 A-D:

- The entire population, defined Parental (P1), was gated by excluding cells at high Forward Scatter – Area (FSC-A) and Side Scatter – Area (SSC-A). Higher SSC-A signals indicate increased granularity and therefore dying cells; high FSC-A signals denote the presence of doublets in the cell suspension. The P1 gate contained an average of 85.5% ± 5.3 cells (Figure 3.10 A)
- The doublet content in the population was further characterized by looking at the FCS-Weight. Cells at high FCS-W were gated out for the actual sorting (Figure 3.10 B),
- Finally, a histogram and a dot plot were generated to define the amount of CD133<sup>+</sup> and CD133<sup>-</sup> cells to be sorted (Figure 3.10 D).

The distribution of CD133-labelled cells did not allow a clear distinction between CD133<sup>+</sup> and CD133<sup>-</sup> cells, since no distinct peaks were observed (Figure 3.10 C). Thus, in order to insure high purity for both populations, a relatively large gap was maintained between the two populations to sort (21.1% ± 8.5) (Figure 3.10 C).

The graph in Figure 3.10 E shows the content of CD133<sup>+</sup> cells analysed before the sortings using the FACS counter (for the MACS sorting), and the FACS sorter (for the FACS sorting). The starting amount of CD133<sup>+</sup> cells in the bulk population (hK2) was the same for both techniques. The amount of CD133<sup>+</sup> cells that could be retrieved at the end of the both sortings was different. The difference depended on the necessity to keep the gap (between CD133<sup>+</sup> and CD133<sup>-</sup> cells) wider during the FACS sorting, so that the purity of both populations could be increased. By doing so, there was a significant loss of CD133<sup>+</sup> cells that could be obtained at the end of FACS sorting compared to the MACS sorting ( $p < 0.05$ ) (Figure 3.10 E).

The MACS sorting was carried out using an antibody against CD133/2 labelled with PE. Microbeads that recognized the PE fluorochrome, and LD columns specifically designed for negative selections, were used. However, the MACS system proved to be inconsistent and highly variable with respect to purity, specifically of the CD133<sup>-</sup> population (Figure 3.10 F). The MACS efficacy calculated according to Equation 1 (Material and Methods, page 56) was 0.49, leading to a purity for the CD133<sup>-</sup> population of 50.8% ± 33.1. Both CD133<sup>+</sup> and CD133<sup>-</sup> populations, when sorted by FACS, displayed a higher purity compared to the populations isolated by MACS ( $p < 0.05$  for both populations) (Figure 3.10 F). This data suggest that the LD columns worked well to obtain a pure CD133<sup>+</sup> population, but not to get a pure CD133<sup>-</sup> population. Therefore, it appeared that the number of CD133<sup>+</sup> cells that needed to be depleted from the total population was too high for the columns to work efficiently (Miltenyi technical support, personal communication).

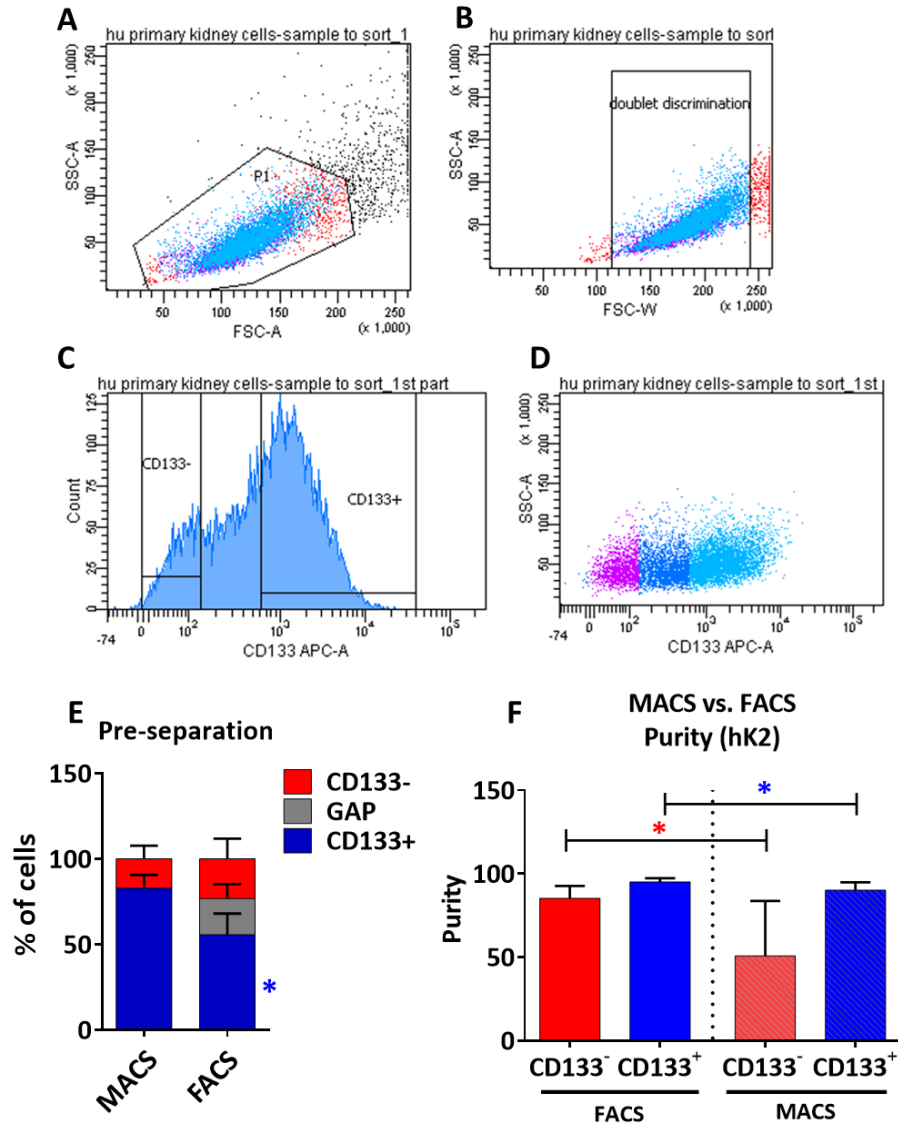


**FIGURE 3.10 FACS SORTING STRATEGY EMPLOYED IN THE STUDY AND COMPARISON WITH MACS**

(A-D) Sorting strategy used to sort the heterogeneous population in CD133<sup>+</sup> and CD133<sup>-</sup> cells. The strategy is detailed in the results section. (E) Histogram showing the expression of CD133 before MACS and before FACS. 6 independent sortings for both techniques were performed on hK2. For the MACS sortings, the FACS Calibur was used, whereas for the FACS sorting, the FACS Aria was used. A t-test was applied to determine significance, \* p<0.05 (F) Histogram showing the purity obtained for both populations after FACS and MACS (n=6). An ANOVA one-way with Dunnet *Post Hoc* was used to establish significance, \* p<0.05.

Based on these results, it was decided to use FACS sorting as the method of choice to separate the entire cell population of the other biological samples into CD133<sup>+</sup> and CD133<sup>-</sup> sub-populations. A summary of the sortings of all samples is shown in Figure 3.11. Higher variability between biological samples was observed due to the differences in the actual amount of CD133<sup>+</sup> cells. The purity of the CD133-based sub-

populations, however, remained considerably high (CD133<sup>+</sup>: 90.7 ± 4.6% vs CD133<sup>-</sup>: 87.6 ± 9.8%).

To sum up, FACS sorting was chosen to sort CD133<sup>+</sup> and CD133<sup>-</sup> cells, because of the consistently high purity (~90%) that could be achieved for all biological samples. However, by using the FACS, less CD133<sup>+</sup> could be obtained because of the technical requirements of the FACS sorter machine.

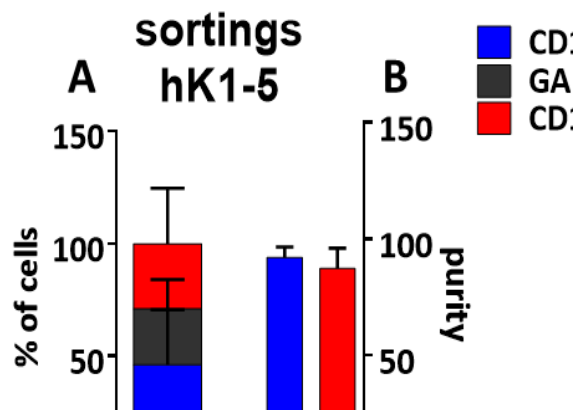


**FIGURE 3.11 SUMMARY OF THE SORTING FOR ALL SAMPLES (hK1-hK5)**

(A) Histogram showing the average distribution of CD133<sup>+</sup> and CD133<sup>-</sup> cells of all samples according to the FACS analysis showed in Figure 3.10. hK1 and hK3 were sorted twice, hK4 and hK5 were sorted once, hK2 was sorted eight times. The error bars represent the SEM. (B) Histogram showing the mean values of purity of CD133<sup>+</sup> and CD133<sup>-</sup> cells for all samples obtained. The error bars represent the SEM.

### 3.2.5 CHARACTERIZATION OF CD133<sup>+</sup> AND CD133<sup>-</sup> POPULATIONS BY IMMUNOFLUORESCENCE

The putative renal progenitor population expressing CD133 and the CD133<sup>-</sup> subpopulation were further characterised for renal progenitor markers, in line with previous studies (Bussolati et al., 2005). Specifically, the expression of the two transcription factors Pax2 and Wt1 was evaluated by immunofluorescence. Pax2 is not expressed in adult kidneys, but it has been shown to co-localize with CD133 (Bussolati et al., 2005; Ye et al., 2011). Wt1 is expressed in the developing kidneys and, in the adult kidneys, by podocytes and parietal epithelial cells (Kabgani et al., 2012). Analyses of both populations were performed by seeding the cells both CD133<sup>+</sup> and CD133<sup>-</sup> populations of all biological samples (hK1, hK2, hK3, hK4, hK5) immediately after sorting, and letting them attach overnight before fixing and staining. Representative



fluorescence images are shown in Figure 3.12. Wt1 was expressed by all cells of the CD133<sup>+</sup> and CD133<sup>-</sup> populations. Pax2, instead, was expressed by 95.7% ± 4.2 of the CD133<sup>+</sup> cells and by 57.3% ± 9.8 of the CD133<sup>-</sup> cells.

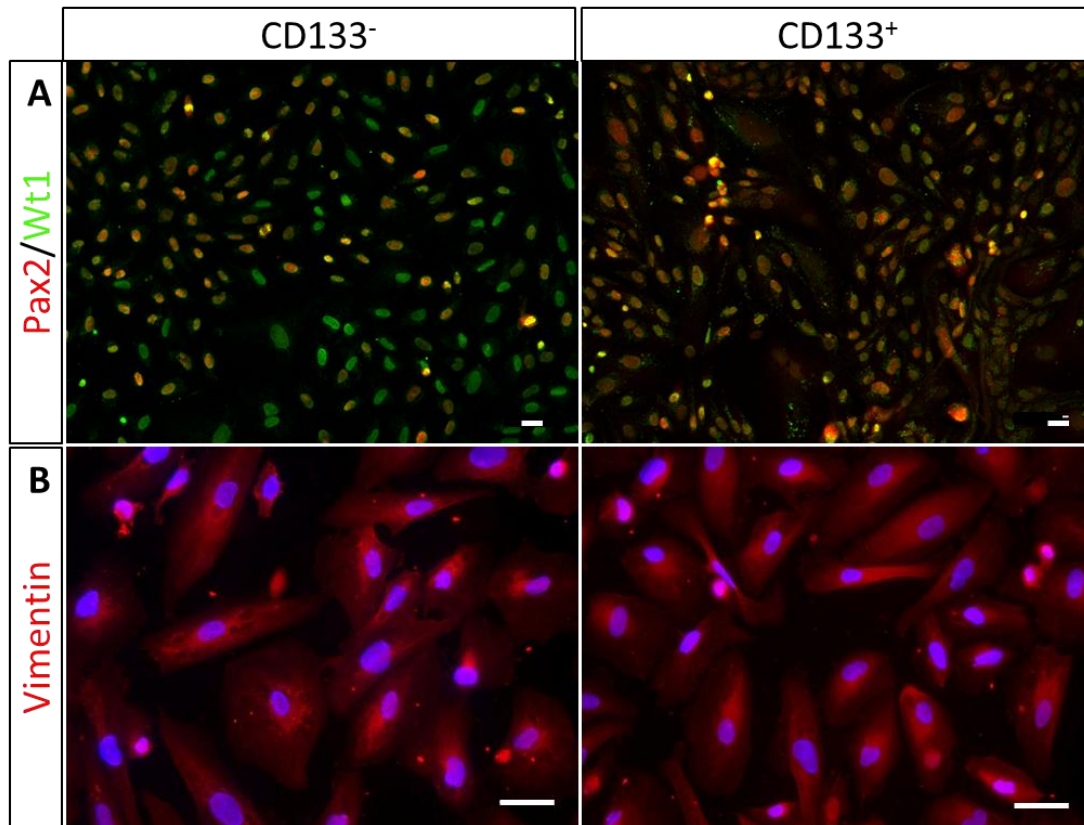


**FIGURE 3.12 EXPRESSION OF RENAL PROGENITOR TRANSCRIPTION FACTORS (WT1, PAX2) AND VIMENTIN**

Representative immunofluorescence images stained for (A) Pax2 (red) and Wt1 (green) in CD133<sup>+</sup> and CD133<sup>-</sup> cells. Notably, 57.3% ± 9.8 of the CD133<sup>-</sup> cells expressed Pax2. For each cell line, 10 random images were taken and the number of Pax2<sup>+</sup> cells was counted for each of them, together with the number of DAPI<sup>+</sup> cells, to get the total amount of cells (B) Representative immunofluorescence image stained for Vimentin (red) in CD133<sup>+</sup> and CD133<sup>-</sup> cells.

Vimentin, a marker of mesenchymal cells, was found to be expressed in the regenerating epithelium after acute damage and by the scattered tubular cells (Smeets et al., 2013; Witzgall et al., 1994). Here, Vimentin was expressed by all CD133<sup>+</sup> cells (Figure 3.12 B), consistently with previous reports in the literature (Bussolati et al., 2013; Lindgren et al., 2011; Smeets et al., 2013). However, also all CD133<sup>-</sup> cells expressed Vimentin, indicating that the marker is expressed *in vitro* by all renal cells regardless CD133 expression.

### 3.2.6 CHARACTERIZATION OF THE CD133<sup>+</sup> AND CD133<sup>-</sup> POPULATIONS IN CULTURE

The results presented so far showed that a population of CD133<sup>+</sup> cells could be efficiently isolated from the children's kidneys. However, the number of CD133<sup>+</sup> cells in culture greatly exceeded that of CD133<sup>-</sup> cells already at passage 2 (Figure 3.13), suggesting that the CD133<sup>+</sup> cells may proliferate and take over in the primary cultures or that most renal cells start expressing CD133 de novo.

Since one of the aims of this project was to isolate a CD133<sup>+</sup> population for cell therapies, it was essential to assess whether the cells were expandable from every donor, and whether the expression of CD133 was maintained during expansion. Therefore, after isolation, the population doubling time for the CD133<sup>+</sup> population for each sample from passage 2 to passage 3 was recorded (Figure 3.13 A). Interestingly, the CD133<sup>+</sup> population from hK5 could not be expanded after sorting. For all the other samples, PD times are shown in Figure 3.15 A. The healthy sample (hK2) gave rise to a CD133<sup>+</sup> population with the lowest PD time of approximately 30 hours. The correlation between the age of the patients and the population doubling time did not give any significant result (Data not shown; p-value 0.4541). However, the differences among the biological samples were significant (Figure 3.13 A) and this might be explained by the different disease status of the patients. However, information about the patients was not available.

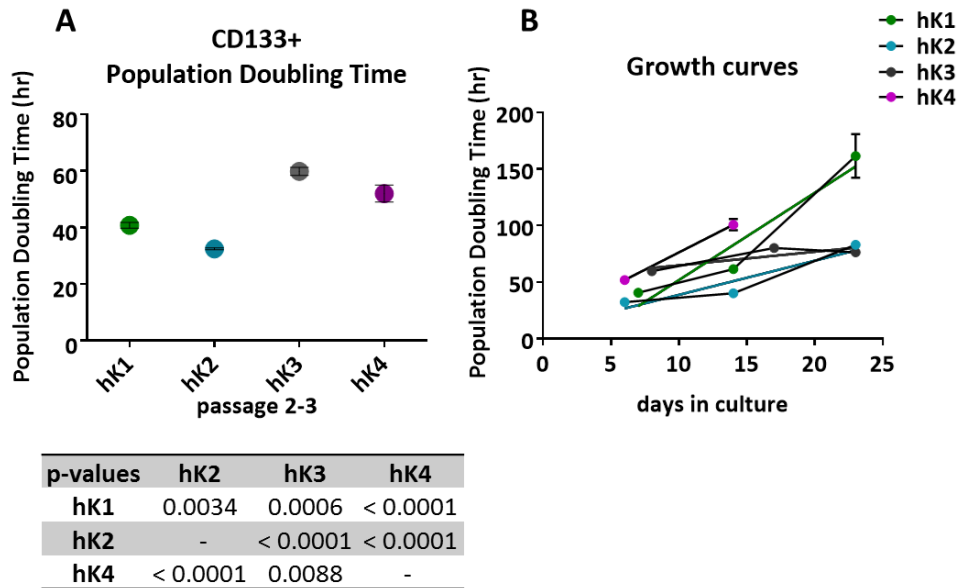


**FIGURE 3.13 CHARACTERIZATION OF CD133<sup>+</sup> POPULATION IN CULTURE**

(A) Population Doubling time (PD time) of four samples (hK1, hK2, hK3, hK4) calculated from passage 2 to passage 3 using the Doubling Time software. An ANOVA test with Dunnett's *Post Hoc* was applied and the p-values of all combinations are listed in (B). (C) PD time of all CD133<sup>+</sup> populations calculated from passage 2 to passage 5. One data point of hK4 was eliminated from the graph since it was too far out from the other samples (1125 hours).

Next, the PD time evaluations were carried out during expansion of the cell populations. The CD133<sup>+</sup> cells were monitored for up to 25 days and counted at every passaging step to obtain the PD time for each passage for each cell line (Figure 3.13 B). For all cell lines, an increase in the PD time was observed at higher passages, indicating that the cells might become senescent over passages. For hK4, the last time point greatly exceeded the PD time of the other samples, reaching 1125 hours. Therefore, hK4 was excluded from further characterizations.

During the sorting process, both CD133<sup>+</sup> and CD133<sup>-</sup> cells were isolated. Figure 3.14 shows representative micrographs of both CD133<sup>+</sup> and CD133<sup>-</sup> cells belonging to hK2 and hK3 five days in culture after sorting. In hK2, the vast majority of the CD133<sup>+</sup> cells maintained a small cuboidal, epithelial-like morphology. By contrast, the CD133<sup>-</sup> cells appeared mainly enlarged and elongated. For hK3, instead, both populations appeared to be quite slow-cycling and did not reach confluency after five days in culture. In the CD133<sup>+</sup> fraction, there were not only small epithelial-like cells but also occasional enlarged cells, also which were also present in the CD133<sup>-</sup> fraction. Small,

compact colonies of epithelial cells, (Fig. 3.14 B) were not unusual to spot in CD133<sup>-</sup> cultures. These colonies may originate from CD133<sup>+</sup> cells, hence representing a contamination of the CD133<sup>+</sup> cells within the CD133<sup>-</sup> population.

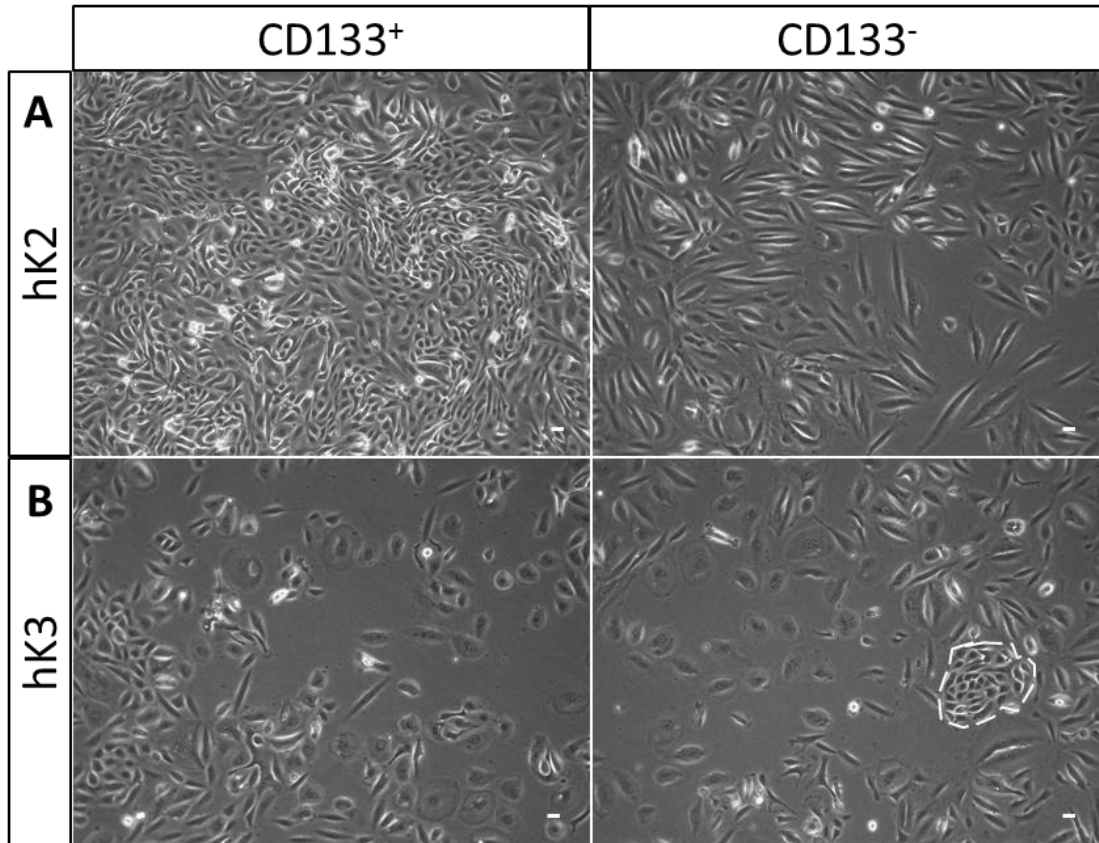


**FIGURE 3.14 BRIGHT FIELD IMAGES OF CD133<sup>+</sup> AND CD133<sup>-</sup> CELLS AT PASSAGE 2**

Bright field images of freshly isolated cells taken five days after the FACS sorting. The dotted line represents a compact colony of epithelial cells, presumably CD133<sup>+</sup> cells. Scale bar represents 50µm.

### 3.2.7 CLONOGENIC POTENTIAL OF CD133<sup>+</sup> AND CD133<sup>-</sup> CELLS

In order to define a progenitor/stem cell as such, it is important to test its potential to self-renew, giving rise to an entire population starting from a single cell. Following this requirement, two methods were used to investigate the clonogenic potential of both populations: Giemsa assay and FACS.

For the Giemsa assay, 100 and 200 CD133<sup>+</sup> or CD133<sup>-</sup> cells at passage two after FACS sorting were seeded in a 6 cm dish (Figure 3.15 A-B). After three weeks in culture, several colonies were observed, each presumably originated from a single cell. The dishes were stained using the Giemsa staining, so that the colonies could be

counted under an inverted microscope. When 100 cells were seeded, both CD133<sup>+</sup> and CD133<sup>-</sup> cells gave rise to around 40 colonies, corresponding to a cloning efficiency of 40%. When 200 cells were seeded, the CD133<sup>-</sup> cells gave rise to almost 80 colonies (cloning efficiency 40%), whereas the CD133<sup>+</sup> cells to about 65 colonies (cloning efficiency 32.5%; t-test, p=0.0198). However, the assay is not entirely reliable, since it is not possible to exclude that two cells in close proximity gave rise to one colony only. Also, some colonies could be found so close to be virtually undistinguishable, and it is not possible to isolate the clones to characterize them further.

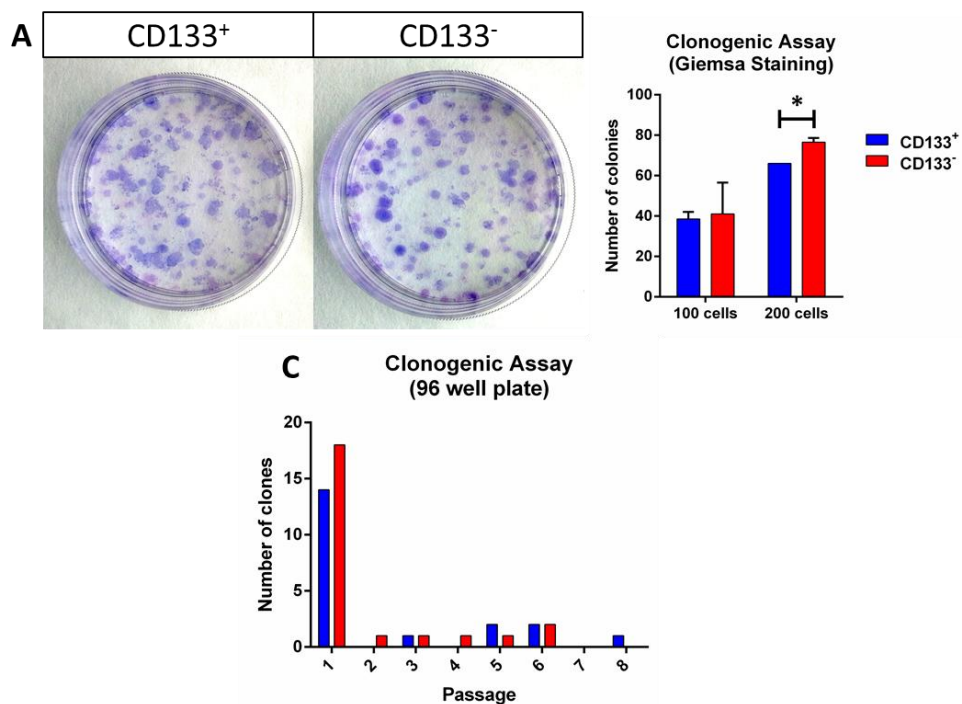


**FIGURE 3.15 CLONOGENIC ASSAY**

(A-B) Giemsa staining. 100 and 200 CD133<sup>+</sup> or CD133<sup>-</sup> cells were seeded in a 6 cm dish after sorting from the heterogeneous population. The dishes contained fresh medium and conditioned medium (1:1) and the cells were left in the incubator for 3 weeks, without a change of medium. After the culture period, the cells were fixed in Methanol, and stained with Giemsa dye, to highlight the cell body. The colonies were scored under an inverted microscope. A un paired t-test was used to establish significance between the CD133<sup>+</sup> and CD133<sup>-</sup> samples, \* p=0.0198, n=3. (C) Sorting on single cells into a 96 well plate from the heterogeneous population. The wells contained fresh medium and conditioned medium (1:1) and the wells were scored for the presence or absence of single cells on day 1. Subsequently, the wells were observed every week until the presence of a confluent well was identified. From the 96 well plate, the colonies were then trypsinized and transferred subsequently to a 48 well plate, 24 well plate, 12 well plate, 6 well plate and 6 cm dish.

To overcome this issue, the CD133<sup>+</sup> and CD133<sup>-</sup> populations were seeded straight after sorting in two 96 well plates at the density of 1 cell per well. Each well contained

a mixture of fresh medium with conditioned medium from the heterogeneous population to better support the growth of the eventual clones. Figure 3.15 shows that both populations were able to give rise to clones. Interestingly, the CD133<sup>+</sup> and CD133<sup>-</sup> cells showed a cloning efficiency of 20% (20 colonies out of 96 wells), and 25% (24 colonies out of 96 wells), respectively (Figure 3.15 C). Most of the clones were found to not expand following the passaging, and only few could be expanded. Having obtained few colonies, the study and the use of clones for following experiments was not pursued further.

Overall, the clonogenic assays performed on both populations do not show any major difference. However, the data suggest that the cell-cell interaction in the 6 cm dish, as for the Giemsa assay, facilitated the growth of colonies.

### **3.2.8 EVALUATION OF THE CD133 EXPRESSION IN BOTH SORTED POPULATIONS DURING EXPANSION**

To ensure that the expression of CD133 was maintained by the whole positive population over passages, and not acquired by the negative population, both CD133<sup>+</sup> and CD133<sup>-</sup> populations from three cell lines (hK1, hK2, and hK3) were monitored for the CD133 expression by FACS over six passages (Figure 3.16 A). After sorting, the number of CD133-expressing cells in the CD133<sup>+</sup> population accounted for more than 95% up to passage 4 to then reach circa 80% at passage 5 and nearly 60% at passage 6. In the CD133<sup>-</sup> population, instead, after sorting, an increase in the number of cells expressing CD133 was reported. From the sorting to passage 3, the number of CD133<sup>+</sup> cells reaches approximately 30% of the whole population, and decreased from passage 5 (Figure 3.16 A). These data can be explained through two mechanisms: the CD133<sup>+</sup> cells proliferated faster than the counterpart or a fraction of the CD133<sup>-</sup> cells started expressing CD133 *de novo*.

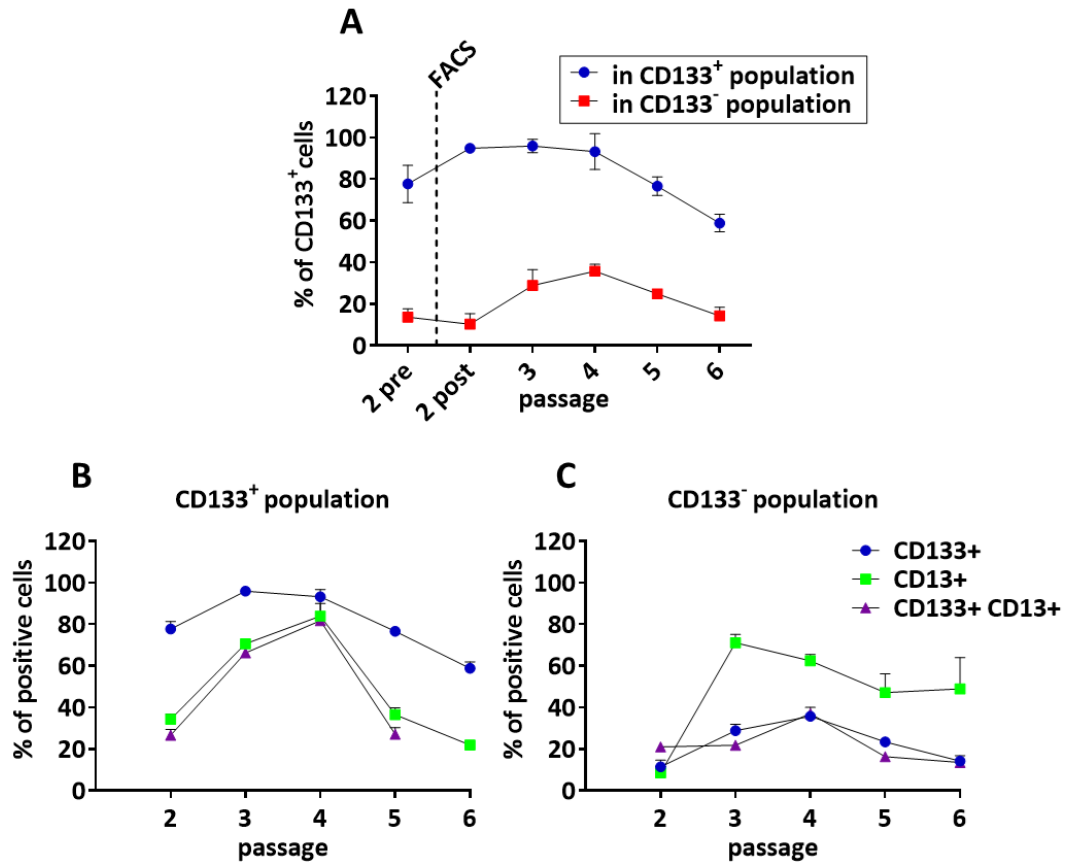


**FIGURE 3.16 CHARACTERIZATION OF CD133<sup>+</sup> AND CD133<sup>-</sup> CELLS DURING EXPANSION**

(A) FACS analysis over 6 passages of changes in CD133 (CD133/2) expression in the CD133<sup>+</sup> and CD133<sup>-</sup> populations of the biological samples hK1, hK2, hK3. (B) FACS analysis over 6 passages of changes in CD13 expression in the CD133<sup>+</sup> population of biological samples hK1, hK2, hK3. CD13 was evaluated alone and together with CD133/2 APC. (C) FACS analysis over 6 passages of changes in CD13 expression in the CD133<sup>-</sup> population of biological samples hK1, hK2, hK3. CD13 was evaluated alone and together with CD133/2 APC. The sorted populations from each sample were expanded twice and the FACS analysis for CD133 was performed in duplicate at each passage. The bars show the SEM.

In addition to the expression of CD133, the two populations were evaluated for the expression of CD13, since it was expressed by a significant portion of the CD133<sup>+</sup> population at passage 2 (Figure 3.8 and Figure 3.16 B-C).

In the CD133<sup>+</sup> population, the amount of the CD13<sup>+</sup> cells increased from passage two onwards, reaching 80% at passage 4. Interestingly, all CD13<sup>+</sup> cells are also CD133<sup>+</sup>. Notably, at passage 5 there is a sudden drop in the expression of CD13, which might reflect a dedifferentiation of the population (Figure 3.16 B). In the CD133<sup>-</sup> population, an exponential increase of the CD13<sup>+</sup> subpopulation was observed. Also in this case, all CD133<sup>+</sup> cells were CD13<sup>+</sup>, but not all CD13<sup>+</sup> cells were CD133<sup>+</sup> positive (Figure 3.16 C).

In summary, the data from the expansion of the cells showed that the positive population maintained the expression of CD133 up to passage 5. In the negative population, it was noted an upregulation of CD133 expression in culture. Importantly, both populations contained a significant fraction of fully-differentiated tubular cells.

Due to these findings, it was decided that in the *in vivo* experiments the cells would be expanded for not more than 4 passages and injected at passage 5, in order to use a relatively pure CD133<sup>+</sup> population. For the negative population a different strategy was chosen: the CD133<sup>-</sup> population was sorted after every passage to remove as many CD133<sup>+</sup> cells as possible. Since the amount of CD133<sup>+</sup> cells did not exceed the 40% of the total number of cells, MACS could be successfully used to achieve a good purity (Data not shown).



### 3.3 DISCUSSION

At the moment, the alternatives for ESRD patients are limited to transplantation and dialysis. However, the shortage of kidneys and the demanding costs of dialysis make it necessary to explore alternative therapies. Cellular therapies might represent this alternative, given that any pure population chosen is tested to be efficacious to ameliorate or slow down the progression of kidney injuries. The beneficial effects of mesenchymal stem cells in preclinical models of kidney injuries are quite established (Grange et al., 2014b). Nevertheless, several groups investigated whether a progenitor population exists in the adult kidney. In 2005, the surface protein CD133, a hallmark of several stem cells and cancer stem cells, was suggested as marker of a putative progenitor population in the adult kidneys, even though its role has not been completely elucidated (Angelotti et al., 2012; Bussolati et al., 2005; Sagrinati et al., 2006).

In the current study, the isolation and characterisation of CD133<sup>+</sup> renal stem/progenitor cells was performed using kidneys biopsies obtained from children. The age range of the samples used was quite wide (6 months to 10 years old) and most patients were hospitalized for recurrent infections, in some cases a consequence of having a duplex kidney. Nevertheless, the CD133<sup>+</sup> population was shown to lie on the Bowman's capsule (BC), and in scattered tubular cells consistent with previous studies (Hansson et al., 2014; Ronconi et al., 2009). In the outer stripe of the medulla, the whole cross-section of the tubuli of the loop of Henle was shown to express CD133. This population may represent the papillary renal stem cells identified in mice (Oliver et al., 2004) and in humans (Bussolati et al., 2013). Therefore, our results show that in children's kidneys, localisation of CD133 expression is consistent with that previously described in adult kidneys, and regardless of the underlying renal disease (Bussolati et al., 2005; Hansson et al., 2014). Interestingly, sporadic CD133<sup>+</sup> cells were spotted inside the glomerulus, especially in hK4 (Figure 3.1). In previous studies, it was hypothesized that human CD133<sup>+</sup> cells migrate from the luminal pole of the BC towards the tuft of the glomerulus to differentiate into podocytes (Ronconi et al., 2009), as it was shown for PEC cells in mice during adolescence (Appel et al., 2009). In the samples of this study, the staining observed inside the glomerulus was more likely

to represent the contribution of parietal epithelial cells to a glomerular lesion, as in the case of glomerulosclerosis, or the dedifferentiation of fully differentiated podocytes in response to glomerular damage (Smeets et al., 2009; Smeets et al., 2011). Since the information about the renal damage of the patients of this study is not available, it is hard to rule out one or the other possibility.

Previously published studies reported that, consistently with the notion of representing stem/progenitor cells in the kidney, CD133<sup>+</sup> cells account for approximately the 0.5-4% of the total number of cells isolated from adult kidneys (Sagrinati et al., 2006). Those evaluations were carried out on freshly isolated cells before plating. In this chapter we have described the isolation and characterisation of five cell lines from 5 biological samples (kidney biopsies). In the cell populations of all biological samples at passage two (P2), after five-to-seven days in culture, the content of CD133<sup>+</sup> cells ranged from 40% (hK4) to over 90% (hK3) (Figure 3.4). The FACS data at P2 suggested that once in culture the CD133<sup>+</sup> cells proliferated quicker than the CD133<sup>-</sup> counterpart. Alternatively, it can be hypothesized that the cells acquired CD133 expression as an adaptation to the culture conditions. It is possible that the medium used in this study, which has been reported to maintain fetal metanephric cells in culture (Price et al., 2007), can eventually play a role in the selective expansion of the CD133<sup>+</sup> population. Initially, the two monoclonal CD133 antibodies CD133/1 (AC133) and CD133/2 (293C3) were used to characterize the isolated populations (Angelotti et al., 2010). It was interesting to notice that there were differences in the number of cells that expressed the two specific epitopes. This finding has never been reported before and it is difficult to explain. The role of CD133/prominin or its glycosylated epitopes in maintaining or defining the stem cell phenotype is still unclear (Fargeas, 2006).

Once in culture, all cell lines looked highly heterogeneous and displayed both compact epithelial colonies and mesenchymal-like cells. A comprehensive analysis of the surface marker profile was performed to characterise the isolated cells. Firstly, the expression of CD24 was assessed, since all CD133<sup>+</sup> have been described to express CD24 (Figure 3.5) (Romagnani and Remuzzi, 2014). Our analysis revealed that virtually all CD133<sup>+</sup> cells in culture expressed CD24, but not all CD24<sup>+</sup> cells expressed CD133.

CD24 has been described as a marker of stem cells and cancer stem cells, restricted to metabolically active cells and progenitor cells and not present on fully differentiated cells (Fang et al., 2010). Similarly to CD133, its role in the context of stem cell properties has not been elucidated. It has been identified on epithelial cells in many organs and is therefore often regarded as an epithelial marker (Fang et al., 2010). Based on our findings and the known characteristics of CD24, we decided to carry out our further studies based on the expression of CD133 only (Bussolati et al., 2005; Ronconi et al., 2009; Sagrinati et al., 2006).

The bulk population was interrogated for a series of markers that would elucidate their phenotype (see Table 3.2). We looked at canonical markers of mesenchymal stem cells (Figure 3.7). CD73 and CD44 were previously shown to be expressed on renal progenitor CD133<sup>+</sup> cells (Bussolati et al., 2005; Bussolati et al., 2013). Conversely, the cells do not express high levels of CD90. The expression of CD90 seems quite controversial in the literature, where in one study CD90 was found in the majority of the cells isolated from adult kidneys (Bussolati et al., 2005), whereas in another study CD90 is expressed in less than 30% of the isolated cells (Metsuyanin et al., 2009). The difference can be explained by different culture conditions used. However, CD90 has also been used to identify and purify fibroblasts in human primary cell lines (Kisselbach et al., 2009). It is therefore a possibility that following the isolation procedure no fibroblasts were isolated in all samples except hK4, which would be consistent with the cell morphology of hK4, where more spindle-like cells were observed (Figure 3.3).

In our analysis, the epithelial markers CD326 (EpCam, Epithelial Cell Adhesion Molecule) and CD324 (E-Cadherin) were present in virtually 100% of the population (Figure 3.8). In particular, EpCam-positive cells displayed considerable homogeneity in the staining intensity, in contrast to analysis performed on human fetal kidney cells by Metsuyanin and colleagues (Metsuyanin et al., 2009). They argued that the presence of EpCam<sup>bright</sup> and EpCam<sup>dim</sup> populations was indicative of the presence of differentiated cells and progenitor cells, respectively. Their conclusion was based on the observation that during fetal development EpCam is expressed in the ureteric bud, comma-shaped and S-shaped bodies, but not in the metanephric mesenchyme (MM)

which contains the renal multipotent progenitor population (Metsuyanin et al., 2009). Thus, according to the hypothesis by Metsuyanin and colleagues, the cell populations isolated in this study would be fully differentiated. Interestingly, EpCam was identified on the surface of regenerating epithelia (Trzpis et al., 2008).

CD13 (aminopeptidase N) is a marker of fully differentiated proximal tubular cells (Baer et al., 1997). Our analysis is the first of its kind to characterize a primary renal population for the expression of CD13 (Figure 3.8). However, recently, the expression of CD13 was shown on CD133<sup>+</sup>/NCAM<sup>-</sup> fetal-derived cells (Pode-Shakked et al., 2016). Here, the results can be interpreted in different ways: If CD133 is a true marker of putative progenitor cells, then CD13 identified a sub-population of progenitor cells already committed towards the tubular fate. Alternatively, if CD133 is acquired in culture as an adaptation to the *in vitro* conditions, then all tubular cells that proliferate in culture would acquire CD133. It needs to be pointed out that the medium used to isolate the cells might play an important role here. Despite its use to culture fetal progenitor cells (Price et al., 2007), the same protocol was retrieved in studies that isolated and cultured proximal tubular cells (Van der Hauwaert et al., 2013). It might be possible, therefore, that the culture conditions used in this study either promote the expansion of progenitor cells with tubular commitment or the upregulation of CD133 expression in cells with tubular commitment.

To obtain a deeper understanding of the heterogeneous status of the primary cultures we had isolated, the putative renal progenitor markers NCAM1 and Tra-1-60 were evaluated (Figure 3.9). NCAM1 (CD56) has been identified in the nephrogenic zone of the developing kidney, and it was also found on a small percentage of adult kidney epithelial cells (Buzhor et al., 2013). Our analysis showed that only a small percentage of CD56<sup>+</sup> cells was detected (with the exception of hK4) in primary cultures of all biological samples, which is consistent with what has been previously described (Metsuyanin et al., 2009).

Tra-1-60, an isoform of the proteoglycan podocalyxin, is expressed in the Bowman's capsule and has been linked to renal epithelial cell polarization and tubulogenesis. However, podocalyxin is also expressed in mature podocytes (Fesenko et al., 2010). Interestingly, in our primary cell populations at least half the cells

expressed Tra-1-60, and in addition, the majority of them also co-expressed CD133. However, the investigation of the features of Tra-1-60<sup>+</sup> cells was not done *in vitro*, so its function in context of progenitor cells remains elusive (Fesenko et al., 2010). It is possible that CD133<sup>+</sup>/Tra-1-60<sup>+</sup> cells represent a progenitor population committed towards podocytes, but there is no evidence in the literature to support this hypothesis.

It should be mentioned as well that it was attempted to generate clonal populations at the start of the project. However, the clones proved to be difficult to expand and characterize (Figure 3.15). Therefore, it was decided to study the bulk population. Further research to dissect even further the heterogeneity observed could involve molecular profiling of a large pool of single CD133<sup>+</sup> cell to exactly determine its phenotypical composition.

The aim of the study was to isolate CD133<sup>+</sup> cells and test their potential in an *in vivo* model of acute kidney injury (chapter 5). As a negative cell population, we envisaged to use CD133<sup>-</sup> cells. Therefore, the samples were sorted for the expression of CD133. Both MACS and FACS technologies were compared to assess which techniques achieved the highest purity in both CD133<sup>+</sup> and CD133<sup>-</sup> cell populations (Figure 3.10). MACS gave a higher yield in terms of cell numbers but a lower purity than FACS. This is in contrast to what has been shown in the literature, where MACS were used to isolate the CD133<sup>+</sup> population (Angelotti et al., 2012; Bussolati et al., 2005; Ronconi et al., 2009; Sagrinati et al., 2006). However, in all these studies, the CD133<sup>+</sup> cells were isolated soon after the dissociation of cells from the tissue, when 1%-4% of the cells are CD133<sup>+</sup> (Bussolati et al., 2005; Sagrinati et al., 2006). Therefore, our inability to isolate a highly pure CD133<sup>-</sup> cell population using MACS was attributed to the high number of CD133<sup>+</sup> cells in the population to sort. Importantly, how FACS and MACS can affect specific stem cell function still remains largely unknown.

Once sorted, the CD133<sup>+</sup> and CD133<sup>-</sup> populations were further characterized by immunofluorescence for the expression of Pax2 and Wt1, two transcription factors expressed in the metanephric mesenchyme (Reidy and Rosenblum, 2009), and Vimentin, a marker for mesenchymal cells which has been also associated with de-differentiation and regenerating epithelia (Smeets et al., 2013). Our analysis showed

that both the CD133<sup>+</sup> and CD133<sup>-</sup> populations expressed Wt1. Since Wt1 is expressed in both PEC and podocytes in mouse and humans (Bussolati et al., 2005; Kabgani et al., 2012), our results are not surprising. Our results also showed that all CD133<sup>+</sup> cells and approximately 60% of the CD133<sup>-</sup> cells expressed Pax2. Pax2 expression had been previously identified *in vitro* in CD133<sup>+</sup> cells by Bussolati and colleagues (Bussolati et al., 2005). Pax2 is not expressed in adult tissues *in vivo*, but was shown to be re-expressed after acute injury on tubular cells (Ye et al., 2011). Here, we observe its expression in the majority of the cells, including CD133<sup>-</sup> cells. Also, both populations also expressed Vimentin, regardless of CD133 expression.

Taken together, the characterization data demonstrated high levels of heterogeneity in the primary cultures, which needs to be further analysed. *In vitro*, the cells express markers that have been identified *in vivo* on regenerating epithelia, including Pax2, EpCam, Vimentin, CD44, Tra-1-60, regardless of the CD133 expression (Asselman et al., 2003; Fesenko et al., 2010; Smeets et al., 2013; Trzpis et al., 2008; Witzgall et al., 1994; Ye et al., 2011). By plating the bulk population, we might be therefore expanding what it would be the population responsible for the regeneration of the tubular epithelium *in vivo*. Whether this population is the PEC or the STC population it cannot be determined, since the marker CD106, that distinguishes between the two putative progenitor populations, was not utilized in this study. Also, since the sorting of the CD133<sup>+</sup> cells was carried out on cells cultured for one or even two passages, it is possible that the CD133<sup>+</sup> cells obtained do not represent the previously reported population (Ronconi et al., 2009; Sagrinati et al., 2006), and were phenotypically altered by the culture conditions. In addition, since the whole kidney was available for one of the patients (hK2), it could have been feasible to separate the tubular and glomerular compartments, and then sort for CD133, to investigate different progenitor potentials in the two renal compartments.

Morphologically, the two isolated populations showed marked differences, since the CD133<sup>+</sup> cells had predominantly a polygonal epithelial-like phenotype, whereas the CD133<sup>-</sup> cells appeared mostly enlarged and elongated. However, even in the CD133<sup>-</sup> fraction, it was not unusual to find small epithelial colonies. Indeed, a further characterization by FACS of both CD133<sup>+</sup> and CD133<sup>-</sup> cells over few passages in culture

showed that there is an increase of the CD133<sup>+</sup> fraction in the CD133<sup>-</sup> population. Importantly, most of the CD133<sup>+</sup> cells were CD13<sup>+</sup> until P5, when a substantial drop in the expression of CD13 was observed. This drop is consistent with the loss of markers specific for the fully differentiated cells, as it was documented for primary proximal tubule cells and podocytes (Okamura et al., 2009; Wilmer et al., 2010). Take together, this data can be interpreted in two ways: i) the progenitor population pre-committed to a tubular fate expands over time, or ii) the CD133<sup>+</sup> cells acquire the CD13 expression in culture, probably fostered by the culture medium.

Finally, the CD133<sup>+</sup> populations were analysed for their population doubling time (PD time) in culture. There were significant differences between the PD times of all samples, which probably reflected the renal health of the patients. Interestingly, one sample (hK5) could not be expanded. The possible differences between samples in terms of expandability have never been investigated, but it should be of great importance when considering autologous cellular therapies.

In summary, in this chapter, it was shown that putative progenitor cells could be isolated from young kidneys. The phenotypical analysis of the samples proved that the progenitor populations were heterogeneous, having both epithelial and mesenchymal characteristics. It would be expected that a progenitor population, isolated through the expression of a *bona fide* marker, such as CD133, would be quite homogeneous. Instead, other subpopulations were identified, carrying fully differentiated markers (CD13) or other putative progenitor markers (CD56 and Tra-1-60). Interestingly, markers associated with the dedifferentiation/regeneration of tubular cells, such as Pax2, Vimentin, and EpCam were also expressed *in vitro*. It is, therefore, possible that the population isolated is the one that had been described to proliferate in response to injury in the tubular compartment. The isolated cells will be tested for differentiation capacity and ability to integrate into an *ex vivo* chimeric assay in the next chapter and for their amelioration potential *in vivo* in chapter 5.





## **4 INVESTIGATING THE ABILITY OF CD133<sup>+</sup> AND CD133<sup>-</sup> CELLS TO DIFFERENTIATE INTO PODOCYTES AND TO INTEGRATE IN A CHIMERIC RUDIMENT**

### **4.1 INTRODUCTION AND AIMS**

In the previous chapter, the isolation of a renal cell population from biopsy tissues obtained from children was reported. Upon isolation, most of the renal cells expressed CD133, marker of renal progenitor cells. The nature of the isolated cells was characterized and compared to the CD133<sup>-</sup> counterpart. The CD133<sup>+</sup> population appeared quite heterogeneous and expressing markers of both epithelial and mesenchymal cells. Importantly, the vast majority of CD133<sup>+</sup> cells expressed CD13, a marker of fully differentiated proximal tubular cells. The CD133<sup>+</sup> population could be expanded in culture for up to 6 passages, but it started losing the expression of the marker by passage 5. Instead, in the CD133<sup>-</sup> fraction, an increase of CD133-expressing cells was observed. It would appear as the CD133<sup>+</sup> population has proliferative potential *in vitro*.

In this chapter, two aspects of the CD133<sup>+</sup> and CD133<sup>-</sup> cells described in chapter 3 will be investigated, in order to demonstrate their renal progenitor potential: (i) the differentiation potential towards a specialized renal cell type; and (ii) the ability of the progenitors to integrate into developing structures of a chimeric rudiment. The first aspect has been used in previous studies to test the putative progenitor population. The second feature is relatively unexplored for the CD133<sup>+</sup> population. In both cases, the CD133<sup>-</sup> will be used as negative control.

If the CD133<sup>+</sup> truly represents a population of renal progenitor cells, it can be expected that they might somehow contribute to the formation of de novo tubuli

during the reorganization of the mouse embryonic renal cells. In contrast, the CD133<sup>-</sup> population would rather occupy the stromal space within the chimera without any sign of integration.

Specifically, the following objectives will be addressed:

1. Investigate the differentiation potential of CD133<sup>+</sup> and CD133<sup>-</sup> cells isolated from young adults kidneys, specifically towards podocytes;
2. Analyse the nephrogenic potential of CD133<sup>+</sup> and CD133<sup>-</sup> cells in the chimeric kidney rudiment assay, in comparison to control reaggregated rudiments and chimeric rudiments using a positive control cell line;
3. Modify the kidney rudiment assay to make it suitable for the LSM.

## 4.2 RESULTS

### 4.2.1 PREPARATION OF CD133<sup>+</sup> AND CD133<sup>-</sup>-GFP-LABELLED

The heterogeneous population of cells isolated from hK2 had been cryopreserved at passage 1 (see chapter 3). In preparation for the reaggregation assay and the *in vivo* study, cells were thawed, and upon attachment, transduced with a pHIV-GFP viral vector using an MOI (Multiplicity of Infection) of 5. The transduced cells were expanded for one passage before sorting for the expression of CD133 using the FACS Aria. The efficiency of transduction was qualitatively confirmed under the fluorescence microscope (Figure 4.1) and quantitatively assessed during the sorting, yielding to 88.3% ± 6.5 of the cell population, over three independent sortings.

The following sorting strategy was pursued to achieve two populations, of either CD133<sup>+</sup> or CD133<sup>-</sup> cells, as shown in Figure 4.2:

- Cells with an FSC-A lower than 70 were considered dead cells and excluded by gating. Higher and SSC-A signals indicated increased granularity and therefore likely dying cells. Therefore, the population of healthy cells, defined as Parental (P1) was considered for further analysis (Figure 4.2 A).
- The doublet content in the population was further characterized using the Forward Scatter-Width (FSC-W) parameter. Cells with high FCS-W were gated out of the actual sorting (Figure 4.2 B).

- Finally, a density plot was generated to define the amount of cells that were either CD133<sup>+</sup>/GFP<sup>+</sup>, CD133<sup>+</sup>/GFP<sup>-</sup>, CD133<sup>-</sup>/GFP<sup>+</sup>, or CD133<sup>-</sup>/GFP<sup>-</sup>. It should be noted that a small fraction of CD133<sup>+</sup> cells is not efficiently transfected with the vector pHIV-GFP, shown in Figure 4.2 C, Q1.

Due to the overall high labelling efficiency, the sortings were based only on the expression of CD133/2 (APC-labelled, FL4). The purity immediately after the sortings was comparable for the two cell types ( $94.9 \pm 3.7\%$  vs.  $92.0 \pm 1.8\%$ , CD133<sup>+</sup> vs. CD133<sup>-</sup>).

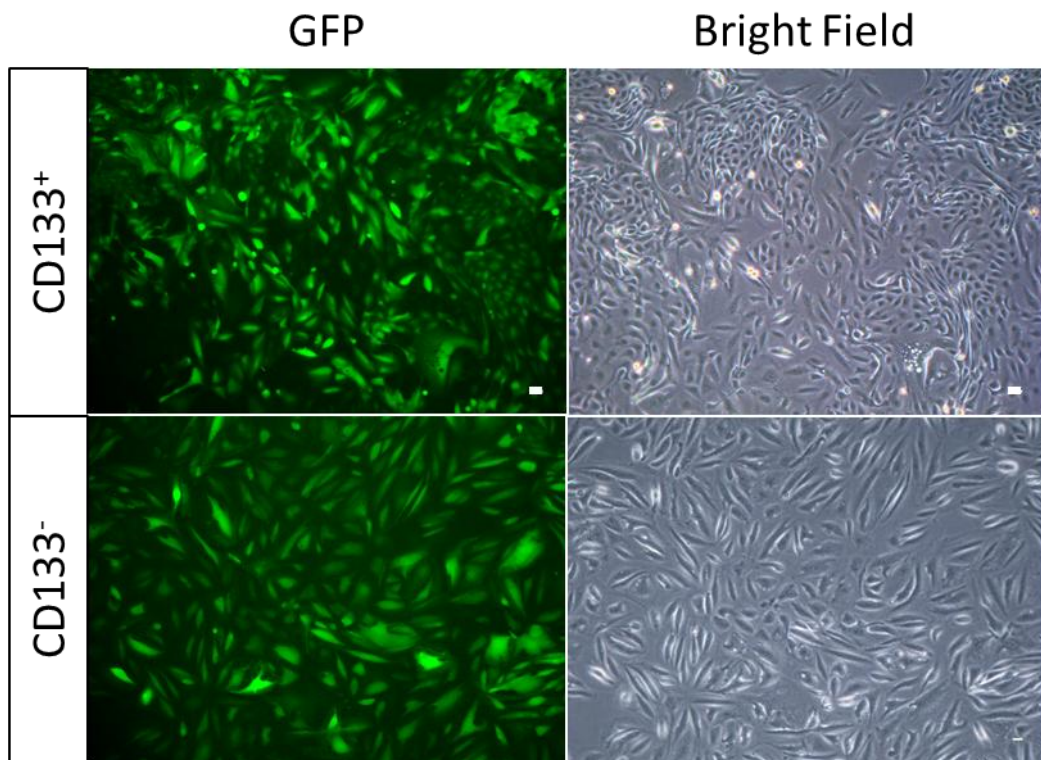


**FIGURE 4.1 MICROGRAPHS OF CD133<sup>+</sup>GFP<sup>+</sup> AND CD133<sup>-</sup>GFP<sup>+</sup> CELLS AT P3**

Representative pictures of CD133<sup>+</sup>GFP<sup>+</sup> cells and CD133<sup>-</sup>GFP<sup>+</sup> cells at P3. All green fluorescence pictures were taken with the same exposure conditions (5 seconds). Scale bars correspond to 50  $\mu\text{m}$ .

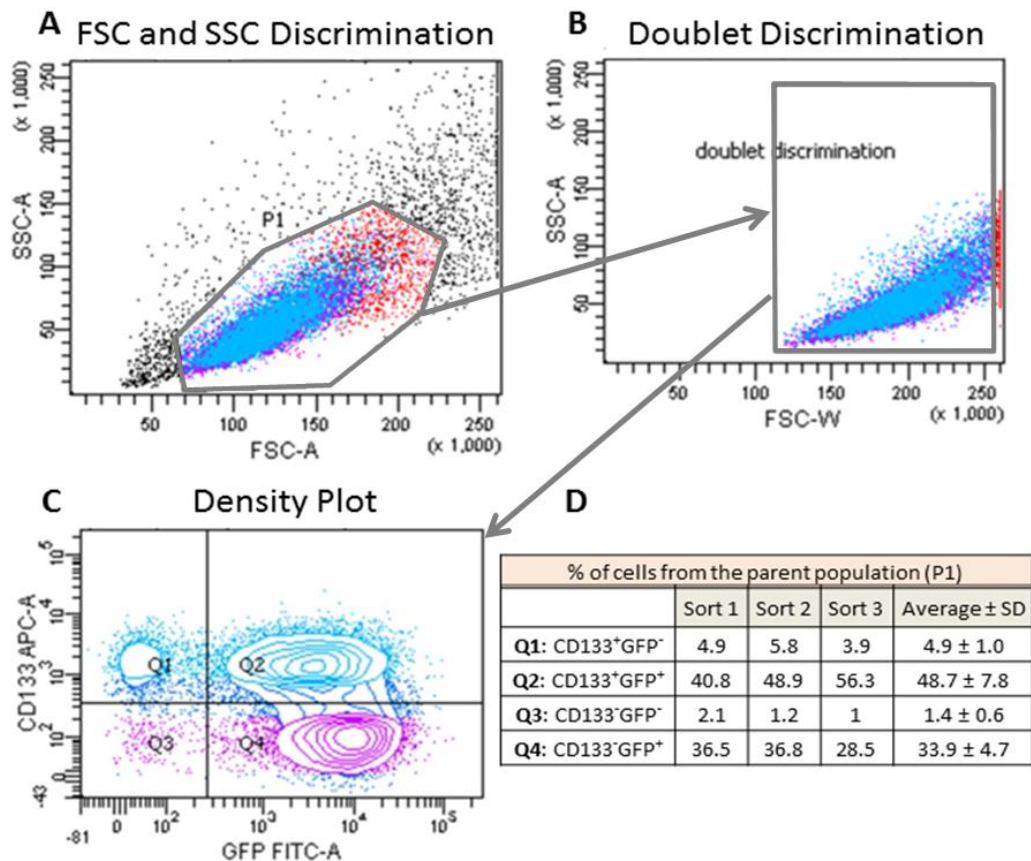


**FIGURE 4.2 SORTING STRATEGY USED TO SORT CD133<sup>+</sup>GFP<sup>+</sup> AND CD133<sup>-</sup>GFP<sup>+</sup>**

(A) Dot Plot showing Forward Scatter-Area (FSC-A) and Side Scatter –Area (SSC-A) used to discriminate healthy and damaged or dying cells. (B) Dot plot of SSC-A and Forward Scatter-Width (FSC-W) used to discriminate doublets, which might represent a false positive signal. (C) Density plot obtained plotting the signal from the excitation of cells with the 488-nm laser (GFP FITC-A, log scale) against the signal from the FL4 laser (APC-A, log scale). Due to the high efficiency of GFP labelling, the CD133<sup>+</sup>GFP<sup>-</sup> population was neglected, and the sorting was based only on the expression of CD133 (Q1+Q2 vs. Q3+Q4) (D) The lentiviral transduction and the sortings were performed three times on independent cryopreserved hK2 cells. The table summarizes the percentages of cells obtained during the three independent sortings, reported according to the quadrants they belonged to.

#### **4.2.2 ANALYSING THE POTENTIAL OF CD133<sup>+/-</sup> RENAL PROGENITOR CELLS TO DIFFERENTIATE INTO PODOCYTES**

The first aim of this part of the study was to assess the differentiation potential of the isolated CD133<sup>+</sup> and CD133<sup>-</sup> cells. Both sorted populations, derived from hK2, were seeded at passage 2 or 3 at low density (10.000 cells/well in a 6 well plate) and treated for seven days with VRAD medium, containing 100 µM of All-Trans-Retinoic Acid (ATRA) and 100 nM Vitamin D3. In parallel, both CD133<sup>+</sup> and CD133<sup>-</sup> cells were treated with VRAD control medium. After seven days, both VRAD-treated populations

showed a drastic change in the proliferation rate and morphology when compared to the populations treated with the VRAD control medium (Figure 4.3). Specifically, both CD133<sup>+</sup> and CD133<sup>-</sup> cells treated with the VRAD medium stopped proliferating and, most importantly, showed an enlarged and arborized cell body, typical of podocytes.

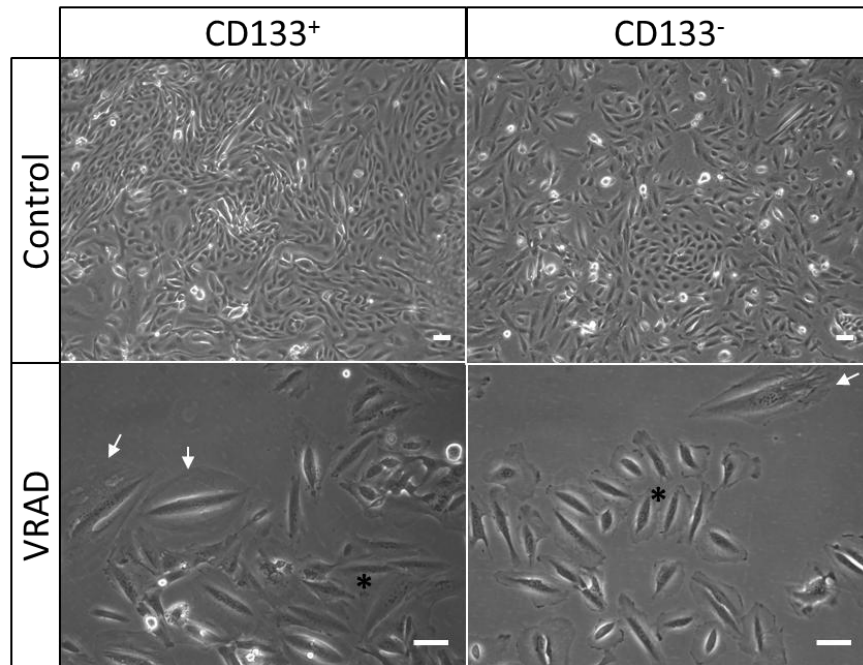


**FIGURE 4.3 REPRESENTATIVE BRIGHT FIELD IMAGES OF CD133<sup>+</sup> AND CD133<sup>-</sup> CELLS CULTURED IN VRAD CONTROL OR FULL VRAD MEDIUM FOR SEVEN DAYS.**

10<sup>4</sup> CD133<sup>+</sup> or CD133<sup>-</sup> cells were seeded in a 6 well plate in HPRC medium overnight. The following day, the medium was changed for either VRAD or control medium and refreshed every two-three days. After 7 days, the cells appeared as in the figure above. The cells in control medium grew as normal. Following treatment with VRAD medium, instead, the cells stopped proliferating, their cell body became enlarged (\*) and arborized cells appeared (indicated by arrowheads). Scale bars represent 50  $\mu$ m.

To compare the differentiated cells, conditionally immortalized podocytes (ciPodo) and primary podocytes were used. ciPodo is an immortalized cell line consisting of proliferative immature podocytes when grown at the permissive temperature of 33°C while when cultured at 37°C for 14 days the cells undergo complete differentiation (Saleem et al., 2002). ciPodo cells grown under differentiating conditions at 37°C had enlarged cell bodies, and some of them were binucleated (Figure 4.4). In addition, primary human podocytes were isolated from hK6 by isolating and plating the glomeruli with or without Bowman's capsule (inset in Figure 4.4 B). After several days in culture, outgrowths of cells could be observed. The outgrowths were passaged for

up to 5 passages. The cells display features of podocytes, including enlarged and arborized cell body and occasional binucleated cells.

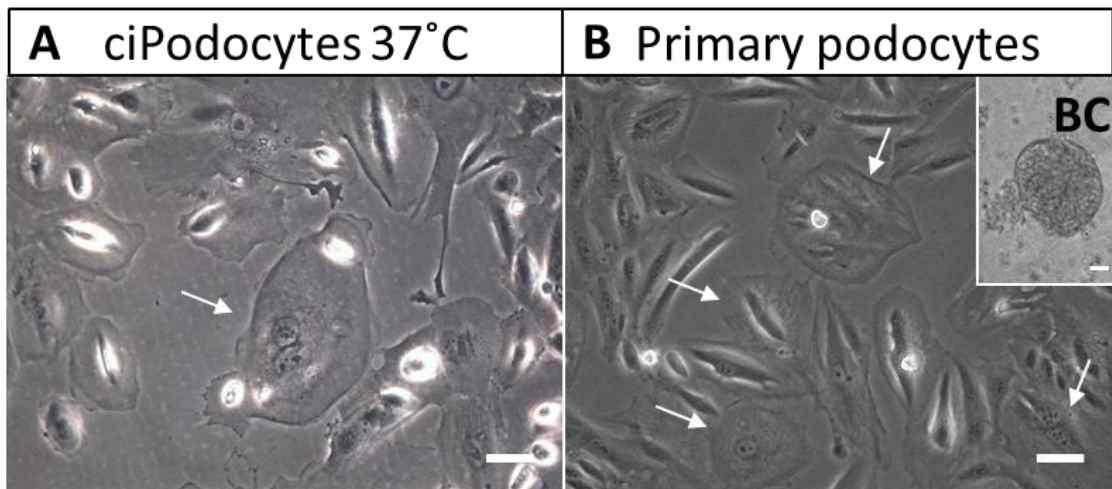


**FIGURE 4.4 REPRESENTATIVE BRIGHT FIELD IMAGES OF DIFFERENTIATED CIPODOCYTES AND PRIMARY HUMAN PODOCYTES IN CULTURE**

(A) ciPodocytes were grown at 33°C until 60% confluence and then grown at 37°C for at least 7 seven days to induce differentiation. Binucleated arborized cells (arrows) were not unusual to spot in culture. (B) Primary podocytes were obtained by plating entire glomeruli with or without Bowman's capsule (BC), as shown in the inset. After at least seven days in RPMI+10% FCS, cells were growing out of the glomeruli. The outgrowths were then passaged for up to 5 passages. Here, P5 hK6 glomerular outgrowths are shown. Arborized, binucleated cells (arrows) can be observed. Scale bars represent 50  $\mu\text{m}$

#### **4.2.2.1 EXPRESSION OF MARKERS OF PODOCYTES**

VRAD- and control-treated CD133<sup>+</sup> and CD133<sup>-</sup> cells were tested for the expression of two podocyte-specific markers: podocin and nephrin. Both proteins are essential for the maintenance of the slit diaphragms in podocytes. Interestingly, following seven days of culture in VRAD medium, both CD133<sup>+</sup> and CD133<sup>-</sup> cells showed the expression of podocin and nephrin (Figure 4.6 A and B). Immunofluorescence for podocin revealed a distribution which overlaps with the cytoskeleton, with occasional stronger staining in the foot processes of some cells. By contrast, nephrin was concentrated on the cortical ring of the cytoskeleton of the cells, especially in the CD133<sup>-</sup> population. Conversely, the cells cultured in control medium for seven days failed to show any staining for Nephrin or Podocin, suggesting that the VRAD medium induced the expression of podocyte-specific markers.

For comparison, immunofluorescence stainings for nephrin and podocin were also performed on primary human podocytes at passage 4 and ciPodo grown at 37°C for ten days. In the ciPodo, podocin displayed the same distribution as the VRAD-treated human cells, closely resembling the pattern previously shown in the literature (Saleem et al., 2002). In the primary human podocytes, instead, podocin appeared not only overlapping with the cytoskeleton, but also or accumulated in the periphery of the cells (Figure 4.6 C).

The nephrin staining in the primary podocytes and ciPodo, instead, was comparable to the staining obtained for the human cells with a diffused distribution in the cytoskeleton and concentrated localization at the cell periphery.

To summarize, it seems that the following stimulation with VRAD medium, both CD133<sup>+</sup> and CD133<sup>-</sup> cells do express markers that are physiologically expressed in podocytes.



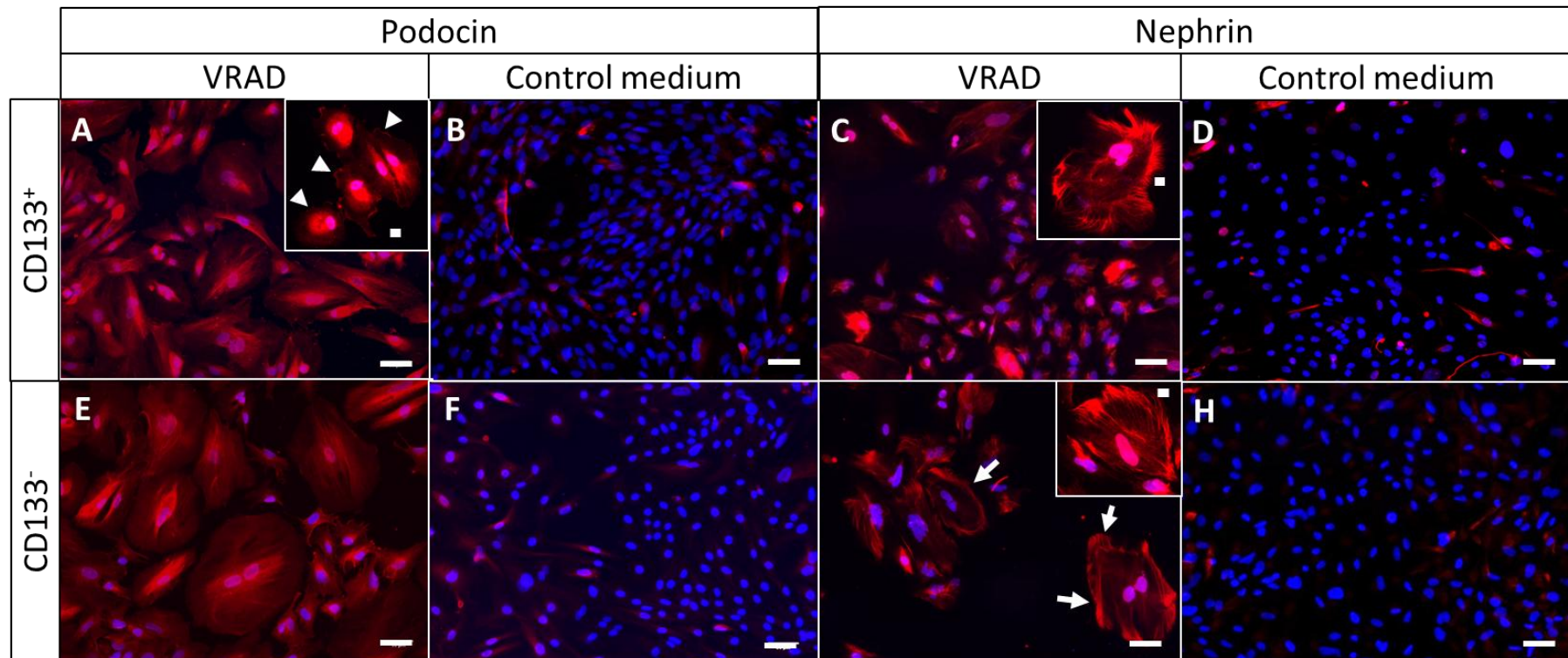


**FIGURE 4.5 EXPRESSION OF PODOCIN AND NEPHRIN IN HUMAN CD133<sup>+</sup> AND CD133<sup>-</sup> CELLS AFTER SEVEN DAYS IN VRAD OR CONTROL MEDIUM**

Representative immunofluorescence images showing (A-D) CD133<sup>+</sup> and (E-H) CD133<sup>-</sup> cells cultured in VRAD or control medium stained for podocin and nephrin (red). 10<sup>4</sup> CD133<sup>+</sup> and CD133<sup>-</sup> cells were seeded in a 6 well plate and let to attach overnight in renal progenitor medium. The day after the medium was changed for VRAD medium or control medium. The assay lasted in total seven days, with two changes of medium. The VRAD medium, but not the control medium, induced the expression of podocin and nephrin. Insets show high magnification images. Arrowheads point towards the accumulation of podocin on the edges of the cells. White arrows indicate the accumulation of nephrin into the cortical ring of the cytoskeleton. Scale bars represent 50  $\mu$ m.



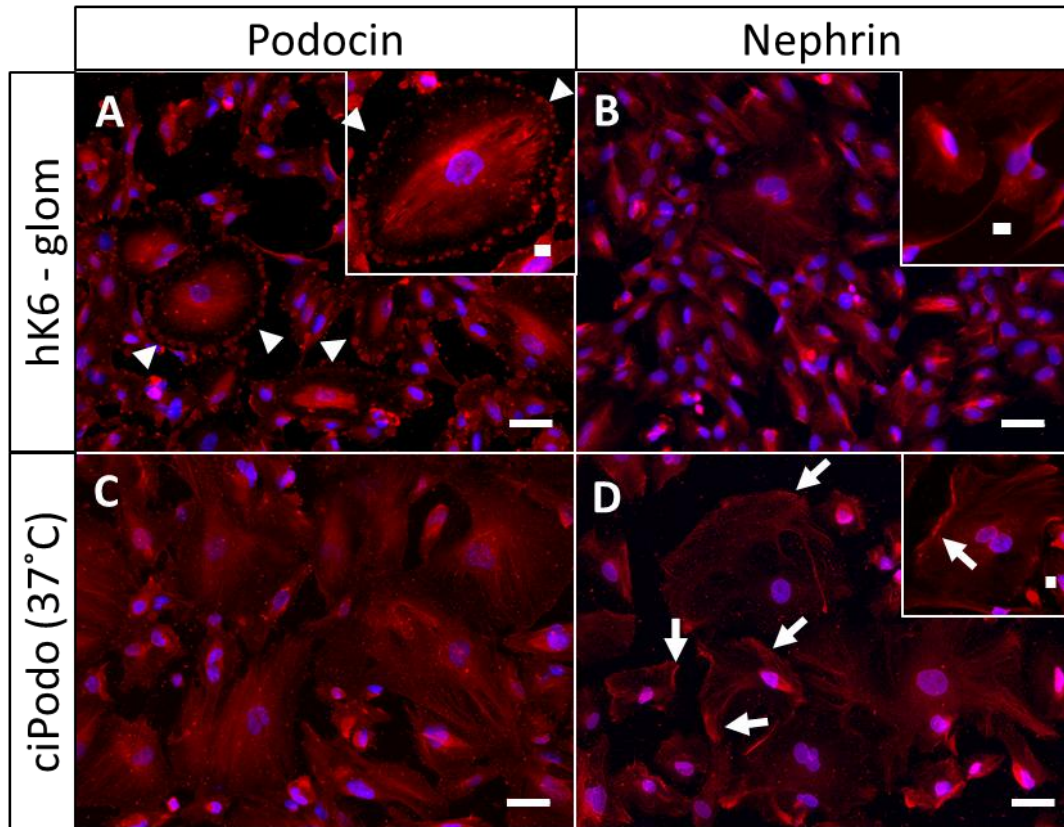


**FIGURE 4.6 REPRESENTATIVE IMMUNOFLUORESCENCE IMAGES SHOWING HK6-DERIVED PRIMARY PODOCYTES AND CIPODOCYTES STAINED FOR PODOCIN AND NEPHRIN**

(A-B) hK6-derived podocytes at passage 4 and (C-D) ciPodocytes grown at 37°C were stained for podocin (red) and nephrin (red). The insets show high magnification images. Arrowheads point towards the accumulation of podocin on the edges of the cells. White arrows indicate the accumulation of nephrin into the cortical ring of the cytoskeleton. Scale bars represent 50  $\mu\text{m}$ .

#### 4.2.2.2 CELL CYCLE ANALYSIS OF DIFFERENTIATED PODOCYTES

In the previous paragraph, it was reported that the VRAD medium was able to induce the expression of podocin and nephrin in both CD133<sup>+</sup> and CD133<sup>-</sup> cells. Podocytes are fully differentiated post-mitotic cells, with a typical arborized morphology and, often, binucleated. With the aim to provide a more comprehensive characterization, the cell cycle of both cell types was analysed by FACS after seven days in either VRAD or control medium.

To start, the ploidy of the cells was taken into account, hypothesising that binucleated cells would be tetraploids.

Upon treatment with VRAD, both cell types presented a significantly higher number of tetraploid cells compared to the control groups (CD133<sup>+</sup>: Ctrl 3.48% ± 1.14 vs VRAD 13.77% ± 1.83 p<0.0001, unpaired t-test; CD133<sup>-</sup>: Ctrl 2.45% ± 1.07 vs VRAD 11.62% ± 1.99 p=0.0116, unpaired t-test) (Figure 4.7 A and B). This increase in tetraploid cells may indicate that following treatment with VRAD medium the number of binucleated cells increased as a consequence of the cells being unable to complete mitosis.

Next, the distribution of the phases of the cell cycle was investigated. Figure 4.7 C shows representative cell cycle histograms obtained by FACS of the CD133<sup>+</sup> cells treated with control medium or VRAD. The results showed that the VRAD treatment significantly increased the population of cells arrested in the G<sub>2</sub>/M phase of the cell cycle (CD133<sup>+</sup>: Ctrl 6.92% ± 0.98 vs VRAD 18.55% ± 1.78, p=0.0014, unpaired t-test; CD133<sup>-</sup>: Ctrl 6.55% ± 0.75 vs VRAD 18.68% ± 3.13, p=0.0243, unpaired t-test; Figure 4.7 D and E). Interestingly, a significant increase in the population of cells in S phase was also observed in both the CD133<sup>+</sup> and CD133<sup>-</sup> population upon treatment (CD133<sup>+</sup>: Ctrl 7.53% ± 0.71 vs VRAD 14.05% ± 1.58, p=0.0159, unpaired t-test; CD133<sup>-</sup>: Ctrl 6.30% ± 0.79 vs VRAD 16.82% ± 2.22, p=0.0216, unpaired t-test). These results suggest that the retinoic acid also potentiated the DNA synthesis in both CD133<sup>+</sup> and CD133<sup>-</sup> populations.

Taken together, these findings indicate that the VRAD medium is responsible for an arrest of the proliferation and a morphological change of the cells. This is supported by the observation that the cells displayed an arborized phenotype, with occasional binucleated cells upon treatment. According to the immunofluorescence data, both treated cell types expressed nephrin and podocin, similarly to primary podocytes and conditionally immortalized podocytes. The analysis of the cell cycle indicated that the retinoic acid slightly stimulated the proliferation of some cells while inducing aberrant mitosis in others.

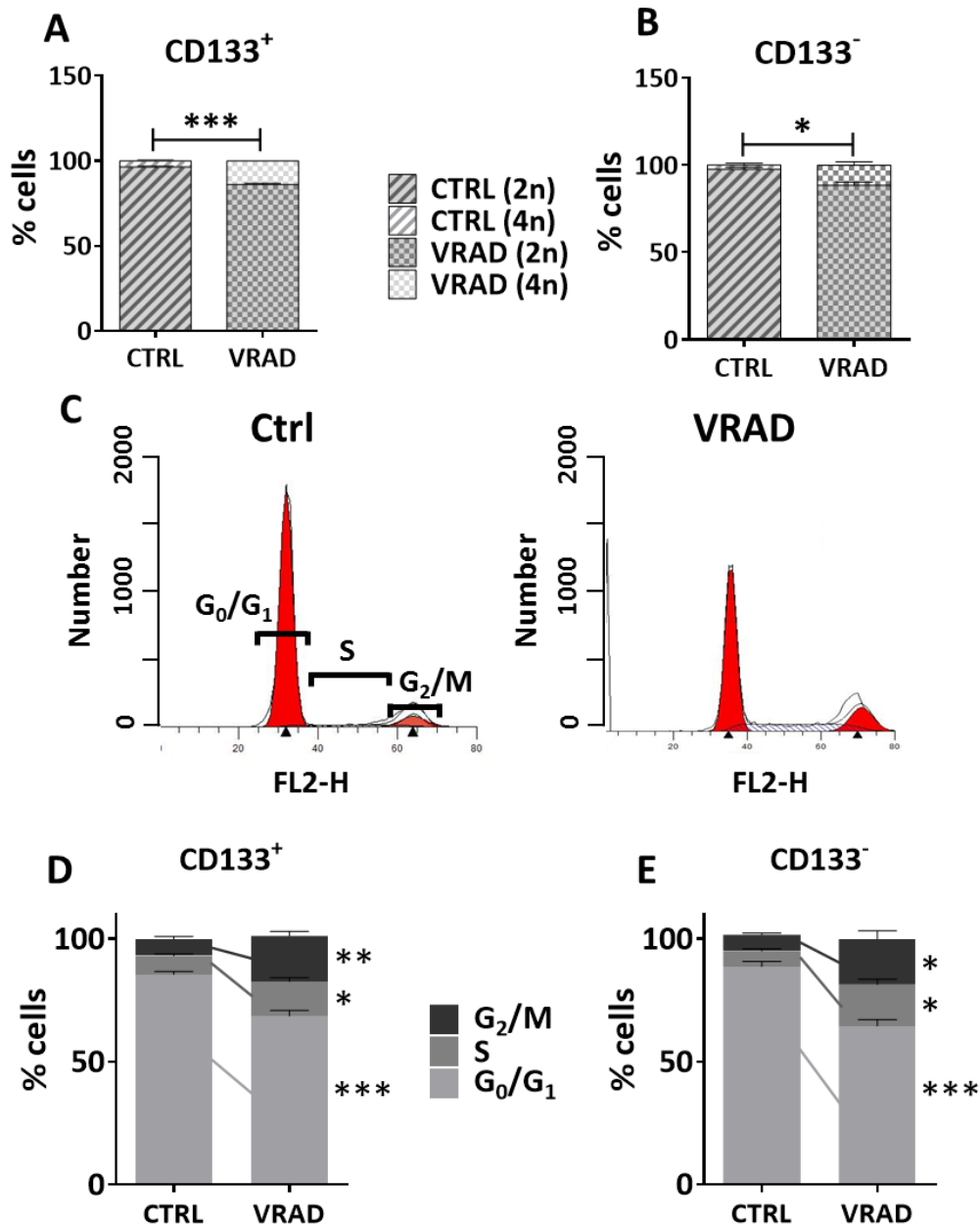


**FIGURE 4.7 CELL CYCLE ANALYSIS OF CD133<sup>+</sup> AND CD133<sup>-</sup> CELLS IN CONTROL AND VRAD MEDIUM**

(A-B) Number of diploid and tetraploid cells in both CD133<sup>+</sup> and CD133<sup>-</sup> cells after seven days in control and VRAD medium. (C) Representative histograms showing the distribution of the cells in the different phases of the cell cycle. (D-E) Distribution of both CD133<sup>+</sup> and CD133<sup>-</sup> cells in the various phases of the cell cycle.

For the generation of the data, at least 15000 events per sample were recorded using a FACS Calibur and the analysis of diploids/tetraploid cells and distribution of the phases of the cell cycle was performed using ModFit LT software. Each dataset comprises two experimental replicates, with three technical replicates per experiment. The t-test was used to determine statistical differences among the treatments. \* p<.05; \*\* .05<p<.01; \*\*\* p<.01

As a next step, I had planned to analyse the gene expression profile of the treated cells, specifically with respect to podocyte-specific markers. However, subsequent to the analysis described above, the VRAD assay failed to provide consistent results. In particular, when it was repeated, using the same cell populations isolated from hK2 or different cell lines at various passages, the cells displayed vacuoles inside the cell body and started dying within two days after the start of the assay (Figure 4.8). Although several conditions were tested, and all reagents changed and carefully diluted, it was not possible to observe the same pattern of differentiation in the populations. Therefore, further analysis of the cells involving the VRAD assay was abandoned.

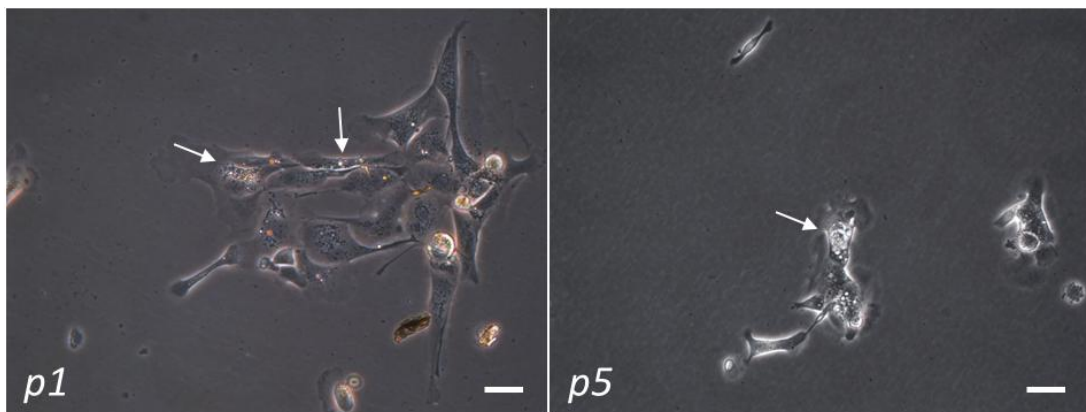


**FIGURE 4.8 REPRESENTATIVE BRIGHT FIELD IMAGES OF HUMAN CELLS TREATED WITH VRAD MEDIUM UNDERGOING CELL DEATH**

The differentiation assay was repeated with several cell types, belonging to hK2 or other samples at passage 1 or passage 5. After the first two successful experiments, the VRAD medium induced cell death in the cells, highlighted by white arrows in the images here, as soon as 2 days after the beginning of the assay. Scale bars represent 50  $\mu\text{m}$ .

#### **4.2.3 THE KIDNEY REAGGREGATION ASSAY AS A TOOL TO EVALUATE THE NEPHROGENIC POTENTIAL OF CD133<sup>+</sup> HUMAN RENAL PROGENITOR CELLS**

The nephrogenic potential of the sorted CD133<sup>+</sup> and CD133<sup>-</sup> populations was tested using the reaggregation assay described by Unbekandt and Davies in 2010, from now on defined as kidney reaggregation assay (KRA) (Unbekandt and Davies, 2010). It was decided to start from embryonic kidneys at a developmental stage of 13.5 days post fertilization (E13.5). The detailed methods are described in section 2.8 of material and methods (page 57). Figure 4.8 A and B show a schematic

representation and a photograph of a kidney rudiment in culture. For the successful organotypic development of the kidney rudiments, it is essential that the cell pellet is positioned at the interface between medium and air.

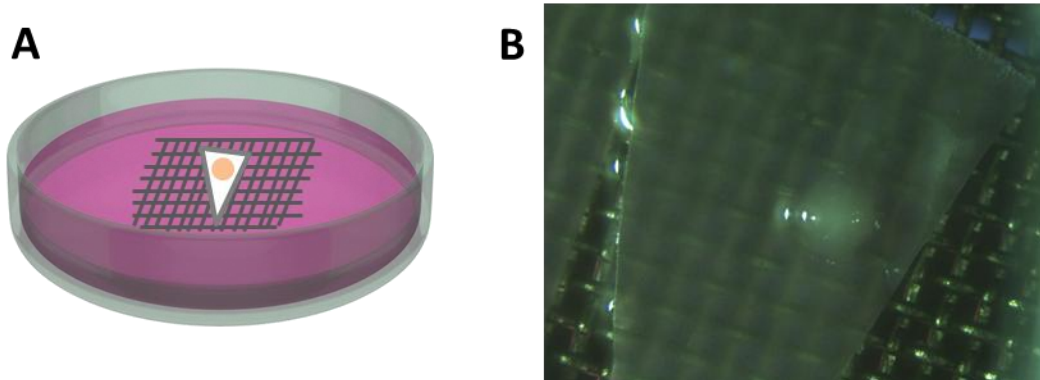


**FIGURE 4.9 KIDNEY REAGGREGATION ASSAY**

The reaggregated rudiment is assembled using embryonic kidney cells isolated from E13.5 embryos. Schematic (A) and image (B) of the set-up of the kidney reaggregation assay. All rudiments are placed on a polycarbonate membrane (1.2  $\mu\text{m}$  pores), which in turn is positioned on top of a metallic grid at the air-medium interface. The ROCK inhibitor is added for the first 24 hours of culture, in order to increase the viability of the mouse cells.

In a typical reaggregated, a total of one hundred thousand cells was used. The following controls were included in the experimental set-up:

- Reaggregated control rudiments: mouse embryonic kidney cells at E13.5 were disaggregated and reaggregated, to verify that following reaggregation there was a recapitulation of the development and the formation of *de novo* structures;
- Positive control chimeric rudiments: mouse embryonic kidney cells at E13.5 were reaggregated with GFP-labelled mouse mesothelial cells mixed in at a ratio of 1:10 (see below for more details).

All chimeric rudiments and the controls were grown up to six days, fixed and stained for Laminin, a marker of basement membrane to highlight renal structures, and Megalin, a marker of proximal tubule cells, or Wt1, a marker of the podocytes in the nephron. Some additional pellets for each experimental group were fixed one and three days after reaggregation, to monitor the development of the structures.

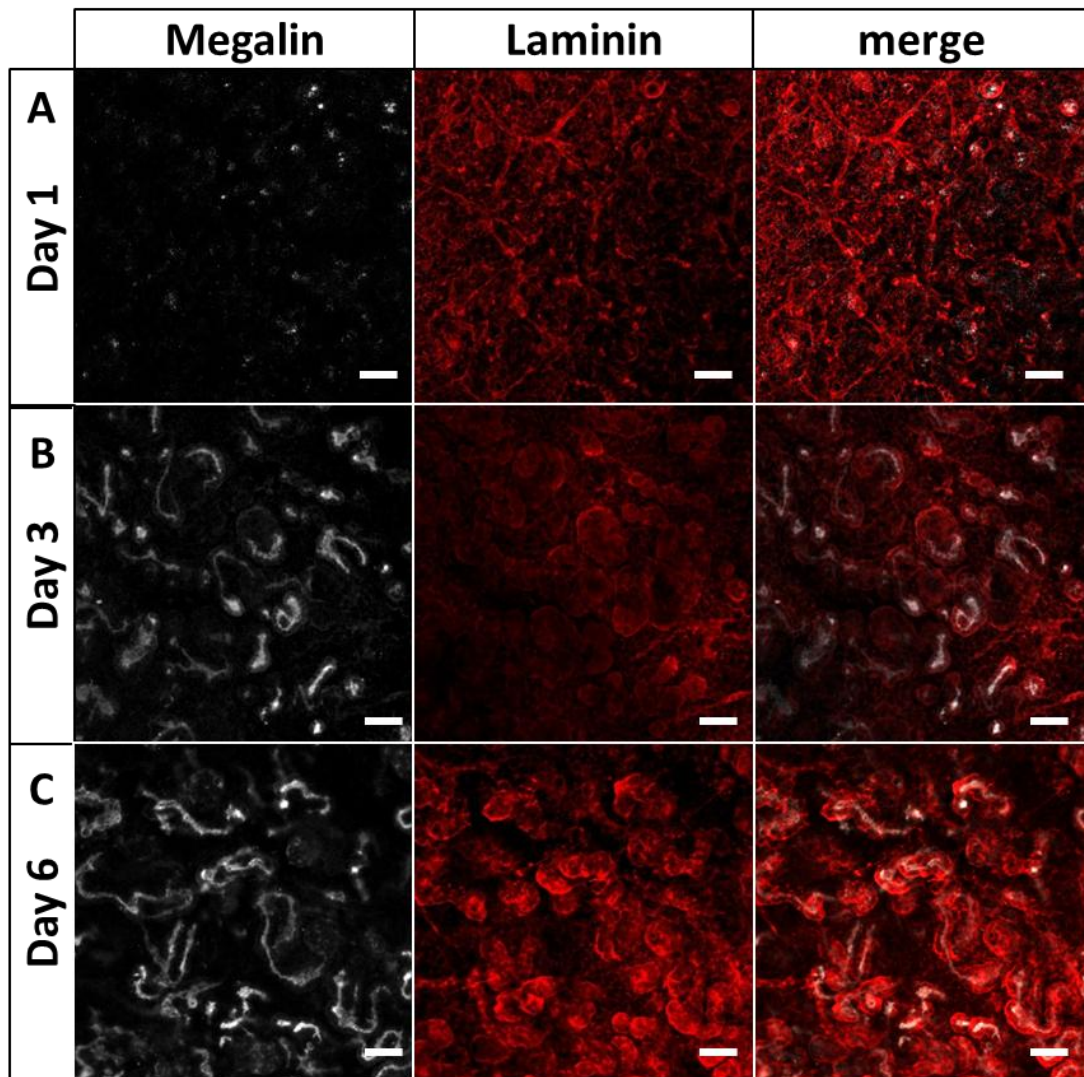
#### **4.2.3.1 CONTROL REAGGREGATED RUDIMENTS**

Figure 4.10 shows the reagggregated control rudiments at day 1, 3 and 6.

The staining at day 1 was performed to confirm that there were no remnant structures after the disaggregation at day 0. In fact, at day 1 (Figure 4.10 A), no structures were observed, besides some cysts that show Megalin staining. At day 3, the rudiments contained tubuli as highlighted by the presence of both Laminin at the basement membrane, and Megalin on the luminal side (Figure 4.10 B). These structures became even more convoluted at day 6 (Figure 4.10 C).

Thus, analysis of the control reagggregated rudiments showed that the mouse embryonic cells recapitulated the development of renal structures that start as cysts at day 1 and elongate and get convoluted over the culture period.





**FIGURE 4.10 CONTROL REAGGREGATED RUDIMENTS AT DAY 1, 3 AND 6**

Representative confocal images of single focal planes of reaggregated rudiments stained for Laminin (red) and Megalin (white) at day 1 (A), 3 (B) and 6 (C). Laminin was used to highlight epithelial structures, whereas Megalin was used to highlight the luminal surface of tubuli. Over time, it is possible to appreciate an increased complexity of the convoluted tubuli. Scale bars represent 50  $\mu\text{m}$ .

Once the technique was established, GFP-labelled mouse mesothelial cells were used as positive control and re-aggregated in a 1:10 ratio (Figure 4.11). In independent studies performed in my laboratory by Sumaya Dauleh (University of Liverpool), mouse mesothelial cells were efficiently used in the rudiment. The chimeric rudiments were analysed six to seven days after reaggregation. At the end point, the cells were found alive and interspersed in the chimera. Therefore, these cells were used as positive control.

The chimeric rudiments were monitored at the day 1, 3 and 6 by confocal microscopy and by fluorescence dissection microscopy. At day 1, the GFP-positive cells were randomly interspersed among the mouse cells, as shown by the single focal plane confocal image (Figure 4.11 A) and by the low magnification fluorescence images using a dissection microscope (Figure 4.11 B). At day 3 and day 6, tubules expressing Megalin were observed, and the GFP-positive cells were interspersed around the crescent tubuli. Figure 4.11 G shows a high magnification confocal image of a chimeric rudiment at day 6. There was no evidence at any time point of an integration of the mesothelial cells into the renal structures. Instead, the cells were often observed in the interstitium, lying on the laminin layer surrounding the tubuli. It cannot be excluded that the mouse mesothelial cells support the growth of the mouse tubuli. While no specific advantage in the tubular growth was observed in the chimeric rudiments in relation to the control rudiments, importantly, the mouse mesothelial cells integrated and spread throughout the chimeric organoid without hindering its development or the formation renal structures. A loss of the mouse mesothelial cells over time was not qualitatively observed (Figure 4.11 B, D, F).



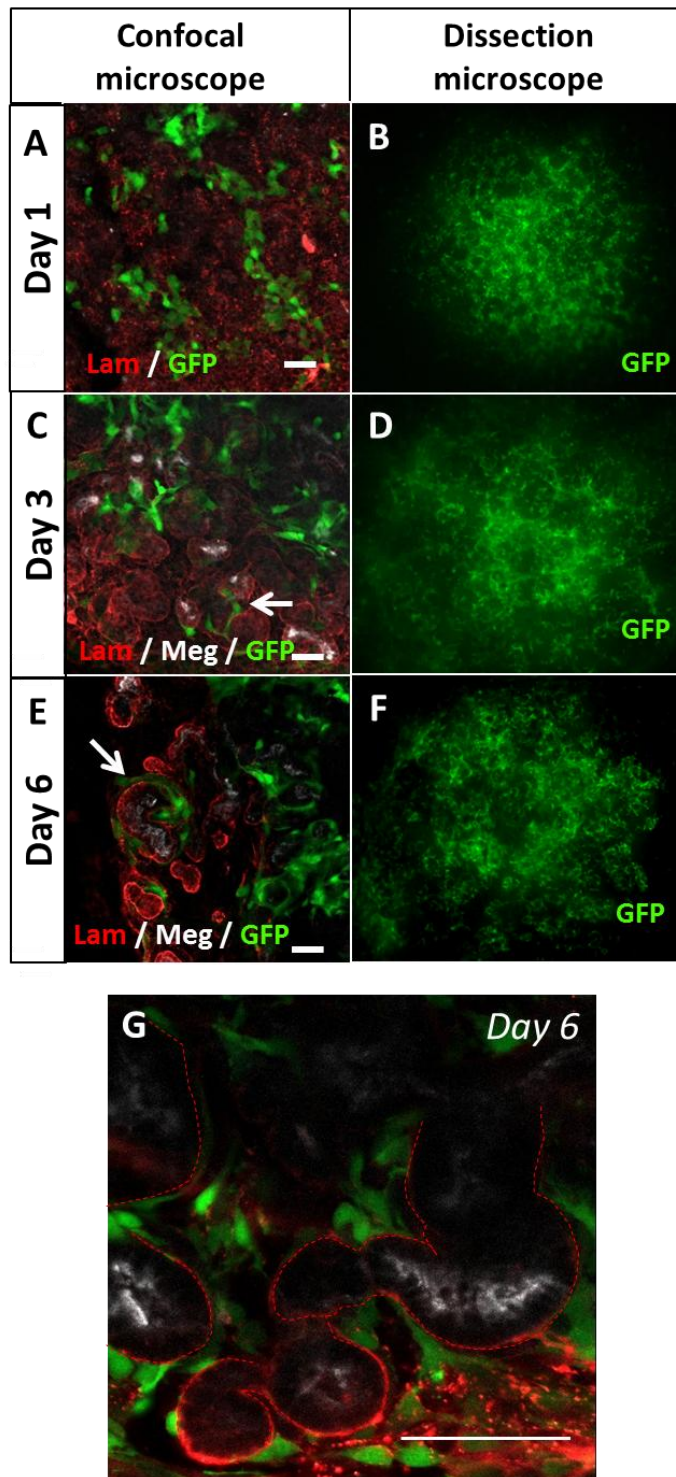


**FIGURE 4.11 CHIMERIC RUDIMENT USING MOUSE MESOTHELIAL CELLS, MONITORED AT 1, 3 AND 6 DAYS**

Representative merged confocal images of single focal planes of chimeric rudiments containing GFP-labelled mouse mesothelial cells stained for Laminin (red) and Megalin (white) at day 1 (A), 3 (C) and 6 (E). Representative fluorescence images taken under the dissection microscope at day 1 (B), 3 (D) and 6 (F). (G) Representative high magnification confocal image of a chimeric rudiment using mouse mesothelial cells. Scale bars represent 50  $\mu\text{m}$ .

#### **4.2.3.2 REAGGREGATED RUDIMENTS USING GFP-LABELLED CD133<sup>-</sup> AND CD133<sup>+</sup> CELLS**

Next, human GFP-labelled CD133<sup>-</sup> and CD133<sup>+</sup> cells were tested for their nephrogenic potential in the KRA at a ratio of 1:10 (Figure 4.12).

At day 1, the CD133<sup>-</sup> cells were randomly interspersed with Laminin-expressing mouse cells (Figure 4.12 A and B). From day 1 to day 3, there was a striking decrease in the number of GFP-positive cells in the rudiment. Figure 4.12 B, D and F show the same chimera imaged at different time points. It appeared that most of the human cells had died in the time frame of two days. Nevertheless, the dying human CD133<sup>-</sup> cells failed to disrupt the development of the renal structures. Both at day 3 and at day 6, most of the GFP-positive cells were detected in the interstitial space outside the developing epithelial structures (Figure 4.12 C and E). A series of focal planes of a z-stack in Figure 4.13 reveals a dying GFP-positive cell. Interestingly, fragments of the dying GFP-expressing CD133<sup>-</sup> cells were detected outside of the renal tubular structures, while one cell could be seen inside the tubule. Of note, this was the only cell spotted inside renal tubular structures in the entire set of experiments. Also, in the z-stack, two cells appeared to be attached to the tubuli, thus colocalizing with the Laminin signal.

The results so far indicate that the human CD133<sup>-</sup> cells died within 2 days after the start of the KRA. The death of considerable numbers of cells failed to prevent the formation of the developmental renal structures. However, given the high rate of cell death in such a short time frame and the observation of only one case of integration, it can be concluded that the latter was a stochastic event rather than active participation of the human cell in the formation of renal structures.

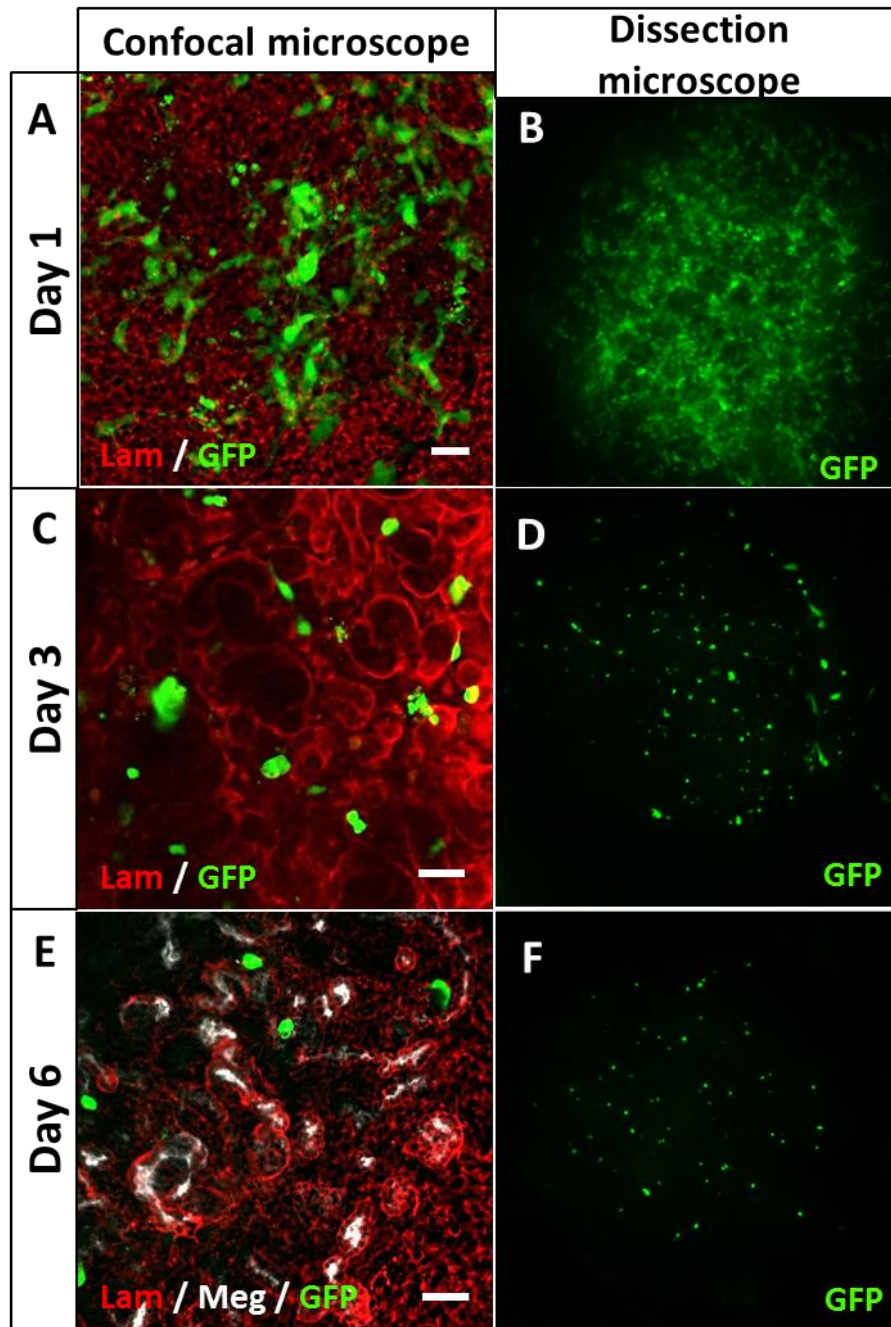


**FIGURE 4.12 CHIMERIC RUDIMENTS USING CD133<sup>+</sup> CELLS, MONITORED AT DAY 1, 3 AND 6**

(A-C-E) Representative merged confocal images of single focal planes of chimeric rudiments containing GFP-labelled human CD133<sup>+</sup> cells stained for Laminin (red) at day 1 (A) and 3 (C) and for both Laminin (red) and Megalin (white) at day 6 (E). (B-D-F) Representative fluorescence images taken under the dissection microscope at day 1 (B), 3 (D) and 6 (F). Scale bars represent 50  $\mu$ m.

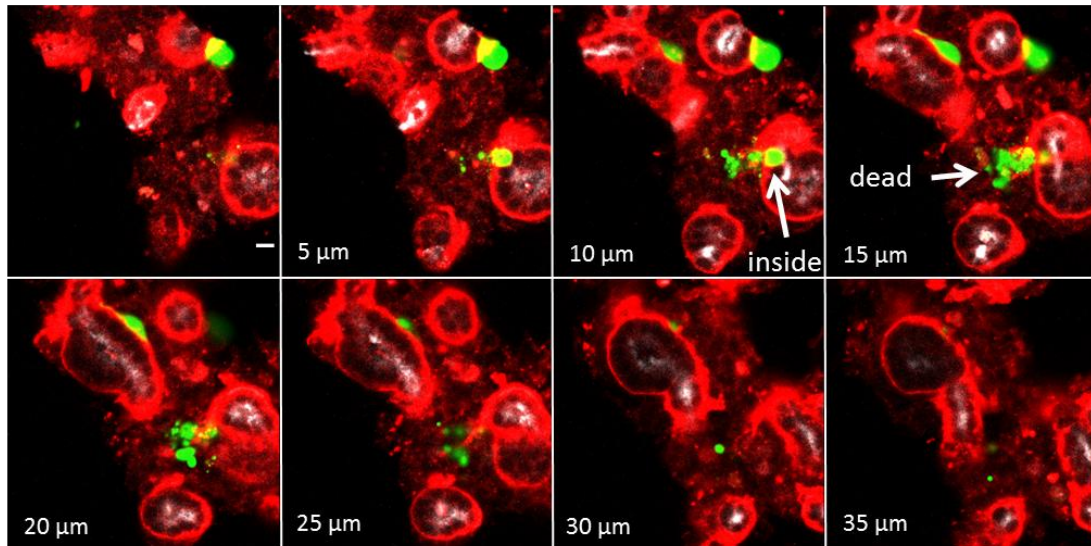


**FIGURE 4.13 CONFOCAL IMAGES SERIES OF A Z-STACK SHOWING A DETAIL OF A CHIMERIC RUDIMENT USING CD133<sup>+</sup> CELLS AT DAY 3**

Detail of a chimeric rudiment with GFP-labelled CD133<sup>+</sup> cells stained for Laminin (red) and Megalin (white). The z-stack has a z-step of 5 μm. Scale bar represents 10 μm. From the images, it is possible to observe 2 cells aligned with the Laminin<sup>+</sup> tubuli, a cell that is inside the cross-section of a tubule, and a dead cell in proximity of a cell. The cell inside the tubule was a rare observation.

Finally, human GFP-labelled CD133<sup>+</sup> cells were tested at a ratio of 1:10 (Figure 4.14). At day 1, the CD133<sup>+</sup> cells were interspersed among the mouse embryonic cells in the chimera. However, by day 6, substantial cell death of the GFP-positive human cells could be observed (Figure 4.14 B, D and F). The surviving cells grouped in the middle of the chimera and failed to integrate into any of the developing renal structures. Furthermore, at day 3, no structures were detected in proximity of the clump of human cells (Figure 4.14 C), and at day 6, a few cysts expressing Wt1 were found close to the human cells (Figure 4.14 E). This observation was consistent throughout all experiments (see page x of M&M). Interestingly, Figure 4.15 the area of the rudiment that did not contain human cells showed a complex network of tubuli. Few isolated cells were spotted in the area containing structures, but not inside the tubuli (see 1 in Figure 4.15).

These results suggest that the human CD133<sup>+</sup> cells grouped together inside the kidney rudiment instead of interspersing, and that these CD133<sup>+</sup> clumps prevented or slowed down the development of renal structures in their direct vicinity, without



disrupting the overall formation of the renal structures in more distant regions of the rudiment.

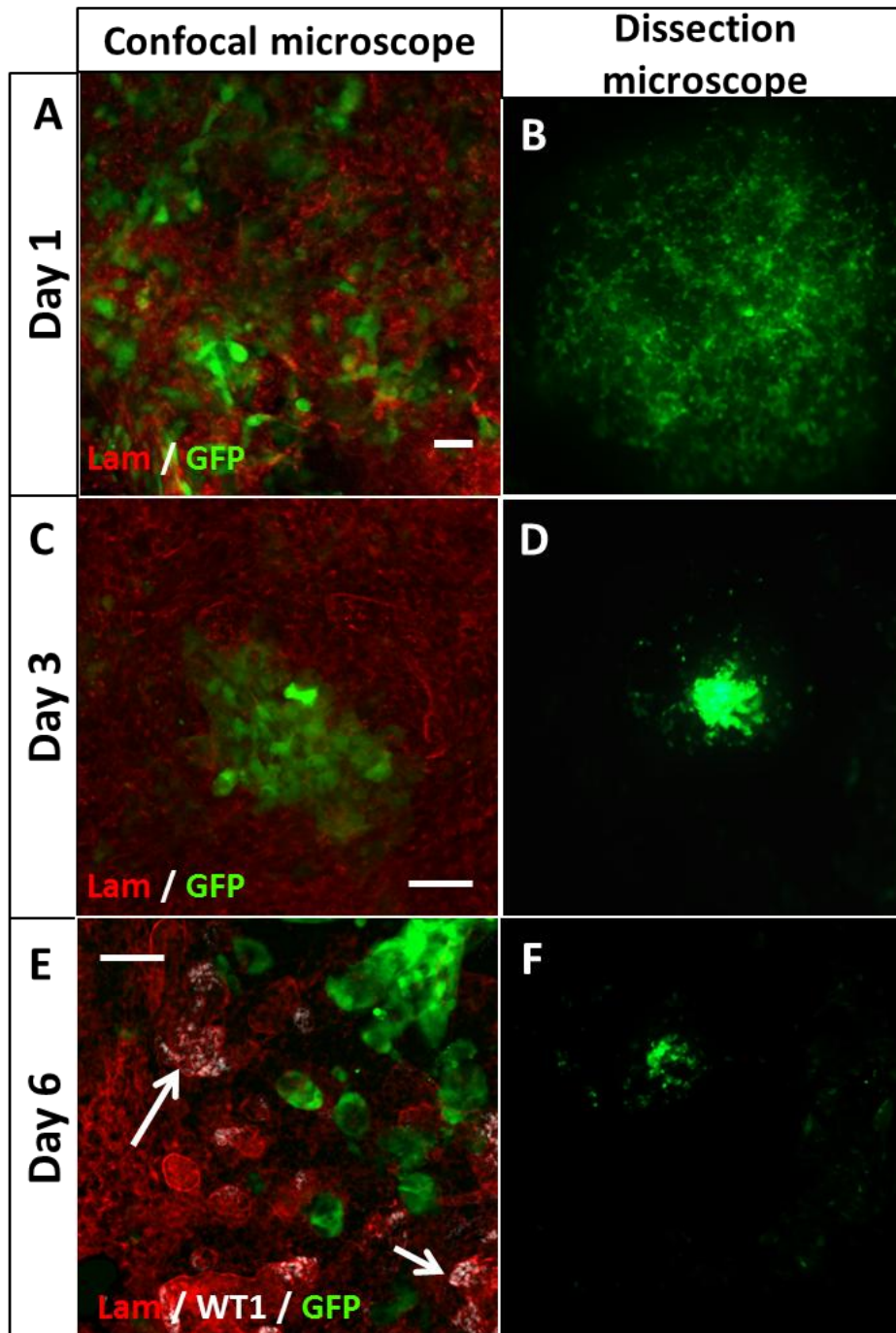


**FIGURE 4.14 CHIMERIC RUDIMENTS USING CD133<sup>+</sup> CELLS, MONITORED AT DAY 1, 3 AND 6**

(A-C-E) Representative merged confocal images of single focal planes of chimeric rudiments containing GFP-labelled human CD133<sup>+</sup> cells stained for Laminin (red) at day 1 (A) and 3 (C) and for both Laminin (red) and Wt1 (white) at day 6 (E). White arrows indicate the presence of small structures stained for Wt1. (B-D-F) Representative fluorescence images taken under the dissection microscope at day 1 (B), 3 (D) and 6 (F). Scale bars represent 50  $\mu$ m

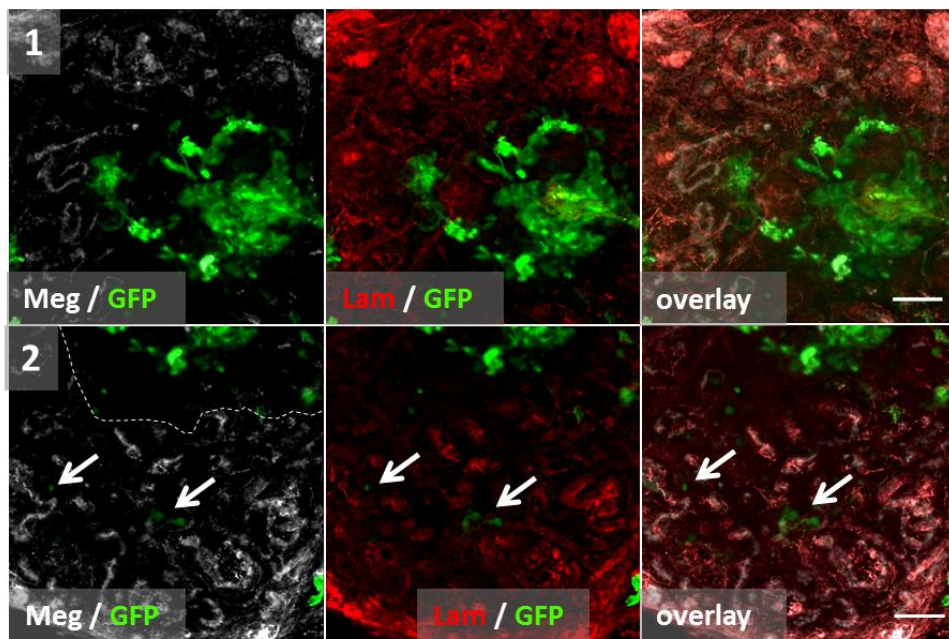
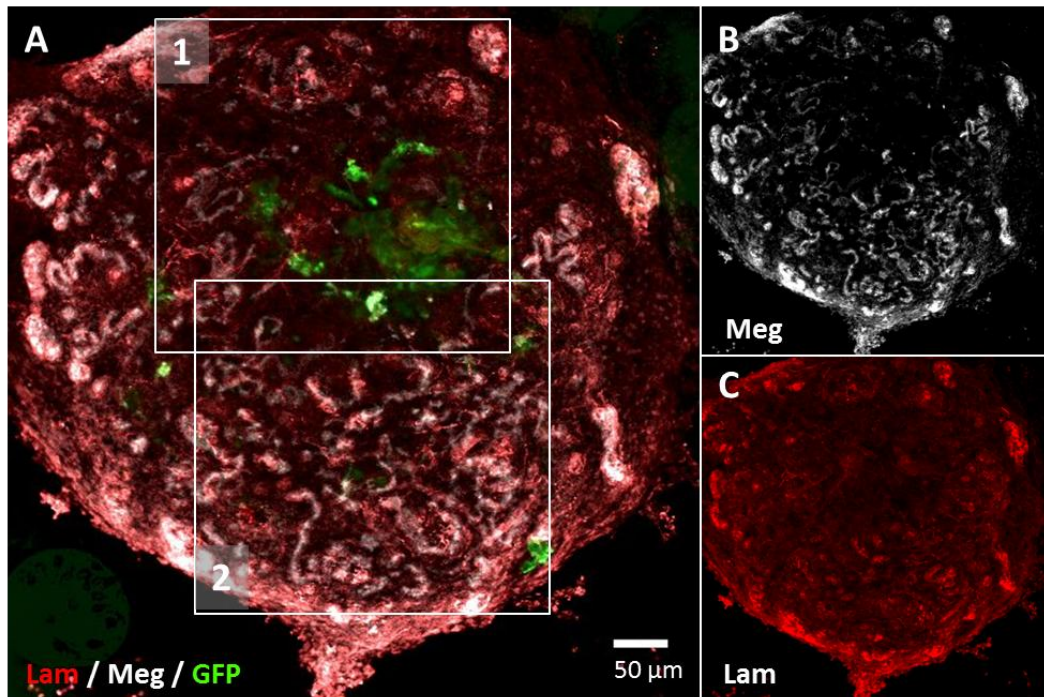


**FIGURE 4.15 SINGLE FOCAL PLANE CONFOCAL IMAGE OF A CHIMERIC RUDIMENT USING CD133<sup>+</sup> CELLS ON DAY 6**

Additional representative images of single focal plane of a chimeric rudiment containing GFP-labelled human CD133<sup>+</sup> cells stained for Laminin (red) and Megalyn (red) at day 6. (A-B-C) Low magnification image showing the chimeric rudiment. The images suggest that there are no developed tubuli in the area where there is the cluster of human cells. (1-2) Two areas of the chimera were imaged at higher magnification. Very few cells were detected interspersed in the rest of the chimera. The arrows indicate 3 human cells close to convoluted tubuli expressing Laminin and Megalyn. The diameter of the rudiment was calculated to be 536  $\mu\text{m}$ . The scale bar represents 50  $\mu\text{m}$ .

Given the inability of the cells of interest to survive in the chimera and to contribute to the formation of renal structure, it was decided to not stain the chimera for additional nephrogenic genes, such as Pax2 or Six2. Instead, the formation of renal embryonic spheroids was pursued, in order to eliminate the membrane as support and image the spheroids in the Light Sheet Fluorescent Microscope (LSFM).

#### **4.2.4 A REFINED KIDNEY REAGGREGATION ASSAY FOR LIGHT SHEET MICROSCOPY**

The KRA as presented in the last section followed the method described by Unbekandt (Unbekandt and Davies, 2010). Being grown on a support, the kidney organoid was partially three dimensional with a dome-like shape. Also, as a result of the technique which requires careful handling of the delicate reaggregated kidney organoids at several critical steps, consistency in the outcome may not be achieved every time. One important drawback of the technique is that rudiments need to be fixed at specific time points for detailed monitoring and analysis of the development of the renal structures. Therefore, the aim was to generate spheroids that could be imaged using the Light-sheet fluorescent microscope, allowing live imaging to track the behaviour of fluorescently labelled cells, in addition to end point high resolution imaging.

To obtain spheroids, a different set-up was devised. A multi-well support disk of approximately 3 cm diameter was shaped from PDMS (Polydimethylsiloxane), a hydrophobic material. A polycarbonate membrane (same as the one used in the conventional assay) was placed underneath the PDMS disk. The multi-well disk was placed in a culture dish and maintained at the medium/air interface by PDMS spacers (Figure 4.16 A). The KRA protocol was followed to the step where mouse embryonic kidney cells were reaggregated. The pellet was composed of one hundred thousand cell, as in the assay involving the membrane. Each pellet was positioned inside one of the wells in the multi-well disk and grown for up to six days. Figure 4.16 B and C shows the arrangement of the PDMS multi-well disk at day 0 and day 6. For endpoint imaging at day 6, the spheroids were fixed and embedded in 1.5% agarose inside a glass capillary (Figure 4.16 D) and imaged using the LSFM. The experiments with the LSFM were performed in collaboration with Dr. Marie Held, Post Doc at the University of Liverpool, who operated the LSFM.

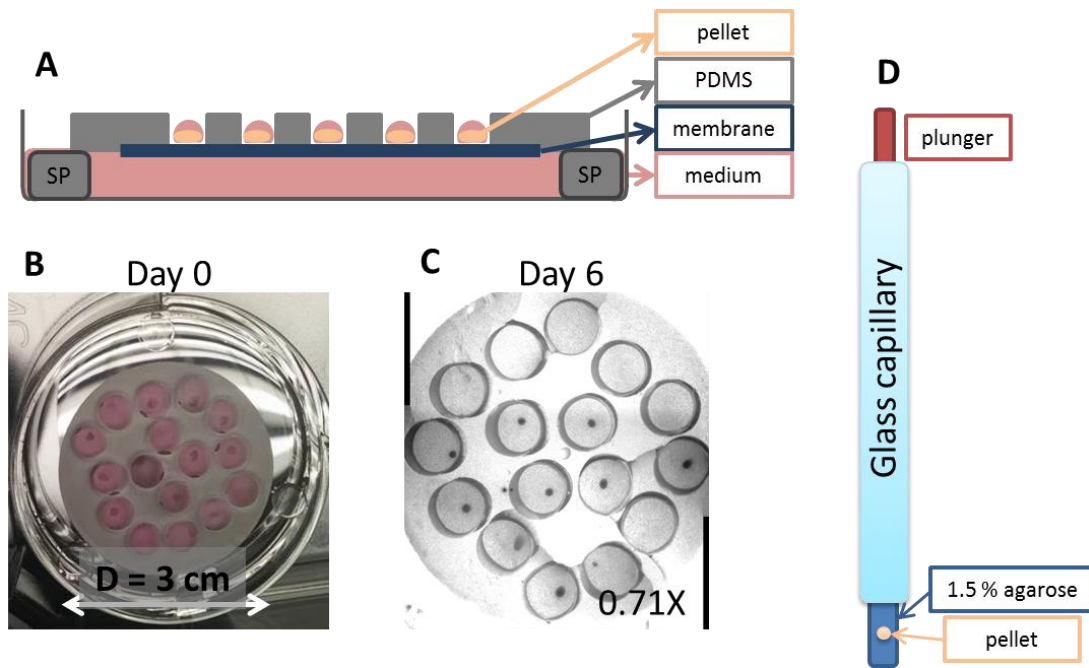


**FIGURE 4.16 MODIFIED KRA, DEvised TO PRODUCE SPHEROIDS TO IMAGE IN THE LSFM**

(A-B) The multi-well support disk is made of PDMS, a hydrophobic material, and a polycarbonate membrane placed underneath; PDMS spacers (SP) allow the membrane to be at the air-medium interface. This set-up offers the right environment for the spheroid to receive nutrients from the medium in the bottom of the dish without attaching to the membrane. (C) Image of the dish taken at the dissection microscope displaying the spheroids inside the PDMS support in medium after 6 days in culture. (D) Glass capillary containing the spheroid that for imaging in the LSFM. The pellet is embedded in 1.5% agarose/3% gelatine and, for the imaging, the embedded spheroid is pushed out of the capillary using a plunger.

During the six days in culture, the spheroids were imaged every day using a dissection microscope. To follow their development and potential growth, the spheroid area was measured daily, assessed with the Fiji software and normalized to the area of the spheroids at day 1. By day 3, the area of the spheroids declined significantly by 30%, to then increase steadily until day 6 (Figure 4.17). These fluctuations in the spheroid area could possibly reflect an initial compaction of the cells that might lead to the development of the structures, followed by an increase in the number of cells over time. In general, at day 6, the diameter of the spheroids was approximately 450  $\mu\text{m}$ .



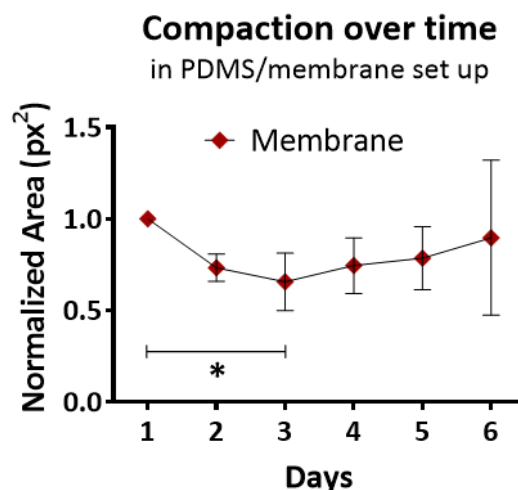


**FIGURE 4.17 COMPACTION OVER TIME OF THE SPHEROIDS**

The graph summarizes the mean and SD of the area measurements for six days of culture (n=8). The area occupied by the spheroids was measured using the Fiji software. The values were normalized to the area of the spheroids at day 1. Each day was compared to day 1 by using a t-test, and only the spheroids at day 3 are statistically smaller in relation to day 1. \* p<0.05

At day 6, the spheroids were fixed and stained using immunofluorescence to investigate the presence of developing renal structures (Figure 4.18). The presence of epithelial structures was confirmed by the presence of Laminin. Inside some of these structures, also Megalin was identified, suggesting the presence of proximal tubuli (Figure 4.18 A). The lectin peanut agglutinin (PNA) was used to stain ureteric bud, collecting duct, and proximal tubules, in cases of primary antibody incompatibility (Phillips et al., 2001). Pax2 was detected in the condensed mesenchyme around the tips of the ureteric buds and inside some ureteric trunks, as indicated in Figure 4.18 B. It appeared that more than one ureteric bud underwent branching. Furthermore, Synaptopodin staining at the tip of the tubuli highlighted the presence of fully developed nephrons (Figure 4.18 C). Altogether, the images point towards the co-presence of different developmental stages in the same spheroid.

Of note, the LSM is equipped with two illumination objectives positioned at 180 degrees to another. The images showed in Figure 4.18 were taken with a single illumination objective, either from the left (A) or the right (B) side. The illumination source explains why the images appear faded out on one side. Because the spheroids

are quite large and compact, it is difficult to image the light-scattering core of the spheroid.

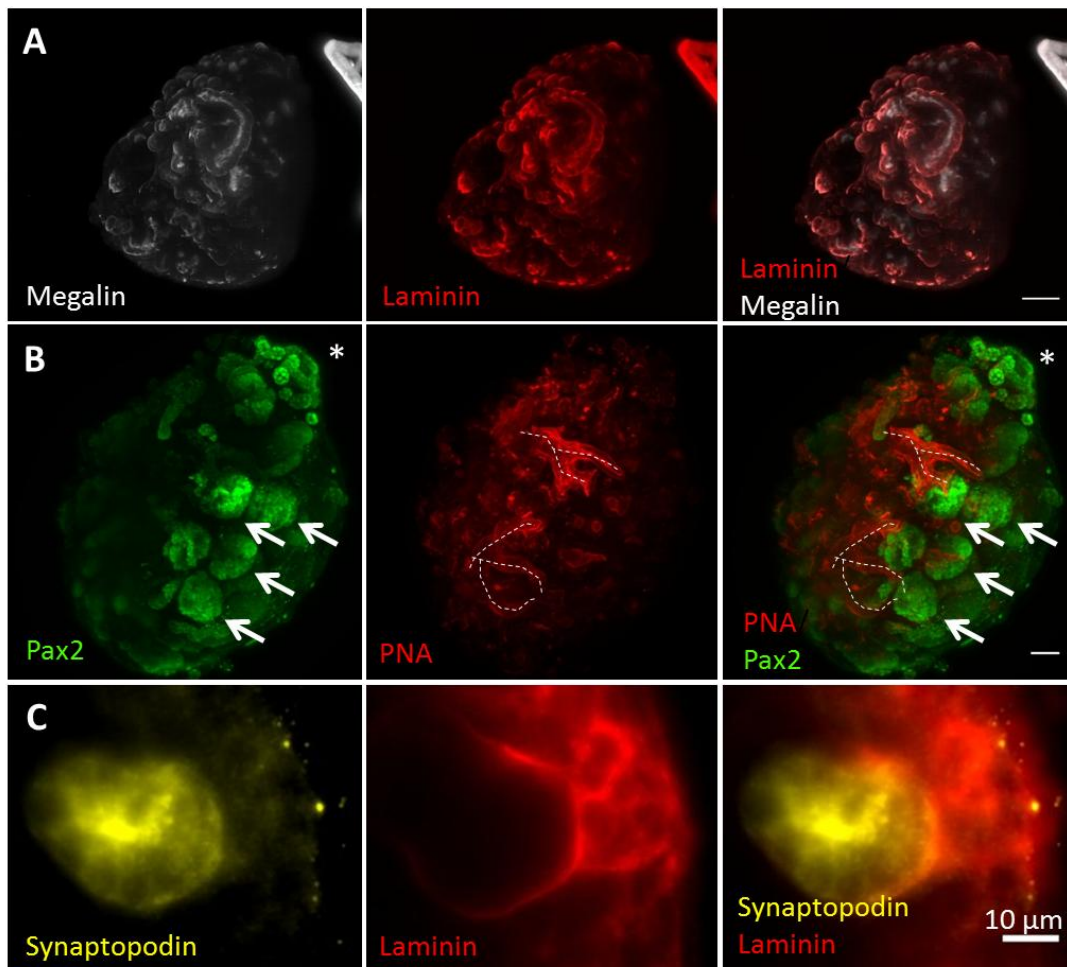


**FIGURE 4.18 REPRESENTATIVE LSFM IMAGES OF THE SPHEROIDS CULTURED FOR SIX DAYS**

Immunofluorescence images taken with the LSFM of a spheroid made of one hundred thousand mouse embryonic cells cultured for six days and fixed in 4% PFA. (A) Spheroid stained for Megalin (white) and Laminin (red) (B) Spheroid stained for Pax2 (green) and PNA (red) The asterisks indicate tubular structures where Pax2 is expressed inside the tubuli, so likely to be the ureteric buds. The white arrows indicate the accumulation of Pax2 in the cap mesenchymes. Dashed lines indicate the branching of two different ureteric buds. (C) Detail of a spheroid showing a nephron stained for Synaptopodin (yellow) and Laminin (red). The stainings highly reflect the physiological localization of the markers. All images are MIPs obtained imaging the spheroid with a single illumination lens. Scale bar represents 50  $\mu\text{m}$ , unless stated otherwise.

#### 4.2.5 FUNCTIONALITY OF THE TUBULI IN THE SPHEROIDS

It had been shown that serially-reaggregated engineered kidneys can transport organic anions and cations into and out of the renal tubuli (Lawrence et al., 2015). To test the functionality of the spheroids obtained in this study, an organic anion uptake

assay was set up by using the anionic 5(6)-carboxyfluorescein (6-CF). 6-CF is transported by the family of organic anion transporters (OATs) through the basolateral and apical surface of the tubular cells.

In this assay, the spheroids were treated at day 5 or 6 with 6-CF, either with or without Probenecid (2.5 mM), an inhibitor of the OAT family and the Mrp efflux pumps. Subsequently, spheroids from both treatment groups were incubated with Probenecid at high concentration (10 mM). In the samples without probenecid treatment at the beginning and high Probenecid at the end, 6-CF was transported into the tubuli, while the inhibitor was expected to prevent the efflux of 6-CF (Lawrence et al., 2015; Rak-Raszewska et al., 2012).

Imaging of the spheroids after the functional uptake assay by LSM showed that spheroids treated with Probenecid at the beginning and the end of the assay contained no 6-CF inside the tubuli (Figure 4.19). By contrast, in the samples treated with probenecid only at the end, 6-CF was found inside the tubuli. The orthogonal views XZ and YZ demonstrate at a single cell level the occurred uptake of 6-CF by the tubular cells. In conclusion, the PDMS multi-well culture system allowed the culture of spheroids, which developed appropriate renal structures, and gained functional physiological properties over time.

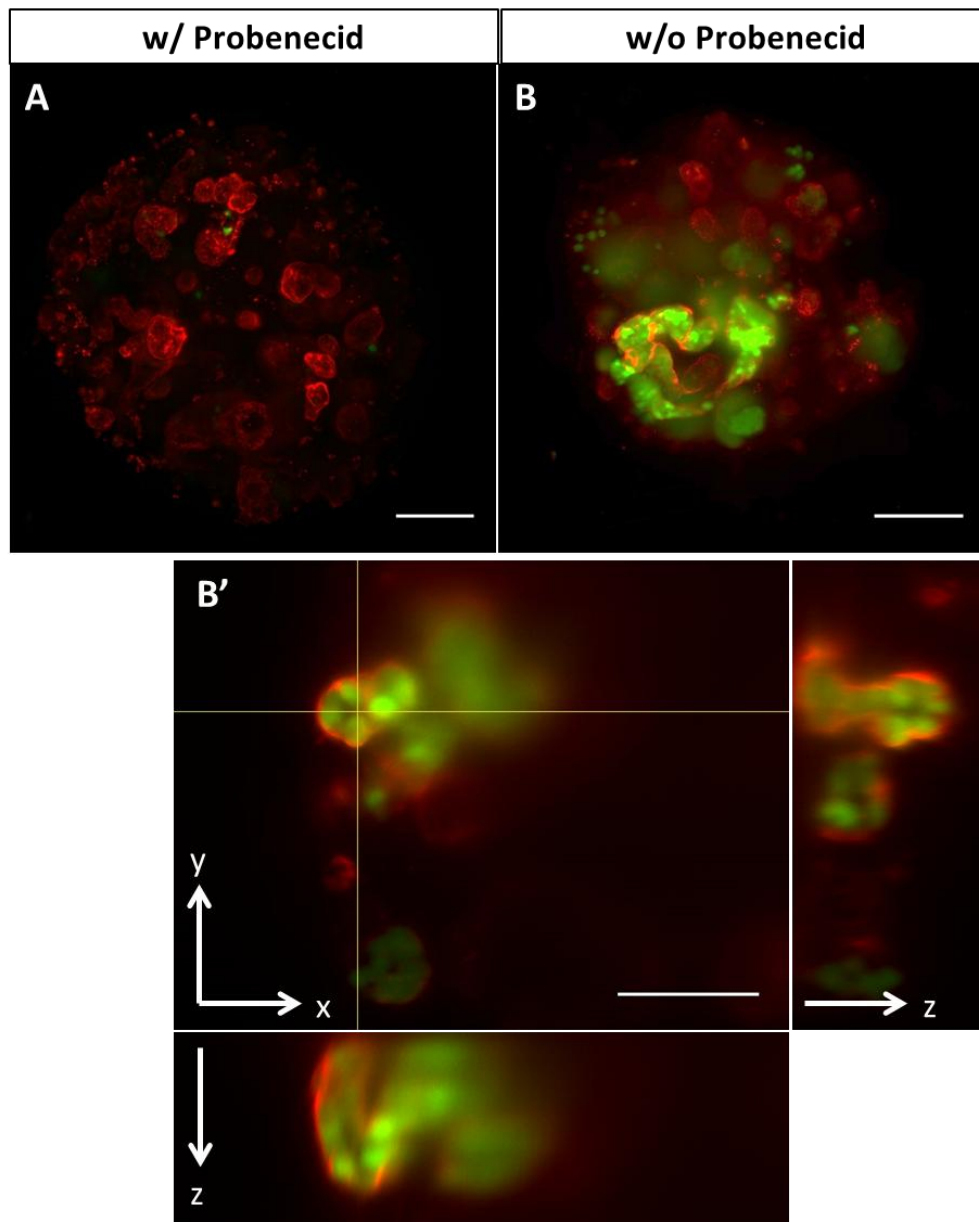


**FIGURE 4.19 ANIONIC UPTAKE ASSAY ON REAGGREGATED CONTROL SPHEROIDS**

Functional anionic uptake assay on spheroids cultured for 5 or 6 days. (A) The samples 'w/ Probenecid' were initially incubated for 1 hour with Probenecid (2.5 mM), 6-CF (1  $\mu$ M, green) and PNA (20  $\mu$ g/ml, red). (B) The control samples (w/o Probenecid) were incubated only with 6-CF and PNA. After the incubation period, both sample groups were incubated with a higher concentration of Probenecid (10 mM), washed and imaged. The images represent MIPs of fused single illumination images. (B') MIP of a detail of a control spheroid. Orthogonal views in XZ and YZ show the fluorescence inside the tubuli in single cells. The assay was repeated 4 times with independent samples. Scale bars represent 100  $\mu$ m.

#### **4.2.6 IN VIVO IMAGING OF KIDNEY SPHEROIDS**

So far, it was shown that the kidney rudiment assay could be adapted to culture conditions that led to the formation of spheroids. Therefore, the final aim of this part of the study was to image live the reaggregation process of mouse embryonic cells and any fluorescently labelled cell of interest. This would serve as a proof of concept experiment, demonstrating that it is possible to observe the developing renal structures in the spheroids in real time using the Light sheet microscope.

Initially, a spheroid consisting only of mouse embryonic cells was embedded in 1.5% agarose and 3% gelatine, which had been previously tested as a compatible combination for the growth of the spheroid (data not shown). The spheroid was imaged from day two every 30 mins for 10 hours using dual illumination to increase the axial and lateral resolution. The embedded spheroid was immersed in a chamber connected to a reservoir continuously supplying fresh medium, to counteract eventual evaporation, and PNA as a vital dye to highlight the developing renal structures. The montage in Figure 4.20 shows a summary of the MIP images every two hours of the spheroid. From the series, it is possible to appreciate the compaction of the spheroid over time and the organization of the cells into small structures, appearing between 6 and 8 hours after the beginning of the imaging.

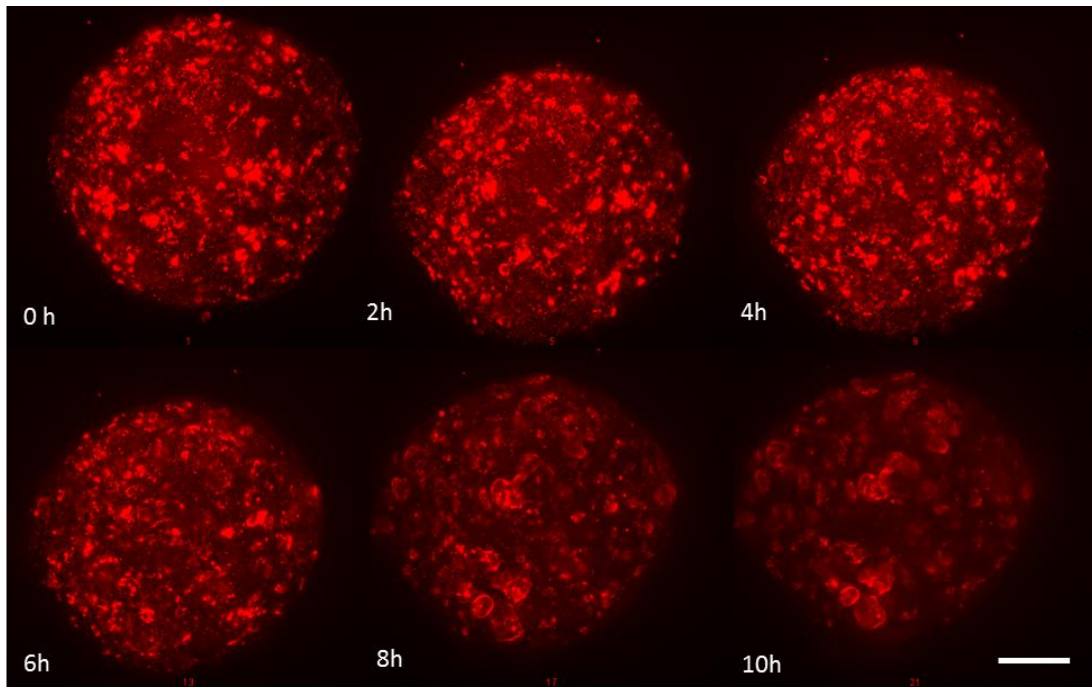


**FIGURE 4.20 SERIES OF LSFM IMAGES OBTAINED DURING THE LIVE IMAGING OF A REAGGREGATED SPHEROID FOR TEN HOURS**

Montage summarizing MIP images of reagggregated rudiments generated using mouse embryonic cells. The spheroid was imaged over a period of 12 hours (0.5 days) at intervals of 30 min with a single illumination. In total, 26 3D stacks in the red fluorescence channel (PNA) were recorded. Each 3D stack contained 247 single frames spaced  $0.65\ \mu\text{m}$  along the z-axis. In the montage, a summary of all images is presented. A continuous supply of medium containing diluted PNA (red) was necessary to keep the spheroid alive and stain developing structures over time. The spheroid compacted over time, passing from  $232\ \mu\text{m}$  at  $t=0\text{h}$  to  $205\ \mu\text{m}$  at  $t=10\text{h}$ . Scale bar represented  $100\ \mu\text{m}$ .

Next, a reagggregated rudiment containing GFP-labelled mouse mesothelial cells was imaged every 30 mins from day 1 over the course of 72 hours. The sample was embedded in 1.5% agarose and 3% gelatine. The montage in Figure 4.21 shows a summary of MIP images of the spheroid every three hours. As previously observed, the spheroid compacted over time. An interesting finding was the high mobility of the GFP-labelled cells in the spheroid, which end-point imaging fails to reveal (Figure 4.21). However, we could observe a number of mitosis events (Figure 4.22). Three problems were identified by imaging this spheroid over a long time period: i) due to the high compaction over time, the core of the spheroid could not be imaged; ii) the imaging chamber can easily get contaminated and the contaminated medium impeded proper light scattering; iii) the spheroid moves in the capillary and after 45 hours of imaging it could not be visualized anymore.



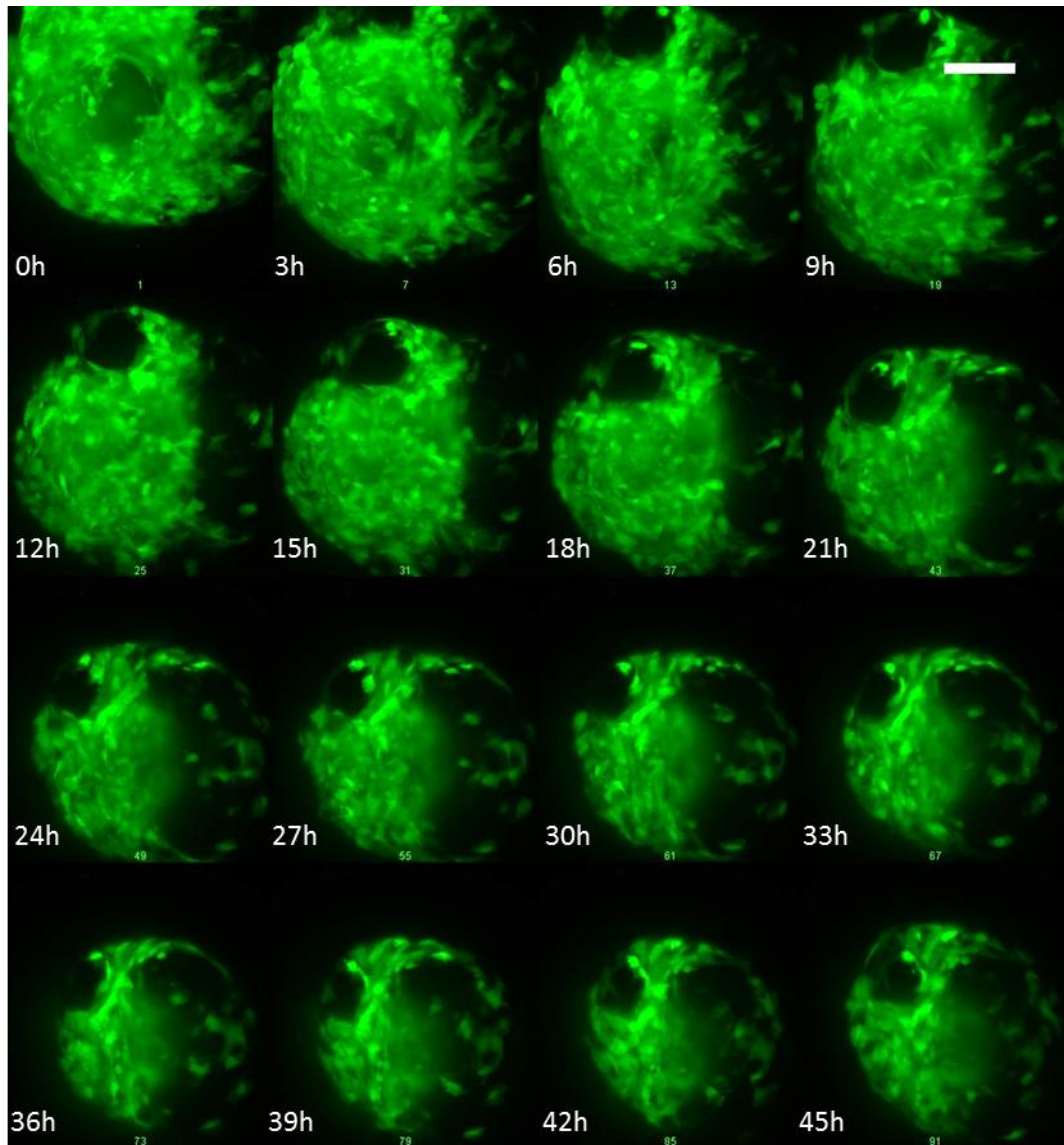


**FIGURE 4.21 SERIES OF LSFM IMAGES OBTAINED DURING THE LIVE IMAGING OF A CHIMERIC SPHEROID CONTAINING MOUSE MESOTHELIAL CELLS FOR FORTY-FIVE HOURS**

Montage reporting MIP images of reaggregated chimeric rudiments generated using mouse embryonic cells. The spheroid was imaged over a period of 63 hours (2.6 days) at intervals of 30 min with a dual illumination. However, the spheroid was visible up to 45 hours. In the first 45 hours, 182 3D stacks with one channel (green channel –GFP mouse mesothelial cells) were recorded. Each 3D stack contained an average of 350 single frames spaced 0.81  $\mu\text{m}$  along the z-axis. A continuous supply of medium was necessary to keep the spheroid alive. The spheroid compacted over time, being around 421 $\mu\text{m}$  at  $t=0$  and reaching 323  $\mu\text{m}$  at  $t=45\text{h}$ . Scale bar represented 100  $\mu\text{m}$ .

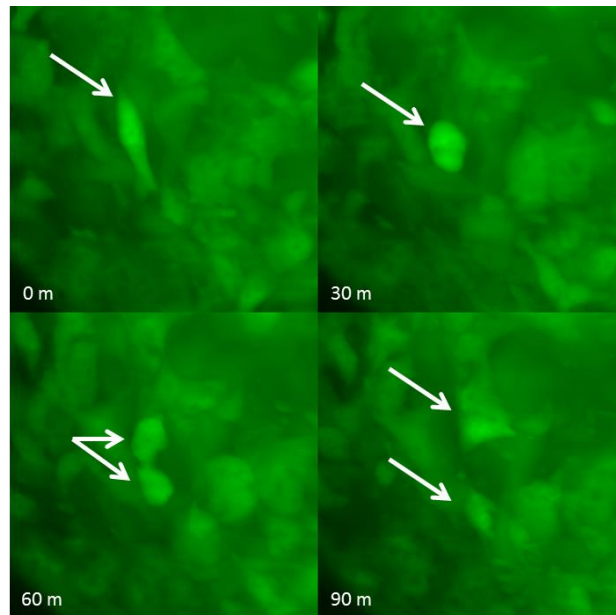


**FIGURE 4.22 SERIES OF LSFM IMAGES OF A DETAIL OF THE CHIMERIC RUDIMENT CONTAINING MOUSE MESOTHELIAL CELLS**

Montage of 4 images belonging to the time series shown in the previous figure. In this image, a cell undergoing mitosis is indicated by the white arrow. This is just one example of several episodes of mitosis happening in the spheroid, suggesting that the environment does not impede cell division.

In the last three paragraphs, a novel approach for the formation of spheroids was presented. The process to form spheroid is very simple and by-passes the critical step of transferring the pellet on top of the membrane, that can easily result in the spreading of the pellet on the membrane. The size of the spheroid is quite consistent ( $\sim 400 \mu\text{m}$ ) as opposed to the size in the conventional KRA that can be very variable. Also, another advantage of the spheroid set-up is given by the lack of contact of the spheroid with the membrane. Last, but not least, the possibility of using the gentle imaging of the LSFM will permit to gather more information compared to the conventional assay. And, in line of principle, the use of a continuous supply of PNA coupled with the use of fluorescently labelled cells can potentially be used to infer live dynamics of the cells in the spheroid at a single cell level and help understand whether the cells actively migrate towards the structures or if their presence inside structures is due to stochastic events. However, a number of optimizations are needed to improve the antibody penetration and, therefore, the imaging of the core, and to prevent contamination of the medium during live experiments.



### 4.3 DISCUSSION

In this chapter, the main aim was to provide a proof that the isolated CD133<sup>+</sup> cells are progenitors. In order to do that, their ability to differentiate into podocytes was tested by culturing the cells *in vitro* with VRAD medium. Alongside, the cells were used in an *ex vivo* kidney reaggregation assay, to assess whether either CD133<sup>+</sup> and CD133<sup>-</sup> cells could integrate into developing structure into the rudiment.

Differentiation is an important parameter for the potency of putative progenitor/stem cells. In the literature, CD133<sup>+</sup> cells were defined multipotent for their ability to differentiate into a broad range of cell types, from renal lineage, like tubular and podocytic, to extra-renal lineages, such as endothelial, neurogenic, osteogenic and adipogenic (Bussolati et al., 2005; Ronconi et al., 2009; Sagrinati et al., 2006). This wider plasticity of the renal CD133<sup>+</sup> cells could be considered an important incentive for clinical applications, specifically for their use in regenerative medicine therapies. However, since the kidney has only limited regenerative potential, it seems unlikely that CD133<sup>+</sup> renal progenitor cells may be able to differentiate into cells not even close in terms of anatomical localization. The unexpected reports of trans-differentiation could therefore be the consequences of the use of specific culture media and their cocktails of growth factors. Thus, the observed morphology would be a result of adaptation to the “new” culture conditions.

Vitamin A (All-trans retinoic acid, ATRA) is a signaling molecule that exerts multiple effects during embryogenesis, by directly or indirectly regulating a broad range of cellular processes, from proliferation to differentiation (Gudas and Wagner, 2011). Many of the primary target genes regulated by ATRA present Retinoic Acid Responsive Elements (RARE) on their promoters. In the glomerulus, nephrin is one of the genes transcriptionally activated by ATRA (Okamura et al., 2009; Suzuki et al., 2003). Retinoic acid and Vitamin D3, another proven activator of nephrin gene expression, were indeed used to induce the differentiation of renal progenitor cells in podocytes in several studies (Arcolino et al., 2016; Bombelli et al., 2013; Kietzmann et al., 2015; Ronconi et al., 2009; Sagrinati et al., 2006). The process was being partially elucidated, and miRNA-193a appeared as a powerful regulator of this differentiation process (Kietzmann et al., 2015). Recently, BIO (6-bromo-indirubin-3'-oxime), an inhibitor of

the glycogen synthase kinases 3 (GS3Ks) was used to enhance further the differentiation ability exerted by the ATRA on hRPC. Besides an upregulation of the nephrin gene and protein, BIO led to an increase in the percentage of quiescent cells in  $G_0/G_1$  accompanied by a reduction of the proportion of the cells in S phase (Lasagni et al., 2015). This redistribution of the phases of the cell cycle is in line with the dogma that podocytes are quiescent post-mitotic cells. However, this is in contrast to the findings from this study. Here, primary human  $CD133^+$  and  $CD133^-$  cells isolated from young adults kidneys were tested for their ability to differentiate into podocytes by culturing them in ATRA and Vitamin D3. An increase in the percentage of cells in the  $G_2/M$  phase of the cell cycle was observed, together with a slight, but significant increase in the proportion of the cells in the S phase. This finding would support the possibility that ATRA induced aberrant mitosis in the cells used in my experiments. In chapter 3, it was reported that the vast majority of the isolated human cells cultured in fetal progenitor medium (Price et al., 2007) expressed a marker of fully differentiated proximal tubular cells (CD13). It can be hypothesized that the cells, being mostly proximal tubule cells-like are not able to fully differentiate into podocytes and, following VRAD treatment they arrest in the  $G_2/M$  phase of the cell cycle. Nevertheless, the expression of nephrin and podocin was confirmed by immunofluorescence and showed to be comparable to the conditionally-immortalized and primary podocytes. Unfortunately, due to subsequent technical problems with the assay, these preliminary findings could not be corroborated.

Despite the impossibility to consistently reproduce the differentiation assay, the assessment of functionality of the differentiated cells is key to confirm the differentiation. Previous reports that exploited the VRAD medium to differentiate putative progenitor cells into podocytes simply relied on immunofluorescence and gene expression to define the cells as fully differentiated podocytes (Angelotti et al., 2012; Bombelli et al., 2013; Ronconi et al., 2009). Alongside with immunofluorescence and gene expression, Arcolino and colleagues (Arcolino et al., 2016) examined the functionality of the neonatal urine progenitors-derived podocytes using the albumin endocytosis assay, generic functional assay for proximal tubular cells and podocytes,

and testing the activity of the podocytes-specific transient receptor potential cation channel (TRPC6) in the presence of  $\text{Ca}^{2+}$ .

Alongside with the differentiation assay, the nephrogenic potential of both  $\text{CD133}^+$  and  $\text{CD133}^-$  cells was investigated in this study. No definite proof of integration was found. All GFP-labelled  $\text{CD133}^-$  cells were found in the interstitial space, in parts closely aligning with the tubular basement membrane. In contrast, most of the GFP-labelled  $\text{CD133}^+$  cells were found aggregated on top of the chimeric rudiment, even if at day one the cells had been randomly interspersed in the rudiments Figure 4.12 and Figure 4.14. The absence of structures in the areas occupied by the cluster of cells, but not in the surrounding areas indicates that the human  $\text{CD133}^+$  cells secreted paracrine factors that halted the recapitulation of the developing structures in their close proximity.

To date, this represents the first study where hPSCs were tested for their capacity to integrate and potentially contribute to the formation of renal structures in the kidney reaggregation assay. A surrogate of the assay was shown by Ward and colleagues. They argued that papillar  $\text{CD133}^+$  cells were able to integrate into embryonic kidney rudiments cultured *ex vivo* for four days (Ward et al., 2011). However, the assay used in this study bypassed the disaggregation and reaggregation of the mouse cells, and the human  $\text{CD133}^+$  cells were injected directly into E12.5 embryonic kidneys in culture. However, due to the experimental design it is possible that the integration shown could be instead due to the accumulation of the cells at the site of injection. In fact, there is no evidence that the human cells were randomly distributed in the embryonic kidney following the injection, but clusters of  $\text{CD133}^+$  cells were detected at day four inside the tubuli (Ward et al., 2011). By contrast, the reaggregation assay helps to understand whether exogenous cells actively contribute to the formation of the developing renal structures and are capable of specifically integrating and differentiating in the correct spatio-temporal fashion.

Only two studies have so far proved the capacity of iPSC- or ESC-derived nephron progenitor cells to engraft into the metanephric mesenchyme or ureteric bud (Takasato et al., 2014; Xia et al., 2013). These results cannot be considered as unexpected, since both nephron progenitor cell populations were in the 'right place'

at the 'right moment' matching in time the developmental stage of the reaggregation assay. The need for matching developmental stages between embryonic cells and exogenous cells is illustrated by the observation that amniotic fluid stem cells failed to integrate into chimeric kidney rudiments unless a genetic modification was introduced, such as the induced expression of GDNF (Xinaris et al., 2015). Importantly, GDNF (glial cell-line-derived neurotrophic factor 1) is one of the essential growth factors expressed by the cells of the metanephric mesenchyme that induce the growth of the ureteric bud. Furthermore, the expression of GDNF was shown to be regulated by the Pax2-expressing cells *in vitro* (Vainio and Lin, 2002). In the previous chapter, both CD133<sup>+</sup> and CD133<sup>-</sup> kidney-derived primary human cells were found to express Pax2. It would be therefore interesting to determine whether the primary renal cells secrete GDNF since they express Pax2.

The reaggregation assay performed in this study failed to show engraftment of the CD133<sup>+</sup> cells. Instead, the CD133<sup>+</sup> cells behaved more similarly to the ESCs used in the rudiment experiments by Takasato and colleagues (Takasato et al., 2014), by forming cysts on top of the chimeric organoids. Interestingly, no convoluted renal structures were identified in the direct vicinity to the cluster of human CD133<sup>+</sup> cells. By contrast, some of the CD133<sup>-</sup> cells were found in-between convoluted tubuli in the interstitial space. For both cell types, though, a complete disruption of the embryonic kidney structures could not be found. If the renal progenitor cells are defined by the expression of CD133, as claimed in the literature, then the CD133<sup>-</sup> cells would more likely represent a heterogeneous population of fully differentiated cells. According to the phenotyping experiments shown in chapter 3, both populations contain a fully differentiated fraction of proximal tubular cells. Yet, despite the observed cell death, the CD133<sup>-</sup> cells were able to remain in the interstitial space of formed structures, even if not in the tubuli, whereas the CD133<sup>+</sup> could not.

An important point needs to be raised about the dynamics of the human renal cells in the reaggregation assay. Previous studies that reported on the engraftment of exogenous cells in the reaggregation rudiments, do not mention any substantial loss of exogenous cells; in most cases high-magnification images are shown to demonstrate the engraftment, if applicable, of the cells tested (Kuzma-Kuzniarska et



al., 2012; Siegel et al., 2010; Song et al., 2012; Xinaris et al., 2012). Xinaris and colleagues mentioned that fewer AFSCs were present in the chimeric rudiments at day five compared to the initial amount (Xinaris et al., 2012). The results from this chapter show a striking difference between day 1 and day 3 in the number of GFP-labelled cells (both CD133<sup>+</sup> and CD133<sup>-</sup> cells) detectable in the same chimeric rudiments, even though a quantitative assessment was not performed. The use of different media combinations failed to prevent the loss of cells over time (data not shown). Hence, one of the conclusions from the KRA experiments is that the mouse embryonic kidney environment does not permit the survival of the human cells for more than two days. It would be important to thoroughly investigate the causes of the human cell loss that was observed in some instances and not in others: is it cell type dependent? An interesting experiment to explore the effect of the secreted factors present in the organoid environment could include the culture and exposure of human cells to the conditioned medium of control reaggregated spheroids: is there an increase in cell death in response to the conditioned medium? Subsequently, the factors present in the conditioned medium could be further analysed to pinpoint their role in the loss of the human cells.

In this chapter, it was shown that both CD133<sup>+</sup> and CD133<sup>-</sup> cells fail to contribute the development of renal structures by using the embryonic kidney reaggregation method introduced by Unbekandt in 2010. In this method, the rudiments become firmly attached to filter membranes, which can lead to issues with light scattering while imaging with the confocal microscope. Also, the imaging of the whole thickness of the sample highly depends on the working distance of the objective used. Nevertheless, as shown above, high-quality images could be acquired. The rudiment formed with the conventional approach is not entirely tri-dimensional; it has more of a dome-like shape. The method was therefore adapted in order to form renal embryonic spheroids. A direct comparison of some features of both systems is offered in Table 4.1. By using the PDMS support, the critical step of transferring the pellet on the membrane is abolished. In the conventional method, in fact, at this point the pellet can disaggregate and break in multiple points or spread on the membrane,

preventing the compaction of the pellet and the recapitulation of the development. By increasing its consistency, it is possible to reduce the amount of animals used.

**TABLE 4.1 DIRECT COMPARISON BETWEEN THE CONVENTIONAL AND THE NOVEL METHOD TO PERFORM THE KIDNEY REAGGREGATION ASSAY (KRA)**

One of the major differences is connected to the shape of the pellet. In the conventional KRA, the pellets assume a dome-like shape, whereas in the novel assay, the pellet becomes a spheroid. In the conventional KRA, the critical step is represented by the transfer of the pellet from the eppendorf to the membrane, where it can break in multiple pieces or spread on the membrane. Losing its compactness, it does not give rise to developing structures. That leads to a high variability between experiments and size of the actual pellet. All these problems are not relevant in the novel approach, since, once the pellet in the hydrophobic environment created by the PDMS and the membrane, it compacts to form a spheroid. Nevertheless, both approaches allow formation of functional structures and allow live imaging. However, the use of the confocal microscope can lead to photo-toxicity and photo-bleaching of the sample, whereas the LSFM does not. \* functionality shown in the literature by (Lawrence et al., 2015; Rak-Raszewska et al., 2012).

	<b>Conventional KRA</b>	<b>Novel KRA</b>
<b>Shape</b>		
<b>Size</b>	Highly variable	~400 µm
<b>Inter-experimental consistency</b>	No	Yes
<b>Direct contact with membrane?</b>	Yes → possible cell migration out of the pellet	No
<b>Antibody penetration</b>	Good	Not good
<b>Formation of structures?</b>	Yes	Yes
<b>Functional tubuli?</b>	Yes*	Yes
<b>Live imaging?</b>	Yes, by confocal → risk of bleaching	Yes, by LSFM → gentle for long term imaging

The novel reaggregation method combines the hydrophobic material PDMS (polydimethylsiloxane) with a polycarbonate membrane. Due to its low cost, easy fabrication and optical transparency, PDMS is the material of choice for microfluidic cell culture (Halldorsson et al., 2015). Here, it was used to create a hydrophobic well

that would support the formation and growth of the spheroids made of embryonic renal cells without promoting their attachment to the membrane. Elected method of the year in 2013 by Nature, the LSFM was chosen to image the spheroids because it presents several advantages over the confocal microscopy. High image capture speed, low phototoxicity and, therefore, lower photobleaching of the samples permit gentle imaging of live organisms that are fluorescently labeled or transparent, e.g. *Caenorhabditis elegans*. The LSFM is affirming itself in many fields, from plant biology to developmental biology, from neuroscience to the histological analysis of tissues (Pampaloni et al., 2015).

Due to the physical arrangement of the microscope, it is possible to rotate the sample and image it from different angles. The optical sections recorded are suitable for imaging reconstruction software such as Fiji or Imaris, which will allow detailed volume rendering of the sample. The amount of additional information that can be gathered using the LSFM is remarkable.

The embryonic renal spheroids that were created using the modified reaggregation method, presented a good distribution of epithelial structures at day six as shown by the expression of Laminin and Megalin. Pax2 was detected in an appropriate spatial arrangement, in both the MM and the UB. Not only so, in some spheroids nephrons expressing Synaptopodin at the tip of Laminin-positive structures were observed, suggesting that all stages of nephron development might be represented. This finding resonates with the lack of the presence and branching of one ureteric bud, which orchestrates the correct series of events during nephrogenesis (Vainio and Lin, 2002). The major drawback of the system was related to the impossibility to image the centre of the spheroid. Compact spheroids like these are difficult to image in their cores, due to antibodies not reaching the centre after fixation at end-point analysis, or due to increased light scattering in the case of live imaging. By comparison, tumor spheres of 1000-3000 cells are routinely imaged using the LSFM (Pampaloni et al., 2013). An alternative method would be the optical

clearing of the spheroid at end points, using one of the several protocols available<sup>3</sup>, whose aim is the reduction of the light scattering and the increase of the optical distance that can be imaged. CLARITY, for example, was used to image large samples (e.g. mouse brains) and showed a high structural resolution and molecular details (Chung and Deisseroth, 2013).

The assessment of the functionality of their renal tubuli was an important quality control for the reaggregated kidney spheroids formed following the novel method. The tubuli of the renal spheroids were able to uptake 6-CF and to be blocked by the OAT inhibitor, Probenecid. This feature implies that the tubuli are functional, as previously shown in the KRA rudiments (Lawrence et al., 2015; Rak-Raszewska et al., 2012). However, not all tubuli in the spheroid control samples appeared stained. This can be explained by two factors: i) the brightness of the tubuli in the front of the spheroid impedes the imaging of the tubuli in the core; ii) some tubuli might be more immature than others and in different developmental stages, as discussed above. However, the OAT family transporters start being expressed from E11.5 in the renal vesicles (Lawrence et al., 2015) and, in the spheroids, the condensed metanephric mesenchyme was observed. Hence, the spheroids represent developmental stages from E10.5-E11.5 onwards. Therefore, the lack of fluorescence in all tubuli might be due to an artifact in imaging.

Finally, live imaging of spheroids without and with GFP-labelled cells was performed. To achieve this, the microscope was combined with a biocompatible sample holder immersed in a perfusion chamber that is supplied continuously with medium and nutrients by dedicated reservoirs, connected to a peristaltic pump (Pampaloni et al., 2014). The GFP-labelled cells were highly active in the spheroid and underwent mitosis, showing that the arrangement supported normal cellular processes to take place. This allowed the live imaging sequence to capture cellular events as they were taking place in real-time. However, as already mentioned for the imaging of fixed spheroids, the core could not be imaged, and it was impossible to

---

<sup>3</sup> Clearing Procedures for Deep Tissue Imaging – Science Lab - Leica Microsystem website <https://www.leica-microsystems.com/science-lab/clarity/clearing-procedures-for-deep-tissue-imaging/>



determine whether GFP-labelled cells would be in the core as well. However, it is important to note that the live imaging experiments described in this thesis represent proof-of-principle studies, and more in-depth experiments are needed to fully explore the capabilities of the novel reaggregation method in combination with the LSFM.

Generally, the LSFM could be used to image spheroids made of stem cells, where the core harbors the quiescent stem cells. The encouraging results above show that mitosis can be detected, and exogenous cells be tracked, widening the type of questions that can be answered.

The versatility of the reaggregation spheroids in combination with the capabilities of the LSFM will open a myriad of possibilities to study cell behaviour in various different applications. Recently, iPSC-derived Six2<sup>+</sup>Sall1<sup>+</sup>Wt1<sup>+</sup>Pax2<sup>+</sup> nephron progenitor cells were plated on low-attachment plates and grown for ten additional days in order to obtain renal organoids that could be used for nephrotoxicity studies (Freedman et al., 2015; Morizane et al., 2015). Importantly, since organoids with sizes in the range of 400µm are ideal for the formation of a hypoxic core, the system may become highly relevant for the study of growth delays or regeneration after drug exposure (Ranga et al., 2014). Alternatively, the cross-talk between different cell types (e.g. tubular and immune cells) could be analysed in great detail. Finally, the LSFM has been proposed for use of in the clinic, to directly address the need for histological analysis of the biopsies of cancer patients (Pampaloni et al., 2015).

The LSFM will facilitate the analysis of organoids in studies on pharmacodynamics/pharmacokinetics, embryonic development, regenerative medicine applications, and tissue engineering. The applications are innumerable and will bring together scientists with a wide range of backgrounds.



## **5 AMELIORATION POTENTIAL OF HUMAN CD133<sup>+</sup> AND CD133<sup>-</sup> IN A CISPLATIN-INDUCED RAT MODEL OF ACUTE KIDNEY INJURY**

### **5.1 INTRODUCTION AND AIMS**

Given its central role in the detoxification and excretion of toxic compounds, the kidney is the major target of exogenous toxicants. Circa 20% of nephrotoxicity is caused by drugs, and this percentage increases with age, to reach up to 66% in the elderly. Nephrotoxicity is one of the key limiting factors of chemotherapeutics for various types of hyperplasia (Perazella, 2012).

In this chapter, a preclinical model of cisplatin-induced acute kidney injury was used to test the potential of human primary CD133<sup>+</sup> and CD133<sup>-</sup> cells to be used as cellular therapeutics. Athymic rats lacking only T cells were used in order to facilitate the survival of the human cells into the rat environment. Renal function was monitored using a novel transcutaneous device that does not require continuous blood or urine samplings as for conventional plasma clearance techniques. Instead, it measures the excretion of the renal marker FITC-Sinistrin after intravenous injection. The excellent safety profile of Sinistrin combined to the successful use of the device in preclinical models make the device a promising tool for the clinic (Scarfe et al., 2015; Schock-Kusch et al., 2009; Schock-Kusch et al., 2011; Steinbach et al., 2014).

The intravenous administration was the chosen route of administration. An important obstacle of this route is represented by the possible entrapment of the cells into the lung capillary bed. From the tail vein, the blood travels through the inferior vena cava all the way to the right ventricle of the heart. From there, the venous blood is distributed to both lungs where the carbon dioxide (CO<sub>2</sub>) is removed. The alveoli are responsible for the oxygenation of the blood that will then be diverted to the rest of the body. The diameter of the interior pulmonary capillaries was measured

to be  $5.15 \pm 1.3 \mu\text{m}$  in SD rats. Therefore, IV-injected cells larger than the pulmonary capillaries, risk to get trapped in the lungs (Kutscher et al., 2010; Leibacher and Henschler, 2016). For instance, Fischer and colleagues demonstrated that the majority of intravenously administered stem cells [mesenchymal stromal cells (MSC), multipotent adult progenitor cells (MAPC), bone marrow-derived mononuclear cells (BMMC) and neural stem cells (NSC)] in rats did not reach the arteriosus system, but were trapped in the pulmonary system and cleared there. The size of the cells made a difference in the pulmonary passage: the smallest cells in the set [BMMC (diameter of  $7 \mu\text{m}$ )] showed a pulmonary passage 30-fold higher than MSCs ( $d \sim 18 \mu\text{m}$ ), followed by MAPC and NSC ( $d = 15$  and  $16 \mu\text{m}$ , respectively) that had a 2-fold increase compared to MSCs. The adhesion properties of the injected cells played a role too: MSCs treated with CD49d (that inactivates VCAM-1) showed a 2-fold increase of pulmonary passage. VCAM-1, adhesion molecule expressed by endothelial cells, might promote the entrapment of the MSCs in the endothelial capillaries in the lungs, impeding the pulmonary passage (Fischer et al., 2009).

Given the previous studies that use  $\text{CD133}^+$  and  $\text{CD133}^-$  cells in acute kidney injury models (introduced extensively in the introduction), it was speculated that the  $\text{CD133}^+$  cells would exert a positive impact on the development of the acute injury induced by cisplatin. On the contrary,  $\text{CD133}^-$  cells serve as a negative control, since their efficacy has never been shown before. The transcutaneous device can be effective in reducing the number of animals used for the experimentation, allowing the longitudinal monitoring of the renal function without the need of sacrificing the animals. It was also hypothesised that, following IV administration, the cells identified by GFP would get trapped in the lungs, and never reach the kidney. In the kidneys, instead, it would be expected to observe PKH26 staining, used to co-stain the cells, as a sign of the release of extracellular vesicles that help the amelioration process.

In this chapter, the main aims that will be addressed in this chapter encompass:

- I) Assess the therapeutic effect of human-derived  $\text{CD133}^+$  and  $\text{CD133}^-$  cells on renal function in a model of acute kidney injury induced in immunodeficient rats (RNU) after cisplatin administration.

- II) Investigate the biodistribution pattern and evaluate the engraftment of the intravenously injected human-derived CD133<sup>+</sup> and CD133<sup>-</sup> cells into the damaged kidney.
- III) Study the role of the innate immune system following the administration of the human renal CD133<sup>+</sup> and CD133<sup>-</sup> cells, to establish possible mechanisms of action of the human cells in the model.

## 5.2 RESULTS

The *in vivo* experiments presented in this chapter were carried out during my secondment in the lab of Prof. Norbert Gretz (Centre for Medical Research, University of Heidelberg, Mannheim, Germany), where I worked in collaboration with Zeneida Herrera Perez (University of Heidelberg) who developed the Cisplatin Rat model.

The cells were transduced and sorted at the University of Liverpool and cultured at the University of Heidelberg for one passage before the injection. Zeneida Herrera Perez performed the injections. The GFP-containing lentivirus (pHIV-GFP) was kindly supplied by Dr. Arthur Taylor (University of Liverpool). The Hematoxylin and Eosin stainings were performed by technical personnel at the University of Heidelberg. The paraffin blocks for other staining procedures were kindly cut by Angela Platt-Higgins, research technician at the University of Liverpool.

### 5.2.1 PREPARATION OF CD133<sup>+</sup> AND CD133<sup>-</sup>-GFP-LABELLED

The heterogeneous population was labelled with GFP lentivirus and sorted for the expression of CD133 only, as shown in paragraph 4.2.1 in chapter 4. For the *in vivo* experiments, it was decided to inject the cells (CD133<sup>+</sup> and CD133<sup>-</sup>) at passage 5, right after the trypsinization at passage 4, when the CD133 expression was expected to be above 90%. According to Figure 3.16, CD133<sup>+</sup> cells start losing considerably the expression of CD133 after 5 days in culture at passage 5 (~80%). The FACS analysis confirmed that  $91.36\% \pm 9.17$  of the CD133<sup>+</sup> cells expressed CD133/2. However, based on the finding that CD133 expression increased in the CD133<sup>-</sup> population during expansion, immunodepletion of CD133<sup>+</sup> cells by MACS was employed to maintain a pure negative population when necessary (Data not shown). Before injection,  $7.01\% \pm 6.00$  of the CD133<sup>-</sup> cells expressed CD133/2 (Figure 5.1).

To include an additional cell labelling method, consistent with previous studies in

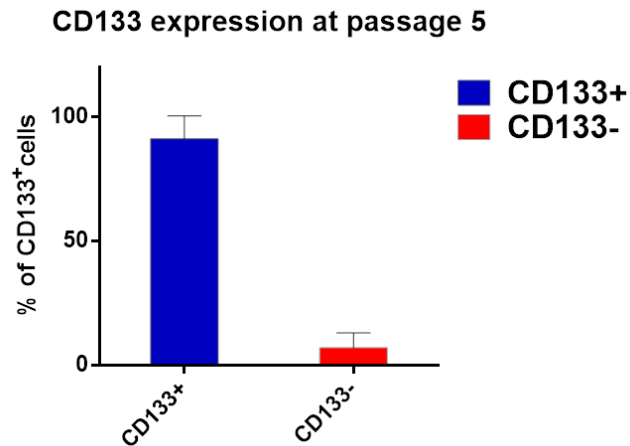


**FIGURE 5.1 CONFIRMATION OF THE PURITY OF BOTH POPULATION AT P5 BEFORE INJECTION *IN VIVO***

FACS analysis of the expression of CD133/2 APC in both CD133<sup>+</sup> and CD133<sup>-</sup> populations at P5, the passage of the injection *in vivo*. Mean values  $\pm$  SEM of three independent sortings and expansions.

the literature (Gupta et al., 2015; Qi and Wu, 2013; Ronconi et al., 2009), both cell populations were incubated before the injection with PKH26. PKH26 is a lipophilic dye with an excitation wavelength of 551 nm and an emission wavelength of 567 nm, which is diluted out upon cell division and can be transferred to the host cells via extracellular vesicles (Li et al., 2013a).

Therefore, all cells were GFP-positive and PKH26-positive and either CD133<sup>+</sup> or CD133<sup>-</sup>. From now on, they will be referred as CD133<sup>+</sup> and CD133<sup>-</sup> cells only.

### 5.2.2 TWO-WEEK STUDY

The experimental design of the two-week study is shown in Figure 5.2. Cisplatin was injected intraperitoneally (IP) at a dose of 7mg/100g BW and the day of cisplatin administration was defined as day 0. Renal function was monitored throughout the study using the GFR transcutaneous device, and measurements were performed before the induction of the damage (baseline) and on days 2, 7 and 14 after Cisplatin injection. Also, blood and urine samples were collected at baseline and days 7 and 14 after the induction of the damage. Day 7 represents the peak of damage (Zeneida Herrera-Perez, personal communication). Three experimental groups were used in this study. The control group received cisplatin on day 0 and saline on day 2 and 7, the

CD133<sup>+</sup>-treated group received cisplatin on day 0 and 1 million CD133<sup>+</sup> cells on day 2 and 7 and the CD133<sup>-</sup>-treated group received cisplatin on day 0 and 1 million CD133<sup>-</sup> cells injected on day 2 and 7. It is important to mention that the GFR measurements on days 2 and 7, and urine and blood collection on day 7 were performed before the injection of a single dose of 1 million CD133<sup>+</sup> or CD133<sup>-</sup> cells.

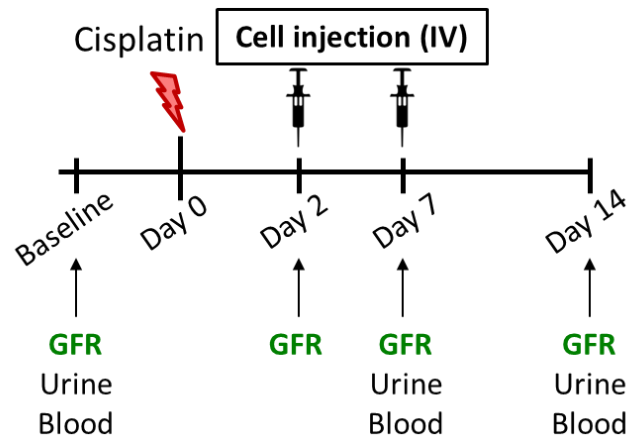


**FIGURE 5.2 EXPERIMENTAL SET-UP OF THE TWO-WEEK STUDY**

### 5.2.2.1 MONITORING THE RENAL FUNCTION USING THE TRANSCUTANEOUS DEVICE

The overview of the GFR measurements over the length of the study is presented in Figure 5.3. The results of FITC-Sinistrin half-life (HL-Sin), serum creatinine and serum urea are reported in Figure 5.3.

At baseline, all rats had comparable HL-Sin, while on day 2 the renal injury was already apparent, as shown by the modest, but not significant increase in HL-Sin. In fact, the measurements on day 2 were used to corroborate the presence of the damage and avoid the injection of cells into animals that did not develop the damage. In fact, 37.5% (12 out of 32 rats) of the animals did not show any increase in HL-Sin at day 2 and were therefore eliminated from the study.

On day 7, both cell-treated groups showed a reduction of the HL-Sin, of 59.1% (CD133<sup>+</sup> cells) and 46.8% (CD133<sup>-</sup> cells), when compared to the control group. Interestingly, there is no significant difference between the groups that received CD133<sup>+</sup> or CD133<sup>-</sup>. These data suggest that the reduction in HL-Sin observed was a consequence of the cell injection. Furthermore, the results indicate that CD133 might not be the exclusive factor responsible for the amelioration of the renal function.

By day 14, a decrease in the HL-Sin was observed in the control group, corroborating the acute type of damage induced by Cisplatin. As mentioned in the introduction, the tubular compartment triggers an offsetting response; the residual proximal tubule cells start proliferating to replace the neighbours lost upon injury, leading to the improvement of the renal function. In the cell-treated groups, the HL-Sin remained at similar levels as on day 7, suggesting that the second injection of CD133<sup>+</sup> or CD133<sup>-</sup> cells did not further ameliorate the renal function.

Altogether, these results suggest that one injection of either CD133<sup>+</sup> or CD133<sup>-</sup> cells two days after the induction of the damage was beneficial in reducing the HL-Sin, and, as a consequence, improving the renal function. Nevertheless, the HL-Sin of each group failed to return to the baseline levels after 14 days (Figure 5.3).

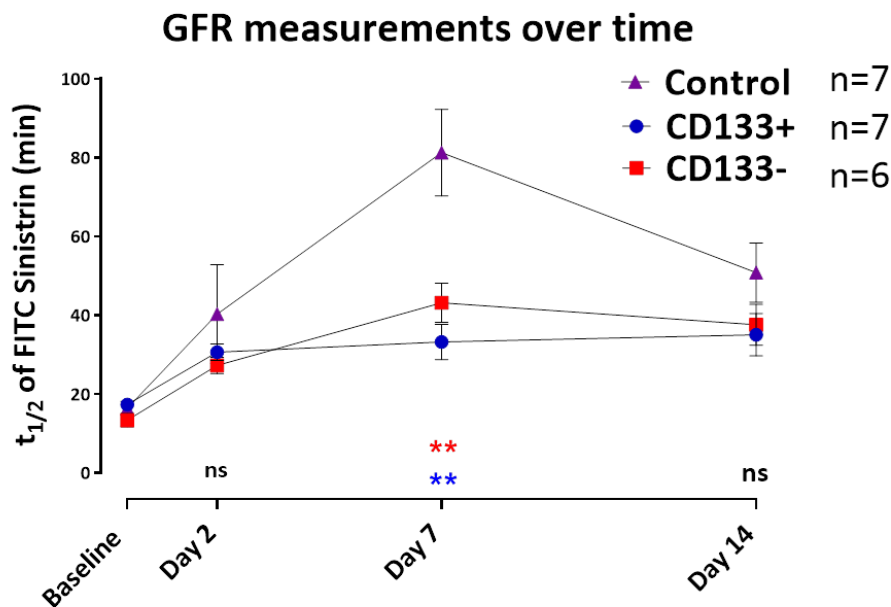


**FIGURE 5.3 HALF-LIFE VALUES OF FITC-SINISTRIN OVER THE TWO WEEKS STUDY OBTAINED USING THE GFR DEVICES**

Mean values  $\pm$  SEM of the HL-Sin over the whole length of the study (CD133<sup>+</sup> group n=6, CD133<sup>-</sup> group n=6, Control group n=7). An ANOVA one-way statistical test with Dunnett *Post Hoc* analysis was applied for each time point to compare the groups \*\* p=0.0026; \*\* p=0.0095.



**TABLE 5.1 MEAN VALUES OF HL-SIN, SERUM CREATININE, AND SERUM UREA ± SEM FOR ALL GROUPS AT ALL TIME-POINTS EVALUATED**

An ANOVA one-way statistical test with Dunnet *Post Hoc* analysis was applied for group to compare baseline values and values at day 14.

HL-Sin p-values: Control: Base vs. 14D p <0.0001; CD133<sup>+</sup>: Base vs. 14D p=0.0237; CD133<sup>-</sup>: Base vs. 14D p=0.0032;

Serum Creatinine p-values: Control: baseline vs. d14 p<0.0001; CD133<sup>+</sup>: baseline vs. d14 p=0.0008; CD133<sup>-</sup>: baseline vs. d14 p<0.0001;

Serum urea p-values: Control: baseline vs. d14 p=0005; CD133<sup>+</sup>: baseline vs. d14 p=ns; CD133<sup>-</sup>: baseline vs. d14p=ns.

		<i>Cisplatin</i>		<i>CD133<sup>+</sup></i>		<i>CD133<sup>-</sup></i>	
<b>HL-Sin (min) ± SEM</b>	<i>B</i>	16.41 ± 1.78	] * * * ]	17.36 ± 1.54	] * * * ]	13.38 ± 1.68	] * * * ]
	<i>D2</i>	40.3 ± 12.51		30.63 ± 2.08		27.25 ± 2.07	
	<i>D7</i>	81.27 ± 11.01		33.21 ± 4.47		43.18 ± 4.96	
	<i>D14</i>	50.83 ± 7.47		35.07 ± 5.38		37.60 ± 5.17	
<b>SCr (mg/dL) ± SEM</b>	<i>B</i>	0.16 ± 0.00	] * * * ]	0.17 ± 0.00	] * * * ]	0.16 ± 0.00	] * * * ]
	<i>D7</i>	1.59 ± 0.55		0.44 ± 0.04		0.56 ± 0.05	
	<i>D14</i>	0.59 ± 0.08		0.39 ± 0.04		0.46 ± 0.02	
<b>SUrea (mg/dL) ± SEM</b>	<i>B</i>	39.64 ± 2.09	] * * * ]	31.8 ± 1.33	] ns ns ns ]	35.23 ± 1.80	] ns ns ns ]
	<i>D7</i>	294.7 ± 94.87		75.84 ± 10.97		107.3 ± 24.82	
	<i>D14</i>	122.1 ± 29.23		63.7 ± 10.4		76.42 ± 12.32	

### 5.2.3 MONITORING SERUM CREATININE AND UREA TO ASSESS FUNCTIONAL RENAL DAMAGE

The magnitude of the renal damage was also evaluated through the measurement of conventional renal biomarkers, such as creatinine and urea in serum and urine (Figure 5.4).

The animals that had received CD133<sup>+</sup> or CD133<sup>-</sup> cells showed a reduction in the serum levels of creatinine and urea when compared to the control animals at day 7 (Figure 5.4 A). Despite similar values for both the CD133<sup>+</sup> and CD133<sup>-</sup>-treated groups, statistical significance in the difference for serum creatinine and for serum urea was only observed in animals that received CD133<sup>+</sup> cells. At day 14, all groups showed comparable values of serum creatinine. However, the serum creatinine levels at day 14 failed to return to baseline levels (Table 5.1).

The results for the serum urea revealed that at day 7 rats from both cell-treated groups had much lower values than control animals, but only in the group that received CD133<sup>+</sup> cells was the difference significant (Figure 5.4 B). However, at day 14 the serum urea levels of the cell-treated groups, but not the control group returned to baseline levels (Table 5.1).

Altogether, the renal serum markers supported the data obtained through the GFR device, revealing an acute phase of the injury in the control animals that was attenuated in both groups of animals after treatment with the cells.

Creatinine and urea were also analysed in the urine of the animals of each experimental group (Figure 5.4 C-D). An increase of urinary creatinine or a decrease in urinary urea would be symptomatic of kidney disease. In the cisplatin model, however, there were no significant differences in the urinary injury markers between groups, with the exception for the CD133<sup>-</sup>-treated group when compared to control group at day 14.

Altogether, these results suggest that even one single injection of either CD133<sup>+</sup> or CD133<sup>-</sup> two days after the initial damage was beneficial in slowing down or even arresting the development of the injury. The transcutaneous measurements showed an improvement of approximately the 50% of the renal function after treatments with both cell types. Serum Creatinine and serum urea were less sensitive, when compared to the HL-Sin and significance could be found only for CD133<sup>+</sup> cells. Finally, urinary Creatinine and Urea failed to highlight any difference in the groups.

Interestingly, all biomarkers used to assess renal function did not return to baseline levels, indicating that the damage is not resolved in 14 days (Table 5.1). The cisplatin dose used in these immunodeficient rats surely induced an acute kidney injury. However, it can be speculated that the damage could progress to a chronic injury in the long-term. An additional set of measurements at a later time point will help in defining the long-term effects of the used dose of cisplatin and the role of the cellular therapies.

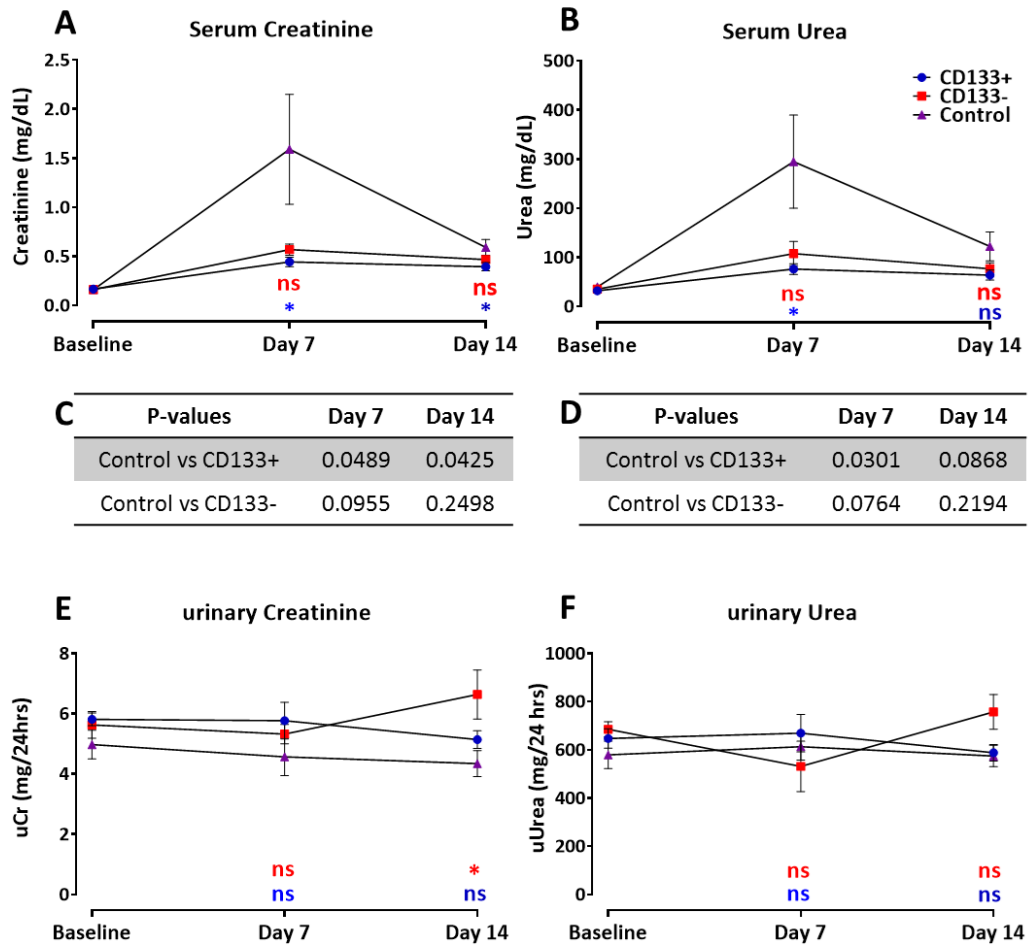


**FIGURE 5.4 SERUM CREATININE AND SERUM UREA VALUES OVER THE TWO WEEKS STUDY IN SERUM AND URINE**

Mean values  $\pm$  SEM of serum creatinine (A), serum urea (B), urinary creatinine (E) and urinary urea (F) at baseline, day 7 and 14. The urinary values were normalized over a 24 hours period. The ANOVA one-way statistical test with Dunnet *Post Hoc* analysis was applied for each time point to compare the groups. (C) and (D) Tables summarizing the p-values of the statistical test at day 7 and day 14. The p-values table for urinary creatinine and urea were not included, because higher than 0.5. uCr (Day 14; Control vs CD133<sup>-</sup>) \* p=0.0138.

### 5.2.3.1 EVALUATING URINARY TIM-1, CYSTATIN C AND ALBUMIN AT D14

In the last decade, there has been intensive research on developing novel renal biomarkers. As explained in the introduction, creatinine and urea are not always suitable biomarkers to detect nephrotoxicity. Specifically, Tim-1 (rat homologue of Kim-1) and cystatin C (Cys-C) were proposed as excellent biomarkers to monitor renal health.

Tim-1, Cys-C and the albumin/creatinine ratio (ACR) were evaluated in the urine for each experimental group at baseline, day 2 and 7. All values were normalized to the amount of urinary creatinine over a 24 hour period (Figure 5.5).

In healthy animals, Tim-1 is not excreted, as shown by the virtual absence of Tim-1 from the urine of all animals at baseline. Upon damage, Tim-1 levels raised significantly in all groups (One-way ANOVA, Tukey *Post Hoc* test,  $p < 0.0001$  for all groups), consistent with the fact that damaged proximal tubule cells shed Tim-1 into the luminal area, and, therefore, the urine. At day 7, both cell-treated groups did not show any major difference in the levels of Tim-1 when compared to the control group. Nevertheless, the urinary concentration of Tim-1 slightly decreased at day 14 for all experimental groups. However, this reduction was not significant and, most importantly, was comparable for all experimental groups (Figure 5.5 A and Table 5.2).

Cys-C is produced at a constant rate from every nucleated cell. It is then reabsorbed and catabolized from the proximal tubule cells. Therefore, in case of tubular damage, the reabsorption capacity of the tubular cells is impaired, and Cys-C is released into the urine. In this study, the urinary levels of Cys-C raised equally in all three groups at day 7. However, the increase was not significant. At day 14, the Cys-C levels remained constant for the CD133<sup>-</sup> group and rose slightly for the CD133<sup>+</sup> and control group. No statistical differences were detected among the groups (Figure 5.5 B and Table 5.2).

Finally, the urinary ACR informs about microalbuminuria. It reflects the status of the filtration barrier in the glomerulus; therefore, it can be informative of the onset of a chronic type of damage. At day 7, it was observed a slight, but not significant increase in the ACR in all groups. At day 14, the control group displayed a significantly higher ACR compared to both cell-treated groups. Importantly, there were no differences among the cell-treated groups (Figure 5.5 C and Table 5.2).

The data relative to the urinary biomarkers Tim-1 and Cys-C were consistent with the onset of an acute kidney injury, but not with the trend observed for HL-Sin, serum creatinine and serum urea. In the data set presented in this paragraph, the cell therapies did not lead to a reduction of the levels of the biomarkers at any time point.

Not only so, all groups showed significantly higher levels of urinary markers at day 14 than at baseline, indicating that some degree of renal damage was still present.

Instead, the ACR data suggested that the human cells prevented leakage of albumin across the filtration barrier in the long term, as shown by the difference at day 14 between the two cell-treated groups and the control group. This finding corroborates the possibility of the onset of chronic kidney disease.

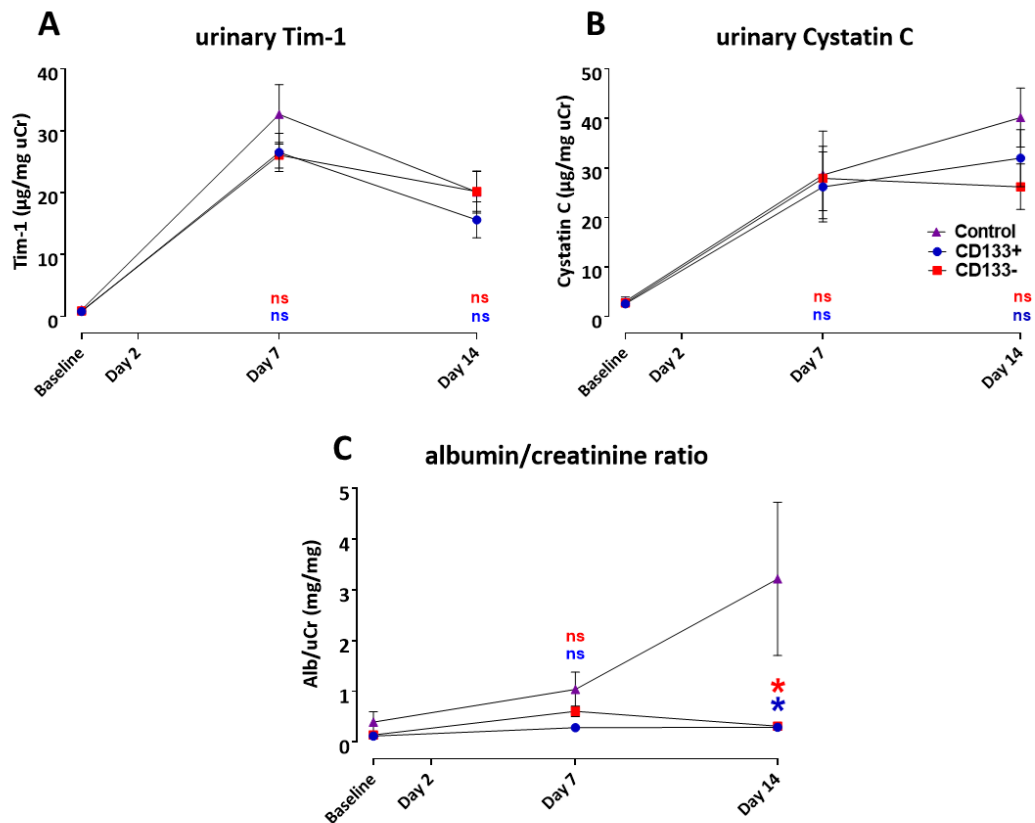


**FIGURE 5.5 URINARY TIM-1, CYS-C AND ALBUMIN OVER THE LENGTH OF THE STUDY**

Mean values  $\pm$  SEM of urinary Tim-1 (A), Cys-C (B) and albumin (C) at baseline, day 7 and day 14. To detect the urinary values of Tim-1 and Cys-C, the urine of 5 animals per group was randomly used. All urinary values were normalized against urinary creatinine. The ANOVA one-way statistical test with Tukey *Post Hoc* analysis was applied for each time point to compare the groups. ACR (Day 14; vs. Control \*  $p=0.215$ , \*  $p=0.0345$ )

**TABLE 5.2 MEAN VALUES ± SEM FOR TIM-1, CYS-C, AND ACR ± SEM FOR ALL GROUPS AT ALL TIME POINTS. THE ANOVA ONE-WAY STATISTICAL TEST WITH TUKEY POST HOC ANALYSIS WAS APPLIED FOR GROUP TO COMPARE BASELINE VALUES AND VALUES AT DAY 14.**

Tim-1 p-values: Control: Base vs. 14D p=0.0031; CD133<sup>+</sup>: Base vs. 14D p=0.0381; CD133<sup>-</sup>: Base vs. 14D p=0.0026;

Cys-C p-values: Control: baseline vs. d14 p=0.0059; CD133<sup>+</sup>: baseline vs. d14 # p=0.0499; CD133<sup>-</sup>: baseline vs. d14 p=ns;

ACR p-values: Control: baseline vs. d14 p=0.0217; CD133<sup>+</sup>: baseline vs. d14 p=ns; CD133<sup>-</sup>: baseline vs. d14 p=ns

		<i>Cisplatin</i>	<i>CD133<sup>+</sup></i>	<i>CD133<sup>-</sup></i>
<b>Tim-1</b> (µg/mg Cr) ± SEM	<i>B</i>	1.10 ± 0.18	0.83 ± 0.08	0.92 ± 0.09
	<i>D2</i>	32.63 ± 4.79	26.51 ± 3.09	26.06 ± 2.05
	<i>D14</i>	20.11 ± 3.40	15.62 ± 2.90	20.20 ± 3.20
<b>Cys-C</b> (µg/mg Cr) ± SEM	<i>B</i>	3.09 ± 1.72	2.56 ± 0.37	2.76 ± 0.69
	<i>D7</i>	28.6 ± 8.83	26.18 ± 7.04	27.89 ± 6.49
	<i>D14</i>	40.16 ± 5.92	31.98 ± 5.72	26.20 ± 4.58
<b>Alb/uCr</b> (mg/mg) ± SEM	<i>B</i>	0.39 ± 0.20	0.11 ± 0.00	0.13 ± 0.02
	<i>D7</i>	1.03 ± 0.34	0.28 ± 0.06	0.60 ± 0.10
	<i>D14</i>	3.21 ± 1.15	0.29 ± 0.06	0.31 ± 0.04

### 5.2.3.2 HISTOLOGICAL EVALUATION OF RENAL INTEGRITY AT DAY 14

The tissue integrity of the kidneys was analysed after Hematoxylin and Eosin staining at day 14. In the control group, several abnormalities, typical of acute tubular injury, were observed (Figure 5.6 A): the tubular cells showed features of undergoing apoptosis, including pyknotic nuclei, and being shed into the lumen, while the remaining epithelium lost the brush border, had a flattened appearance and the tubular lumen was disproportionally enlarged. By contrast, in the two cell-treated groups, cellular debris in the luminal area and flattened epithelia were rarely observed. Instead, regenerating tubuli with almost intact brush borders were detectable (Figure 5.6 B-C). In all groups, glomeruli appeared intact and morphologically normal.

In order to quantify the histological damage, the luminal area of the tubuli was measured using the imaging software Fiji for each experimental group in a blinded fashion. The results are summarized in Figure 5.8 D, showing that the mean luminal

area of the groups that received either CD133<sup>+</sup> or CD133<sup>-</sup> cells was significantly smaller than the average luminal area of the control group.

Further correlation analysis revealed a significant coefficient of correlation between the computed luminal area and the HL-Sin at day 14 (Table 5.1 E) in the control group (p-value <0.05). Also, the CD133<sup>+</sup>-treated group showed a significant correlation coefficient. This correlation indicates that it might be possible to infer the actual tissue damage by measuring the renal function through the transcutaneous device. Higher animal numbers would be required to fully test this hypothesis.

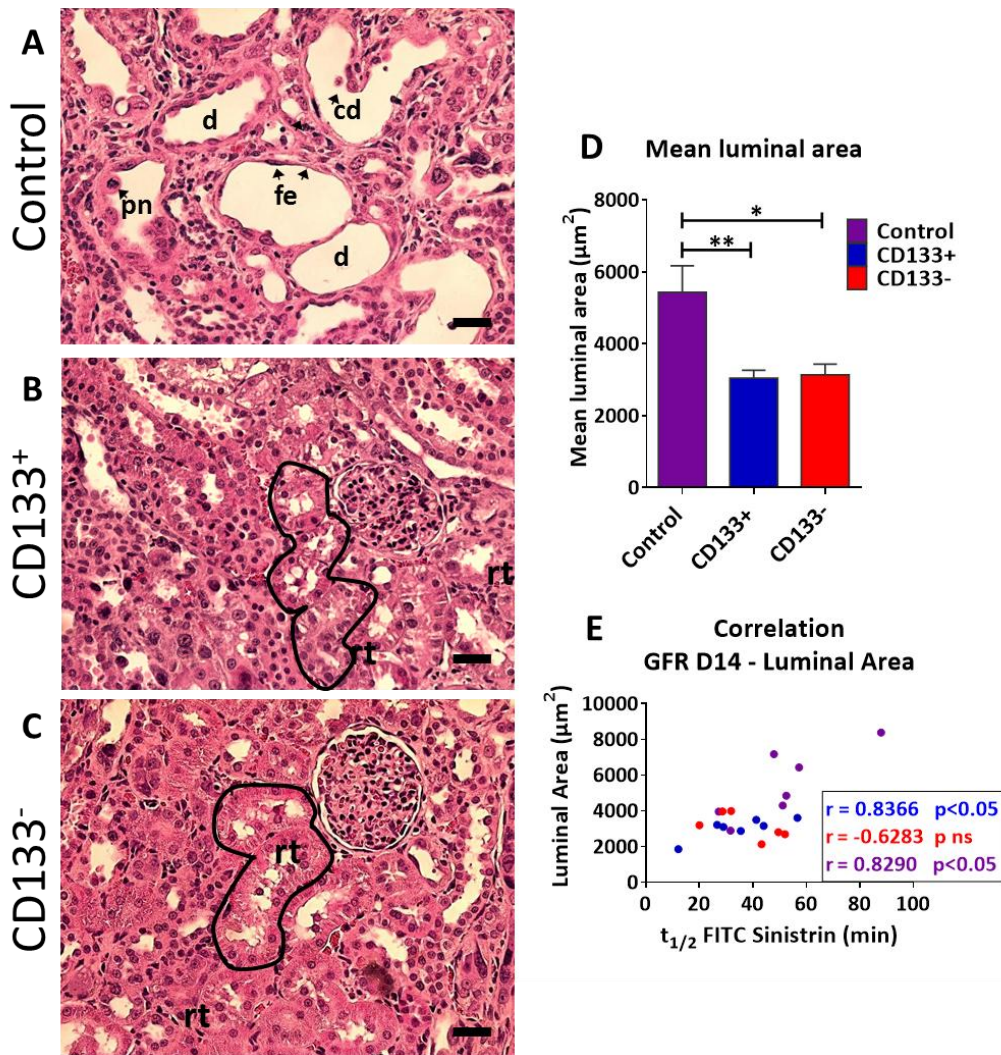


**FIGURE 5.6 EVALUATION OF THE RENAL INTEGRITY AT DAY 14**

(A-C) Representative images for each experimental group of H&E-stained paraffin sections of the kidney. The scale bars represent 50µm. (D) Mean luminal area ± SEM. The luminal area was measured using the imaging software Fiji, applying the black and white threshold to at least 10 images per animal. The ANOVA one-way statistical test with Dunnett *Post Hoc* analysis was applied to compare the groups. (E) Pearson correlation between the HL-Sin values at day 14 and the luminal area at day 14.

Abbreviations: pn – Pyknotic nuclei, cd – cellular debris, fe – flat epithelium, (d – dilated tubuli, rt – regenerating tubuli, surrounded by the black solid line.

### 5.2.3.3 CORRELATION OF BIOMARKERS WITH HISTOLOGY AND HL-SIN VALUES

Since the conventional biomarkers, serum creatinine and urea, still represent the gold standard in the clinic to detect acute kidney injury, the correlation between the HL-Sin values and the serum biomarkers values was tested (Figure 5.7). None of the conventional biomarkers significantly correlated with the HL-Sin values, probably



indicating a difference in the accumulation of serum creatinine and urea following injury and the excretion rate of FITC-Sinistrin following injury.

Also, the values of the luminal areas were tested for their correlation with the serum biomarkers. However, even in this instance, no significance was found, highlighting that both biomarkers might not be sensitive enough to infer the tissue integrity in the three experimental groups.

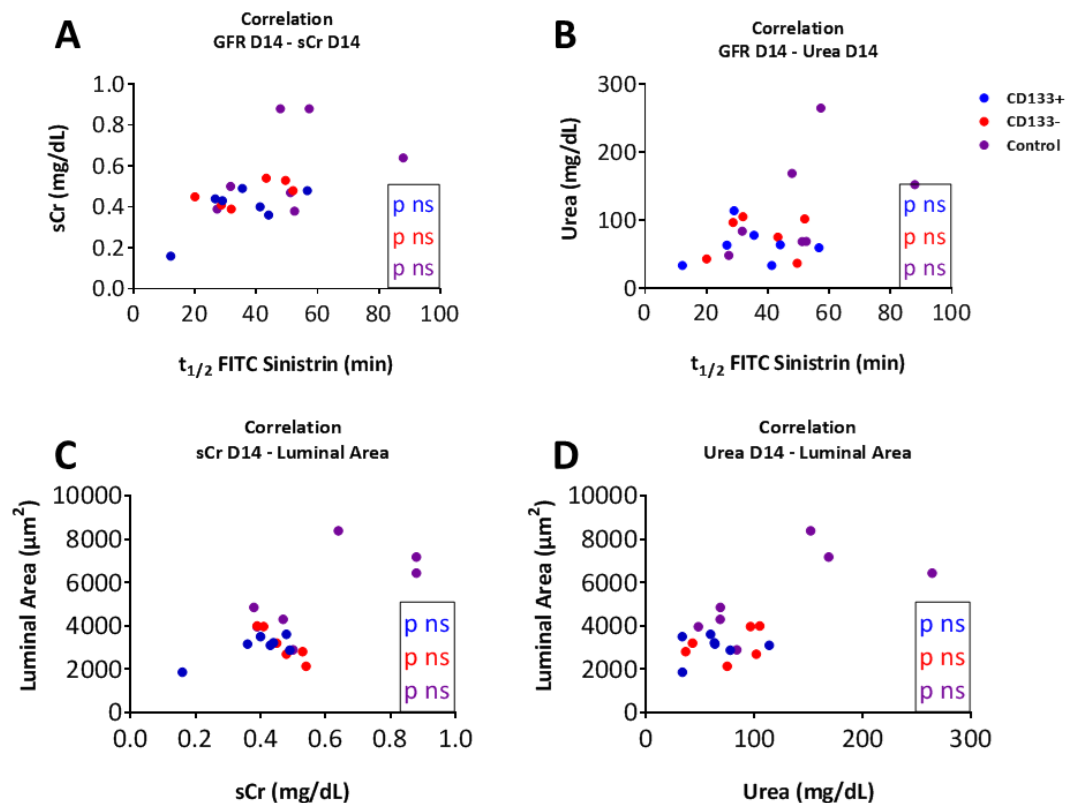


**FIGURE 5.7 CORRELATION OF SERUM BIOMARKERS WITH HL-SIN AND LUMINAL AREA VALUES**

(A) Pearson correlation between the HL-Sin values at day 14 and the serum Creatinine values at day 14. (B) Pearson correlation between the HL-Sin values at day 14 and the serum Urea values at day 14. (C) Pearson correlation between the luminal area at day 14 and the serum Creatinine values at day 14. (D) Pearson correlation between the luminal area at day 14 and the serum Urea values at day 14. P values are indicated in the insets.

#### 5.2.3.4 HISTOLOGICAL EVALUATION OF RENAL FIBROSIS AT DAY 14

Renal fibrosis occurs when there is an excessive accumulation of extracellular matrix, specifically collagen, in the tubular-interstitial space. This excessive accumulation leads to the formation of scar tissue, with consequent loss of tissue or

organ function. In the kidney, progressive loss of function would undoubtedly lead to ESRD.

To measure fibrosis, paraffin sections from kidneys of the three experimental groups were stained for Masson's Trichrome, a histological staining technique efficient in detecting early fibrosis where blue staining marks matrix elements, including both basement membrane and collagen (Street et al., 2014). Five images of the cortex were stitched together to visualise the differences among the groups throughout a larger section of the kidneys including cortex and parts of the medulla (Figure 5.8 A-C). The stitched images show that the cortical epithelium of the control group was completely damaged as the most proximal tubular epithelia were flattened, and the luminal dilation was high (Figure 5.9 A). By contrast, sections from kidneys of the groups that received human cells revealed a more organized cortex, with smaller dilated tubuli and regenerating tubular epithelia (Figure 5.9 B, C). Between the two cell-treated groups, the CD133<sup>-</sup> treated group appeared to have tubuli with larger lumen that could not be completely appreciated in the H&E single images.

The blue staining as indicator of matrix deposition was quantified using the colour threshold function of the imaging software Fiji, and the results are shown in Figure 5.8 D. While the mean tissue area identified as fibrotic for all control animals was larger than for the cell-treated animal groups, these differences were not significant. Examples of staining of the two extremes (highest fibrotic area and lowest fibrotic area) are shown in the two insets. Since fibrosis develops slowly in damaged tissue it is not surprising that significant differences could not be observed at day 14. The fibrotic area was also measured using the histological stain Picrosirius Red where the collagen deposition is stained bright red. However, similar results were obtained and no differences noted (data not shown).

In conclusion, the results presented so far demonstrate that the injection of CD133<sup>+</sup> or CD133<sup>-</sup> cells have beneficial effects on kidney function and tubular structure in cisplatin-injured rats. However, the data fail to show any difference in fibrosis in the kidneys between control and cell-treated animals.

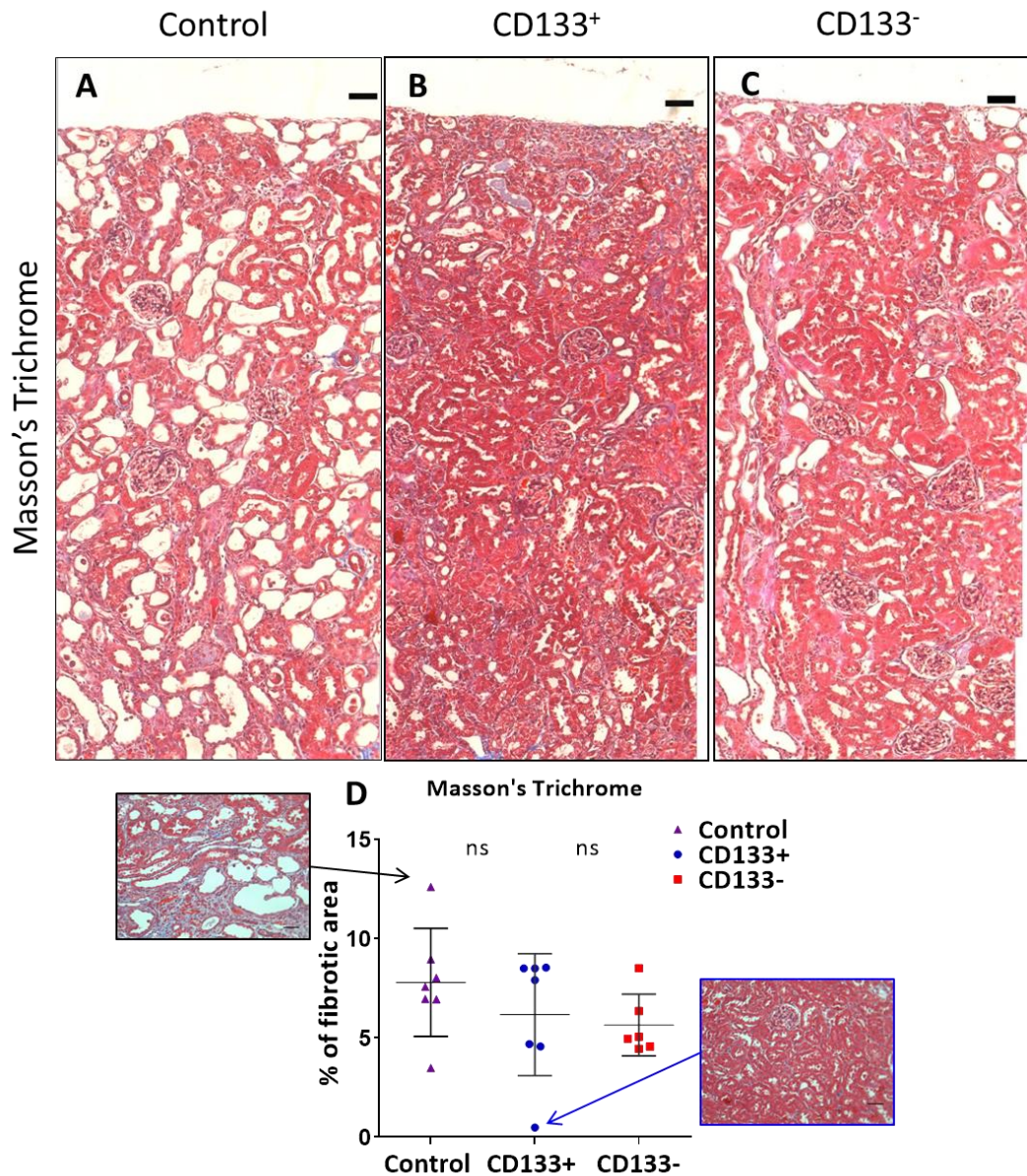


**FIGURE 5.8 EVALUATION OF FIBROSIS AT DAY 14 AFTER CISPLATIN INJURY**

Representative stitched images of Masson's Trichrome staining of kidney sections from control group (A), CD133<sup>+</sup>-treated group (B), and CD133<sup>-</sup>-treated group (C) animals. (D) Quantification of the fibrotic area in histological kidney sections of animals of all groups after processing of at least 10 images per animal per group. An ANOVA one-way statistical test with Dunnett *Post Hoc* analysis was applied to compare the groups. The bars represent the SEM. The insets show representative images of the animals with the highest and lowest fibrotic area.

### 5.2.3.5 LOCALIZATION OF PKH26<sup>+</sup>/GFR<sup>+</sup> CELLS AT DAY 14 IN LUNGS AND KIDNEYS

Once the therapeutic efficacy of the cells has been proved, the following aim was to localize the CD133<sup>+</sup> or CD133<sup>-</sup> cells at day 14 in order to assess whether the benefit that the cells exert are due to their engraftment in the renal tissue. Given the

administration route used in the study, lungs were also collected for analysis. A GFP antibody was used to identify unequivocally the human cells, while PKH26 was detected due to its fluorescence properties (Excitation maximum 551 nm, Emission maximum 567 nm).

In the lungs, no GFP-positive cells were detectable in the lungs. However, small dots of PKH26 stain could be identified in clusters in the lung sections (Figure 5.9 A-B). In the kidneys, GFP-positive cells could not be detected; it is important to note that strong autofluorescence in the tubuli, especially in the green channel, was visible (compare with lung sections). PKH26 staining could be identified in the two cell-treated groups. As observed in the lungs, the PKH26 staining appeared as red spots close to the nuclei of either tubular cells or interstitial cells (Figure 5.9 D-F).

The results showed in this paragraph provide compelling evidence for the passage of the cells through the lungs, where the PKH26 staining is stronger than in the kidneys. At the end of the experiment, however, the GFP-positive cells could not be identified, suggesting that the expression of GFP or the entire cells might have been lost in the two-weeks. It is noteworthy that, especially in the control group, there are cells that are autofluorescent in the green and red channel, highlighted in Fig 10 C and F with arrowheads. These cells might represent immune cells, such as macrophages (Njoroge et al., 2001).

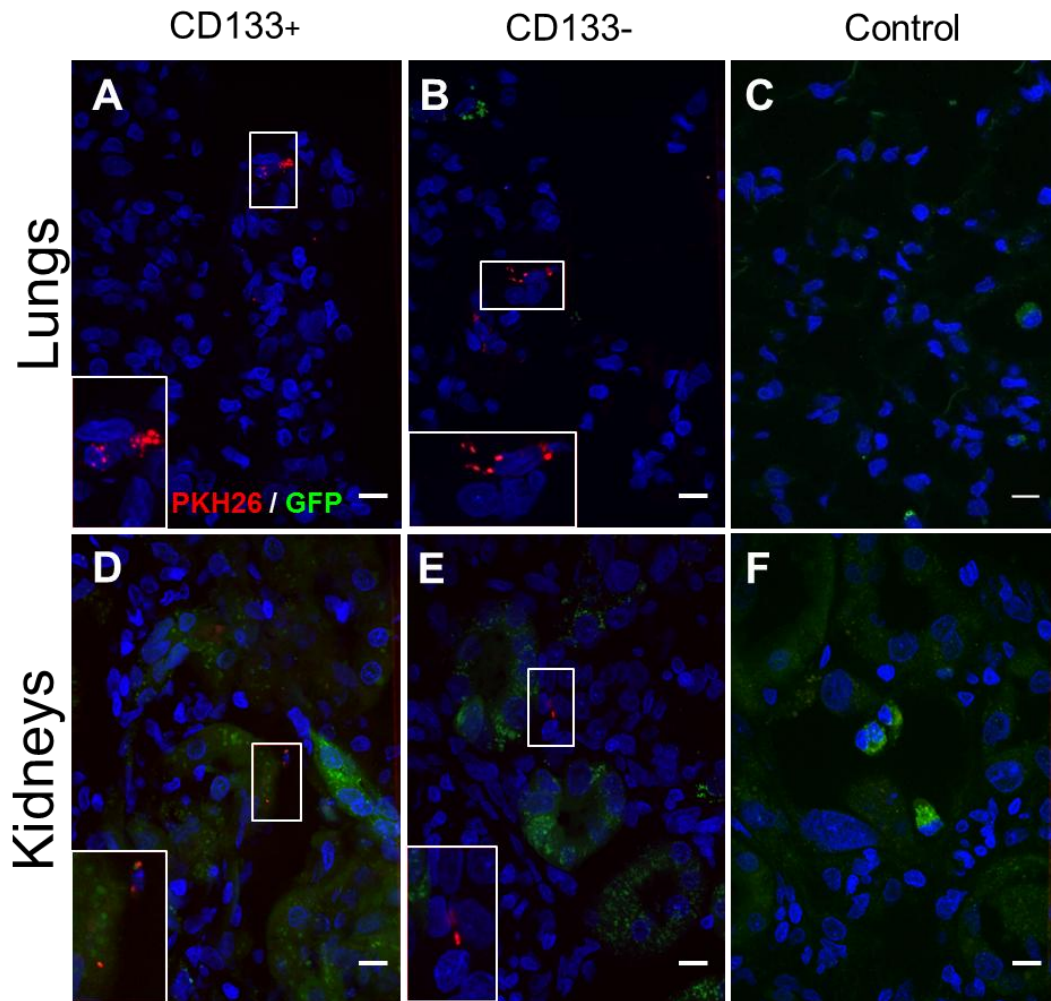


**FIGURE 5.9 LOCALIZATION OF GFP AND PKH26 IN LUNGS AND KIDNEYS AT DAY 14**

Maximum intensity projection (MIP) confocal images of a representative animal per experimental group in lungs (A-C) and kidneys (D-F).

## 5.2.4 BIODISTRIBUTION STUDY

### 5.2.4.1 LOCALIZATION OF CD133<sup>+</sup> PKH26<sup>+</sup>/GFR<sup>+</sup> CELLS IN LUNGS, KIDNEYS

The two-week study failed to provide a definite answer about the exact localization and fate of the cells. It was clearly demonstrated that the cells were not present in the kidneys. To elucidate the biodistribution pattern after the injection, a short-term study was performed (Figure 5.10). In this study,  $1 \times 10^6$  CD133<sup>+</sup> GFP<sup>+</sup>/PKH26 labelled cells were injected in 6 animals on day 2. Two animals each were then sacrificed at 1, 6 and 24 hours after cell administration, and lungs, kidneys were collected for further analysis. Two animals served as vehicle control as they were injected with PBS and sacrificed 1 hour after the injection.

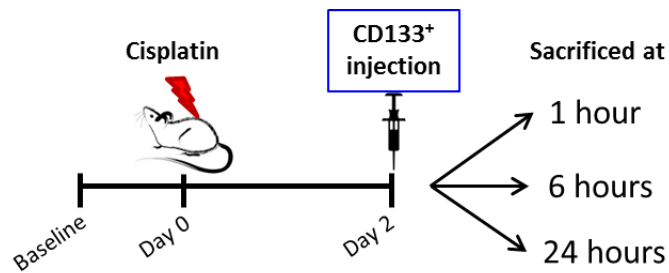


**FIGURE 5.10 EXPERIMENTAL SET-UP OF THE BIODISTRIBUTION STUDY**

One hour after the injection, clusters of CD133<sup>+</sup> cells were present in the lungs, showing both GFP and PKH26 staining. Interestingly, some cells displayed an abnormal nucleus. At 6 hours, some human cells appeared fragmented (Figure 5.11 B), while others appeared intact (Figure 5.11 C). Importantly, PKH26 stain was spotted even if no intact human cell was found. At 24 hours, no more GFP<sup>+</sup> cells could be detected. However, positive areas for PKH26 were revealed (Figure 5.11 D).

In the kidneys, the staining pattern did not differ from what observed at day 14. No CD133<sup>+</sup> cells were detected in the kidneys at any of the time point analysed, while PKH26 appeared as small red dots around the cell nuclei (Figure 5.12C). Therefore, even in the short-term biodistribution study we could exclude the presence of GFP-positive cells in the kidneys.

These results suggest that, following intravenous injection, the cells get entrapped in the lungs and disappear within 24 hours. Notably, the PKH26 was not confined to the GFP labelled cells (see Figure 5.11 B and C) and it was observed even when no GFP labelled cells could be stained in the lungs. It can be speculated that extracellular vesicles released by the cell body are responsible for this punctuate pattern in both lungs and kidneys. On this regard, it has been shown that PKH26 can be released from cells bound to extracellular vesicles (Li et al., 2013a).



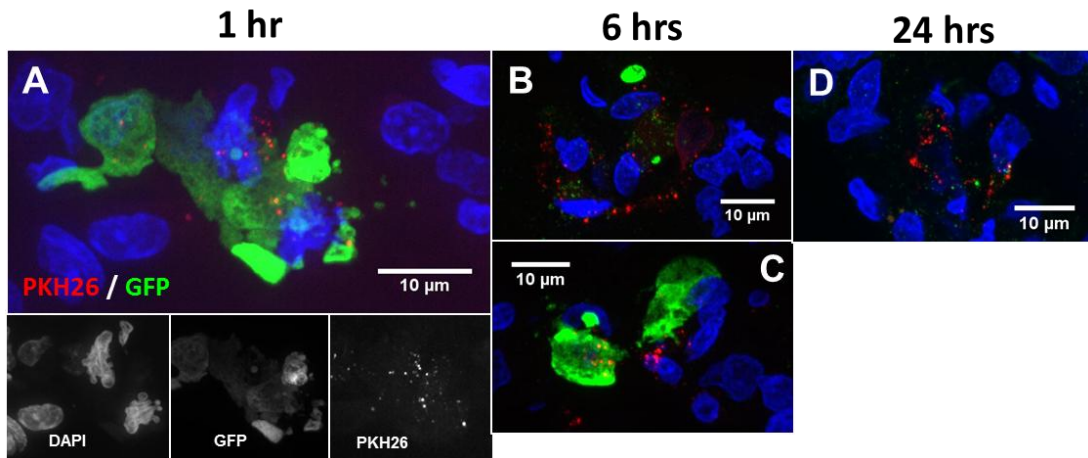


**FIGURE 5.11 LOCALIZATION OF HUMAN CD133<sup>+</sup> CELLS IN THE LUNGS 1, 6 AND 24 HOURS AFTER INJECTION**

(A-D) Representative MIP confocal images of the lungs of the animals at the three time points showing PKH26 staining and GFP staining. The images were taken by applying the same exposure for each channel. (C) Representative confocal image of the kidney cortex of a 1-hour animal showing PKH26 staining close to the glomerulus.

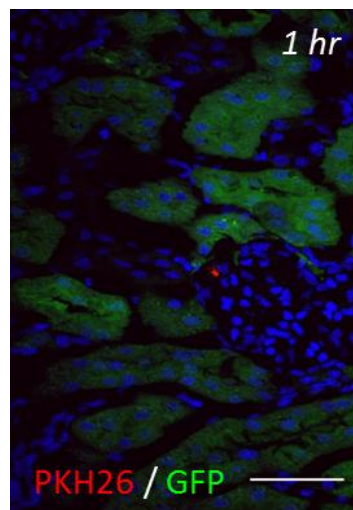


**FIGURE 5.12 LOCALIZATION OF HUMAN CD133<sup>+</sup> CELLS IN THE KIDNEY 1 HOUR AFTER INJECTION**

Representative MIP confocal image of the kidney cortex of a 1-hour animal showing PKH26 staining close to the glomerulus. No GFP<sup>+</sup> cell was detected.

#### **5.2.4.2 ROLE OF MACROPHAGES IN THE LUNGS AND KIDNEYS IN THE BIODISTRIBUTION STUDY**

The results presented so far would indicate that the human cells were trapped in the lungs after IV administration and disappeared within the following 24 hours. It was postulated that macrophages could play a role in the disappearance of the cells in the

lungs. Therefore, sections were analysed for the expression of macrophage markers, specifically CD68, which has been well established as a pan-macrophage marker.

Resident macrophages are present in most organs, including lungs. In the control animals, resident macrophages were seen interspersed throughout the tissue (Figure 5.13 A). In lungs from animals 1 hour after cell administration, GFP-positive cells were surrounded by CD68-positive cells (Figure 5.13 B, E). At 6 hours, this pattern was maintained, with clusters of CD68-positive cells surrounding GFP-positive cells (Figure 5.13 C-F). Interestingly, the PKH26 signal localized with the signal coming from the CD68 cells, suggesting that macrophages might be involved in the phagocytosis of possible by-products released by the human cells (Supplementary videos 5.1 and 5.2). At 24 hours, the clusters of CD68<sup>+</sup> cells were still evident in several locations, however, GFP positive cells could not be identified (Figure 5.13 D).

In summary, these results suggest an instrumental role of macrophages in the disappearance of the human cells from the lungs. Whether the macrophages observed in the lungs were recruited from the circulation or resulted from the proliferation of the resident macrophages was not established.



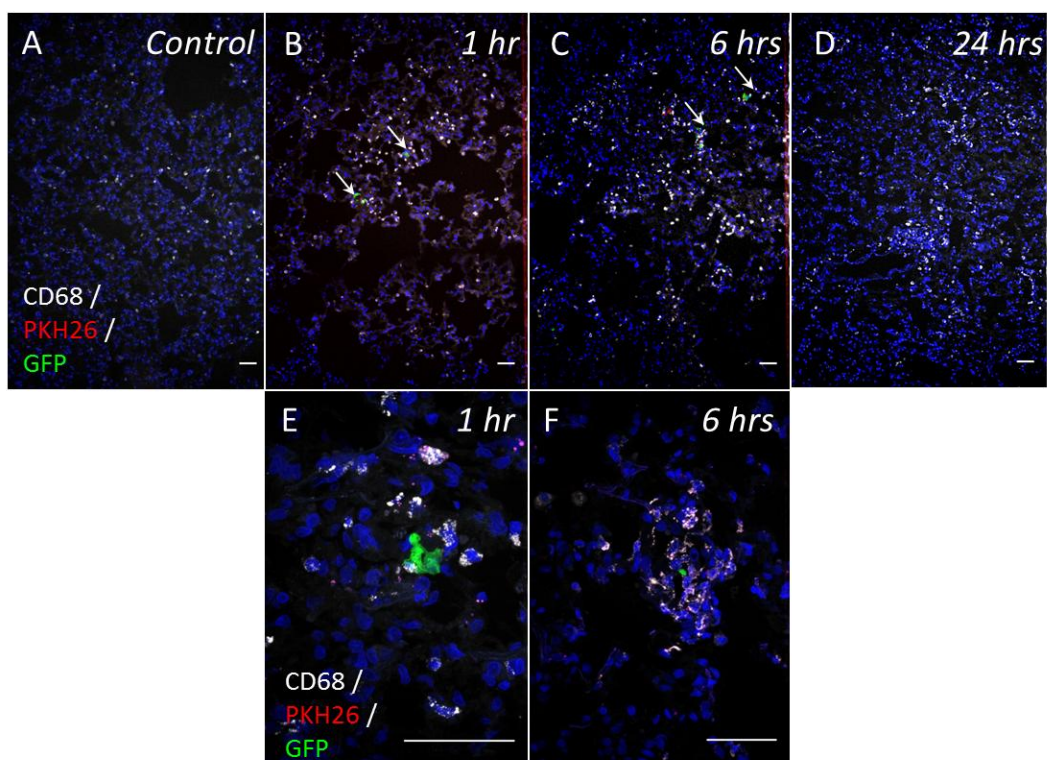


**FIGURE 5.13 MACROPHAGE INFILTRATION IN THE LUNGS**

(A-F) Representative MIPs confocal images of the lungs of the animals at all time points showing PKH26 (red), GFP (green) and CD68 (white). The images were taken with the same exposure for the different channels across different samples. The scale bar represents 50  $\mu\text{m}$ .

In the kidneys, a slight increase in the distribution of infiltrating macrophages was observed in the cell treated animals when compared to the control group (Figure 5.14). However, the differences were not striking.

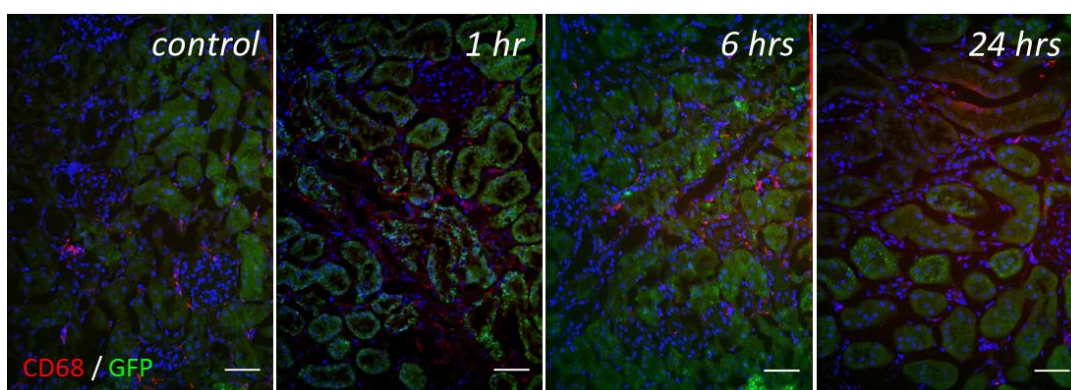


**FIGURE 5.14 MACROPHAGES INFILTRATION IN THE KIDNEYS IN THE BIODISTRIBUTION STUDY**

Representative MIPs confocal images of the lungs of the animals at all time points showing GFP (green), CD68 (red) and DAPI (blue). The images were taken with the same exposure for the different channels across different samples. The scale bar represents 100  $\mu\text{m}$ .

#### **5.2.4.3 EFFECTS OF THE HUMAN CELLS ON THE HOST RENAL EPITHELIUM: PROLIFERATION**

The major consequence of the cisplatin uptake into the tubular epithelial cells is the apoptosis of the cell. Since the human cells appear to influence the renal function and histology of the cisplatin-injured kidneys, it was important to address the mechanism through which the cells act on the damaged kidney tissues. To address these questions, the kidneys of all animals of the long-term study were analysed for markers of proliferation.

The proliferating cells were identified using the marker Ki67, which is expressed during all phases of the cell cycle ( $G_1$ , S,  $G_2$ , and mitosis), but is absent from resting cells ( $G_0$ ). Quantitatively, a bit less than twice as many proliferative cells were detected in the control group than in both cell-treated groups. Of note, rare proliferating cells were detected in the Bowman's capsule, indicated by an arrow in the CD133<sup>+</sup> image (Figure 5.15 B).

Therefore, at day 14, the control group showed a significantly higher number of proliferative cells. The data might indicate that the cell-treated animals might have had a regenerative advantage given by the injection of the cells. Two different mechanisms could be taken into account: the cells have the ability to prevent tubular apoptosis, or they accelerated the regeneration process. The approach followed in this paragraph does not clarify which one might be the actual mechanism. Also, the Ki67<sup>+</sup> cell in the BC in the CD133<sup>+</sup> group might indicate a sort of response of putative progenitor cells to the damage induced by cisplatin.

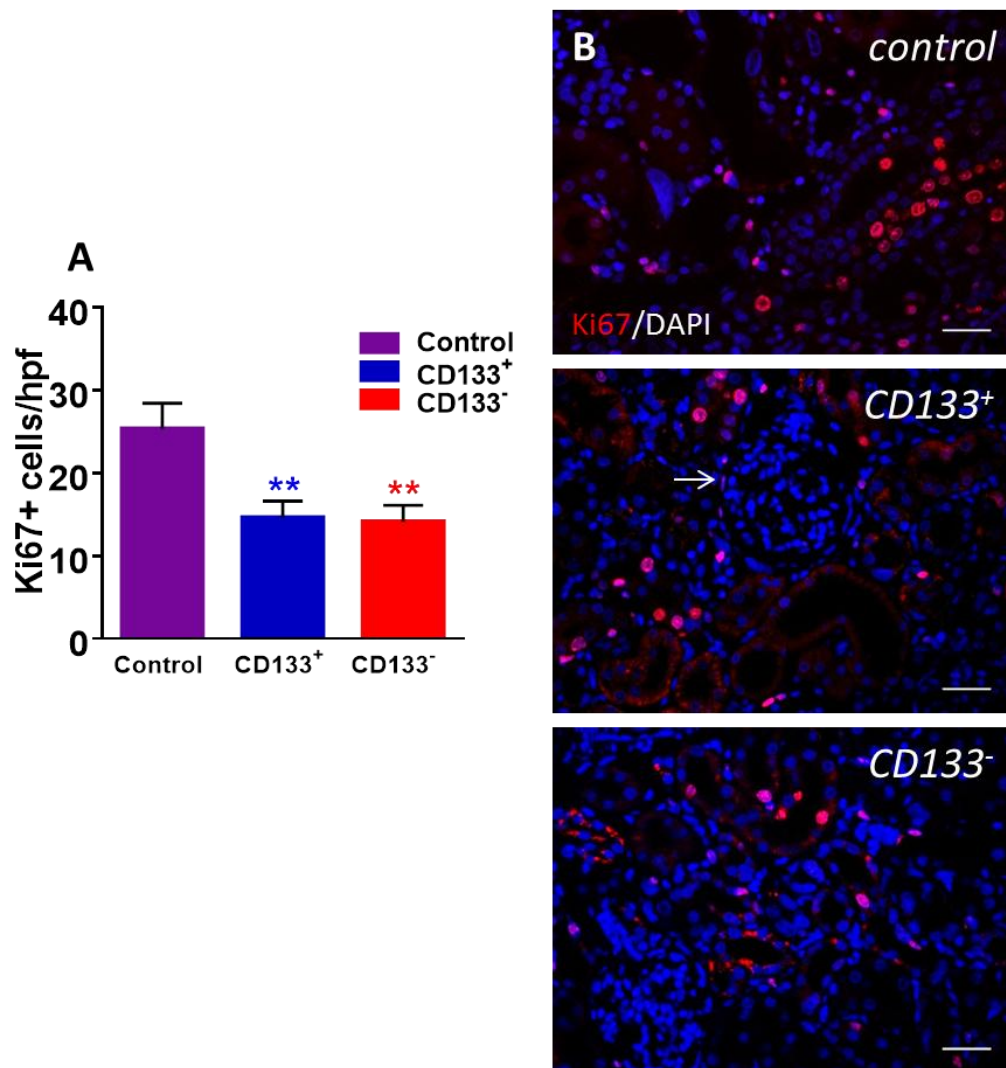


**FIGURE 5.15 EFFECTS OF THE HUMAN CELLS ON THE PROLIFERATION OF THE HOST EPITHELIUM AT 14 DAYS**

(A) Histogram bar showing the average amount of KI67<sup>+</sup> cells  $\pm$  SEM per high power field (hpf) obtained counting at least 10 random images taken across the whole kidney. The ANOVA one-way statistical test with Tukey *Post Hoc* analysis was applied to compare the groups \*\*  $p=0.0091$  \*\*  $p=0.0086$  (B) Representative fluorescence images of each experimental group showing Ki67 staining (red). In the CD133<sup>+</sup> group, the white arrow points to a proliferating cell in the Bowman's capsule. The scale bars represent 50  $\mu$ m.

### 5.3 DISCUSSION

One of the final aims of the characterization of progenitor/stem cells is testing their capabilities to ameliorate tissue injury by either fostering the regeneration of the damaged organ or preventing further damage due to the primary insult. In the previous chapters, human renal putative progenitor cells expressing CD133 were isolated from children's kidneys, expanded in culture and phenotypically characterized. The isolated cells failed to survive and integrate into developing structures of an *ex vivo* chimeric reaggregation assay. In this chapter, both CD133<sup>+</sup> and CD133<sup>-</sup> populations were finally injected in an immunodeficient rat model of acute kidney injury, induced by cisplatin, to determine their potential as cellular therapeutics.

On one hand, the beneficial effects of kidney-derived CD133<sup>+</sup> cells have been reported in different preclinical models of kidney injury, both acute and chronic [reviewed in (Bussolati and Camussi, 2015)]. On the other side of the spectrum, the efficacy of a broad range of stem cells has been assessed in models of cisplatin-induced acute kidney injury in rats (summarized in Table 5.4). Regardless of the origin of the cells, either rat or human, common results of all those studies include: i) amelioration of the renal function, assessed by serum creatinine and/or BUN; ii) engraftment of the cells in the damaged kidneys; iii) improvement of the renal histology; iv) increase of proliferation markers and/or decrease of apoptotic markers in the acute phase of the injury. Also, lipophilic dyes, such as PKH26, were used to label the cells before their intravenous administration into the animals.

In this study, a novel transcutaneous device was used. It was instrumental for two reasons. Firstly, it permitted non-invasive measurements of the renal function throughout the length of the study. Also, it allowed a pre-screening of the animals so that only animals that did develop some sort of damage were used in the control or cell-treated group. In the perspective of a preclinical study of regenerative medicine therapies, it is paramount to assess the validity of the damage to avoid wasting precious human cells and prevent misleading and non-informative results. It is also true that the model chosen, being acute, allows this kind of precautions to be put in place. In contrast, models of progressive chronic kidney injury do not concede the

same freedom, since first signs of damage can be appreciated several days after the induction of the damage.

By using the device, at the peak of damage (day7), an amelioration of the renal function of at least 50% in both cell-treated groups compared to controls was reported and supported by the concomitant reduction of azotemia (Figure 5.3 and Figure 5.4). By day 14, the differences between the control and the cell-treated groups were attenuated, corroborating the onset of an offsetting regenerative response in the host epithelium in the control animals after damage (Humphreys, 2014; Kusaba et al., 2014). To a certain extent, the results provided here are consistent with a number of studies that point towards the beneficial effect of human CD133<sup>+</sup> cells *in vivo* [see (Bussolati and Camussi, 2015)]. Unexpectedly, CD133<sup>-</sup> cells provided the same sort of functional benefit to the animals, contrary to what has been shown in other models of AKI (Angelotti et al., 2012; Sagrinati et al., 2006). Therefore, the lack of CD133 on the renal cells did not compromise the success of the cell therapy, posing its relevance into question.

With the aim of extending the panel of non-invasive biomarkers to monitor the renal function, Cystatin-C and Tim-1 were measured in the urine. Both biomarkers are regarded as promising in clinical practise for a major stability and increased sensitivity than serum creatinine (Baxmann et al., 2008). In this study, both markers reflected the damaged status of the kidney, rising considerably above the baseline levels upon renal impairment. However, the injected cells failed to reduce the levels of both biomarkers in the urine at any time point. Urinary Cystatin-C emerged as marker of acute kidney injury in the urine (Conti et al., 2006; Herget-Rosenthal et al., 2004; Uchida and Gotoh, 2002). To date, the dynamics of both Cystatin-C and Tim-1 have been investigated in preclinical disease models and in patients with kidney diseases, but not in preclinical models of regenerative medicine therapies (Song et al., 2009; Vaidya et al., 2006). Only in one study, human renal-derived erythropoietin-containing cells injected in a chronic kidney model led to a reduction in the levels of Kim-1 (Yamaleyeva et al., 2012). Importantly, a sustained expression of Kim-1 has been recently associated with renal fibrosis (Humphreys et al., 2013), opening some speculations about the long term effects of the high levels of Kim-1 seen in this study.

To sum up, at the peak of damage, some markers pointed towards a beneficial effect of the cells on renal function (Table 5.3). Most importantly, the two cell types did have comparable therapeutic effects on the model. Alongside, the data indicate that by day 14 the damage is not completely resolved (Figure 5.1 and Table 5.2), not even in the cell-treated groups. It can be expected that the cells would have an impact on the renal health in the long term, as evidenced by the higher levels of microalbuminuria in control animals at day 14 compared to the cell-treated groups. Future research would need additional end points to investigate the dynamics of all markers, to monitor the eventual progression to chronic disease, and to assess the role of the human cells in the long term.

**TABLE 5.3 SUMMARY OF THE THERAPEUTIC EFFECTS EXERTED BY BOTH CELL TYPES (CD133<sup>+</sup> AND CD133<sup>-</sup>) COMPARED TO THE CONTROL GROUP.**

All entries are relative to the acute phase of the damage (day 7), making exception for Albumin-to-Creatinine ratio (ACR), Histological Damage and Fibrosis. \* difference observed at day 14; # difference not significant; X = no difference.

	<b>CD133<sup>+</sup></b>	<b>CD133<sup>-</sup></b>
Half Life FITC-Sinistrin	↓59.1%	↓46.8%
sCreatinine	↓72.3%	↓64.7%#
BUN	↓74.2%	↓63.6%#
Tim-1	X	X
Cystatin C	X	X
ACR*	↓72.8%	↓41.7%
Histological damage *	↓43.8%	↓42.2%
Fibrosis*	N/A	N/A

The histology data confirm a major impact of the cells on the renal architecture. Typical features of renal damage, including flat epithelia and dilated tubuli, were qualitatively and quantitatively reduced in the cell-treated groups (Figure 5.6). Notably, the values measured with the transcutaneous device could be correlated with the

luminal dilation, suggesting its potential use as predictive tool to infer the severity of the renal damage. Although this finding needs to be supported by a larger number of samples, it would be of great value in the clinic.

Despite the histological improvements, no difference in fibrosis between the groups was detected at day 14. Fibrosis is the result of a cascade of events that take time to shape the tissue architecture. In fact, Peng and colleagues, reported a decrease in the fibrotic area as a consequence of the injection of umbilical cord-derived MSCs six weeks after cisplatin administration (Peng et al., 2013). However, Angelotti and colleagues reported marked differences in renal fibrosis already after 15 days in a mouse model of rhabdomyolysis (Angelotti et al., 2012). The onset of fibrosis is most probably model-dependent and determined by the severity of the model used.

Having found that both cell types positively impacted on renal health, a crucial question was posed about whether the human CD133<sup>+</sup> cells homed to the kidneys after intravenous administration, as previously reported (Angelotti et al., 2012; Grange et al., 2014a; Ronconi et al., 2009). In these studies, exogenous dyes, such as PKH26, were used to label and subsequently track the cells. The lipophilic nature of the dye implies its retention in extracellular vesicles released from the cells, in addition to its loss upon division. In fact, lipophilic dyes have been extensively used to label specifically extracellular vesicles before administration (Bruno et al., 2009; Cantaluppi et al., 2012; Imai et al., 2015). Once *in vivo*, the transplanted cells are exposed to an incredibly dynamic environment that might stimulate them to deliver specific signals (including proteins and miRNAs) through the release of paracrine factors, specifically extracellular vesicles (EVs). EVs are vesicles of 40-100 nm of diameter released by many types of cells. The vesicles originate from the budding of cell membrane and carry protein, lipids, mRNA, miRNA and non-coding RNAs (Raposo and Stoorvogel, 2013). mRNAs and miRNAs are particularly important, because involved in transcription, cell proliferation and immune regulation, delivering a complex set of messages to the target cells. In the kidney, MSCs-derived vesicles promoted tubular regeneration and protected tubular cells from apoptosis in AKI models, homing to the affected organ (Bruno et al., 2012; Bruno et al., 2009; Gatti et al., 2011; Grange et al., 2014b). If the cells are labelled only with these dyes, the EVs

might entrap the dye during their biogenesis. In this study, it was preferred to accompany the exogenous label PKH26 with a genetic tag (GFP) to track the living cells and their by-products. By doing so, it was demonstrated that no living cells were present at day 14 in the kidneys or in the lungs. However, PKH26 staining was observed in both kidneys and lungs, indicating the passage of the cells through the lungs and maybe through the kidneys or the release of paracrine factors released from the cells containing PKH26. This study reports conflicting results compared to a broad range of studies where lipophilic-like dyes were spotted in the kidneys. A common conclusion of all the studies that use PKH26 as only labelling agent is that human cells, either CD133<sup>+</sup> or not, efficiently homed to the affected organ (Angelotti et al., 2012; Gupta et al., 2015; Qi and Wu, 2013; Sagrinati et al., 2006).

To shed light on the fate of the human cells, rats that received CD133<sup>+</sup> cells were sacrificed 1, 6 and 24 hours after IV administration. The results unequivocally demonstrated the presence of human cells in the lungs 1 hour after the injection, as determined by both the GFP and the PKH26 staining (Figure 5.11). The appearance of the nuclei leads to believe that the cells are undergoing apoptosis. However, 24 hours after the injection, the human cells disappeared. In the kidneys, only some spots of PKH26 were visible in the interstitial cells, and no GFP staining was found (Figure 5.11 and Figure 5.12). It seems plausible to believe that the cells got trapped in the network of thin capillaries of the lungs. Since they still showed efficacy in improving kidney function and architecture, it can be speculated that EVs were released by the human cells while trapped in the lungs. This would explain the presence of PKH26 staining in the kidneys and lungs in the two-week study. More investigations are needed to understand the fate of the cells or their by-products soon after injection. On logical grounds, how would a human cell get to the tubuli/glomeruli? Would that take place through the interstitial capillaries or through the glomerular filtration barrier? In the glomeruli, it might be reasoned that the cells get stuck in the glomerular capillaries. However, how the cells might get into the tubuli might be physiologically more complicated and need an in-depth investigation. Imaging technologies for preclinical models are bridging that gap of knowledge about the *in vivo* biodistribution of the cells after IV injection. Bioluminescence is one of those technologies that allow this type of investigations (Heslop et al., 2015). MSCs injected



in an AKI model were seen in the lungs after IV injection, and in the kidneys after intra-arterial injection (Togel et al., 2008). Or, in a mouse model of cerebral hypoxia-ischemia, it was shown that IV-injected multipotent neural stem cells did not reach the brain. Instead, they stopped in the lungs and were cleared within 7 days (Pendharkar et al., 2010).

On the basis of the abnormal morphology of the human cells observed in the lungs one hour after injection, we propose that they die. This would explain the paucity in GFP signal 6 and 24 hours after the injection, while the PKH26 signal persists. It was hypothesised that phagocytic cells, identified through the presence of CD68, might play an important role in the disappearance of the human cells (Ferenbach and Hughes, 2008). The analysis revealed that 1 hour after the injection CD68-positive cells grouped around the human cells in the lungs, while from 6 hours onwards, clusters of CD68 positive cells were observed around remnants of GFP-positive (Figure 5.13). It was then speculated that the human cells died and thereby attracted macrophages, which in turn phagocytosed the human cells, leaving just GFP-positive fragments behind. It cannot be excluded that the injected cells could be susceptible to cisplatin, and might die following uptake of cisplatin while in the circulation. This hypothesis, however, would imply the presence of cisplatin into the circulation 2 days after the induction of the damage. By that time point, the evidence of damage would suggest that the drug reached the kidneys, where it exerted its nephrotoxic action during its excretion. Nevertheless, the susceptibility of kidney-derived cells has not been tested in this study, so it cannot be ruled out completely.

While dying, apoptotic cells expose phosphatidylserine (PtdSer) on the outer surface of the cell membrane. PtdSer is generally recognised as one of the so-called “eat me” signals that triggers the engulfment of the dying cell by phagocytosis through specific PtdSer receptors, including TIM-4, BAI 1, and Stabilin-2. Macrophages were shown to be attracted by PtdSer on the apoptotic cell surface and to secrete anti-inflammatory cytokines following the phagocytosis (Fadok et al., 1992). *In vivo*, PtdSer-carrying liposomes were uptaken by either resident or circulating macrophages after IV injection in a rat model of MI (myocardial infarction), attenuating inflammation in the infarcted area and improving cardiac function (Harel-Adar et al., 2011). Thum and

colleagues postulated the hypothesis that apoptotic cells could be used in myocardial infarction models to stimulate macrophages to secrete anti-inflammatory cytokines, such as IL-10 and TGF- $\beta$ . These cytokines would suppress the expression of pro-inflammatory cytokines, such as TNF- $\alpha$ , IL6 and IL-1 $\beta$ , in the infarcted area (Thum et al., 2005). This hypothesis could be applied ideally to any type of tissue, and it might explain the functional renal amelioration observed in the model used in this study even if a concrete proof of integration of the human cells is missing. A plethora of signals might be involved in the cross-talk between the dying cells and the macrophages; some of these molecules are on the inner or outer membrane of the dying cell while others are released into the circulation (Hochreiter-Hufford and Ravichandran, 2013; Poon et al., 2014).

The fact that both injected cell types in this study reduce the acute phase of the damage may indicate that the apoptotic phase induced by cisplatin is prevented or quickly remediated. As mentioned, the ability of transplanted cells to foster proliferation of the host epithelium was the proposed mechanism of action of several types of stem cells injected (see Table 5.4). In this study, the proliferation profile at day 14 showed a higher number of dividing cells in the control group than the cell-treated groups. It can be speculated that the human cells provided an extra help for the regeneration of the host epithelium earlier in the timeline, so that by day 14 there are less proliferating cells in the cell-treated groups. This speculation would benefit from an intermediate end point for the histological analysis.

To conclude, in this study, the injection of both CD133<sup>+</sup> and CD133<sup>-</sup> cells into the tail vein of animals with AKI led to the reduction of the blood levels of functional biomarkers (HL-Sin, serum creatinine, BUN) and the preservation of the renal tissue. Those features were not accompanied by a conclusive evidence of the engraftment of the cells into the renal tissue. Instead, intact human cells were spotted in the lungs soon after injection, but not at the end of the study. In contrast, PKH26 signal was observed in lungs and kidney in both the biodistribution and two-week study. It is therefore proposed that PKH26 is not a reliable marker for the *in vivo* tracking of transplanted cells. In the lungs, CD68-expressing cells were seen in close proximity to human cells already 1 hour after cell injection, leading to believe that macrophages

might be involved in the phagocytosis of the human cells. It can be postulated that the amelioration of the renal function was partially mediated by the extracellular vesicles released from the human cells and partially by the release of anti-inflammatory cytokines from the macrophages while phagocytising the human cells in the lungs. Both hypotheses need further investigations, in the view of their great implications in simplifying cellular therapies in the clinical setting.

**TABLE 5.4 COMPARATIVE TABLE OF ALL STUDIES FOUND IN LITERATURE USING RAT CISPLATIN-INDUCED ACUTE KIDNEY INJURY MODELS. ALL STUDIES REPORTED USE SD RATS.**

Dose of Cis	Cells used				Are cells in the kidney?	Are the lungs analysed ?	End points D (D post injection )	Cell-treated group versus control group				Ref
	Type (species)	Num. Cell label	Day of injection post CDP	Injection route				sCr and BUN	Attenuation of structural damage	Apoptotic markers	Proliferation markers	
7 mg/Kg	Fetal kidney stem cells (rat)	2 x 10 <sup>6</sup> PKH26 <sup>+</sup>	D5	IV	PKH26 found in the kidneys, overlays with AQP1	No	D5 (0)	= vs ctrl	N/A	N/A	N/A	(Gupta et al., 2015)
						No	D8 (3)	↓ vs ctrl	Yes	↓ vs ctrl	↑ vs ctrl	
						No	D12 (7)	↓ vs ctrl	Yes	↓ vs ctrl	↑ vs ctrl	
6 mg/Kg	BM MSC (rat)	1 x 10 <sup>6</sup> PKH26 <sup>+</sup>	D4	IV	PKH26 found in the peritubular cells	No	D8 (4)	↓ vs ctrl	Yes	↓ vs ctrl	↑ vs ctrl	(Qi and Wu, 2013)
6 mg/kg	UC MSC (human)	2 x 10 <sup>6</sup> CM-Dil	D1	IV	CM-Dil found in the kidneys 4 weeks after injection	No	D5 (4)	↓ vs ctrl	Yes	↓ vs ctrl	↑ vs ctrl	(Peng et al., 2013)
							W6	= vs ctrl	Fibrosis attenuated	Anti-apoptotic proteins ↑ vs ctrl	N/A	
10 mg/Kg	Ad-MSC (human)	5 x 10 <sup>5</sup> BrdU	D1	IV	Yes, in tubular epithelial cells	No	D3 (2)	↓ vs ctrl	Yes	↓ vs ctrl	N/A	(Kim et al., 2012)

Abbreviations: BM-MSC Bone Marrow-derived Mesenchymal Stem cells; UC-MSC Umbilical Cord-derived Mesenchymal Stem Cells; Ad-MSC Adipose tissue-derived Mesenchymal Stem Cells; BrdU Bromodeoxyuridine; D day; W week; IV intravenous injection; N/A Non Applicable

## 6 CONCLUSIONS

In the past decade, several studies investigated the presence of renal progenitor cells in the adult kidney. In most of those studies, CD133 was the marker of choice to isolate this population. The CD133<sup>+</sup> renal progenitor cells displayed i) a significant proliferation and clonogenic potential *in vitro*, ii) notable plasticity *in vitro*, being able to differentiate in different cell types, both renal and extra-renal, iii) amelioration of renal function and tissue structure following injection into preclinical models of kidney injury, allegedly led by the engraftment of the cells in the host tissue (Angelotti et al., 2012; Bussolati et al., 2005; Bussolati et al., 2013; Grange et al., 2014a; Ronconi et al., 2009; Sagrinati et al., 2006).

In this chapter, the key findings of each part of this thesis will be summarized and put into the context of a possible clinical translation of the cell therapy using CD133<sup>+</sup>, where possible. Figure 6.1 summarizes the key points that emerged from each step of the project.

In this thesis, the general aim was to investigate the presence of CD133<sup>+</sup> cells in human kidneys obtained from children. In the samples used in this study, the localization of CD133 corroborated previous studies where CD133 was expressed by the cells of the Bowman's capsule, defined Parietal Epithelial Cell (PEC), and by scattered tubular cells (Angelotti et al., 2012; Ronconi et al., 2009). Once the correct anatomical location of the CD133<sup>+</sup> cells was confirmed, a population of renal cells was isolated and plated, without selecting at passage 0 for the CD133<sup>+</sup> cells, as it has been reported (Bussolati et al., 2005; Ronconi et al., 2009; Sagrinati et al., 2006).

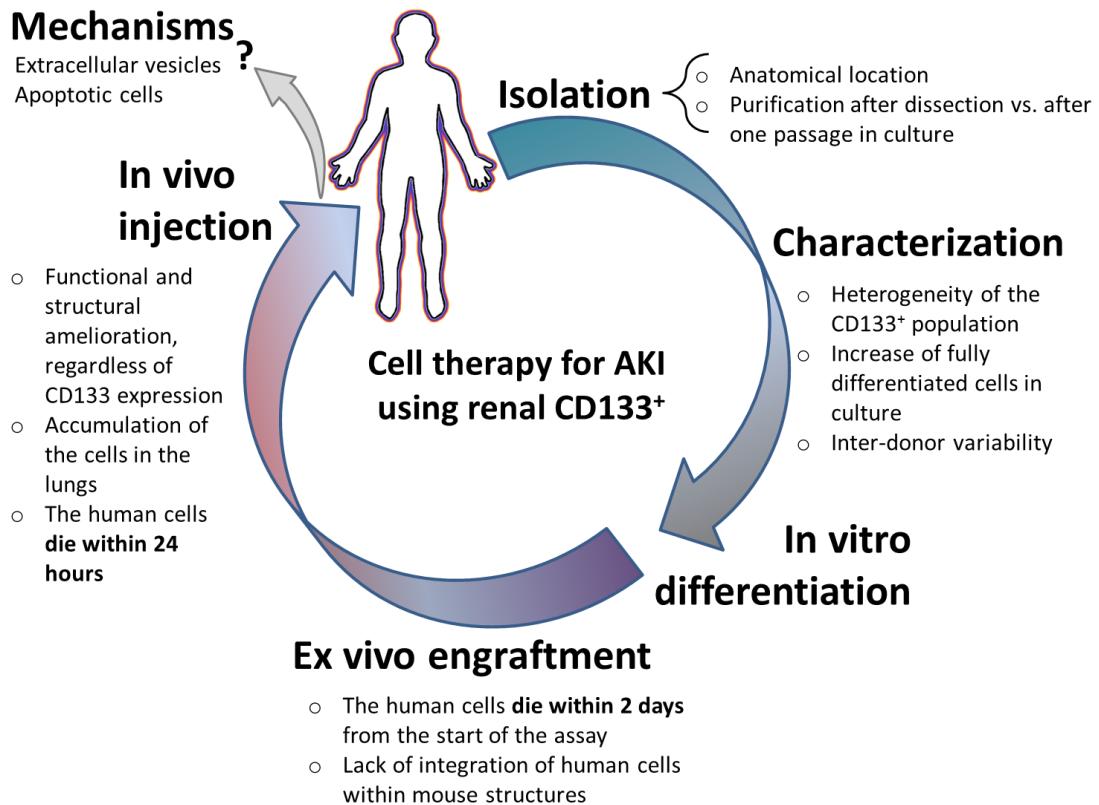


**FIGURE 6.1 SCHEMATIC SUMMARY OF THE KEY POINTS IDENTIFIED IN THIS THESIS.**

In this scheme, all relevant phases of this thesis about the use of CD133<sup>+</sup> as therapeutics are shown. Each part of the project provided significant insights into possible hurdles of CD133<sup>+</sup>-cell based therapies. The drawbacks are particularly evident for the *in vitro* section, where the CD133<sup>+</sup> were shown to be heterogeneous in their surface marker profile. When the cells were tested for their ex vivo engraftment and in vivo amelioration potential, some congruence was observed: the human cells die within few days in the mouse/rat environment. Nevertheless, both CD133<sup>+</sup> and CD133<sup>-</sup> cells improved renal function and tissue architecture. This suggests a role for paracrine factors or apoptotic cells as modulators of the damage, possibly through immunomodulation. It is important to note that these are just speculations and require further study.

The observations of the renal cells *in vitro* led to key conclusions:

At passage 1, most of the renal cells expressed CD133, although in vivo the amount of CD133<sup>+</sup> was reported to be between 0.5% and 4% (Bussolati et al., 2005). Whether this extensive expression was determined by a more sustained proliferation of the CD133<sup>+</sup> cells that quickly took over in culture or by the acquisition of the marker as adaptation to the culture conditions could not be established with the experiments shown in this thesis.

A significant proportion of the CD133<sup>+</sup> cells expressed CD13, a marker of proximal tubule cells. This finding indicates that the isolation protocol and/or the culture

conditions used in this study led to the differentiation of the renal progenitors towards a proximal tubular fate or allowed the enrichment of a population of fully differentiated proximal tubule cells that acquired CD133 in culture.

The CD133<sup>+</sup> population is highly heterogeneous. This heterogeneity resonated with the presence of several subpopulations, most notably expressing epithelial markers (CD24), putative progenitor markers (NCAM/Tra-1-60) or fully differentiated renal cell markers (CD13). To provide a more comprehensive characterization, the CD133<sup>-</sup> cells were analysed as negative control population alongside for the same surface markers. Interestingly, the two populations failed to show remarkable differences regarding surface markers (Table 3.2, Results chapter 3). Once again, the lack of a distinct profile for the CD133<sup>+</sup> cells might be due to the culture conditions that preconditioned the bulk population. The heterogeneity of the CD133<sup>+</sup> population could have potentially been addressed if the population had been purified after the isolation, as previously done by the seminal studies about CD133<sup>+</sup>. Experimentally, the two approaches should be compared to select the method that guarantees the highest purity and homogeneity.

Each CD133<sup>+</sup> cell line isolated from a different donor showed different population doubling times, possibly reflecting the age or the health status of the donor.

If the final aim is to devise a cellular therapy using primary CD133<sup>+</sup> cells as therapeutics, several challenges which could hamper the translation of the therapy in clinical settings need to be factored into the risk-benefit analysis of such therapies. Firstly, the procedure to obtain a renal biopsy is invasive, and the tissue biopsy is quite small. Alternatively, full kidneys can be used to isolate some cells. However, due to the shortage of kidneys, autologous therapies as alternative might be quite unrealistic. Secondly, the approach used to purify the CD133<sup>+</sup> cells, whether directly after dissection or after one passage in culture, might assure an adequate number of cells. As shown in this study, plating the cells and select for CD133 afterward resulted in a high number of CD133<sup>+</sup> cells, but the heterogeneity of the population could be a drawback. Also, cell lines obtained from patients with underlying renal conditions might behave differently *in vitro*. In this study, for example, CD133<sup>+</sup> cells isolated from two patients (hK5, hK4) could not be serially expanded. Therefore, a therapy using

CD133 cells might require a case-by-case assessment and in some cases a contingency plan, such as an allogeneic cell therapy, needs to be readily available.

Although impressive progress has been made to understand the real potential of this population, *in vitro* as *in vivo*, the use of these cells as therapeutics and their translation to the clinic is still elusive. Some lessons can be learnt from the therapies that use mesenchymal stem cells. At the moment, there are no active clinical trials where stem cells are used in patients with acute kidney injury (clinicaltrials.gov – April 2016). Interestingly, one study which is currently recruiting participants, will use mesenchymal stromal cells in patients with solid organ cancers affected by cisplatin-induced acute renal failure (NCT01275612). This trial would represent an explorative dose-finding study to establish safety and efficacy of autologous MSC transplantation. Initially, the cells will be isolated, expanded *ex vivo* and reinfused systemically in the patient at a concentration of  $10^6$  cells per Kg of Body Weight. From there, the amount of injected cells will be escalated accordingly. Serum creatinine and NGAL and NAG will be the biomarkers evaluated. The enormous amount of cells needed for *in vivo* human cell therapy at the moment might not be compatible with the amount of CD133<sup>+</sup> cells that can be isolated from a renal biopsy. More exploratory and comprehensive studies need to be performed to understand the scalability of the cell therapies from preclinical to clinical settings.

After phenotyping, the isolated cells were tested for their potential to differentiate into a specialized renal cell, such as podocytes. Despite their extensive use in several studies, the differentiation conditions failed to provide successful insights into the potential of the renal cells in this study. Nevertheless, preliminary results showed the upregulation of podocytic markers, such as podocin and nephrin, following stimulation of both CD133<sup>+</sup> and CD133<sup>-</sup> cell types with Retinoic Acid.

The *ex vivo* reaggregation assay was then used to investigate the engraftment of the human CD133<sup>+</sup> and CD133<sup>-</sup> cells into developing embryonic renal structures. Key findings from the *ex vivo* assay include:

Most of the human cells died over the first three days. The difference between the rudiments at day one and day three after the start of the assay is striking and indicates that either the human cells failed to have the right conditions to proliferate or even



survive in the system, or that there were death signals released by the mouse cells that impacted on the human cell survival.

The few cells that survived at day 3 and 6 failed to show any engraftment, and if they did, it would be more plausible to consider it a stochastic integration.

So far, the reaggregation assay using human cells has been proved successful only when using nephron progenitor cells obtained after differentiation of hESCs or hiPSCs (Takasato et al., 2014; Xia et al., 2013). Human somatic stem cells, such as mesenchymal stem cells or amniotic stem cells, failed to engraft in large number unless genetically modified to express GDNF (Kuzma-Kuzniarska et al., 2012; Xinaris et al., 2015). This evidence strongly indicates that the main issue is not the species of the cell of interest, but the type of cells that are mixed with the mouse cells. Nephron progenitor cells or cells expressing GDNF can actively participate in the development of the structures, probably because they can release/receive the appropriate signals during the shaping of the structures.

Beyond the isolation of a viable population of CD133<sup>+</sup>, a significant milestone was to test the therapeutic effect of these cells in immunodeficient rats with acute kidney injury induced by cisplatin.

Both CD133<sup>+</sup> and CD133<sup>-</sup> positively impacted on the renal health of the rats. The degree of amelioration was comparable for the two cell types and was corroborated by conventional serum biomarkers and the half-life of FITC-Sinistrin as a measure of GFR using the transcutaneous device. This effects might be explained by two mechanisms: i) there is a progenitor population that is common to the CD133<sup>+</sup> and CD133<sup>-</sup> populations; or ii) fully differentiated cells are somehow able to improve renal function. Clearly, more mechanistic studies are needed to elucidate how the amelioration takes place. However, the data indicate that any renal cell type independent of CD133 expression shows efficacy, eliminating all problems related to purification, phenotyping, and expansion of a specific population.

The intravenous injection of the human cells led to an accumulation of the cells in the lungs and not in the kidneys. It is not surprising that the cells were found in the lungs soon following injection. In our group, further experiments were conducted

using the primary CD133<sup>+</sup> and CD133<sup>-</sup> cells transduced with a luciferase construct to facilitate *in vivo* bioluminescence imaging. Once injected IV in SCID mice affected by Adriamycin-induced nephropathy, the cells accumulated in the lungs (Figure 6.2).

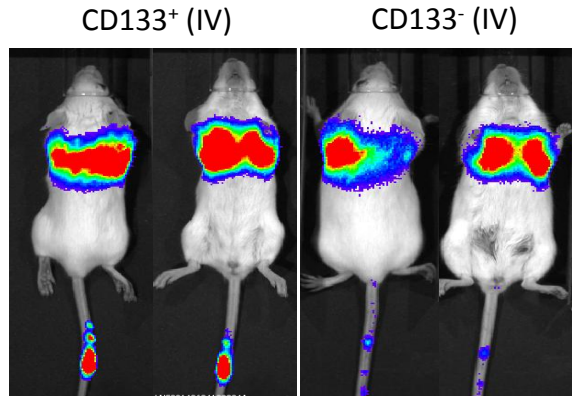


**FIGURE 6.2 BIOLUMINESCENCE IMAGING OF HUMAN CD133<sup>+</sup> AND CD133<sup>-</sup> CELLS INJECTED INTO SCID MICE AFFECTED BY ADRIAMYCIN-INDUCED CHRONIC KIDNEY INJURY.**

Both CD133<sup>+</sup> and CD133<sup>-</sup> cell populations were transduced with a Luciferase lentivirus after sorting and injected at passage five into SCID mice with chronic kidney disease induced by Adriamycin. 750 thousand cells were injected into each mouse through the tail vein. The bioluminescence was measured 30 minutes after injection. Luciferin was injected 15 minutes before the imaging. In this panel, two animals per cell type are shown. Image courtesy of Lauren Scarfe (University of Liverpool).

Most of the studies that employed renal progenitor cells *in vivo* did not use any imaging technology able to track the cells. Instead, the tracking was often entrusted to the PKH26 only. In light of the findings shown in this thesis, all studies that show PKH26 labelling in the kidneys after IV injection could be interpreted differently: the cells might release extracellular vesicles that entrap PKH26 within the lipidic shell and reach the affected organ. In chapter 5, the absence of GFP<sup>+</sup> cells in the kidney and the presence of sporadic PKH26 labelling in the shape of vesicles in the kidneys was shown. In the lungs, the release of what can be interpreted as vesicles retaining PKH26 was even more evident, as the GFP<sup>+</sup>/PKH26<sup>+</sup> cells were clearly identifiable at 1 and 6 hours after injection, whereas at 24 hours only PKH26 was left. This piece of evidence leads the next key finding.

The cells in the lungs disappeared within 24 hours from the injection. At 24 hours after the injection, there was no evidence of intact cells in the lungs or the kidneys. However, as already mentioned, the fact the PKH26 was found in the lungs at 24 hours might indicate that the cells stayed there at least for some hours; and, since the cells

were not retrieved in the kidneys either, it is plausible that they died in the lungs. The disappearance of the human cells in less than 24 hours might be determined by the phagocytic activity of macrophages, identified through the expression of CD68. The distribution of the CD68<sup>+</sup> cells appeared to be affected by the distribution of the human cells in the lungs. In fact, already after one hour, macrophages were seen in close proximity of the human cells. By 24 hours, clusters of CD68<sup>+</sup> cells were identified in the lungs, where no human cells could be spotted. In vitro co-cultures of intact primary cells with macrophages could further elucidate the mechanisms of interaction and show if a phagocytosis of the cells takes place. This experiment could be brought even a step further by studying co-cultures of primary apoptotic cells with macrophages.

The use of apoptotic cells in therapies is not a new concept. Numerous studies have studied the effects of apoptotic cell injections, mainly splenocytes, in cardiac and bone marrow transplantation. Apoptotic cells, on one side, down-modulate inflammation and immunity, and, on the other hand, modulate the functions of antigen presenting cells (dendritic cells and macrophages) and their immunoregulatory potential, following phagocytosis (Morelli and Larregina, 2010). Overall, the use of apoptotic cells to modulate the renal damage could be an exciting avenue for future therapies, once their efficacy is proven.

To conclude, this study indicated that CD133<sup>+</sup> cells might not be the best therapeutics for therapies for renal diseases. Instead, the study of systems that modulate these cells *in vivo* would be more appealing as recent studies suggest (Lasagni et al., 2015). Also, the present thesis enlightens two possible scenarios for future research: the use of extracellular vesicles and their eventual modulatory properties, and the use of apoptotic cells to stimulate anti-inflammatory responses within the animal. The first scenario appears to be promising, as demonstrated by the studies of EVs released from MSCs used in preclinical models of AKI (Bruno et al., 2012; Bruno et al., 2009).

While the debate about the existence of renal progenitor cell population will continue for a long time to come, one aspect requires attention now: the patient.



## LIST OF REFERENCES

Abrahamson, M., Olafsson, I., Palsdottir, A., Ulvsback, M., Lundwall, A., Jensson, O., and Grubb, A. (1990). Structure and expression of the human cystatin C gene. *Biochem J* 268, 287-294.

Ahmadi, H., Baharvand, H., Ashtiani, S.K., Soleimani, M., Sadeghian, H., Ardekani, J.M., Mehrjerdi, N.Z., Kouhkan, A., Namiri, M., Madani-Civi, M., *et al.* (2007). Safety analysis and improved cardiac function following local autologous transplantation of CD133(+) enriched bone marrow cells after myocardial infarction. *Curr Neurovasc Res* 4, 153-160.

Akcay, A., Nguyen, Q., and Edelstein, C.L. (2009). Mediators of inflammation in acute kidney injury. *Mediators of inflammation* 2009, 137072.

Angelotti, M.L., Lazzeri, E., Lasagni, L., and Romagnani, P. (2010). Only anti-CD133 antibodies recognizing the CD133/1 or the CD133/2 epitopes can identify human renal progenitors. *Kidney international* 78, 620-621; author reply 621.

Angelotti, M.L., Ronconi, E., Ballerini, L., Peired, A., Mazzinghi, B., Sagrinati, C., Parente, E., Gacci, M., Carini, M., Rotondi, M., *et al.* (2012). Characterization of renal progenitors committed toward tubular lineage and their regenerative potential in renal tubular injury. *Stem cells* 30, 1714-1725.

Appel, D., Kershaw, D.B., Smeets, B., Yuan, G., Fuss, A., Frye, B., Elger, M., Kriz, W., Floege, J., and Moeller, M.J. (2009). Recruitment of podocytes from glomerular parietal epithelial cells. *Journal of the American Society of Nephrology: JASN* 20, 333-343.

Arcolino, F.O., Zia, S., Held, K., Papadimitriou, E., Theunis, K., Bussolati, B., Raaijmakers, A., Allegaert, K., Voet, T., Deprest, J., *et al.* (2016). Urine of Preterm Neonates as a Novel Source of Kidney Progenitor Cells. *Journal of the American Society of Nephrology: JASN*.

Asselman, M., Verhulst, A., De Broe, M.E., and Verkoelen, C.F. (2003). Calcium oxalate crystal adherence to hyaluronan-, osteopontin-, and CD44-expressing injured/regenerating

tubular epithelial cells in rat kidneys. *Journal of the American Society of Nephrology : JASN* 14, 3155-3166.

Baboolal, K., McEwan, P., Sondhi, S., Spiewanowski, P., Wechowski, J., and Wilson, K. (2008). The cost of renal dialysis in a UK setting—a multicentre study. *Nephrology, dialysis, transplantation : official publication of the European Dialysis and Transplant Association - European Renal Association* 23, 1982-1989.

Baer, P.C., Nockher, W.A., Haase, W., and Scherberich, J.E. (1997). Isolation of proximal and distal tubule cells from human kidney by immunomagnetic separation. Technical note. *Kidney international* 52, 1321-1331.

Bailly, V., Zhang, Z., Meier, W., Cate, R., Sanicola, M., and Bonventre, J.V. (2002). Shedding of kidney injury molecule-1, a putative adhesion protein involved in renal regeneration. *J Biol Chem* 277, 39739-39748.

Bauer, N., Fonseca, A.V., Florek, M., Freund, D., Jaszai, J., Bornhauser, M., Fargeas, C.A., and Corbeil, D. (2008). New insights into the cell biology of hematopoietic progenitors by studying prominin-1 (CD133). *Cells Tissues Organs* 188, 127-138.

Baxmann, A.C., Ahmed, M.S., Marques, N.C., Menon, V.B., Pereira, A.B., Kirsztajn, G.M., and Heilberg, I.P. (2008). Influence of muscle mass and physical activity on serum and urinary creatinine and serum cystatin C. *Clinical journal of the American Society of Nephrology : CJASN* 3, 348-354.

Berger, K., Bangen, J.M., Hammerich, L., Liedtke, C., Floege, J., Smeets, B., and Moeller, M.J. (2014). Origin of regenerating tubular cells after acute kidney injury. *Proc Natl Acad Sci U S A* 111, 1533-1538.

Bombelli, S., Zipeto, M.A., Torsello, B., Bovo, G., Di Stefano, V., Bugarin, C., Zordan, P., Vigano, P., Cattoretti, G., Strada, G., *et al.* (2013). PKH(high) cells within clonal human nephrospheres provide a purified adult renal stem cell population. *Stem cell research* 11, 1163-1177.

Bonventre, J.V. (2003). Dedifferentiation and proliferation of surviving epithelial cells in acute renal failure. *Journal of the American Society of Nephrology : JASN* 14 *Suppl 1*, S55-61.

Bonventre, J.V., Vaidya, V.S., Schmouder, R., Feig, P., and Dieterle, F. (2010). Next-generation biomarkers for detecting kidney toxicity. *Nat Biotechnol* 28, 436-440.

Bourseau-Guilmain, E., Griveau, A., Benoit, J.P., and Garcion, E. (2011). The importance of the stem cell marker prominin-1/CD133 in the uptake of transferrin and in iron metabolism in human colon cancer Caco-2 cells. *PLoS one* 6, e25515.

Brinkkoetter, P.T., Ising, C., and Benzing, T. (2013). The role of the podocyte in albumin filtration. *Nature reviews Nephrology* 9, 328-336.

Bruno, S., Grange, C., Collino, F., Deregibus, M.C., Cantaluppi, V., Biancone, L., Tetta, C., and Camussi, G. (2012). Microvesicles derived from mesenchymal stem cells enhance survival in a lethal model of acute kidney injury. *PLoS one* 7, e33115.

Bruno, S., Grange, C., Deregibus, M.C., Calogero, R.A., Saviozzi, S., Collino, F., Morando, L., Busca, A., Falda, M., Bussolati, B., *et al.* (2009). Mesenchymal stem cell-derived microvesicles protect against acute tubular injury. *Journal of the American Society of Nephrology : JASN* 20, 1053-1067.

Bucaloiu, I.D., Kirchner, H.L., Norfolk, E.R., Hartle, J.E., 2nd, and Perkins, R.M. (2012). Increased risk of death and de novo chronic kidney disease following reversible acute kidney injury. *Kidney international* 81, 477-485.

Bussolati, B., Bruno, S., Grange, C., Buttiglieri, S., Deregibus, M.C., Cantino, D., and Camussi, G. (2005). Isolation of renal progenitor cells from adult human kidney. *The American journal of pathology* 166, 545-555.

Bussolati, B., and Camussi, G. (2015). Therapeutic use of human renal progenitor cells for kidney regeneration. *Nature reviews Nephrology* 11, 695-706.

Bussolati, B., Lauritano, C., Moggio, A., Collino, F., Mazzone, M., and Camussi, G. (2013). Renal CD133(+)/CD73(+) progenitors produce erythropoietin under hypoxia and prolyl hydroxylase inhibition. *Journal of the American Society of Nephrology : JASN* 24, 1234-1241.

Bussolati, B., Moggio, A., Collino, F., Aghemo, G., D'Armento, G., Grange, C., and Camussi, G. (2012). Hypoxia modulates the undifferentiated phenotype of human renal inner medullary CD133+ progenitors through Oct4/miR-145 balance. *Am J Physiol Renal Physiol* 302, F116-128.

Buzhor, E., Harari-Steinberg, O., Omer, D., Metsuyanin, S., Jacob-Hirsch, J., Noiman, T., Dotan, Z., Goldstein, R.S., and Dekel, B. (2011). Kidney spheroids recapitulate tubular organoids leading to enhanced tubulogenic potency of human kidney-derived cells. *Tissue Eng Part A* 17, 2305-2319.

Buzhor, E., Omer, D., Harari-Steinberg, O., Dotan, Z., Vax, E., Pri-Chen, S., Metsuyanin, S., Pleniceanu, O., Goldstein, R.S., and Dekel, B. (2013). Reactivation of NCAM1 defines a subpopulation of human adult kidney epithelial cells with clonogenic and stem/progenitor properties. *The American journal of pathology* 183, 1621-1633.

Camici, M. (2005). Renal glomerular permselectivity and vascular endothelium. *Biomed Pharmacother* 59, 30-37.

Canis, M., Lechner, A., Mack, B., Zengel, P., Laubender, R.P., Koehler, U., Heissmeyer, V., and Gires, O. (2013). CD133 induces tumour-initiating properties in HEK293 cells. *Tumour Biol* 34, 437-443.

Cantaluppi, V., Gatti, S., Medica, D., Figliolini, F., Bruno, S., Deregibus, M.C., Sordi, A., Biancone, L., Tetta, C., and Camussi, G. (2012). Microvesicles derived from endothelial progenitor cells protect the kidney from ischemia-reperfusion injury by microRNA-dependent reprogramming of resident renal cells. *Kidney international* 82, 412-427.

Cao, Q., Harris, D.C., and Wang, Y. (2015). Macrophages in kidney injury, inflammation, and fibrosis. *Physiology (Bethesda)* 30, 183-194.

Carlone, D.L., and Breault, D.T. (2012). Tales from the crypt: the expanding role of slow cycling intestinal stem cells. *Cell Stem Cell* 10, 2-4.

Chawla, L.S., Amdur, R.L., Amodeo, S., Kimmel, P.L., and Palant, C.E. (2011). The severity of acute kidney injury predicts progression to chronic kidney disease. *Kidney international* 79, 1361-1369.

Chawla, L.S., Eggers, P.W., Star, R.A., and Kimmel, P.L. (2014). Acute kidney injury and chronic kidney disease as interconnected syndromes. *N Engl J Med* 371, 58-66.

Chawla, L.S., and Kimmel, P.L. (2012). Acute kidney injury and chronic kidney disease: an integrated clinical syndrome. *Kidney international* 82, 516-524.

Chung, K., and Deisseroth, K. (2013). CLARITY for mapping the nervous system. *Nat Methods* 10, 508-513.

Ciarimboli, G., Deuster, D., Knief, A., Sperling, M., Holtkamp, M., Edemir, B., Pavenstadt, H., Lanvers-Kaminsky, C., am Zehnhoff-Dinnesen, A., Schinkel, A.H., *et al.* (2010). Organic cation transporter 2 mediates cisplatin-induced oto- and nephrotoxicity and is a target for protective interventions. *The American journal of pathology* 176, 1169-1180.

Ciarimboli, G., Lancaster, C.S., Schlatter, E., Franke, R.M., Sprowl, J.A., Pavenstadt, H., Massmann, V., Guckel, D., Mathijssen, R.H., Yang, W., *et al.* (2012). Proximal tubular secretion of creatinine by organic cation transporter OCT2 in cancer patients. *Clinical cancer research : an official journal of the American Association for Cancer Research* 18, 1101-1108.

Ciarimboli, G., Ludwig, T., Lang, D., Pavenstadt, H., Koepsell, H., Piechota, H.J., Haier, J., Jaehde, U., Zisowsky, J., and Schlatter, E. (2005). Cisplatin nephrotoxicity is critically mediated via the human organic cation transporter 2. *The American journal of pathology* 167, 1477-1484.



Conti, M., Moutereau, S., Zater, M., Lallali, K., Durrbach, A., Manivet, P., Eschwege, P., and Loric, S. (2006). Urinary cystatin C as a specific marker of tubular dysfunction. *Clin Chem Lab Med* *44*, 288-291.

Corbeil, D., Fargeas, C.A., and Jaszai, J. (2014). CD133 might be a pan marker of epithelial cells with dedifferentiation capacity. *Proc Natl Acad Sci U S A* *111*, E1451-1452.

Corbeil, D., Marzesco, A.M., Fargeas, C.A., and Huttner, W.B. (2010). Prominin-1: a distinct cholesterol-binding membrane protein and the organisation of the apical plasma membrane of epithelial cells. *Subcell Biochem* *51*, 399-423.

Cukuranovic, R. (2005). Age related anatomical and functional characteristics of human kidney. *Facta Universitatis Med Biol* *12*, 61-69.

Definition, A. (2012). Section 2: AKI Definition. *Kidney inter, Suppl* *2*, 19-36.

Dekel, B., Metsuyanin, S., Schmidt-Ott, K.M., Fridman, E., Jacob-Hirsch, J., Simon, A., Pinthus, J., Mor, Y., Barasch, J., Amariglio, N., *et al.* (2006). Multiple imprinted and stemness genes provide a link between normal and tumor progenitor cells of the developing human kidney. *Cancer Res* *66*, 6040-6049.

Delanaye, P., and Mariat, C. (2013). The applicability of eGFR equations to different populations. *Nature reviews Nephrology* *9*, 513-522.

Delanghe, J.R., and Speckaert, M.M. (2011). Creatinine determination according to Jaffe-what does it stand for? *NDT Plus* *4*, 83-86.

Doery, A.J., Ang, E., and Ditchfield, M.R. (2015). Duplex kidney: not just a drooping lily. *J Med Imaging Radiat Oncol* *59*, 149-153.

Dominici, M., Le Blanc, K., Mueller, I., Slaper-Cortenbach, I., Marini, F., Krause, D., Deans, R., Keating, A., Prockop, D., and Horwitz, E. (2006). Minimal criteria for defining multipotent mesenchymal stromal cells. The International Society for Cellular Therapy position statement. *Cytotherapy* *8*, 315-317.

dos Santos, N.A., Carvalho Rodrigues, M.A., Martins, N.M., and dos Santos, A.C. (2012). Cisplatin-induced nephrotoxicity and targets of nephroprotection: an update. *Archives of toxicology* *86*, 1233-1250.

Ebeling, C.G., and Jorgensen, E.M. (2013). Two views on light sheets. *Nat Biotechnol* *31*, 992-993.

Edelstein, C.L. (2008). Biomarkers of acute kidney injury. *Adv Chronic Kidney Dis* *15*, 222-234.

Fadok, V.A., Voelker, D.R., Campbell, P.A., Cohen, J.J., Bratton, D.L., and Henson, P.M. (1992). Exposure of phosphatidylserine on the surface of apoptotic lymphocytes triggers specific recognition and removal by macrophages. *J Immunol* 148, 2207-2216.

Fang, X., Zheng, P., Tang, J., and Liu, Y. (2010). CD24: from A to Z. *Cell Mol Immunol* 7, 100-103.

Fanos, V., Castagnola, M., and Faa, G. (2015). Prolonging nephrogenesis in preterm infants: a new approach for prevention of kidney disease in adulthood? *Iran J Kidney Dis* 9, 180-185.

Fargeas, C.A. (2006). Prominin-1 (CD133): from progenitor cells to human diseases. *Future Lipidol* 1, 213-225.

Faubel, S., Lewis, E.C., Reznikov, L., Ljubanovic, D., Hoke, T.S., Somerset, H., Oh, D.J., Lu, L., Klein, C.L., Dinarello, C.A., *et al.* (2007). Cisplatin-induced acute renal failure is associated with an increase in the cytokines interleukin (IL)-1beta, IL-18, IL-6, and neutrophil infiltration in the kidney. *The Journal of pharmacology and experimental therapeutics* 322, 8-15.

Faubel, S., Ljubanovic, D., Reznikov, L., Somerset, H., Dinarello, C.A., and Edelstein, C.L. (2004). Caspase-1-deficient mice are protected against cisplatin-induced apoptosis and acute tubular necrosis. *Kidney international* 66, 2202-2213.

Ferenbach, D., and Hughes, J. (2008). Macrophages and dendritic cells: what is the difference? *Kidney international* 74, 5-7.

Ferguson, M.A., Vaidya, V.S., and Bonventre, J.V. (2008). Biomarkers of nephrotoxic acute kidney injury. *Toxicology* 245, 182-193.

Fesenko, I., Franklin, D., Garnett, P., Bass, P., Campbell, S., Hardyman, M., Wilson, D., Hanley, N., and Collins, J. (2010). Stem cell marker TRA-1-60 is expressed in foetal and adult kidney and upregulated in tubulo-interstitial disease. *Histochem Cell Biol* 134, 355-369.

Fink, H.A., Ishani, A., Taylor, B.C., Greer, N.L., MacDonald, R., Rossini, D., Sadiq, S., Lankireddy, S., Kane, R.L., and Wilt, T.J. (2012). In *Chronic Kidney Disease Stages 1-3: Screening, Monitoring, and Treatment* (Rockville (MD)).

Fischer, U.M., Harting, M.T., Jimenez, F., Monzon-Posadas, W.O., Xue, H., Savitz, S.I., Laine, G.A., and Cox, C.S., Jr. (2009). Pulmonary passage is a major obstacle for intravenous stem cell delivery: the pulmonary first-pass effect. *Stem cells and development* 18, 683-692.

Florek, M., Bauer, N., Janich, P., Wilsch-Braeuninger, M., Fargeas, C., Marzesco, A.-M., Ehninger, G., Thiele, C., Huttner, W., and Corbeil, D. (2007). Prominin-2 is a cholesterol-binding protein associated with apical and basolateral plasmalemmal protrusions in polarized epithelial cells and released into urine. *Cell and Tissue Research* 328, 31-47.

Fong, C.Y., Peh, G.S., Gauthaman, K., and Bongso, A. (2009). Separation of SSEA-4 and TRA-1-60 labelled undifferentiated human embryonic stem cells from a heterogeneous cell population using magnetic-activated cell sorting (MACS) and fluorescence-activated cell sorting (FACS). *Stem Cell Rev* 5, 72-80.

Freedman, B.S., Brooks, C.R., Lam, A.Q., Fu, H., Morizane, R., Agrawal, V., Saad, A.F., Li, M.K., Hughes, M.R., Werff, R.V., *et al.* (2015). Modelling kidney disease with CRISPR-mutant kidney organoids derived from human pluripotent epiblast spheroids. *Nat Commun* 6, 8715.

Fuchs, E. (2009). The tortoise and the hair: slow-cycling cells in the stem cell race. *Cell* 137, 811-819.

Ganeva, V., Unbekandt, M., and Davies, J.A. (2011). An improved kidney dissociation and reaggregation culture system results in nephrons arranged organotypically around a single collecting duct system. *Organogenesis* 7, 83-87.

Gatti, S., Bruno, S., Deregibus, M.C., Sordi, A., Cantaluppi, V., Tetta, C., and Camussi, G. (2011). Microvesicles derived from human adult mesenchymal stem cells protect against ischaemia-reperfusion-induced acute and chronic kidney injury. *Nephrology, dialysis, transplantation : official publication of the European Dialysis and Transplant Association - European Renal Association* 26, 1474-1483.

Gong, L., Cui, Z., Yu, X., Wei, Y., Peng, J., and Leng, X. (2012). Hexokinase II in CD133+ and CD133- hepatoma BEL-7402 Cells. *Pathol Oncol Res* 18, 377-381.

Grange, C., Moggio, A., Tapparo, M., Porta, S., Camussi, G., and Bussolati, B. (2014a). Protective effect and localization by optical imaging of human renal CD133+ progenitor cells in an acute kidney injury model. *Physiol Rep* 2, e12009.

Grange, C., Tapparo, M., Bruno, S., Chatterjee, D., Quesenberry, P.J., Tetta, C., and Camussi, G. (2014b). Biodistribution of mesenchymal stem cell-derived extracellular vesicles in a model of acute kidney injury monitored by optical imaging. *Int J Mol Med* 33, 1055-1063.

Gross, A., Schoendube, J., Zimmermann, S., Steeb, M., Zengerle, R., and Koltay, P. (2015). Technologies for Single-Cell Isolation. *Int J Mol Sci* 16, 16897-16919.

Gudas, L.J., and Wagner, J.A. (2011). Retinoids regulate stem cell differentiation. *Journal of cellular physiology* 226, 322-330.

Gupta, A.K., Jadhav, S.H., Tripathy, N.K., and Nityanand, S. (2015). Fetal kidney stem cells ameliorate cisplatin induced acute renal failure and promote renal angiogenesis. *World J Stem Cells* 7, 776-788.

Haldorsson, S., Lucumi, E., Gomez-Sjoberg, R., and Fleming, R.M. (2015). Advantages and challenges of microfluidic cell culture in polydimethylsiloxane devices. *Biosensors & bioelectronics* *63*, 218-231.

Hallgrímsson, B., Benediktsson, H., and Vize, P.D. (2003). 11 - Anatomy and Histology of the Human Urinary System. In *The Kidney*, P.D.V.S.W.B.L. Bard, ed. (San Diego: Academic Press), pp. 149-164.

Han, W.K., Alinani, A., Wu, C.L., Michaelson, D., Loda, M., McGovern, F.J., Thadhani, R., and Bonventre, J.V. (2005). Human kidney injury molecule-1 is a tissue and urinary tumor marker of renal cell carcinoma. *Journal of the American Society of Nephrology : JASN* *16*, 1126-1134.

Han, W.K., Bailly, V., Abichandani, R., Thadhani, R., and Bonventre, J.V. (2002). Kidney Injury Molecule-1 (KIM-1): a novel biomarker for human renal proximal tubule injury. *Kidney international* *62*, 237-244.

Hanigan, M.H., and Devarajan, P. (2003). Cisplatin nephrotoxicity: molecular mechanisms. *Cancer therapy* *1*, 47-61.

Hansson, J., Hultenby, K., Cramnert, C., Ponten, F., Jansson, H., Lindgren, D., Axelson, H., and Johansson, M.E. (2014). Evidence for a morphologically distinct and functionally robust cell type in the proximal tubules of human kidney. *Hum Pathol* *45*, 382-393.

Haraldsson, B., Nystrom, J., and Deen, W.M. (2008). Properties of the glomerular barrier and mechanisms of proteinuria. *Physiol Rev* *88*, 451-487.

Harari-Steinberg, O., Metsuyanin, S., Omer, D., Gnatek, Y., Gershon, R., Pri-Chen, S., Ozdemir, D.D., Lerenthal, Y., Noiman, T., Ben-Hur, H., *et al.* (2013). Identification of human nephron progenitors capable of generation of kidney structures and functional repair of chronic renal disease. *EMBO Mol Med* *5*, 1556-1568.

Harel-Adar, T., Ben Mordechai, T., Amsalem, Y., Feinberg, M.S., Leor, J., and Cohen, S. (2011). Modulation of cardiac macrophages by phosphatidylserine-presenting liposomes improves infarct repair. *Proc Natl Acad Sci U S A* *108*, 1827-1832.

Harrison-Bernard, L.M. (2009). The renal renin-angiotensin system. *Adv Physiol Educ* *33*, 270-274.

Heilman, R.L., Smith, M.L., Kurian, S.M., Huskey, J., Batra, R.K., Chakkera, H.A., Katariya, N.N., Khamash, H., Moss, A., Salomon, D.R., *et al.* (2015). Transplanting Kidneys from Deceased Donors With Severe Acute Kidney Injury. *Am J Transplant* *15*, 2143-2151.

Herget-Rosenthal, S., Poppen, D., Husing, J., Marggraf, G., Pietruck, F., Jakob, H.G., Philipp, T., and Kribben, A. (2004). Prognostic value of tubular proteinuria and enzymuria in nonoliguric acute tubular necrosis. *Clin Chem* 50, 552-558.

Heslop, J.A., Hammond, T.G., Santeramo, I., Tort Piella, A., Hopp, I., Zhou, J., Baty, R., Graziano, E.I., Proto Marco, B., Caron, A., *et al.* (2015). Concise review: workshop review: understanding and assessing the risks of stem cell-based therapies. *Stem cells translational medicine* 4, 389-400.

Heyman, S.N.K.M.R.S.R.C. (2010). In vivo models of acute kidney injury. *Drug Discovery Today: Disease Models* 7, 51-56.

Heymsfield, S.B., Arteaga, C., McManus, C., Smith, J., and Moffitt, S. (1983). Measurement of muscle mass in humans: validity of the 24-hour urinary creatinine method. *Am J Clin Nutr* 37, 478-494.

Hochreiter-Hufford, A., and Ravichandran, K.S. (2013). Clearing the dead: apoptotic cell sensing, recognition, engulfment, and digestion. *Cold Spring Harbor perspectives in biology* 5, a008748.

Humphreys, B.D. (2014). Kidney injury, stem cells and regeneration. *Current opinion in nephrology and hypertension* 23, 25-31.

Humphreys, B.D., Czemiak, S., DiRocco, D.P., Hasnain, W., Cheema, R., and Bonventre, J.V. (2011). Repair of injured proximal tubule does not involve specialized progenitors. *Proc Natl Acad Sci U S A* 108, 9226-9231.

Humphreys, B.D., Xu, F., Sabbiseti, V., Grgic, I., Movahedi Naini, S., Wang, N., Chen, G., Xiao, S., Patel, D., Henderson, J.M., *et al.* (2013). Chronic epithelial kidney injury molecule-1 expression causes murine kidney fibrosis. *J Clin Invest* 123, 4023-4035.

Ichimura, T., Bonventre, J.V., Bailly, V., Wei, H., Hession, C.A., Cate, R.L., and Sanicola, M. (1998). Kidney injury molecule-1 (KIM-1), a putative epithelial cell adhesion molecule containing a novel immunoglobulin domain, is up-regulated in renal cells after injury. *J Biol Chem* 273, 4135-4142.

Imai, T., Takahashi, Y., Nishikawa, M., Kato, K., Morishita, M., Yamashita, T., Matsumoto, A., Charoenviriyakul, C., and Takakura, Y. (2015). Macrophage-dependent clearance of systemically administered B16BL6-derived exosomes from the blood circulation in mice. *J Extracell Vesicles* 4, 26238.

Ishida, S., Lee, J., Thiele, D.J., and Herskowitz, I. (2002). Uptake of the anticancer drug cisplatin mediated by the copper transporter Ctr1 in yeast and mammals. *Proc Natl Acad Sci U S A* 99, 14298-14302.

Jahan-Tigh, R.R., Ryan, C., Obermoser, G., and Schwarzenberger, K. (2012). Flow cytometry. *J Invest Dermatol* 132, e1.

Jang, H.R., and Rabb, H. (2015). Immune cells in experimental acute kidney injury. *Nature reviews Nephrology* 11, 88-101.

Jarad, G., and Miner, J.H. (2009). Update on the glomerular filtration barrier. *Current opinion in nephrology and hypertension* 18, 226-232.

Kabgani, N., Grigoleit, T., Schulte, K., Sechi, A., Sauer-Lehnen, S., Tag, C., Boor, P., Kuppe, C., Warsow, G., Schordan, S., *et al.* (2012). Primary cultures of glomerular parietal epithelial cells or podocytes with proven origin. *PLoS one* 7, e34907.

Kalluri, R., and Weinberg, R.A. (2009). The basics of epithelial-mesenchymal transition. *J Clin Invest* 119, 1420-1428.

Kamei, N., Kwon, S.M., Alev, C., Nakanishi, K., Yamada, K., Masuda, H., Ishikawa, M., Kawamoto, A., Ochi, M., and Asahara, T. (2013). Ex-vivo expanded human blood-derived CD133+ cells promote repair of injured spinal cord. *J Neurol Sci* 328, 41-50.

Karbanova, J., Missol-Kolka, E., Fonseca, A.V., Lorra, C., Janich, P., Hollerova, H., Jaszai, J., Ehrmann, J., Kolar, Z., Liebers, C., *et al.* (2008). The stem cell marker CD133 (Prominin-1) is expressed in various human glandular epithelia. *J Histochem Cytochem* 56, 977-993.

Kaushal, G.P., Kaushal, V., Hong, X., and Shah, S.V. (2001). Role and regulation of activation of caspases in cisplatin-induced injury to renal tubular epithelial cells. *Kidney international* 60, 1726-1736.

Kemper, K., Sprick, M.R., de Bree, M., Scopelliti, A., Vermeulen, L., Hoek, M., Zeilstra, J., Pals, S.T., Mehmet, H., Stassi, G., *et al.* (2010). The AC133 epitope, but not the CD133 protein, is lost upon cancer stem cell differentiation. *Cancer Res* 70, 719-729.

Keppler, A., Gretz, N., Schmidt, R., Kloetzer, H.M., Groene, H.J., Lelongt, B., Meyer, M., Sadick, M., and Pill, J. (2007). Plasma creatinine determination in mice and rats: an enzymatic method compares favorably with a high-performance liquid chromatography assay. *Kidney international* 71, 74-78.

Kietzmann, L., Guhr, S.S., Meyer, T.N., Ni, L., Sachs, M., Panzer, U., Stahl, R.A., Saleem, M.A., Kerjaschki, D., Gebeshuber, C.A., *et al.* (2015). MicroRNA-193a Regulates the Transdifferentiation of Human Parietal Epithelial Cells toward a Podocyte Phenotype. *Journal of the American Society of Nephrology : JASN* 26, 1389-1401.

Kim, J.H., Park, D.J., Yun, J.C., Jung, M.H., Yeo, H.D., Kim, H.J., Kim, D.W., Yang, J.I., Lee, G.W., Jeong, S.H., *et al.* (2012). Human adipose tissue-derived mesenchymal stem cells protect kidneys from cisplatin nephrotoxicity in rats. *Am J Physiol Renal Physiol* 302, F1141-1150.

- Kintzel, P.E. (2001). Anticancer drug-induced kidney disorders. *Drug Saf* 24, 19-38.
- Kisselbach, L., Merges, M., Bossie, A., and Boyd, A. (2009). CD90 Expression on human primary cells and elimination of contaminating fibroblasts from cell cultures. *Cytotechnology* 59, 31-44.
- Koitaishi, K., Okamoto, K., Arirto, M., Sato, T., Nagai, K., Kurokawa, M.S., Suematsu, N., Yasuda, T., Kimura, K., and Kato, T. (2011). Micro-sieving: isolation of whole glomeruli from a single renal needle biopsy sample. *Nephron Clin Pract* 117, c225-229.
- Kolaczowska, E., and Kubes, P. (2013). Neutrophil recruitment and function in health and inflammation. *Nat Rev Immunol* 13, 159-175.
- Kusaba, T., and Humphreys, B.D. (2014). Reply to Corbeil et al.: Dedifferentiation and multipotency. *Proc Natl Acad Sci U S A* 111, E1453.
- Kusaba, T., Lalli, M., Kramann, R., Kobayashi, A., and Humphreys, B.D. (2014). Differentiated kidney epithelial cells repair injured proximal tubule. *Proc Natl Acad Sci U S A* 111, 1527-1532.
- Kutscher, H.L., Chao, P., Deshmukh, M., Singh, Y., Hu, P., Joseph, L.B., Reimer, D.C., Stein, S., Laskin, D.L., and Sinko, P.J. (2010). Threshold size for optimal passive pulmonary targeting and retention of rigid microparticles in rats. *Journal of controlled release : official journal of the Controlled Release Society* 143, 31-37.
- Kuzma-Kuzniarska, M., Rak-Raszewska, A., Kenny, S., Edgar, D., Wilm, B., Fuente Mora, C., Davies, J.A., and Murray, P. (2012). Integration potential of mouse and human bone marrow-derived mesenchymal stem cells. *Differentiation; research in biological diversity* 83, 128-137.
- Lardon, J., Corbeil, D., Huttner, W.B., Ling, Z., and Bouwens, L (2008). Stem cell marker prominin-1/AC133 is expressed in duct cells of the adult human pancreas. *Pancreas* 36, e1-6.
- Lasagni, L., Angelotti, M.L., Ronconi, E., Lombardi, D., Nardi, S., Peired, A., Becherucci, F., Mazinghi, B., Sisti, A., Romoli, S., *et al.* (2015). Podocyte Regeneration Driven by Renal Progenitors Determines Glomerular Disease Remission and Can Be Pharmacologically Enhanced. *Stem cell reports* 5, 248-263.
- Lassnigg, A., Schmidlin, D., Mouhieddine, M., Bachmann, L.M., Druml, W., Bauer, P., and Hiesmayr, M. (2004). Minimal changes of serum creatinine predict prognosis in patients after cardiothoracic surgery: a prospective cohort study. *Journal of the American Society of Nephrology : JASN* 15, 1597-1605.
- Lawrence, M.L., Chang, C.H., and Davies, J.A. (2015). Transport of organic anions and cations in murine embryonic kidney development and in serially-reaggregated engineered kidneys. *Sci Rep* 5, 9092.

Lee, S., Kim, W., Moon, S.O., Sung, M.J., Kim, D.H., Kang, K.P., Jang, Y.B., Lee, J.E., Jang, K.Y., and Park, S.K. (2006). Rosiglitazone ameliorates cisplatin-induced renal injury in mice. *Nephrology, dialysis, transplantation : official publication of the European Dialysis and Transplant Association - European Renal Association* 21, 2096-2105.

Leibacher, J., and Henschler, R. (2016). Biodistribution, migration and homing of systemically applied mesenchymal stem/stromal cells. *Stem cell research & therapy* 7, 7.

Leung, K.C., Tonelli, M., and James, M.T. (2013). Chronic kidney disease following acute kidney injury-risk and outcomes. *Nature reviews Nephrology* 9, 77-85.

Li, P., Zhang, R., Sun, H., Chen, L., Liu, F., Yao, C., Du, M., and Jiang, X. (2013a). PKH26 can transfer to host cells in vitro and vivo. *Stem cells and development* 22, 340-344.

Li, Q., Zhang, X., Peng, Y., Chai, H., Xu, Y., Wei, J., Ren, X., Wang, X., Liu, W., Chen, M., *et al.* (2013b). Comparison of the sorting efficiency and influence on cell function between the sterile flow cytometry and immunomagnetic bead purification methods. *Prep Biochem Biotechnol* 43, 197-206.

Lieberthal, W., Triaca, V., and Levine, J. (1996). Mechanisms of death induced by cisplatin in proximal tubular epithelial cells: apoptosis vs. necrosis. *Am J Physiol* 270, F700-708.

Lindgren, D., Bostrom, A.K., Nilsson, K., Hansson, J., Sjolund, J., Moller, C., Jirstrom, K., Nilsson, E., Landberg, G., Axelson, H., *et al.* (2011). Isolation and characterization of progenitor-like cells from human renal proximal tubules. *The American journal of pathology* 178, 828-837.

Little, M.H. (2006). Regrow or repair: potential regenerative therapies for the kidney. *Journal of the American Society of Nephrology: JASN* 17, 2390-2401.

Liu, M., Chien, C.C., Burne-Taney, M., Molls, R.R., Racusen, L.C., Colvin, R.B., and Rabb, H. (2006). A pathophysiologic role for T lymphocytes in murine acute cisplatin nephrotoxicity. *Journal of the American Society of Nephrology: JASN* 17, 765-774.

Lopez-Giacoman, S., and Madero, M. (2015). Biomarkers in chronic kidney disease, from kidney function to kidney damage. *World J Nephrol* 4, 57-73.

Marchal, G., Verbeken, E., Oyen, R., Moerman, F., Baert, A.L., and Lauweryns, J. (1986). Ultrasound of the normal kidney: a sonographic, anatomic and histologic correlation. *Ultrasound Med Biol* 12, 999-1009.

Medema, J.P. (2013). Cancer stem cells: the challenges ahead. *Nat Cell Biol* 15, 338-344.

Metsuyanin, S., Harari-Steinberg, O., Buzhor, E., Omer, D., Pode-Shakked, N., Ben-Hur, H., Halperin, R., Schneider, D., and Dekel, B. (2009). Expression of stem cell markers in the human fetal kidney. *PLoS one* 4, e6709.



Miller, R.P., Tadagavadi, R.K., Ramesh, G., and Reeves, W.B. (2010). Mechanisms of Cisplatin nephrotoxicity. *Toxins* 2, 2490-2518.

Mizrak, D., Brittan, M., and Alison, M. (2008). CD133: molecule of the moment. *The Journal of pathology* 214, 3-9.

Morelli, A.E., and Larregina, A.T. (2010). Apoptotic cell-based therapies against transplant rejection: role of recipient's dendritic cells. *Apoptosis* 15, 1083-1097.

Morzane, R., Lam, A.Q., Freedman, B.S., Kishi, S., Valerius, M.T., and Bonventre, J.V. (2015). Nephron organoids derived from human pluripotent stem cells model kidney development and injury. *Nat Biotechnol* 33, 1193-1200.

Murray, P.J., Allen, J.E., Biswas, S.K., Fisher, E.A., Gilroy, D.W., Goerdt, S., Gordon, S., Hamilton, J.A., Ivashkiv, L.B., Lawrence, T., *et al.* (2014). Macrophage activation and polarization: nomenclature and experimental guidelines. *Immunity* 41, 14-20.

Murray, P.J., and Wynn, T.A. (2011). Protective and pathogenic functions of macrophage subsets. *Nat Rev Immunol* 11, 723-737.

Neuzil, J., Stantic, M., Zobalova, R., Chladova, J., Wang, X., Prochazka, L., Dong, L., Andera, L., and Ralph, S.J. (2007). Tumour-initiating cells vs. cancer 'stem' cells and CD133: what's in the name? *Biochem Biophys Res Commun* 355, 855-859.

Njoroge, J.M., Mitchell, L.B., Centola, M., Kastner, D., Raffeld, M., and Miller, J.L. (2001). Characterization of viable autofluorescent macrophages among cultured peripheral blood mononuclear cells. *Cytometry* 44, 38-44.

Okamura, M., Takano, Y., Saito, Y., Yao, J., and Kitamura, M. (2009). Induction of nephrin gene expression by selective cooperation of the retinoic acid receptor and the vitamin D receptor. *Nephrology, dialysis, transplantation : official publication of the European Dialysis and Transplant Association - European Renal Association* 24, 3006-3012.

Oliver, J.A., Maarouf, O., Cheema, F.H., Martens, T.P., and Al-Awqati, Q. (2004). The renal papilla is a niche for adult kidney stem cells. *J Clin Invest* 114, 795-804.

Ozkok, A., and Edelstein, C.L. (2014). Pathophysiology of cisplatin-induced acute kidney injury. *Biomed Res Int* 2014, 967826.

Pabla, N., and Dong, Z. (2008). Cisplatin nephrotoxicity: mechanisms and renoprotective strategies. *Kidney international* 73, 994-1007.

Palevsky, P.M. (2012). Chronic-on-acute kidney injury. *Kidney international* 81, 430-431.

Pampaloni, F., Ansari, N., and Stelzer, E.H. (2013). High-resolution deep imaging of live cellular spheroids with light-sheet-based fluorescence microscopy. *Cell Tissue Res* 352, 161-177.

Pampaloni, F., Berge, U., Marmaras, A., Horvath, P., Kroschewski, R., and Stelzer, E.H. (2014). Tissue-culture light sheet fluorescence microscopy (TC-LSFM) allows long-term imaging of three-dimensional cell cultures under controlled conditions. *Integr Biol (Camb)* 6, 988-998.

Pampaloni, F., Chang, B.J., and Stelzer, E.H. (2015). Light sheet-based fluorescence microscopy (LSFM) for the quantitative imaging of cells and tissues. *Cell Tissue Res* 360, 129-141.

Pendharkar, A.V., Chua, J.Y., Andres, R.H., Wang, N., Gaeta, X., Wang, H., De, A., Choi, R., Chen, S., Rutt, B.K., *et al.* (2010). Biodistribution of neural stem cells after intravascular therapy for hypoxic-ischemia. *Stroke; a journal of cerebral circulation* 41, 2064-2070.

Peng, X., Xu, H., Zhou, Y., Wang, B., Yan, Y., Zhang, X., Wang, M., Gao, S., Zhu, W., Xu, W., *et al.* (2013). Human umbilical cord mesenchymal stem cells attenuate cisplatin-induced acute and chronic renal injury. *Exp Biol Med (Maywood)*.

Perazella, M.A. (2012). Onco-nephrology: renal toxicities of chemotherapeutic agents. *Clinical journal of the American Society of Nephrology : CJASN* 7, 1713-1721.

Phillips, C.L., Arend, L.J., Filson, A.J., Kojetin, D.J., Clendenon, J.L., Fang, S., and Dunn, K.W. (2001). Three-dimensional imaging of embryonic mouse kidney by two-photon microscopy. *The American journal of pathology* 158, 49-55.

Pleniceanu, O., Harari-Steinberg, O., and Dekel, B. (2010). Concise review: Kidney stem/progenitor cells: differentiate, sort out, or reprogram? *Stem cells* 28, 1649-1660.

Pode-Shakked, N., Pleniceanu, O., Gershon, R., Shukrun, R., Kanter, I., Bucris, E., Pode-Shakked, B., Tam, G., Tam, H., Caspi, R., *et al.* (2016). Dissecting Stages of Human Kidney Development and Tumorigenesis with Surface Markers Affords Simple Prospective Purification of Nephron Stem Cells. *Sci Rep* 6, 23562.

Poon, I.K., Lucas, C.D., Rossi, A.G., and Ravichandran, K.S. (2014). Apoptotic cell clearance: basic biology and therapeutic potential. *Nat Rev Immunol* 14, 166-180.

Portilla, D., Dai, G., McClure, T., Bates, L., Kurten, R., Megyesi, J., Price, P., and Li, S. (2002). Alterations of PPARalpha and its coactivator PGC-1 in cisplatin-induced acute renal failure. *Kidney international* 62, 1208-1218.

Price, K.L., Long, D.A., Jina, N., Liapis, H., Hubank, M., Woolf, A.S., and Winyard, P.J. (2007). Microarray interrogation of human metanephric mesenchymal cells highlights potentially important molecules in vivo. *Physiological genomics* 28, 193-202.

Puelles, V.G., Hoy, W.E., Hughson, M.D., Diouf, B., Douglas-Denton, R.N., and Bertram, J.F. (2011). Glomerular number and size variability and risk for kidney disease. *Current opinion in nephrology and hypertension* 20, 7-15.

- Qi, S., and Wu, D. (2013). Bone marrow-derived mesenchymal stem cells protect against cisplatin-induced acute kidney injury in rats by inhibiting cell apoptosis. *Int J Mol Med* 32, 1262-1272.
- Rak-Raszewska, A., Hauser, P.V., and Vainio, S. (2015). Organ In Vitro Culture: What Have We Learned about Early Kidney Development? *Stem Cells Int* 2015, 959807.
- Rak-Raszewska, A., Wilm, B., Edgar, D., Kenny, S., Woolf, A.S., and Murray, P. (2012). Development of embryonic stem cells in recombinant kidneys. *Organogenesis* 8, 125-136.
- Ramesh, G., and Reeves, W.B. (2002). TNF-alpha mediates chemokine and cytokine expression and renal injury in cisplatin nephrotoxicity. *J Clin Invest* 110, 835-842.
- Ramesh, G., and Reeves, W.B. (2003). TNFR2-mediated apoptosis and necrosis in cisplatin-induced acute renal failure. *Am J Physiol Renal Physiol* 285, F610-618.
- Ramesh, G., and Reeves, W.B. (2004). Inflammatory cytokines in acute renal failure. *Kidney international Supplement*, S56-61.
- Ramesh, G., and Reeves, W.B. (2005). p38 MAP kinase inhibition ameliorates cisplatin nephrotoxicity in mice. *Am J Physiol Renal Physiol* 289, F166-174.
- Ranga, A., Gjorevski, N., and Lutolf, M.P. (2014). Drug discovery through stem cell-based organoid models. *Adv Drug Deliv Rev* 69-70, 19-28.
- Raposo, G., and Stoorvogel, W. (2013). Extracellular vesicles: exosomes, microvesicles, and friends. *J Cell Biol* 200, 373-383.
- Razzaque, M.S., Koji, T., Kumatori, A., and Taguchi, T. (1999). Cisplatin-induced apoptosis in human proximal tubular epithelial cells is associated with the activation of the Fas/Fas ligand system. *Histochem Cell Biol* 111, 359-365.
- Reidy, K.J., and Rosenblum, N.D. (2009). Cell and molecular biology of kidney development. *Seminars in nephrology* 29, 321-337.
- Reynaud, E.G., Peychl, J., Huisken, J., and Tomancak, P. (2015). Guide to light-sheet microscopy for adventurous biologists. *Nat Methods* 12, 30-34.
- Ricci, Z., Cruz, D., and Ronco, C. (2008). The RIFLE criteria and mortality in acute kidney injury: A systematic review. *Kidney international* 73, 538-546.
- Ricci, Z., Cruz, D.N., and Ronco, C. (2011). Classification and staging of acute kidney injury: beyond the RIFLE and AKIN criteria. *Nature reviews Nephrology* 7, 201-208.
- Ries, F., and Klastersky, J. (1986). Nephrotoxicity induced by cancer chemotherapy with special emphasis on cisplatin toxicity. *American journal of kidney diseases : the official journal of the National Kidney Foundation* 8, 368-379.

Rinkevich, Y., Lindau, P., Ueno, H., Longaker, M.T., and Weissman, I.L. (2011). Germ-layer and lineage-restricted stem/progenitors regenerate the mouse digit tip. *Nature* 476, 409-413.

Rinkevich, Y., Montoro, D.T., Contreras-Trujillo, H., Harari-Steinberg, O., Newman, A.M., Tsai, J.M., Lim, X., Van-Amerongen, R., Bowman, A., Januszzyk, M., *et al.* (2014). In vivo clonal analysis reveals lineage-restricted progenitor characteristics in mammalian kidney development, maintenance, and regeneration. *Cell Rep* 7, 1270-1283.

Romagnani, P., and Remuzzi, G. (2014). CD133+ renal stem cells always co-express CD24 in adult human kidney tissue. *Stem cell research* 12, 828-829.

Ronconi, E., Sagrinati, C., Angelotti, M.L., Lazzeri, E., Mazzinghi, B., Ballerini, L., Parente, E., Becherucci, F., Gacci, M., Carini, M., *et al.* (2009). Regeneration of glomerular podocytes by human renal progenitors. *Journal of the American Society of Nephrology : JASN* 20, 322-332.

Sagrinati, C., Netti, G.S., Mazzinghi, B., Lazzeri, E., Liotta, F., Frosali, F., Ronconi, E., Meini, C., Gacci, M., Squecco, R., *et al.* (2006). Isolation and characterization of multipotent progenitor cells from the Bowman's capsule of adult human kidneys. *Journal of the American Society of Nephrology : JASN* 17, 2443-2456.

Sahni, V., Choudhury, D., and Ahmed, Z. (2009). Chemotherapy-associated renal dysfunction. *Nature reviews Nephrology* 5, 450-462.

Saleem, M.A., O'Hare, M.J., Reiser, J., Coward, R.J., Inward, C.D., Farren, T., Xing, C.Y., Ni, L., Mathieson, P.W., and Mundel, P. (2002). A conditionally immortalized human podocyte cell line demonstrating nephrin and podocin expression. *Journal of the American Society of Nephrology : JASN* 13, 630-638.

Sanchez-Gonzalez, P.D., Lopez-Hernandez, F.J., Lopez-Novoa, J.M., and Morales, A.I. (2011). An integrative view of the pathophysiological events leading to cisplatin nephrotoxicity. *Crit Rev Toxicol* 41, 803-821.

Scarfe, L., Rak-Raszewska, A., Geraci, S., Darssan, D., Sharkey, J., Huang, J., Burton, N.C., Mason, D., Ranjzad, P., Kenny, S., *et al.* (2015). Measures of kidney function by minimally invasive techniques correlate with histological glomerular damage in SCID mice with adriamycin-induced nephropathy. *Sci Rep* 5, 13601.

Schock-Kusch, D., Sadick, M., Henninger, N., Kraenzlin, B., Claus, G., Kloetzer, H.M., Weiss, C., Pill, J., and Gretz, N. (2009). Transcutaneous measurement of glomerular filtration rate using FITC-sinistrin in rats. *Nephrology, dialysis, transplantation : official publication of the European Dialysis and Transplant Association - European Renal Association* 24, 2997-3001.

Schock-Kusch, D., Xie, Q., Shulhevich, Y., Hesser, J., Stsepankou, D., Sadick, M., Koenig, S., Hoecklin, F., Pill, J., and Gretz, N. (2011). Transcutaneous assessment of renal function in

conscious rats with a device for measuring FITC-sinistrin disappearance curves. *Kidney international* 79, 1254-1258.

Schold, J.D., and Segev, D.L. (2012). Increasing the pool of deceased donor organs for kidney transplantation. *Nature reviews Nephrology* 8, 325-331.

Scott, R.P., and Quaggin, S.E. (2015). Review series: The cell biology of renal filtration. *J Cell Biol* 209, 199-210.

Sebinger, D.D., Unbekandt, M., Ganeva, V.V., Ofenbauer, A., Werner, C., and Davies, J.A. (2010). A novel, low-volume method for organ culture of embryonic kidneys that allows development of cortico-medullary anatomical organization. *PLoS one* 5, e10550.

Shi, M., Ishikawa, M., Kamei, N., Nakasa, T., Adachi, N., Deie, M., Asahara, T., and Ochi, M. (2009). Acceleration of skeletal muscle regeneration in a rat skeletal muscle injury model by local injection of human peripheral blood-derived CD133-positive cells. *Stem cells* 27, 949-960.

Shmelkov, S.V., Butler, J.M., Hooper, A.T., Hormigo, A., Kushner, J., Milde, T., St Clair, R., Baljevic, M., White, I., Jin, D.K., *et al.* (2008). CD133 expression is not restricted to stem cells, and both CD133+ and CD133- metastatic colon cancer cells initiate tumors. *J Clin Invest* 118, 2111-2120.

Shmelkov, S.V., St Clair, R., Lyden, D., and Rafii, S. (2005). AC133/CD133/Prominin-1. *Int J Biochem Cell Biol* 37, 715-719.

Siegel, N., Rosner, M., Unbekandt, M., Fuchs, C., Slabina, N., Dolznig, H., Davies, J.A., Lubec, G., and Hengstschlager, M. (2010). Contribution of human amniotic fluid stem cells to renal tissue formation depends on mTOR. *Human molecular genetics* 19, 3320-3331.

Singbartl, K., and Kellum, J.A. (2012). AKI in the ICU: definition, epidemiology, risk stratification, and outcomes. *Kidney international* 81, 819-825.

Singh, A.P., Junemann, A., Muthuraman, A., Jaggi, A.S., Singh, N., Grover, K., and Dhawan, R. (2012). Animal models of acute renal failure. *Pharmacol Rep* 64, 31-44.

Smeets, B., Angelotti, M.L., Rizzo, P., Dijkman, H., Lazzeri, E., Mooren, F., Ballerini, L., Parente, E., Sagrinati, C., Mazzinghi, B., *et al.* (2009). Renal progenitor cells contribute to hyperplastic lesions of podocytopathies and crescentic glomerulonephritis. *Journal of the American Society of Nephrology : JASN* 20, 2593-2603.

Smeets, B., Boor, P., Dijkman, H., Sharma, S.V., Jirak, P., Mooren, F., Berger, K., Bornemann, J., Gelman, I.H., Floege, J., *et al.* (2013). Proximal tubular cells contain a phenotypically distinct, scattered cell population involved in tubular regeneration. *The Journal of pathology* 229, 645-659.

Smeets, B., Kuppe, C., Sicking, E.M., Fuss, A., Jirak, P., van Kuppevelt, T.H., Endlich, K., Wetzels, J.F., Grone, H.J., Floege, J., *et al.* (2011). Parietal epithelial cells participate in the formation of sclerotic lesions in focal segmental glomerulosclerosis. *Journal of the American Society of Nephrology : JASN* 22, 1262-1274.

Song, B., Smink, A.M., Jones, C.V., Callaghan, J.M., Firth, S.D., Bernard, C.A., Laslett, A.L., Kerr, P.G., and Ricardo, S.D. (2012). The directed differentiation of human iPS cells into kidney podocytes. *PLoS one* 7, e46453.

Song, J., Czemiak, S., Wang, T., Ying, W., Carlone, D.L., Breault, D.T., and Humphreys, B.D. (2011). Characterization and fate of telomerase-expressing epithelia during kidney repair. *Journal of the American Society of Nephrology : JASN* 22, 2256-2265.

Song, S., Meyer, M., Turk, T.R., Wilde, B., Feldkamp, T., Assert, R., Wu, K., Kribben, A., and Witzke, O. (2009). Serum cystatin C in mouse models: a reliable and precise marker for renal function and superior to serum creatinine. *Nephrology, dialysis, transplantation : official publication of the European Dialysis and Transplant Association - European Renal Association* 24, 1157-1161.

Steinbach, S., Krolop, N., Strommer, S., Herrera-Perez, Z., Geraci, S., Friedemann, J., Gretz, N., and Neiger, R. (2014). A pilot study to assess the feasibility of transcutaneous glomerular filtration rate measurement using fluorescence-labelled sinistrin in dogs and cats. *PLoS one* 9, e111734.

Stevens, L.A., and Levey, A.S. (2005). Measurement of kidney function. *Med Clin North Am* 89, 457-473.

Stevens, L.A., and Levey, A.S. (2009). Measured GFR as a confirmatory test for estimated GFR. *Journal of the American Society of Nephrology : JASN* 20, 2305-2313.

Street, J.M., Souza, A.C., Alvarez-Prats, A., Horino, T., Hu, X., Yuen, P.S., and Star, R.A. (2014). Automated quantification of renal fibrosis with Sirius Red and polarization contrast microscopy. *Physiol Rep* 2.

Sulemanji, M., and Vakili, K. (2013). Neonatal renal physiology. *Semin Pediatr Surg* 22, 195-198.

Suzuki, A., Ito, T., Imai, E., Yamato, M., Iwatani, H., Kawachi, H., and Hori, M. (2003). Retinoids regulate the repairing process of the podocytes in puromycin aminonucleoside-induced nephrotic rats. *Journal of the American Society of Nephrology : JASN* 14, 981-991.

Tadagavadi, R.K., Gao, G., Wang, W.W., Gonzalez, M.R., and Reeves, W.B. (2015). Dendritic Cell Protection from Cisplatin Nephrotoxicity Is Independent of Neutrophils. *Toxins* 7, 3245-3256.

Tadagavadi, R.K., and Reeves, W.B. (2010). Endogenous IL-10 attenuates cisplatin nephrotoxicity: role of dendritic cells. *J Immunol* *185*, 4904-4911.

Takano, Y., Yamauchi, K., Hiramatsu, N., Kasai, A., Hayakawa, K., Yokouchi, M., Yao, J., and Kitamura, M. (2007). Recovery and maintenance of nephrin expression in cultured podocytes and identification of HGF as a repressor of nephrin. *Am J Physiol Renal Physiol* *292*, F1573-1582.

Takasato, M., Er, P.X., Becroft, M., Vanslambrouck, J.M., Stanley, E.G., Elefanty, A.G., and Little, M.H. (2014). Directing human embryonic stem cell differentiation towards a renal lineage generates a self-organizing kidney. *Nat Cell Biol* *16*, 118-126.

Tenstad, O., Roald, A.B., Grubb, A., and Aukland, K. (1996). Renal handling of radiolabelled human cystatin C in the rat. *Scand J Clin Lab Invest* *56*, 409-414.

Thum, T., Bauersachs, J., Poole-Wilson, P.A., Volk, H.D., and Anker, S.D. (2005). The dying stem cell hypothesis: immune modulation as a novel mechanism for progenitor cell therapy in cardiac muscle. *J Am Coll Cardiol* *46*, 1799-1802.

Toback, F.G. (1992). Regeneration after acute tubular necrosis. *Kidney international* *41*, 226-246.

Togel, F., Yang, Y., Zhang, P., Hu, Z., and Westenfelder, C. (2008). Bioluminescence imaging to monitor the in vivo distribution of administered mesenchymal stem cells in acute kidney injury. *Am J Physiol Renal Physiol* *295*, F315-321.

Trzpis, M., McLaughlin, P.M., van Goor, H., Brinker, M.G., van Dam, G.M., de Leij, L.M., Popa, E.R., and Harmsen, M.C. (2008). Expression of EpCAM is up-regulated during regeneration of renal epithelia. *The Journal of pathology* *216*, 201-208.

Trzpis, M., Popa, E.R., McLaughlin, P.M., van Goor, H., Timmer, A., Bosman, G.W., de Leij, L.M., and Harmsen, M.C. (2007). Spatial and temporal expression patterns of the epithelial cell adhesion molecule (EpCAM/EGP-2) in developing and adult kidneys. *Nephron Experimental nephrology* *107*, e119-131.

Uchida, K., and Gotoh, A. (2002). Measurement of cystatin-C and creatinine in urine. *Clinica chimica acta; international journal of clinical chemistry* *323*, 121-128.

Uchino, S. (2010). Creatinine. *Curr Opin Crit Care* *16*, 562-567.

Unbekandt, M., and Davies, J.A. (2010). Dissociation of embryonic kidneys followed by reaggregation allows the formation of renal tissues. *Kidney international* *77*, 407-416.

Vaidya, V.S., and Bonventre, J.V. (2006). Mechanistic biomarkers for cytotoxic acute kidney injury. *Expert Opin Drug Metab Toxicol* *2*, 697-713.

Vaidya, V.S., Ferguson, M.A., and Bonventre, J.V. (2008). Biomarkers of acute kidney injury. *Annu Rev Pharmacol Toxicol* **48**, 463-493.

Vaidya, V.S., Ramirez, V., Ichimura, T., Bobadilla, N.A., and Bonventre, J.V. (2006). Urinary kidney injury molecule-1: a sensitive quantitative biomarker for early detection of kidney tubular injury. *Am J Physiol Renal Physiol* **290**, F517-529.

Vainio, S., and Lin, Y. (2002). Coordinating early kidney development: lessons from gene targeting. *Nat Rev Genet* **3**, 533-543.

Van Biesen, W., Vanholder, R., and Lameire, N. (2006). Defining acute renal failure: RIFLE and beyond. *Clinical journal of the American Society of Nephrology: CJASN* **1**, 1314-1319.

Van der Hauwaert, C., Savary, G., Gnemmi, V., Glowacki, F., Pottier, N., Bouillez, A., Maboudou, P., Zini, L., Leroy, X., Cauffiez, C., *et al.* (2013). Isolation and characterization of a primary proximal tubular epithelial cell model from human kidney by CD10/CD13 double labeling. *PLoS one* **8**, e66750.

Vanholder, R., Lameire, N., Annemans, L., and Van Biesen, W. (2015). Cost of renal replacement: how to help as many as possible while keeping expenses reasonable? *Nephrology, dialysis, transplantation : official publication of the European Dialysis and Transplant Association - European Renal Association*.

Vaughan, M.R., Pippin, J.W., Griffin, S.V., Krofft, R., Fleet, M., Haseley, L., and Shankland, S.J. (2005). ATRA induces podocyte differentiation and alters nephrin and podocin expression in vitro and in vivo. *Kidney international* **68**, 133-144.

Vinken, P., Starckx, S., Barale-Thomas, E., Looszova, A., Sonee, M., Goeminne, N., Versmissen, L., Buyens, K., and Lampo, A. (2012). Tissue Kim-1 and urinary clusterin as early indicators of cisplatin-induced acute kidney injury in rats. *Toxicol Pathol* **40**, 1049-1062.

Vize, P.D. (2003). 1 - Introduction: Embryonic Kidneys and Other Nephrogenic Models. In *The Kidney*, P.D.V.S.W.B.L. Bard, ed. (San Diego: Academic Press), pp. 1-6.

Wang, D., and Lippard, S.J. (2005). Cellular processing of platinum anticancer drugs. *Nature reviews Drug discovery* **4**, 307-320.

Wang, Y.K., Zhu, Y.L., Qiu, F.M., Zhang, T., Chen, Z.G., Zheng, S., and Huang, J. (2010). Activation of Akt and MAPK pathways enhances the tumorigenicity of CD133+ primary colon cancer cells. *Carcinogenesis* **31**, 1376-1380.

Ward, H.H., Romero, E., Welford, A., Pickett, G., Bacallao, R., Gattone, V.H., 2nd, Ness, S.A., Wandinger-Ness, A., and Roitbak, T. (2011). Adult human CD133/1(+) kidney cells isolated from papilla integrate into developing kidney tubules. *Biochim Biophys Acta* **1812**, 1344-1357.



Wei, Q., Dong, G., Franklin, J., and Dong, Z. (2007). The pathological role of Bax in cisplatin nephrotoxicity. *Kidney International* 72, 53-62.

Weigmann, A., Corbeil, D., Hellwig, A., and Huttner, W.B. (1997). Prominin, a novel microvilli-specific polytopic membrane protein of the apical surface of epithelial cells, is targeted to plasmalemmal protrusions of non-epithelial cells. *Proc Natl Acad Sci U S A* 94, 12425-12430.

Wilm, B., and Murray, P. (2015). Amniotic Fluid Stem Cells within Chimeric Kidney Rudiments Differentiate to Functional Podocytes after Transplantation into Mature Rat Kidneys. *Journal of the American Society of Nephrology : JASN*.

Wilmer, M.J., Saleem, M.A., Masereeuw, R., Ni, L., van der Velden, T.J., Russel, F.G., Mathieson, P.W., Monnens, L.A., van den Heuvel, L.P., and Levtchenko, E.N. (2010). Novel conditionally immortalized human proximal tubule cell line expressing functional influx and efflux transporters. *Cell Tissue Res* 339, 449-457.

Witzgall, R., Brown, D., Schwarz, C., and Bonventre, J.V. (1994). Localization of proliferating cell nuclear antigen, vimentin, c-Fos, and clusterin in the postischemic kidney. Evidence for a heterogeneous genetic response among nephron segments, and a large pool of mitotically active and dedifferentiated cells. *J Clin Invest* 93, 2175-2188.

Wong, G., Howard, K., Chapman, J.R., Chadban, S., Cross, N., Tong, A., Webster, A.C., and Craig, J.C. (2012). Comparative survival and economic benefits of deceased donor kidney transplantation and dialysis in people with varying ages and co-morbidities. *PloS one* 7, e29591.

Xia, Y., Nivet, E., Sancho-Martinez, I., Gallegos, T., Suzuki, K., Okamura, D., Wu, M.Z., Dubova, I., Esteban, C.R., Montserrat, N., *et al.* (2013). Directed differentiation of human pluripotent cells to ureteric bud kidney progenitor-like cells. *Nat Cell Biol* 15, 1507-1515.

Xinaris, C., Benedetti, V., Novelli, R., Abbate, M., Rizzo, P., Conti, S., Tomasoni, S., Corna, D., Pozzobon, M., Cavallotti, D., *et al.* (2015). Functional Human Podocytes Generated in Organoids from Amniotic Fluid Stem Cells. *Journal of the American Society of Nephrology : JASN*.

Xinaris, C., Benedetti, V., Rizzo, P., Abbate, M., Corna, D., Azzollini, N., Conti, S., Unbekandt, M., Davies, J.A., Morigi, M., *et al.* (2012). In vivo maturation of functional renal organoids formed from embryonic cell suspensions. *Journal of the American Society of Nephrology : JASN* 23, 1857-1868.

Yamaleyeva, L.M., Guimaraes-Souza, N.K., Krane, L.S., Agcaoili, S., Gyabaah, K., Atala, A., Aboushwareb, T., and Yoo, J.J. (2012). Cell therapy with human renal cell cultures containing

erythropoietin-positive cells improves chronic kidney injury. *Stem cells translational medicine* 1, 373-383.

Ye, Y., Wang, B., Jiang, X., Hu, W., Feng, J., Li, H., Jin, M., Ying, Y., Wang, W., Mao, X., *et al.* (2011). Proliferative capacity of stem/progenitor-like cells in the kidney may associate with the outcome of patients with acute tubular necrosis. *Hum Pathol* 42, 1132-1141.

Yin, A.H., Miraglia, S., Zanjani, E.D., Almeida-Porada, G., Ogawa, M., Leary, A.G., Olweus, J., Kearney, J., and Buck, D.W. (1997). AC133, a novel marker for human hematopoietic stem and progenitor cells. *Blood* 90, 5002-5012.

Yokota, N., Burne-Taney, M., Racusen, L., and Rabb, H. (2003). Contrasting roles for STAT4 and STAT6 signal transduction pathways in murine renal ischemia-reperfusion injury. *Am J Physiol Renal Physiol* 285, F319-325.

Zhang, B., Ramesh, G., Norbury, C.C., and Reeves, W.B. (2007). Cisplatin-induced nephrotoxicity is mediated by tumor necrosis factor-alpha produced by renal parenchymal cells. *Kidney international* 72, 37-44.

Zobalova, R., McDermott, L., Stantic, M., Prokopova, K., Dong, L.F., and Neuzil, J. (2008). CD133-positive cells are resistant to TRAIL due to up-regulation of FLIP. *Biochem Biophys Res Commun* 373, 567-571.